Pore-Scale Modelling of Three-Phase Flow

Mohammad Piri
Centre for Petroleum Studies
Department of Earth Science and Engineering
Imperial College London
London SW7 2AZ, UK

A thesis submitted in fulfillment of the requirements for
the degree of Doctor of Philosophy of the University of London
and the Diploma of Imperial College

December, 2003

Abstract

We present a three-dimensional network model to simulate two- and three-phase capillary dominated processes at the pore level. The displacement mechanisms incorporated in the model are based on the physics of multi-phase flow observed in micromodel experiments. All the important features of immiscible fluid flow at the pore-scale, such as wetting layers, spreading layers of the intermediate-wet phase, hysteresis and wettability alteration are implemented in the model. Wettability alteration allows any values for the advancing and receding oil/water, gas/water and gas/oil contact angles to be assigned. Multiple phases can be present in each pore or throat (element), in wetting and spreading layers, as well as occupying the centre of the pore space. In all, some thirty different generic fluid configurations for two- and three-phase flow are analyzed. Double displacement and layer reformation are implemented as well as direct two-phase displacement and layer collapse events. Every element has a circular, square or triangular cross-section. A random network that represents the pore space in Berea sandstone is used in this study. The model computes relative permeabilities, saturation paths, and capillary pressures for any displacement sequence. A methodology to track a given three-phase saturation path is presented that enables us to compare predicted and measured relative permeabilities on a point-by-point basis. A new and robust displacement based clustering algorithm is presented. We predict measured relative permeabilities for two-phase flow in a water-wet system. We then successfully predict the steady-state oil, water and gas three-phase relative permeabilities measured by Oak [1]. We also study secondary and tertiary gas injection into media of different wettability and initial oil saturation and interpret the results in terms of pore-scale displacement processes.

The list of publications as a result of this research is as follows:

- M.J. Blunt, M.D. Jackson, **M. Piri**, and P.H. Valvatne. Detailed physics, predictive capabilities and macroscopic consequences for pore-network models of multiphase flow. *Advances in Water Resources*, **25**(8-12):1069-1089, 2002.
- **M. Piri**, and M.J. Blunt. Pore-scale modeling of three-phase flow in mixed-wet systems. *Paper SPE 77726, Proceedings of the SPE Annual Technical Conference and Exhibition, San Antonio, Texas, 29 September-2 October*, 2002.
- P.H. Valvatne, **M. Piri**, X. Lopez, and M.J. Blunt. Predictive pore-scale modeling of single and multiphase flow. *Transport in Porous Media* (in press)
- **M. Piri**, and M.J. Blunt. Three-dimensional mixed-wet random pore-scale network model of two- and three-phase flow in porous media. *Physical Review E* (submitted).

Acknowledgments

Firstly and most importantly, I would like to express my deepest gratitude to the Almighty and the All-knowing Allah, who, if you believe in him, will never dash your hopes.

Martin holds a place very close to my heart. I am extremely fortunate to have him as my very close friend and supervisor. I have enormously benefited from his invaluable scientific and spiritual support, advice, and continuous encouragement throughout my work with him. Martin, I am deeply affected by your integrity and commitment. Thank you so much.

Imperial College London, in particular the Department of Earth Science and Engineering - Center for Petroleum Studies - is very special to me. This is because of the excellent people that I have had the honor of working with. I would like to take this opportunity to thank them, especially the faculty, students and staff for their support, guidance and friendship. It means a lot to me.

I feel fortunate to have made so many good friends during my time here. I wish to thank them all, too many to name, but here are a few: Eguono-Oghene Obi, Per H. Valvatne, Hiroshi Okabe, Mohammed Al-Gharbi, Pascal Audigane, Maryam Khorram, Alimirza Gholipour, Robert Leckenby, Reza Banki, Branko Bijeljic, Azzan Al-Yaarubi, Rifaat A. M. Al-Mjeni, Ali Dehghani, Arash Soleimani, Ginevra Di Donato, Hooman Sadrpanah, Thomas von Schroeter, Djamel Ouzzane, and Xavier Lopez.

My gratitude extends to Prof. Ken S. Sorbie from Heriot-Watt University, and Prof. Peter R. King from Imperial College London, for serving on my examination committee.

A special mention with my sincere gratefulness goes to Prof. Pål-Eric Øren from Statoil for his continuous and invaluable comments throughout my work on Pore-Scale Modelling. I also feel indebted to the following people for their comments, stimulating discussions and encouragements: Prof. Dave Waldren, Dr. Carlos A. Grattoni , Dr. M.I.J. van Dijke, Dr. Matthew D. Jackson, Prof. Tadeusz W. Patzek,

Prof. Abbas Firoozabadi, and Prof. Muhammad Sahimi.

I would like to acknowledge the sponsors of Imperial College Consortium on Pore-Scale Modelling, i.e. BHP, EPSRC, Gaz de France, JNOC, PDVSA-Intevep, Schlumberger, Shell, Statoil, and the UK Department of Trade and Industry, for their generous and continued support of my research.

I also wish to try and express my gratitude to Dr. Mike Ala, Prof. Alain C. Gringarten and Dr. Hamid Hatamian for their kind help and attention before and after I started at Imperial College.

Last, but by no means least, is my family. I would like to thank them for their love, kindness, encouragement, and understanding. Mom, Dad, Lamia, Amoo Reza, Fatemeh, Masoomeh, Ali, Elaheh, Cobra, and Morteza, with love I dedicate this thesis, that I have worked very hard for, to you.

Contents

List of Figures

List of Tables

Chapter 1

Introduction

The simultaneous flow of three phases - oil, water and gas - in porous media is of great interest in many areas of science and technology, such as petroleum reservoir and environmental engineering. Three fluid flow occurs in enhanced oil recovery schemes including tertiary gas injection into oil and water, gas cap expansion, solution gas drive, gravity drainage, water flooding with different initial oil and gas saturations, steam injection, thermal flooding, depressurization below the bubble point, and water alternate gas (WAG) injection. In an environmental context three-phase flow occurs when a non-aqueous phase liquid (NAPL), leaking from an underground storage tank for instance, migrates through the unsaturated zone and may coexists with water and air (gaseous phase).

In order to understand fluid flow in porous media, one needs to know the constitutive relationships between macroscopic properties of the system such as relative permeabilities, capillary pressures, and fluid saturations. These relationships are used in macroscopic partial differential equations to describe the transport of fluid. The determination of constitutive relationships is complicated as they are dependent on the fluids' properties, the pore space, and the saturation history.

Experimental measurements of three-phase relative permeabilities and capillary pressures have been the subject of several studies [1–30], but they are extremely difficult to perform and at low saturation the results are very uncertain [16, 23, 31, 32]. Two independent fluid saturations are required to define a three-phase system and there is an infinite number of possible fluid arrangements making a comprehensive suite of experimental measurements for all three-phase displacements impossible. This is why numerical simulations of three-phase flow almost always rely on available empirical correlations to predict relative permeability and capillary pressure from measured two-phase properties [4, 20, 22, 33–54]. These models may

give predictions that vary as much as an order of magnitude from each other, or from direct measurements, since they have little or no physical basis [43, 53, 55].

It is important to have a reliable physically-based tool that can provide plausible estimates of macroscopic properties. Any theoretical or numerical approach to this problem not only needs a *detailed understanding* of the multiphase displacement mechanisms at the pore level but also an accurate and realistic characterization of the *structure* of the porous medium [56]. During the last two decades our knowledge of the physics of two- and three-phase flow at the pore level has considerably increased through experimental investigation of displacements in core samples and micromodels [57–72]. To describe the geometry of the pore space several authors have developed different statistical [73–75] and process based [76–78] techniques. In addition the pore space can be imaged directly using micro CT tomography [79, 80]. An example of a three-dimensional pore space image of a sandstone is shown in Fig. (1.1). It is possible to simulate multi-phase flow directly on a three-dimensional pore-space image by solving Navier Stokes equations or by using Lattice-Boltzman techniques [81–84]. However, for capillary controlled flow with multiple phases, these methods become cumbersome and computationally expensive.

An attractive alternative approach is to describe the pore space as a network of pores connected by throats with some idealized geometry (see Fig.(1.2)) [78, 85]. Then a series of displacement steps in each pore or throat are combined to simulate multiphase flow. Fatt [86–88] initiated this approach by using a regular two-dimensional network to find capillary pressure and relative permeability. Since then, the capabilities of network models have improved enormously and have been applied to describe many different processes. Table 1.1 lists some of the recent applications of network modelling. Recent advances in pore-scale modelling have been reviewed by Celia *et al.* [89], Blunt [90], and Blunt *et al.* [91].

For a random close packing of spheres Bryant and co-workers were able to predict permeability, elastic and electrical properties and relative permeability [107, 111, 244]. Øren *et al.* extended this approach by reconstructing a variety of sandstones and generating topologically equivalent networks from them. Using these networks several authors have been able to predict relative permeability and oil recovery for a variety of systems [76–78, 118, 127, 132, 136].

In this work we extend this predictive approach to three-phase flow. Before reviewing previous three-phase network models in detail, we review the fundamentals of contact angles, spreading coefficient and wettability alteration as well as spreading and wetting layers.

Table 1.1: Network and percolation type modelling references.

Aspect	Reference(s)
Two-phase flow	[55, 57, 76–78, 92–137]
Three-phase flow	[56, 132, 138–156]
Artificial neural networks (ANN)	[156–158]
Mercury porosimetry	[110, 159–163]
Effects of pore-size distributions	[88, 104, 164]
Electrical resistivity	[165–170]
Dissolution of NAPL (1)	[171–179]
Nucleation, SGD (2) and bubble growth	[180–183]
Gas condensates	[184–188]
Drying processes	[189–195]
Evaporation of a binary liquid	[196]
Moisture transport	[197]
Rate effects and dynamic modelling	[115, 145, 186, 198–206]
Multiphase flow in fractures	[207–212]
Dispersion	[213]
Foam flow	[214, 215]
Flow in polymer gels	[216]
Biological activity in porous media	[217, 218]
Non-Darcy effects	[219]
Gravity driven displacements	[171, 220, 221]
Imbibition into cement pastes	[222]
Bubble transport	[223]
Applications of critical analysis	[224, 225]
Non-Newtonian flow	[226]
Asphalt precipitation	[227–229]
Fluid imbibition into paper	[230]
Deactivation of immobilized glucose	[231, 232]
Diffusion and reaction	[233, 234]
Packed chromatographic columns	[235–241]
Biofiltering	[242]
Interfacial velocity calculation	[243]

1. Non-Aqueous Phase Liquid

2. Solution Gas Drive

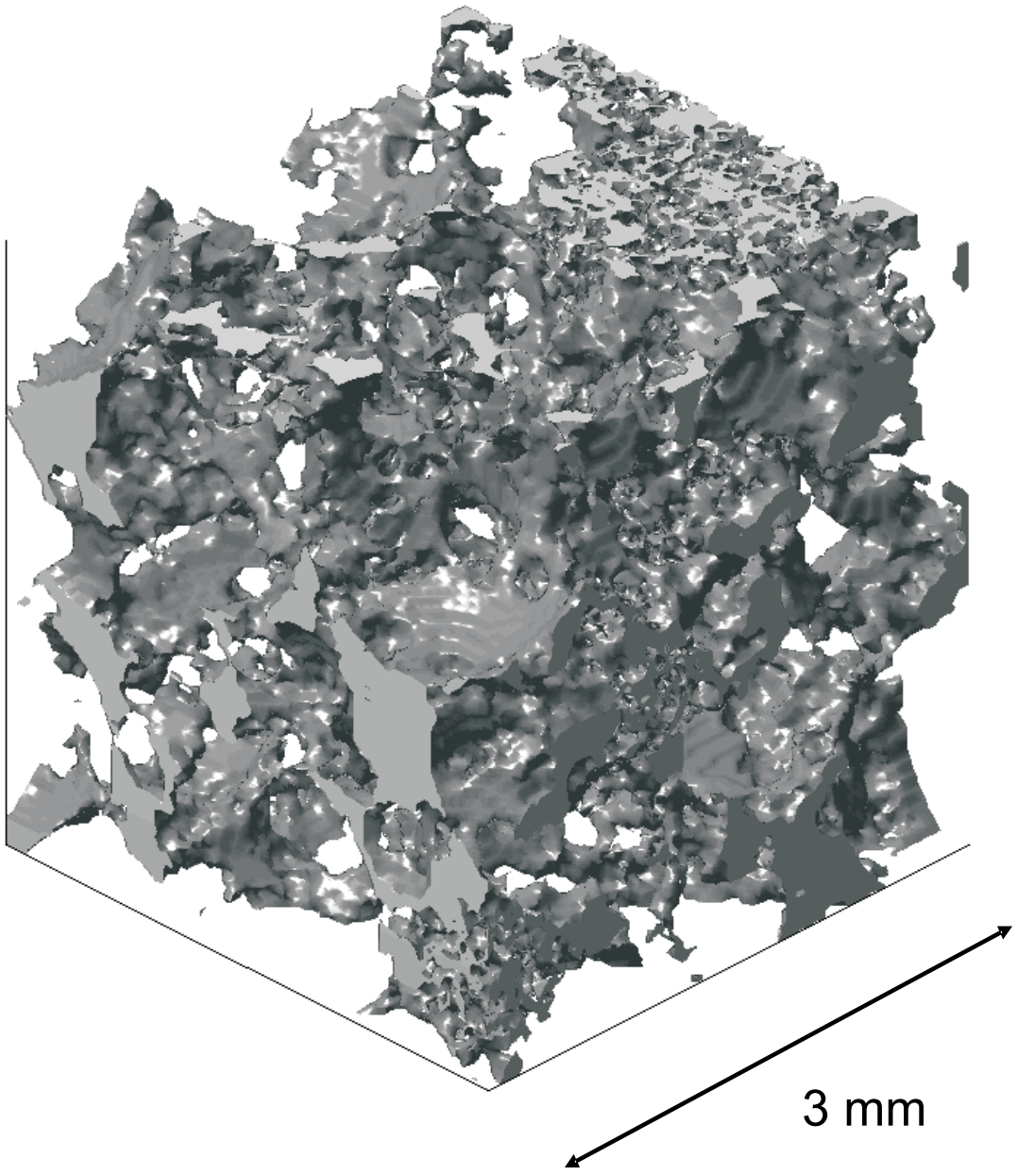

Figure 1.1: The void space of a sandstone produced by process based simulation [76–78].

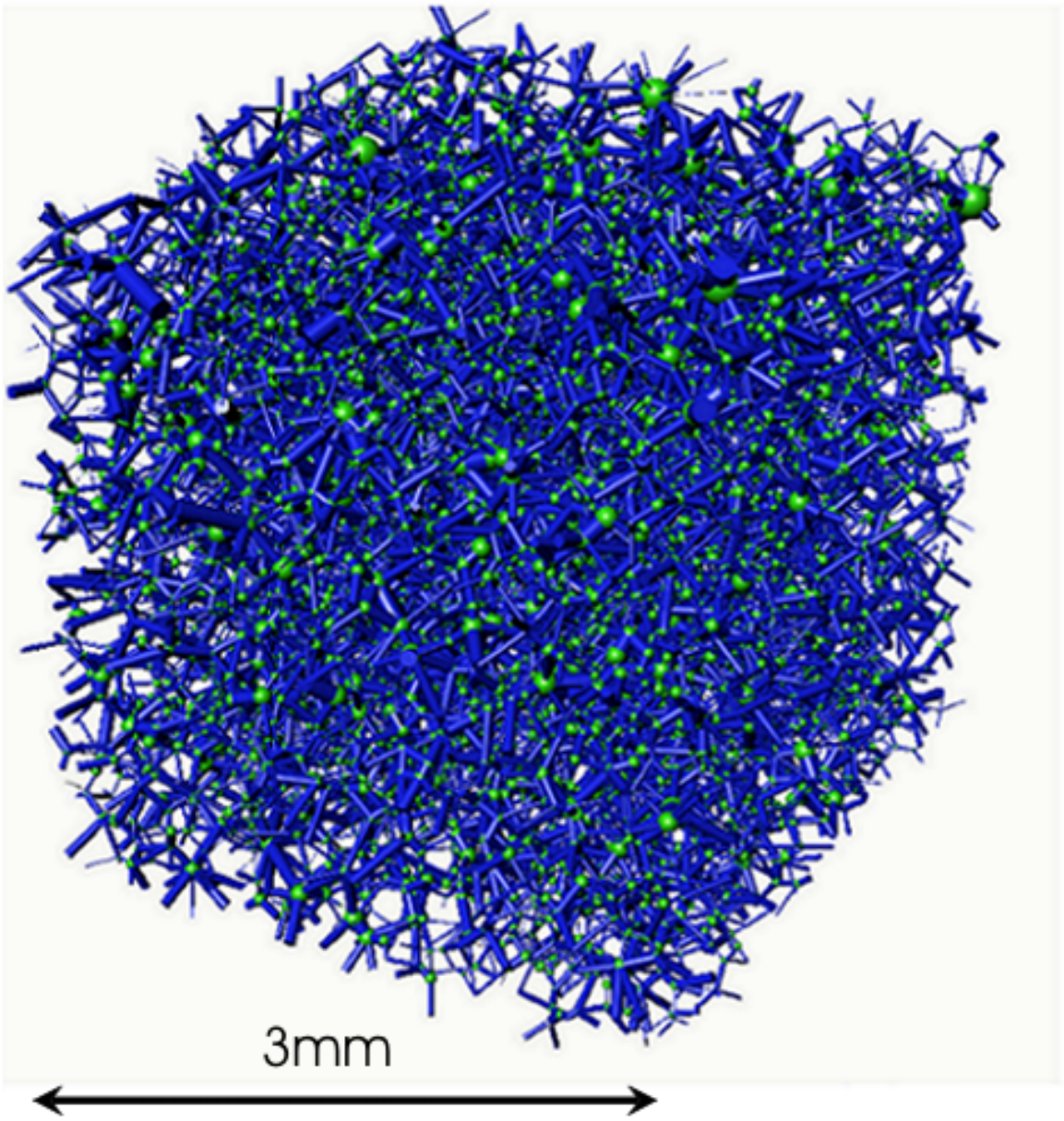

Figure 1.2: The Berea network used in this work. The network is a disordered lattice of pores connected by throats. The network topology, the radii of the pores and throats, their shapes and their volumes are all determined from a three-dimensional representation of the pore space of the system of interest (see Fig.(1.1)). This network will be used to predict two- and three-phase relative permeabilities (see Table (4.2) for dimensions and statistics of the network).

Chapter 2

Physics of Three-Phase Flow at the Pore-Level

2.1 Spreading Coefficients and Interfacial Tensions

The ability of oil to spread on water in the presence of gas is described by the *spreading coefficient* which is a representation of the force balance where the three phases meet. If the interfacial tensions are found by contacting pairs of pure fluids in the absence of the third, the coefficient is called *initial* and is defined by [245]:

$$C_s^i = \sigma_{gw} - \sigma_{go} - \sigma_{ow} \tag{2.1}$$

where σ is an interfacial tension between two phases labeled o, w, and g to stand for oil, water, and gas respectively. However, when three phases are present simultaneously, the interfacial tensions are different from those in two-phase systems. For instance, the gas/water interfacial tension may be significantly lower than its two-phase value because oil may cover the interface by a thin film of molecular thickness [246]. The other two-phase interfacial tensions may also vary when the third phase is present. If the three phases remain long enough in contact, thermodynamic equilibrium will be reached when liquids become mutually saturated. In these circumstances the spreading coefficient is named *equilibrium* and is given by Eq. (2.2), which is either negative or zero [245].

$$C_s^{eq} = \sigma_{gw}^{eq} - \sigma_{go}^{eq} - \sigma_{ow}^{eq} \tag{2.2}$$

Three-phase systems may be divided into one of the following cases (see Fig.

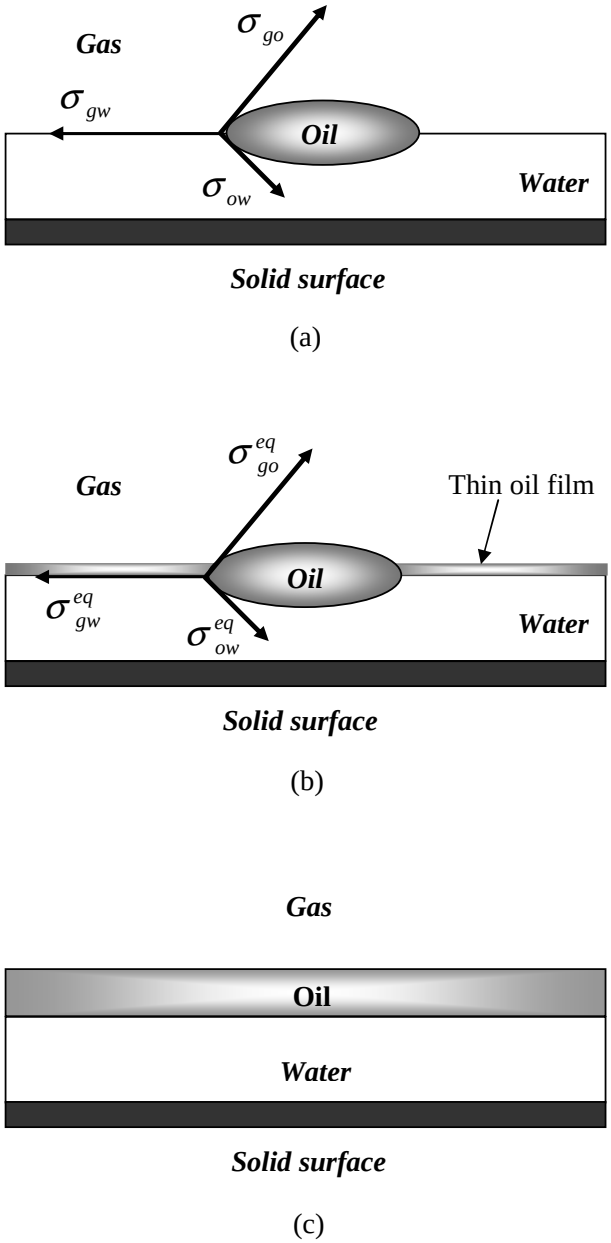

Figure 2.1: Different three-phase systems: (a) Non-spreading, $C_s^i < 0$, (b) Partially spreading, $C_s^i > 0$ and $C_s^{eq} < 0$(c) Spreading, $C_s^i > 0$ and $C_s^{eq} \approx 0$.

(2.1)): (a) *Non-spreading*, $C_s^i < 0$: a blob of oil will remain stationary on water, for example CS_2 on water [245]. (b) *Partially spreading*, $C_s^i > 0$ and $C_s^{eq} < 0$: where a quick initial spreading happens and then when the water surface is covered by a thin oil film, oil retracts to a lens. An example is benzene on water. (c) *Spreading*, $C_s^i > 0$ and $C_s^{eq} \approx 0$: in this case, oil spreads on water and excess oil makes the film thicker and thicker. When the thickness of the oil film is larger than the range of

intermolecular forces the equilibrium spreading coefficient becomes zero. Soltrol, a mixture of hydrocarbons, is an example of this case [71].

In the rest of the work, we will drop the superscript *eq* and always assume that we are dealing with interfacial tensions at equilibrium.

2.2 Three-Phase Contact Angles

The contact angle is defined as the angle between the two-phase line and the solid surface measured through the denser phase. In a three phase system a horizontal force balance can be written for each of the three pairs of fluids, i.e. oil-water, gas-water, and gas-oil, residing on a solid to obtain Young's equation (see Fig. (2.2)):

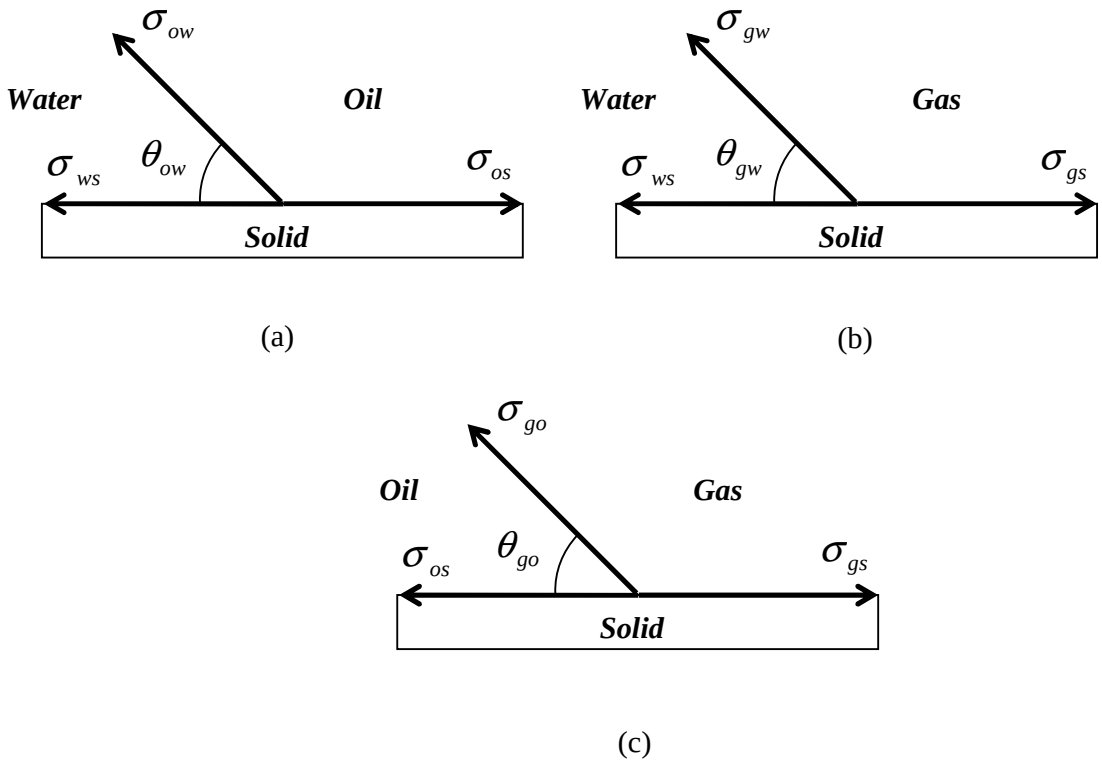

Figure 2.2: Horizontal force balance in three two-phase systems: (a) oil/water/solid, (b) gas/water/solid, and (c) gas/oil/solid.

$$\sigma_{os} = \sigma_{ws} + \sigma_{ow}\cos\theta_{ow} \tag{2.3}$$

$$\sigma_{gs} = \sigma_{ws} + \sigma_{gw}\cos\theta_{gw} \tag{2.4}$$

$$\sigma_{gs} = \sigma_{os} + \sigma_{go}\cos\theta_{go} \tag{2.5}$$

A constraint on the three-phase contact angles and interfacial tensions in mutual equilibrium can be derived by manipulation of Eqs.(2.3)-(2.5):

$$\sigma_{gw}\cos\theta_{gw} = \sigma_{go}\cos\theta_{go} + \sigma_{ow}\cos\theta_{ow} \tag{2.6}$$

Eq. (2.6) was derived first by Bartell & Osterhoff [247] in the context of solid/oil/water systems and rediscovered by Zhou & Blunt [246] in contaminant hydrology. This constraint has many implications for three-phase processes. For instance consider a three-phase strongly oil-wet system, i.e. $\theta_{ow} \approx \pi$. At ambient conditions, typical interfacial tensions for water/n-alkane systems are $\sigma_{go} = 20\, mN/m$ and $\sigma_{ow} = 50\, mN/m$ [245]. This means $\sigma_{gw}\cos\theta_{gw} < 0$ which in turn implies $\theta_{gw} > \frac{\pi}{2}$. The analysis above for oil-wet systems indicates that gas is not the most non-wetting phase in the presence of water.

Blunt [248] showed in a n phase system there are $\frac{n(n-1)}{2}$ contact angles, $\frac{(n-1)(n-2)}{2}$ constraints and $(n-1)$ independent contact angles. In three-phase systems, only two of the contact angles need to be defined independently.

Van Dijke *et al.* [152] presented a linear relationship to find gas/oil and gas/water contact angles from the oil/water contact angle and interfacial tensions which also satisfies the constraint given by Eq. (2.6):

$$\cos\theta_{go} = \frac{1}{2\sigma_{go}}\{C_s\cos\theta_{ow} + C_s + 2\sigma_{go}\} \tag{2.7}$$

$$\cos\theta_{gw} = \frac{1}{2\sigma_{gw}}\{(C_s + 2\sigma_{ow})\cos\theta_{ow} + C_s + 2\sigma_{go}\} \tag{2.8}$$

2.3 Wettability Alteration and Contact Angle Hysteresis

Wettability is the ability of one fluid to spread on a solid and form a wetting film [146]. Based on the oil/water contact angle, porous media with different wettability can be categorized into three main groups: water-wet, neutrally-wet and oil-wet corresponding to oil/water contact angles being less than, close to and larger than $\frac{\pi}{2}$ respectively.

While most clean rock surfaces in contact with refined oils are water-wet, few, if any, oil reservoirs are completely water-wet. This is because of direct contact of crude oil with the solid surface which changes its wettability by adsorption of the polar components of the crude or the presence of naturally oil-wet minerals within

the rock. This makes any values of oil/water and consequently gas/water and gas/oil contact angles possible [249–253]. Kovscek *et al.* [251] developed a model where the wettability of the rock surface is assumed to be altered by the direct contact of oil. Before a porous medium is invaded by oil it is assumed to be full of water and water-wet. Once it is invaded by oil, a thin film of water prevents oil touching the solid surface directly. But at a threshold capillary pressure, this film can collapse and allows oil to contact the solid surface and change its wettability. Regions of the pore space not contacted by oil remain water-wet.

The contact angle also depends on the direction of displacement. This difference between *advancing*, i.e. wetting phase displacing the non-wetting one, and *receding*, i.e. non-wetting phase displacing the wetting one, contact angles may be as large as 50° - 90° [245, 254, 255] depending on surface roughness, surface heterogeneity, swelling, rearrangement or alteration of the surface by solvent [245].

To accommodate any type of displacement process, we assign eight contact angles to each pore and throat: θ_{ow}^{PD} (oil displacing water in an element that has not changed its wettability before), θ_{gw}^{PD} (gas displacing water in an element that has not changed its wettability before), and six contact angles when the wettability has been altered: θ_{ow}^{a} (water displacing oil), θ_{ow}^{r} (oil displacing water), θ_{gw}^{a} (water displacing gas), θ_{gw}^{r} (gas displacing water), θ_{go}^{a} (oil displacing gas), θ_{go}^{r} (gas displacing oil).

There is an ambiguity in defining a third contact angle from Eq. (2.6) if advancing and receding values are different. For instance, imagine water is being injected into oil and gas where the appropriate gas/water and oil/water contact angles to be used are θ_{gw}^{a} and θ_{ow}^{a} respectively. Now if one uses Eq. (2.6) to find the third contact angle, θ_{go}, it is not clear that the calculated value is the advancing or receding gas/oil contact angle. This problem is also evident when one uses Eqs. (2.7) and (2.8), where it is not known, for example, which oil/water contact angle, i.e. advancing or receding, should be used to calculate receding gas/oil contact angle needed, for example, in gas injection into oil and water.

In this work, we first decide on the values of two of the contact angles and then calculate the third one using Eq. (2.6). We use θ_{ow}^{r} and θ_{go}^{r} to calculate a θ_{gw}. We also use θ_{ow}^{a} and θ_{go}^{a} to find another value of θ_{gw}. The smaller of two values of θ_{gw} is considered as receding and the larger one as the advancing value. We always make sure in every single pore and throat, the receding contact angle for each phase is less than or equal to the advancing value, i.e. $\theta_{ij}^{r} \leq \theta_{ij}^{a}$.

2.4 Spreading and Wetting Layers

During primary drainage, oil can occupy centres of the pore space, leaving water as a wetting layer in the corners and crevices of the pore space. During subsequent cycles of water and/or gas injection these water layers are still present and maintain continuity of water.

After gas injection into an element containing oil in the centre and water in wetting layers, gas will occupy the centre and it is possible that oil will remain in a layer sandwiched between the gas and water. These are called *spreading* layers; as we discuss later their stability is related to the spreading coefficient, contact angles, corner angles and capillary pressures, and are likely to be present in spreading systems.

Later, we will present detailed analysis of possible pore space configurations in terms of displacement history, contact angles and spreading coefficient. However, to motivate the critique of previous pore-scale models of three-phase flow, we need to emphasize the definition of some key terms.

A spreading system has $C_s = 0$ and oil spontaneously forms layers between water and gas in the pore space. A non-spreading system has $C_s < 0$ and while oil layers can also be present [72, 256, 257] they tend to be stable for more restricted range of capillary pressures. Also, we refer to wetting and spreading *layers* - these layers are typically a few microns in thickness and have a *non-negligible* hydraulic conductivity and maintain phase continuity. In contrast, *films* are of molecular thickness (of order a nanometer) and have *negligible* conductivity and do *not* contribute to phase continuity - where present films simply modify the apparent, or equilibrium, interfacial tensions, as discussed above.

Chapter 3

Literature Review

3.1 Previously Developed Three-Phase Pore-Scale Network Models

Here we present a detailed review of previously developed three-phase network models.

Heiba *et al.* [138] extended statistical network modelling previously used for two-phase systems [96, 108] to three-phase flow. A Bethe lattice, or Cayley network was used to represent the porous medium. Relative permeabilities were calculated from Stinchcombe's formula [258] using new series approximations from percolation theory. Only a single phase could occupy a throat. A given fluid was considered to be able to flow only when the site that it occupied was a member of a continuous flow path from the inlet to the outlet. The displacement of one phase by another was controlled by accessibility and local entry capillary pressure. Six groups of displacement were considered: gas into oil, oil into gas, gas into water, water into gas, water into oil, and oil into water. Two spreading systems were investigated where in the first one gas and water were displacing oil while in the second case water and oil were displacing oil and gas. The results showed that the gas and water relative permeabilities were functions of only their own saturations. Oil layers prevented the direct contact of gas and water. Oil isoperms were found to be strongly curved, meaning that the oil relative permeability was not only a function of its own saturation. Extensions of the theory to handle the complications involved by the effects of wettability and phase swelling due to mass transfer were also discussed. It was concluded that three-phase relative permeabilities are generally path functions rather than state functions (function of saturation only) except in particular situa-

tions such as when two phases are separated by the third. This model used rather simple networks and displacement rules.

Soll & Celia [139] developed a computational model of capillary-dominated two- and three-phase movement at the pore level to simulate capillary pressure-saturation relationships in a water-wet system. Regular two- or three-dimensional networks of pores, connected to each other by throats, were used to represent the porous medium. Hysteresis was modelled by using advancing and receding values for the contact angles for each pair of fluids. Every pore was able to accommodate one fluid at a time as well as wetting layers. Viscous forces were considered to be negligible but the effects of gravity were included to modify the local capillary pressures. In order to reproduce their micromodel experiments [66], oil as a spreading phase was allowed to advance ahead of a continuous invasion front. Several pores could be filled simultaneously. This model was the first to incorporate layer flow in three-phase network modelling albeit in a rather *ad hoc* fashion. The results were compared with capillary pressure-saturation results and fluid distributions from the two- and three-fluid micromodel experiments. The amount of oil layer flow was used as a fitting parameter. Predicted two-phase air/water and oil/water capillary pressures were in good agreement with measured values [66] although the model did not so successfully match three-phase data. The model was not used to calculate relative permeabilities.

Øren *et al.* [140] described details of the pore level displacement mechanisms taking place during immiscible gas injection into waterflood residual oil (tertiary gas injection) which then were incorporated into a two-dimensional strongly water-wet square network model with rectangular links and spherical pores in order to compute oil recovery in spreading and non-spreading systems. Simulated recoveries compared very well with the measured values from micromodel experiments [63, 64]. The authors described a double drainage mechanism where gas displaces trapped oil that displaces water allowing immobile oil to become connected boosting oil recovery. Oil recovery decreased with decreasing spreading coefficient. In non-spreading systems, the probability of direct gas-water displacement was high and capillary fingering of gas resulted in early gas breakthrough and low oil recovery. In spreading systems, oil reconnection was more effective and direct gas/oil displacement was preferred. It was concluded that a simple invasion percolation algorithm [94, 259] including the spreading layers works well in mimicking the complex three-phase behaviour seen in micromodels. In this work, relative permeabilities were not calculated.

Pereira *et al.* [56, 147] developed a dynamic two-dimensional network model for

drainage-dominated three-phase flow in strongly water- and oil-wet systems when both capillary and viscous forces were important. The displacement mechanisms in spreading and non-spreading systems were described by generalization of two-phase displacement mechanisms. Both pores and throats were assumed to be lenticular in cross-section allowing wetting and spreading layers to be present. No volumes were allocated to the throats and layers and there was no pressure drop in the pores. Resistance to the flow through the throats was modelled using the mean hydraulic radius concept, i.e. twice the ratio of area open to flow to *wetted perimeter*. Pressure of a fluid in a throat was an interpolation of pressures of the same fluid in the neighbouring pores. Trapping of different fluids was considered only for non-spreading systems. Coalescence and reconnection of trapped clusters was also simulated. Pores could be occupied by two or three *bulk* fluids at the same time separated by *flat* interface(s). The simulated recoveries at gas breakthrough were compared against measured values in micromodels [64]. As in Øren *et al.* [140], a large difference between the recoveries in spreading and non-spreading systems was reported for water-wet cases due to existence of oil layers in the spreading systems. The highest recovery, 85%, was found for the oil-wet case. This was because continuous wetting layers prevented trapping of oil. The oil recovery was much lower, 14%, for the water-wet case in a non-spreading system. This was because there were no spreading layers of oil. Even when layers were present for the spreading system, the oil recovery was much lower, 40%, in a water-wet medium than for the oil-wet case. Water in water-wet systems played the same role as oil in oil-wet systems – water recoveries in water-wet spreading and non-spreading systems were high. It was confirmed that the high oil recoveries were due to the presence of wetting or spreading oil layers, despite the fact that the conductance of a layer of water or oil in a throat was only around 1% of the conductance of a throat full of a single phase. In non-spreading systems, direct water displacement by gas was preferred over gas-oil-water double displacement leading to low oil recovery. An order of magnitude reduction in the simulated conductivity of the oil layers decreased oil recovery and made the behaviour of the spreading system similar to that of a non-spreading system. Also a reduction in initial oil saturation for tertiary gas injection decreased the oil recovery. This was true for both spreading and non-spreading systems indicating that the recovery of the intermediate wetting phase is strong function of saturation history. This was reported to be consistent with experiments by Dria *et al.* [23] and Oak [1, 21]. It was also concluded that the recovery of the wetting fluid is independent of the saturation history. Relative permeabilities were

not calculated in this work.

Paterson *et al.* [141] developed a water-wet percolation model to study the effects of spatial correlations in the pore size distributions on three-phase relative permeabilities and residual saturations. This was an extension of their previous work on two-phase systems [117]. Fractal maps derived from fractional Brownian and Levy motion (fBm and fLm) were used to assign pore size. A simple site percolation model with trapping was used. Trapping was incorporated based on Hoshen-Kopelman algorithm [260]. In three-phase simulations direct displacement of oil and water by gas and also double drainage were implemented. The model assigned the same volume to all pores and so the fraction of sites occupied by a phase gave its saturation. All the sites were assumed to have the same conductivity regardless of their radii. The simulation results for correlated properties showed lower residual saturations in comparison to uncorrelated ones. Incorporating a bedding orientation to the spacial-correlations had a major impact on relative permeability. When the bedding was parallel to the flow direction, the relative permeabilities were greater and residual saturations lower than those when bedding was perpendicular to the flow. This was also the case for two-phase relative permeabilities [117]. The effects of spreading coefficient were also studied. Similar to previous authors [56, 140, 147] it was shown that the less negative the spreading coefficient, the lower the final residual oil saturation. For more negative spreading coefficients direct gas to oil and gas to water displacements are preferred over double drainage. This effect was more significant for correlated systems.

Fenwick & Blunt [142, 143] developed a three-phase network model for strongly water-wet systems. A regular cubic network composed of pores and throats with equilateral triangular or square cross-sections was used. Oil/water and gas/water contact angles were considered to be zero. Two and three-phase displacement mechanisms including oil layer flow observed in micromodel experiments were incorporated in the model. Double drainage was generalized to allow any of six types of double displacement where one phase displaces a second that displaces a third as observed by Keller *et al.* [72]. The model was able to simulate any sequence of oil, water and gas injection. Using a geometrical analysis, a criterion for stability of oil layers was derived which was dependent on oil/water and gas/oil capillary pressures, contact angles, equilibrium interfacial tensions, and the corner half angle. It was argued that oil layers could be present even for negative spreading coefficient systems. Using a simple calculation [246] it was shown that the layers are of order a micron across or thicker in the corners, roughness and grooves of the pore space. The work was

the first to estimate conductance of an oil layer which then was used to compute oil relative permeability. It was shown that at low oil saturation the oil relative permeability should vary quadratically with saturation, as observed experimentally [13, 261–263].

It was shown that in three-phase systems relative permeabilities and oil recoveries are strong functions of saturation path. An iterative methodology which coupled a physically-based network model with a 1-D three-phase Buckley-Leverett simulator was developed in order to find the correct saturation path for a given process with known initial condition and injection fluid [143]. This enabled the network model to compute the properties for the right displacement sequence. The three-phase relative permeabilities were called self-consistent when the saturation path that was used by the network model to compute them will be exactly produced by the conventional three-phase Buckley-Leverett simulator if the network model relative permeabilities were used in the flow equations to compute the macroscopic flow. Self-consistent relative permeabilities for secondary and tertiary gas injection into different initial oil saturations were presented. The resultant saturation paths compared well qualitatively with experimental data by Grader & O'Meara [13]. The paths in the oil/water vs. gas/oil capillary pressure space were all located in the region where oil layers were stable meaning that oil did not get trapped. Oil relative permeabilities for different initial conditions were different from each other, consistent with several experimental studies [1, 2, 16, 25, 43].

Mani & Mohanty [144, 145] also used a regular cubic network of pores and throats to simulate three-phase flow in water-wet systems. Pores and throats were considered to be spherical and cylindrical respectively. The oil/water capillary pressure was fixed at its original value during the gas invasion processes. The parameters of the network were tuned to match two-phase mercury-air experimental capillary pressures for Berea sandstone [92].

Both dynamic and quasi-static simulations were carried out. The work had two important features: (I) Dynamic simulation of capillary-controlled gas invasion, where it was assumed each phase pressure was not constant across the network. (II) Re-injection of the produced fluids at the outlet of the medium into the inlet in order to simulate larger systems. This was used to see whether trapped oil ganglia become reconnected by double drainage to form spanning clusters. The two-phase processes were simulated at low capillary number using traditional quasi-static assumptions. Pressure drops across pores were ignored. The model included fluid flow through wetting and spreading layers. A fixed conductance was assigned to

oil layers. For the capillary pressure histories used, no stable oil layers were observed in both spreading and non-spreading systems. Gas invasion was modelled by three displacement mechanisms: direct gas/water, direct gas/oil, and double drainage. For each displacement a potential was considered which was the difference between the pressures of two involved fluids minus the threshold capillary pressure of the displacement. The displacement with the largest potential was carried out first. Re-injection of fluids was simulated by replacing the fluid distribution in the inlet zone by the fluids in the outlet zone. The process was terminated after steady state was reached at the imposed pressure conditions, i.e. when no further gas invasion was possible at the imposed capillary pressure. The final oil saturation in spreading systems was zero. The capillary pressure curves obtained from dynamic and quasi-static simulations were virtually identical. For non-spreading systems with a low oil/water capillary pressure, drainage of water and oil occurred with similar probability. Displacement of water from the medium created trapped oil clusters that were surrounded by gas. Due to the assumed absence of oil layers in non-spreading systems, oil ganglia could not be displaced by gas at any gas/oil capillary pressure. The water relative permeability was a function of the water saturation alone for both two-phase and three-phase systems, and was not dependent on the saturation history, spreading coefficient and the imposed oil/water capillary pressure. Similarly, for spreading three-phase systems, it was shown that gas relative permeability is a function of its own saturation only and do not depend on the imposed oil/water capillary pressure. But for non-spreading systems, the three-phase gas relative permeability was different from the two-phase drainage curves and were dependent on the oil/water capillary pressure, spreading coefficient and the saturation history. The three-phase oil relative permeability was a function of the oil saturation, the imposed oil/water capillary pressure, the spreading coefficient and the saturation history in both spreading and non-spreading systems. The effect of spreading coefficient and saturation history on three-phase relative permeability was consistent with other network modelling studies [56, 140, 142, 143, 147] and experimental measurements [1, 2, 16, 25, 43].

Laroche *et al.* [125, 146] developed a pore network model to predict the effects of wettability heterogeneities with different patterns and spatial distributions on displacement mechanisms, sweep efficiency, and fluid distribution in gas injection into oil and water. A dalmatian type of wettability heterogeneity was used with continuous water-wet surfaces enclosing discontinuous regions of oil-wet surfaces or vice-versa. A series of three-phase glass micro-model experiments with different

wettabilities were also carried out. Measured oil/water contact angles for the water-wet and oil-wet surfaces were 0° and 105° respectively. n-Dodecane, water, and nitrogen were the three fluids used in the experiments. All the two-phase interfacial tensions, densities, and viscosities were measured. The initial spreading coefficient was $7.3mN/m$ and hence the oil was assumed to be spreading. The capillary number throughout the experiments was approximately 10^{-5} indicating capillary controlled displacement. A 2-D regular pore and throat network was used to simulate the experiments. All the throats had triangular cross-sections while the pores were circular cylinders. The pore and throat size distributions were similar to those of Berea sandstone. Saturations, conductances, and relative permeabilities were calculated using similar techniques to Fenwick & Blunt [142]. The fluid distributions at the end of two- and three-phase simulations were in good qualitative agreement with those found experimentally.

Hui & Blunt [264, 265] developed a mixed-wet model of three-phase flow for a bundle of capillary tubes. The tubes had different sizes and were equilateral triangle in cross-section. Wettability alteration was modelled by changing the wettability of surfaces that came into contact with oil after primary drainage. This enabled the model to simulate three-phase flow with any combination of oil/water, gas/water, and gas/oil contact angles. In all some ten fluid configuration were considered. Primary drainage, water flooding, and tertiary gas injection were simulated. The effects of wettability, spreading coefficient and initial oil saturation on relative permeabilities were investigated. Possible configuration changes during each process along with the threshold capillary pressure of each change were presented. The stability of layers in different configurations and capillary pressures at which they collapse was discussed. We will extend this approach to study 30 different possible fluid configurations in three-phase flow and will incorporate them in a three-dimensional random network model.

Lerdahl *et al.* [149] used the technique developed by Bakke *et al.* [76] to reconstruct a three-dimensional void space, Fig. (1.1), and then convert it to a pore and throat network, Fig. (1.2), for use in a water-wet network model to study drainage-dominated three-phase flow. Simulated results were compared successfully against the experimental data by Oak [1]. We will use a similar network in our studies and also compare our predictions against Oak's experiments [1]. In our study we will compare results on a point-by-point basis using our saturation tracking algorithm and extend the model to mixed-wet systems following the approach of Hui & Blunt [264, 265].

Larsen *et al.* [150] used a water-wet three-dimensional cubic pore network model based on the work of Fenwick & Blunt [142, 143] to simulate a series of micromodel experiments of WAG (water alternate gas) injection processes. All the pores and throats were assumed to have square cross-sections. The network model was used in an iterative procedure similar to the one used by Fenwick & Blunt [143] to find self-consistent saturation paths. Three WAG injections with different gas/water injection ratios were carried out.

Van Dijke *et al.* [151–153] presented a process-based mixed-wet model of three-phase flow using a bundle of capillary tubes with circular cross-sections to study the saturation dependencies of capillary pressures and relative permeabilities for spreading and non-spreading systems. Larger pores were considered to be oil-wet and the smaller ones water-wet. It was shown that based on interfacial tensions and contact angles the three-phase saturation space could be divided up to three different regions with a different intermediate-wet phase. The relative permeability of this phase was a function of two saturations. Also the capillary pressure between the most wetting and non-wetting phases is dependent on two saturations. The relative permeabilities of the other two phases were a function of only their own saturation in this region. The authors extended this approach to determine the functional dependency of relative permeability and capillary pressure for media of arbitrary wettability.

Van Dijke *et al.* [154, 155] developed a regular three-dimensional three-phase network model for systems with different wettability expanding on thier previous studies on bundles of capillary tubes. Every element was allowed to have a different oil/water contact angle and Eqs. (2.7) and (2.8) were used to determine the gas/oil and gas/water contact angles [152]. While layers were not incorporated explicitly in saturation or conductance computations, they were allowed to establish continuity of different phases. The model was a cubic array of only throats with a circular cross-section. The coordination number could be changed by removing throats from the network. An extensive series of simulations of three-phase flow was performed. For networks with a high coordination number, the saturation dependencies were qualitatively similar to those predicted for capillary bundles. As the coordination number was reduced, connectivity was impaired and trapping became significant. The authors also compared their network simulations with micromodel experiments of WAG [266, 267] where there were repeated cycles of water and gas flooding. To reproduce the results, they incorporated multiple displacements where a train trapped clusters may displace each other until there is invasion into a connected

phase. They suggested that such multiple displacements were significant in WAG flooding. While certainly such displacements were observed in the micromodel experiments, we suggest that in three-dimensional displacements the phases are likely to be better connected and so the movement of trapped ganglia is less significant. We will only consider double displacements in this work.

The conclusion of this section is that while many three-phase pore-scale displacement mechanisms are well understood, and the generic functionality of relative permeability has been discussed, three-phase network models to date have not addressed the full range of possible configurations in mixed-wet systems and their predictive powers are limited.

The network model described here combines three essential components: ***(1)*** a description of the pore space and its connectivity that mimics *real* systems; ***(2)*** a physically-based model of *wettability alteration*; and ***(3)*** a *full description of fluid configurations* for two- and three-phase flow. This will enable us to predict three-phase relative permeabilities for media of arbitrary wettability using geologically realistic networks.

Comparison of the experimental and predicted relative permeabilities in three-phase systems is only possible if both have identical saturation paths. This is because macroscopic properties in three-phase systems are strongly dependent on saturation history of the system. In this work, we present an algorithm to simulate experimental saturation paths and predict relative permeabilities to compare with measured values.

Chapter 4

Displacement Mechanisms

4.1 Porous Medium

In recent years, several advances have been made in the construction of realistic representations of porous media. Øren, Bakke and co-workers [76–78] have developed random network models based on the pore space geometry of the rock of interest. The model is derived either from a direct three-dimensional image of the pore space obtained from micro CT scanning, or from simulating the geological processes by which the rock was formed, see Fig.(1.1). Many other authors have also developed techniques to derive pore structures from a variety of measurements [75, 80, 107, 111, 130, 163, 244, 268–278]. While such approaches are not routine, and the correct pore-space characterization of carbonates is very much an open question, for simple sandstones there are reliable methods for determining an equivalent network structure that attempts to mimic the properties of the real pore space.

In cross-section, individual pores and throats are often modelled as triangles and high-order polygons [279, 280]. This allows wetting phase to occupy the corners when the non-wetting phase fills the centre. As well as triangular cross-section elements, authors have used geometries with circular [154, 155], square [142, 143, 150], star-shape [112, 166, 168–170], and lenticular [56, 147] cross-sections (see Fig.(4.1)) to represent pores and throats.

The network model in this work reads as input any two or three-dimensional regular or random network comprised of pores connected by throats. Each pore or throat is assigned a total volume, an inscribed radius and a shape. The inscribed radius is used to assign a capillary entry pressure during multiphase flow. In this model the pore and throats have a scalene triangular, square or circular cross-section. The cross-section has the same shape factor G (ratio of cross-sectional area, A, to

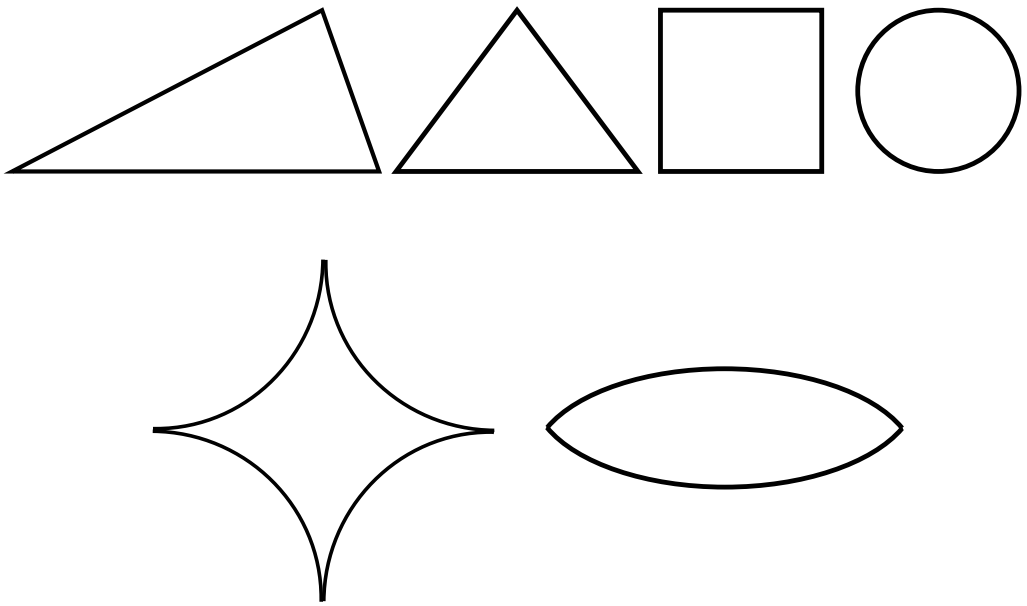

Figure 4.1: Elements with different cross-sectional shape.

perimeter, P, squared) [280] as the real system from which the network is derived:

$$G = \frac{A}{P^2} \tag{4.1}$$

A clay volume is associated with the network. This represents an immobile volume that remains water saturated throughout all displacements. It can be adjusted to match the observed connate water saturation [76–78]. Table (4.1) lists all the parameters that the model reads to recognize a network. A Berea network is used for the modelling studies in this work. A network of pores and throats is generated that presents the topology of the void space of the rock of interest (see Fig. (1.2)). The pores and throats have sizes and shapes that reproduce the principal geometric features of the three-dimensional image (see Fig. (1.2)) [77]. Table (4.2) lists the network statistics. Fig. (4.2) compares the pore and throat size distributions of the network.

4.2 Pore and Throat Cross-Sectional Shapes

- ***Triangular Elements***

  An irregular triangle with the corner half angles of α_1, α_2, and α_3 and the convention of $0 \leq \alpha_1 \leq \alpha_2 \leq \alpha_3 \leq \frac{\pi}{2}$, see Fig. (4.3), is considered. The α_1

Table 4.1: Network parameters read by the model consistent with the networks generated by Øren, Bakke and co-workers [76–78].

No.	Item
1	Total number of pores and throats
2	Length, width and depth of the network
3	Volume of each pore and throat
4	X, Y, and Z coordinations of each pore
5	Inscribed radius of each pore and throat
6	Number of connecting pore(s) to each pore (1)
7	Index of connecting pore(s) to each pore
8	Whether each pore is at the inlet
9	Whether each pore is at the outlet
10	Index of the throat connecting two pores
11	Shape factor of each pore and throat
12	Clay pore volume
13	Index of the first and second connecting pores to each throat
14	Micro-porosity volume in each throat
15	Spacing (2)
16	Length of the first and second pore connecting to each throat
17	Length of each throat

1. Coordination number of each pore
2. Distance between the centres of the two connecting pores

and α_2 are two corner half angles associated with the base of the triangle and R is the inscribed radius which is related to the area, A, and perimeter, P, of the element through [280]:

$$R = \frac{2A}{P} = 2PG \tag{4.2}$$

Since the cross-section is a composition of six triangles with equal height of r (see Fig. (4.3)), from elementary geometry A is given by [281]:

$$A = \frac{R^2}{4G} = R^2 \sum_{i=1}^{3} \cot \alpha_i \tag{4.3}$$

Since $\alpha_3 = \frac{\pi}{2} - \alpha_1 - \alpha_2$, the shape factor $G = A/P^2$ is then given by:

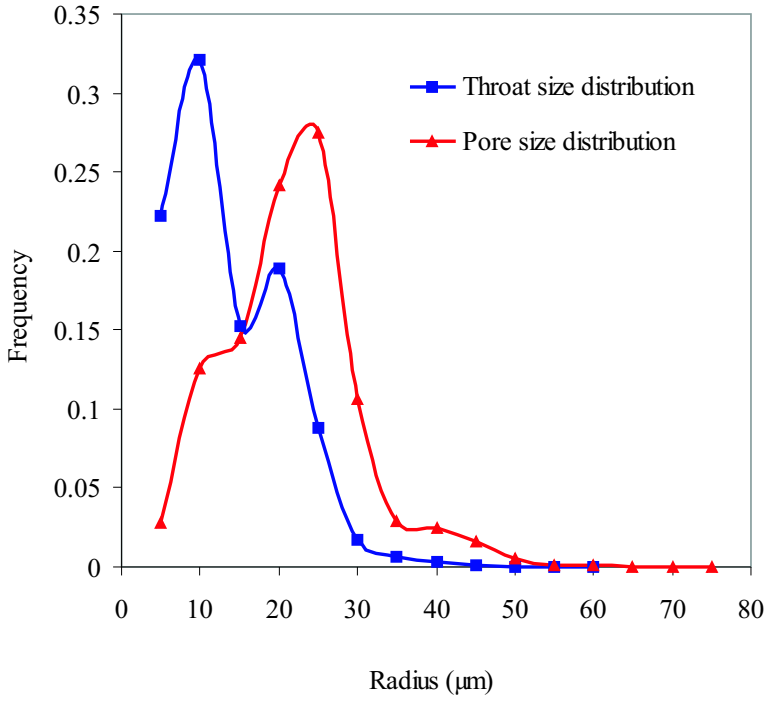

Figure 4.2: Pore and throat size distributions for the Berea network.

$$G = \frac{1}{4}\left[\sum_{i=1}^{3} \cot \alpha_i\right]^{-1} = \frac{1}{4} \tan \alpha_1 \tan \alpha_2 \cot(\alpha_1 + \alpha_2) \tag{4.4}$$

The shape factor for irregular triangles ranges from *zero* corresponding to a slit-like element to $\frac{\sqrt{3}}{36} \approx 0.048113$ belonging to equilateral triangles. A given value of G corresponds to a range of triangles where the limits of the range are denoted by $\alpha_{2,\,min}$ and $\alpha_{2,\,max}$ which in turn correspond to the triangles where $\alpha_{2,\,min} = \alpha_1 = \alpha$ and $\alpha_{2,\,max} = \frac{\pi}{4} - \frac{\alpha_1}{2}$, see Fig. (4.4). The shape factor is related to $\alpha_{2,\,min}$ and $\alpha_{2,\,max}$ by [77, 280]:

$$G = \frac{1}{4}\left[\frac{2}{\tan \alpha_{2,\,min}} + \tan(2\alpha_{2,\,min})\right]^{-1} \tag{4.5}$$

$$G = \frac{\sin(2\alpha_1)}{2}\left[2 + \frac{\sin(2\alpha_1)}{\sin(2\alpha_{2,\,max})}\right]^{-2} = \frac{\sin(2\alpha_{2,\,max})\cos(2\alpha_{2,\,max})}{4\left[1 + \cos(2\alpha_{2,\,max})\right]^2} \tag{4.6}$$

For a given G the value of α_2 is selected randomly ($\alpha_{2,\,min} \leq \alpha_2 \leq \alpha_{2,\,max}$).

Table 4.2: Berea network statistics.

Item	Throats	Pores	Total
Number	26146	12349	38495
Porosity excl. clay (%)	4.562	13.746	18.309
Porosity incl. clay (%)	6.238	17.785	24.024
Average shape factor	0.035	0.033	0.034
Triangular cross-sections (%)	90.729	95.506	92.261
Square cross-sections (%)	7.542	4.324	6.510
Circular cross-sections (%)	1.729	0.170	1.229
ASCHA (deg.)(1)	15.235	13.744	14.751
AWCHA (deg.)(2)	48.828	49.215	48.954
Minimum radius (μm)	0.903	3.623	0.903
Maximum radius (μm)	56.850	73.539	73.539
Average radius (μm)	10.970	19.167	13.60
Connected to the inlet	254	0	254
Connected to the outlet	267	0	267
Isolated clusters	-	-	3
Isolated	3	6	9
Minimum coordination number	-	1	-
Maximum coordination number	-	19	-
Average coordination number	-	4.192	-
Clay volume (%)	1.676	4.039	5.715
K_{abs} (cal. box: 0.05-0.95) (mD)	-	-	3055
X dimension (mm)	-	-	3
Y dimension (mm)	-	-	3
Z dimension (mm)	-	-	3

1. Average Sharpest Corner Half Angle
2. Average Widest Corner Half Angle

Then Eq. (4.4) is used to find the corresponding value of α_1. And finally $\alpha_3 = \frac{\pi}{2} - \alpha_1 - \alpha_2$.

- ***Rectangular and Circular Elements***

The shape factor for rectangular cross-section elements with all corner half angles being equal to $\frac{\pi}{4}$ is $\frac{1}{16}$ while for circular cross-section elements $G = \frac{1}{4\pi}$.

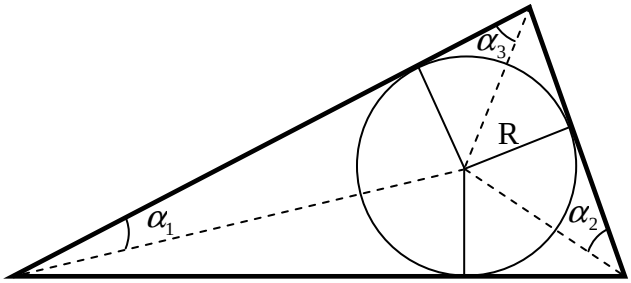

Figure 4.3: An element with irregular triangular cross-section.

4.3 Pressure Difference Across an Interface

To find the pressure difference across an interface, we use the Young-Laplace equation:

$$P_i - P_j = \sigma_{ij}(\frac{1}{r_1} + \frac{1}{r_2}) \qquad (ij = ow, gw, go) \tag{4.7}$$

where ow, gw, and go stand for oil/water, gas/water, and gas/oil respectively, r_1 and r_2 are the principal radii of curvature, and P_i and P_j are pressures of the phases on either sides of the interface.

There are two types of interface (see Fig.(4.5)), *(I)*: *Main Terminal Menisci (MTM)* [280], which is the invading meniscus at the pore/throat junction separating wetting and non-wetting fluids. The shape of such a meniscus is assumed to be spherical meaning that the two radii of curvature are the same ($r_1 = r_2 = r$). The pressure difference across an MTM is then given by (see Fig.(4.6)):

$$P_i - P_j = \frac{2\sigma_{ij}}{r} = \frac{2\sigma_{ij}\cos\theta}{R} \tag{4.8}$$

where R is the radius of the capillary pore. In the case of non-circular cross-section capillaries, R would be the inscribed radius. *(II)*: *Arc Menisci (AM)*, which is the interface at a corner of a non-circular element. It is assumed that the curvature of the interface is negligible in the plane perpendicular to that of the paper meaning that the principal radii of curvature would be $r_1 = r$ and $r_2 = \infty$ [245, 280]. The pressure difference across such an interface is given by:

$$P_i - P_j = \frac{\sigma_{ij}}{r} \tag{4.9}$$

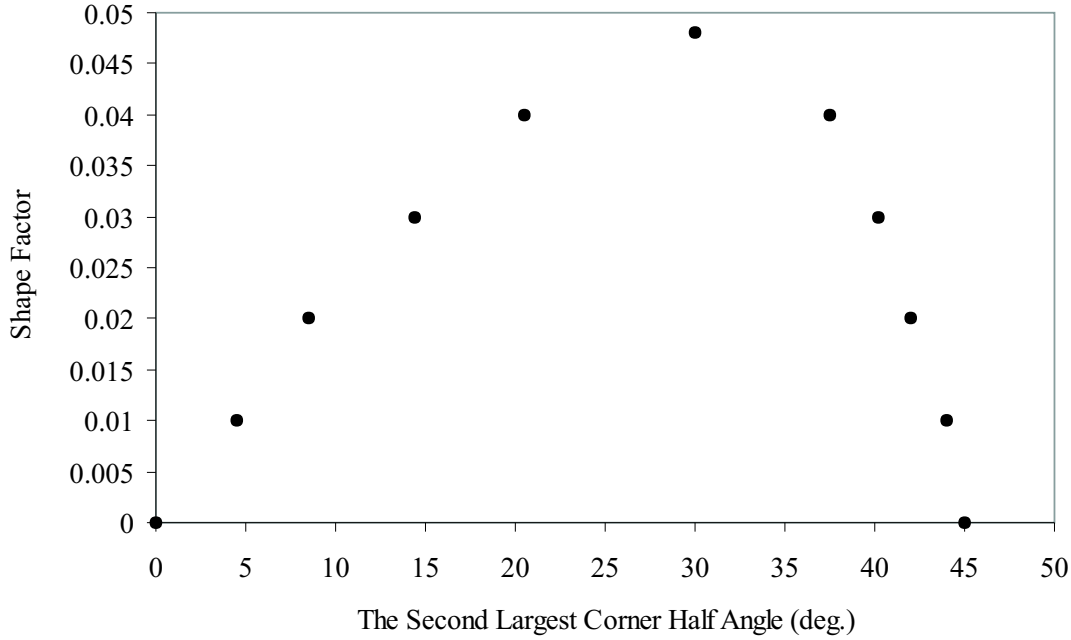

Figure 4.4: Distribution of shape factor vs. the second largest corner half angle in irregular triangles triangles.

4.4 Displacement Mechanisms

4.4.1 Drainage

Drainage in a capillary element is referred to an event where a *wetting* phase is displaced by a *non-wetting* phase with a *positive* capillary pressure. Drainage occurs by a *piston-like* mechanism (see Fig. (4.7)-(a)). Imagine a capillary element filled by a wetting phase with a non-wetting phase having access at one end of it where it forms an MTM. The capillary pressure, $P_{c,ij}$, is simply the pressure difference across the interface:

$$P_{c,ij} = P_i - P_j \qquad (ij = ow, gw, go) \tag{4.10}$$

An increase in $P_{c,ij}$ results in the MTM hinging at the entrance of the element which may remove a small amount of the wetting phase. If the increase in the capillary pressure continues, at some threshold capillary pressure the MTM enters the element with a fixed drainage curvature and receding contact angle [280]. While the MTM displaces the wetting phase from the centre of the element may allow – in

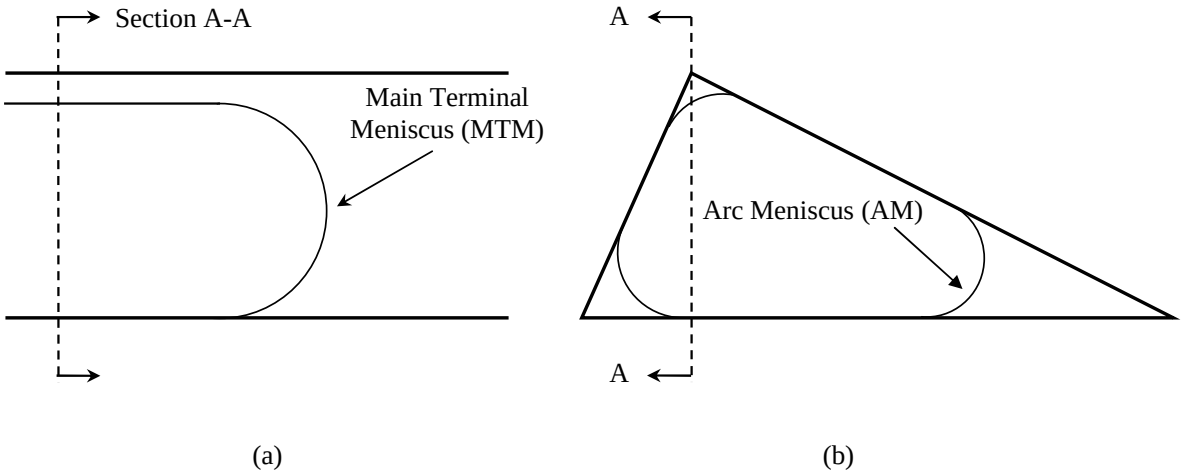

Figure 4.5: Different types of interface (a) Main Terminal Menisci (MTM), and (b) Arc Menisci(AM).

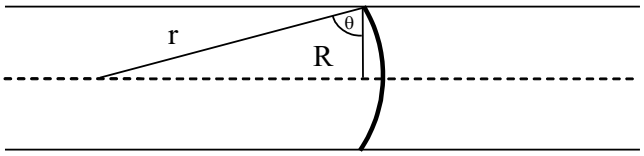

Figure 4.6: Spherical meniscus in a capillary.

non-circular elements and only if the receding contact angle is *less* than $(\frac{\pi}{2} - \alpha)$ – the residual of the displaced phase to remain at the corners creating *new* AM's. If the effects of gravity are *ignored* then the curvature of the AM's will be *exactly the same* as that of the invading MTM meaning that the volume of the wetting fluid that is left at the corners depends on the curvature of the invading MTM or, in other words, on the *threshold* capillary pressure of the displacement which in turn is a function of cross-sectional shape of the element [280]. The threshold capillary pressure is found using the theory that was originally suggested by Mayer and Stowe [282], developed by Princen [283–285] and applied independently by Lenormand *et al.* [57] (called MS-P theory).

The MS-P theory is based on equating the curvature of AM's left at the corners by the displacement to that of the invading MTM. The method has been applied by several authors to derive expressions to compute threshold capillary pressures of piston-like displacement in elements with circular and different angular cross-sections such as those by Legait [286] for capillary tubes with variable square cross-sections and different contact angles, by Mason & Morrow [280] for water-wet irregular tri-

angles which was later extend by Morrow [287] to include the effects of contact angle and contact angle hysteresis in equilateral triangles, and by Van Dijke & Sorbie [288] for three-phase threshold capillary pressures in elements with non-circular cross-section and different wettability. Here we present the generalization of the model by Ma *et al.* [289] to regular n-sided (polygon) elements and Øren *et al.* [77] and Patzek [127] to irregular triangles.

1. ***Cylindrical Elements***

   Conservation of energy for the displacement translates to equating the virtual work of the MTM movement to the change in the surface free energy (see Fig.(4.7)-(b)):

   $$P_c A_{eff} dx = \sigma_{1s} L_{1s} dx - \sigma_{2s} L_{2s} dx \tag{4.11}$$

   where A_{eff} is the cross-sectional area occupied by the non-wetting phase, L_{1s} and L_{2s} are the lengths of phase-1-solid and phase-2-solid interfaces in the cross-sectional plane. For cylindrical tubes, A_{eff} is equal to the cross-sectional area, and lengths L_{1s} and L_{2s} are the same and equal to the perimeter of the tube. If Young's equation is written as:

   $$\sigma_{1s} - \sigma_{2s} = \sigma_{12} \cos\theta \tag{4.12}$$

   then Eq. (4.11) can be reordered as:

   $$\frac{P_c}{\sigma_{12}} = \frac{L \cos\theta}{A} = \frac{P_{eff}}{A_{eff}} = \frac{2 \cos\theta}{R} \tag{4.13}$$

   where P_{eff} is the effective perimeter.

   $$P_{eff} = L \cos\theta \tag{4.14}$$

2. ***Regular n-Sided Elements***

   Similar to the cylindrical elements conservation of energy can be written for tubes with angular cross-sections. The only difference is that AM's may be left at the corners by the displacement (see Fig.(4.7)-(c)). Equating the displacement work to the surface free energy change gives:

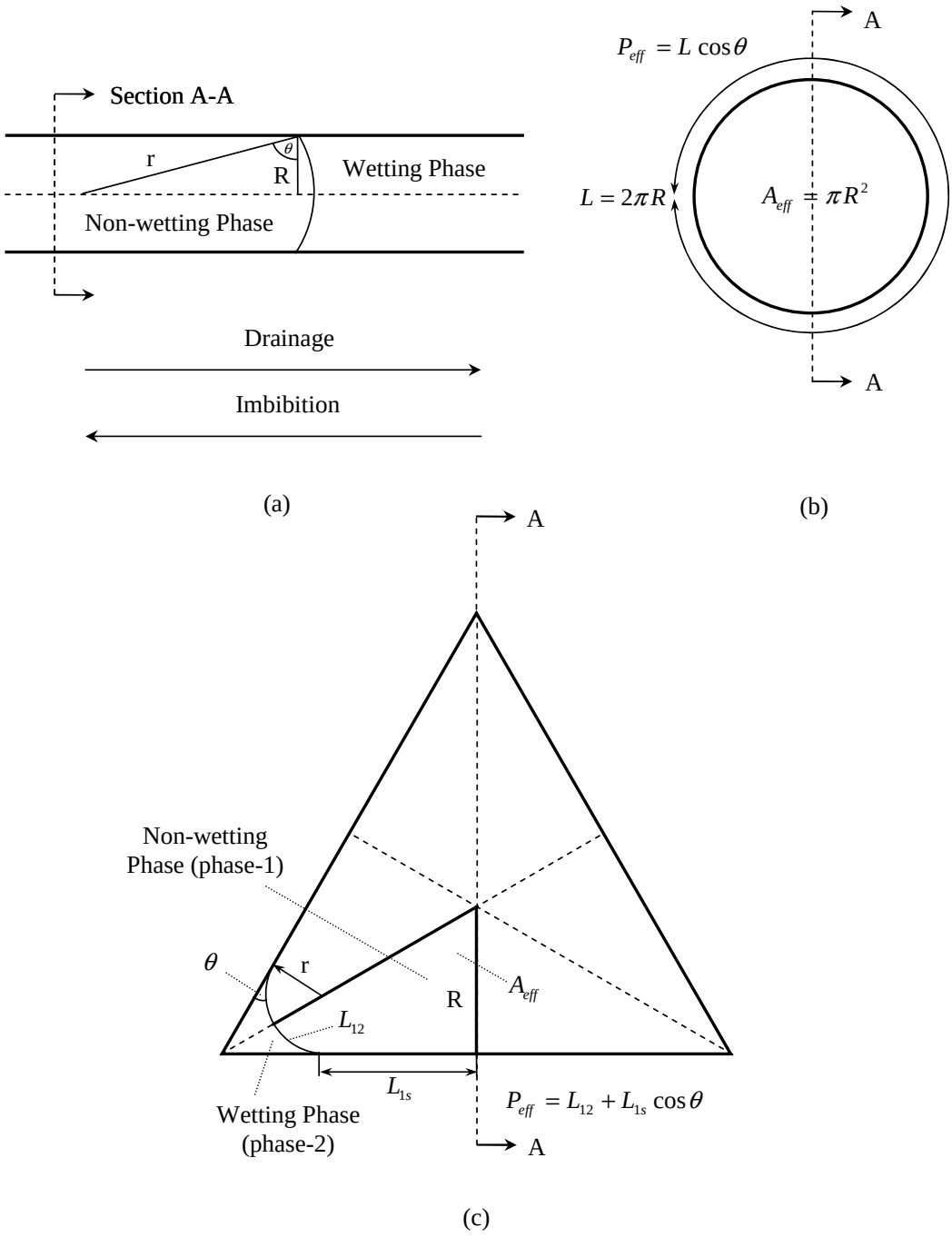

Figure 4.7: Effective perimeter and area for tubes with cylindrical and regular angular cross-section [289].

$$P_c A_{eff} dx = (L_{12}\sigma_{12} + L_{1s}\sigma_{1s} - L_{1s}\sigma_{2s})dx \tag{4.15}$$

where L_{12} is the length of the AM between wetting and non-wetting phases.

Using Young's equation (see Eq. (4.12)), Eq. (4.15) can be rewritten as follows:

$$\frac{P_c}{\sigma_{12}} = \frac{1}{r_d} = \frac{L_{12} + L_{1s}\cos\theta}{A_{eff}} = \frac{P_{eff}}{A_{eff}} \tag{4.16}$$

where

$$P_{eff} = L_{12} + L_{1s}\cos\theta \tag{4.17}$$

In a piston-like drainage, the general relationship between normalized curvature of the MTM, $C_{n,d}$, contact angle and corner half angle is given by:

$$\left[\frac{\cos^2\theta_1}{\tan\alpha} - \frac{\sin 2\theta_1}{2} - (\frac{\pi}{2} - \alpha - \theta_1)\right]\frac{1}{C_{n,d}^2} - \frac{\cos\theta_1}{\tan\alpha}\frac{2}{C_{n,d}} + \frac{1}{\tan\alpha} = 0 \tag{4.18}$$

where

$$C_{n,d} = \frac{R}{r_d} \tag{4.19}$$

The solution is:

$$C_{n,d} = \cos\theta_1 + \sqrt{\frac{\tan\alpha}{2}[\sin 2\theta_1 + \pi - 2\alpha - 2\theta_1))]} \qquad \theta_1 < \frac{\pi}{2} - \alpha \tag{4.20}$$

where θ_1 is given in Tables (4.3), (4.4), (4.5), and (4.6) for different conditions when Eq. (4.20) is used. The threshold capillary pressure is related to the normalized curvature by:

$$P_{c,d} = \frac{\sigma_{12}C_{n,d}}{R} \tag{4.21}$$

If the θ_1 is larger than $\frac{\pi}{2} - \alpha$ then the displacement won't leave any AM's at the corners and the normalized curvature of drainage is given by:

$$C_{n,d} = 2\cos\theta_1 \qquad \frac{\pi}{2} - \alpha < \theta_1 < \frac{\pi}{2} \tag{4.22}$$

3. ***Irregular Triangular Elements***

For an angular cross-section element, the conservation of energy equations are the same as those of the n-sided regular tubes, i.e. Eqs. (4.15), (4.16), and (4.17). For a piston-like drainage, the effective area is given by:

$$A_{eff} = A - r_d^2 \sum_{i=1}^{n} \left[\frac{\cos\theta_2 \cos(\theta_2 + \alpha_i)}{\sin\alpha_i} - (\frac{\pi}{2} - (\theta_2 + \alpha_i)) \right] = \frac{R^2}{4G} - r_d^2 S_1 \quad (4.23)$$

where n is the number of corners that do have an AM formed by the displacement and θ_2 is the angle that the AM's left at the corners by the displacement make with the wall towards the corner rather than the centre which is not necessarily the contact angle. Tables (4.3), (4.4), (4.5), and (4.6) give the θ_2 for different circumstances.

$$L_{1s} = \frac{R}{2G} - 2r_d \sum_{i=1}^{n} \frac{\cos(\theta_2 + \alpha_i)}{\sin\alpha_i} = \frac{R}{2G} - 2r_d S_2 \quad (4.24)$$

$$L_{12} = 2r_d \sum_{i=1}^{n} (\frac{\pi}{2} - \theta_2 - \alpha_i) = r_d S_3 \quad (4.25)$$

From Eqs. (4.16), (4.23), (4.24), and (4.25):

$$r_d = \frac{R\cos\theta_1 [-1 \pm \sqrt{1 + (4GD / \cos^2\theta_2)}]}{4GD} \quad (4.26)$$

where

$$D = S_1 - 2S_2\cos\theta_2 + S_3 \quad (4.27)$$

From two roots given by Eq. (4.26) the r_d which is smaller than R is the valid one. The threshold capillary pressure is:

$$P_c = \frac{\sigma}{r_d} = \frac{\sigma(1 + 2\sqrt{\pi G})\cos\theta_1}{R} F_d(\theta_2, G, E) \quad (4.28)$$

where

$$F_d(\theta_2, G, E) = \frac{1 + \sqrt{1 - (4GE / \cos^2\theta_2)}}{1 + 2\sqrt{\pi G}} \tag{4.29}$$

$$E = \sum_{i=1}^{3} \cos\theta_2 \frac{\cos(\theta_2 + \alpha_i)}{\sin\alpha_i} - [\frac{\pi}{2} - \theta_2 - \alpha_i] \tag{4.30}$$

The F_d depends on the corner half angles and is *not* universal for a given G. When AM's are present at all corners, E will be dependent on only θ_2 and F_d is universal for a given G and is given by:

$$E = -\pi + 3\theta_2 - 3\sin\theta_2\cos\theta_2 + \frac{\cos^2\theta_2}{4G} \tag{4.31}$$

One should note that $F_d(\theta_2 = 0, G, E) = 1$ regardless of number of present AM's at the corners.

4.4.2 Imbibition

An event in which a *non-wetting* phase is displaced by a *wetting* phase at a *positive* capillary pressure is called imbibition (see Fig. (4.7)-(a)) and may be carried out with advancing contact angle by three different types of displacement mechanism: (I) *piston-like*, (II) *snap-off*, and (III) *pore-body filling*.

(I) Piston-like Mechanism (Displacement by MTM)

An MTM might be present at one end of the element filled by the non-wetting phase which might be either an old one created by drainage or a new one formed by the wetting phase arriving at the entrance of the element by an invasion percolation process [94, 259]. If there is contact angle hysteresis then when the capillary pressure drops, the MTM hinges from the receding contact angle towards the advancing value while it stays pinned at its position. If the capillary pressure is lowered enough, the advancing contact angle is reached and it is only then that the MTM invades the element with the imbibition curvature that would be different from that of drainage. If there is no contact angle hysteresis, with a small reduction in the capillary pressure the MTM enters the tube with the same curvature at which drainage took place. While the capillary pressure is reduced, the AM's left at the corners – if there are any – adjust their contact angles to have curvatures the same as that of the invading MTM. This is while they stay pinned at their positions acquired at the end of the

Table 4.3: Threshold capillary pressures for piston-like and pore-body filling displacements with layers of the invading phase contributing to the displacement - oil to water, gas to water and gas to oil.

Item	Cross-section	Contact Angle Range	Equation(s)
1	Triangular	$\theta_{ij} < \frac{\pi}{2} - \alpha_1(1)$	(4.28)-(4.30)
2	Triangular	$\theta_{ij} < \theta_{extreme}(4)$ & $\theta_{ij} \geq \frac{\pi}{2} - \alpha_1$	(4.13)
3	Triangular	$\theta_{ij} \geq \theta_{extreme}$ & $\theta_{ij} \geq \frac{\pi}{2} - \alpha_1$	(4.34)-(4.41),(4.46),(4.64)-(4.66)
4	Square	$\theta_{ij} < \frac{\pi}{4}$	(4.20)-(4.21)
5	Square	$\theta_{ij} < \theta_{extreme}$ & $\theta_{ij} \geq \frac{\pi}{4}$	(4.13)
6	Square	$\theta_{ij} \geq \theta_{extreme}$ & $\theta_{ij} \geq \frac{\pi}{4}$	(4.34)-(4.41),(4.43),(4.64)-(4.66)
7	Circular	$0 \leq \theta_{ij} \leq \pi$	(4.13)

Item	$\theta_1(2)$	θ_2	θ	Comment
1	$\theta_{ij}(3)$	θ_{ij}	—	—
2	—	—	θ_{ij}	—
3	(5)	$\pi - \theta_{ij}$	θ_{ij}	Iterative
4	θ_{ij}	—	—	—
5	—	—	θ_{ij}	—
6	(5)	$\pi - \theta_{ij}$	θ_{ij}	Iterative
7	—	—	θ_{ij}	—

1. α_1 is the half angle of the sharpest corner.
2. θ_1 is the contact angle that interface moved with last time.
3. $\theta_{ij} = \theta^r_{ij}$, $ij = ow, go, gw$ - $\theta_{ow} = \theta^{PD}_{ow}$ and $\theta_{gw} = \theta^{PD}_{gw}$ for displacement of water by gas and oil during primary drainage respectively.
4. $\theta_{extreme} = \pi - \theta_3$, where θ_3 is calculated using Eqs. (4.47) and (4.44) for elements with triangular and square cross-sections respectively.
5. It can be either $\pi - \theta_1$ or θ_1 based on the type of the AM that θ_1 belongs to. It is the angle that the AM makes with the surface towards the apex of the corner.

drainage. The angles may be called *hinging*. The MTM meets the AM's with zero contact angle and the maximum contact angle it reaches before the invasion is the advancing value. An AM can move only when the hinging contact angle is as large as the advancing contact angle.

The threshold capillary pressure under which the piston-like imbibition may take place can be found again using the MS-P theory but the difference with the case where the theory was applied to find threshold capillary pressure of the drainage is

Table 4.4: Threshold capillary pressures for piston-like and pore-body filling displacements with layers of the invading phase contributing to the displacement - water to oil, water to gas, and oil to gas.

Item	Cross-section	Contact Angle Range	Equation(s)
1	Triangular	$\theta_{ij} > \frac{\pi}{2} + \alpha_1(1)$	(4.28)-(4.30)
2	Triangular	$\theta_{ij} \geq \theta_{extreme}(4)$ & $\theta_{ij} \leq \frac{\pi}{2} + \alpha_1$	(4.13)
3	Triangular	$\theta_{ij} < \theta_{extreme}$ & $\theta_{ij} \leq \frac{\pi}{2} + \alpha_1$	(4.34)-(4.41),(4.46),(4.64)-(4.66)
4	Square	$\theta_{ij} > \frac{3\pi}{4}$	(4.45)
5	Square	$\theta_{ij} \geq \theta_{extreme}$ & $\theta_{ij} \leq \frac{3\pi}{4}$	(4.13)
6	Square	$\theta_{ij} < \theta_{extreme}$	(4.34)-(4.41),(4.43),(4.64)-(4.66)
7	Circular	$0 \leq \theta_{ij} \leq \pi$	(4.13)

Item	θ_1(2)	θ_2	θ	Comment
1	θ_{ij}(3)	$\pi - \theta_{ij}$	—	—
2	—	—	θ_{ij}	—
3	(5)	θ_{ij}	θ_{ij}	Iterative
4	—	θ_{ij}	—	—
5	—	—	θ_{ij}	—
6	(5)	θ_{ij}	θ_{ij}	Iterative
7	—	—	θ_{ij}	—

1. α_1 is the half angle of the sharpest corner.
2. θ_1 is the contact angle that interface moved with last time.
3. $\theta_{ij} = \theta_{ij}^a$, $ij = ow, go, gw$.
4. $\theta_{extreme} = \theta_3$, where θ_3 is calculated using Eqs. (4.47) and (4.44) for elements with triangular and square cross-sections respectively.
5. It can be either $\pi - \theta_1$ or θ_1 based on the type of the AM that θ_1 belongs to. It is the angle that the AM makes with the surface towards the apex of the corner.

that the three-phase contact line is fixed in the imbibition and the hinging contact angle is changing while in the drainage the three-phase contact line was moving and the receding contact angle was fixed.

1. ***Cylindrical Elements***

   The threshold capillary pressure is found using Eq. (4.13) with the advancing contact angle.

2. ***Regular n-Sided Elements***

Table 4.5: Threshold capillary pressures for piston-like and pore-body filling displacements with *no* layers of the invading phase contributing to the displacement - oil to water, gas to water and gas to oil.

Cross-section	Contact Angle Range	Equation(s)	θ_1	θ_2	θ	Comment
Triangular	$\theta_{ij} < \frac{\pi}{2} - \alpha_1$	(4.28)-(4.30)	θ_{ij}	θ_{ij}	—	—
Triangular	$\theta_{ij} \geq \frac{\pi}{2} - \alpha_1$	(4.13)	—	—	θ_{ij}	—
Square	$\theta_{ij} < \frac{\pi}{4}$	(4.20)-(4.21)	θ_{ij}	—	—	—
Square	$\theta_{ij} \geq \frac{\pi}{4}$	(4.13)	—	—	θ_{ij}	—

Table 4.6: Threshold capillary pressures for piston-like and pore-body filling displacements with *no* layers of the invading phase contributing to the displacement - water to oil, water to gas, and oil to gas.

Cross-section	Contact Angle Range	Equation(s)	θ_1	θ_2	θ	Comment
Triangular	$\theta_{ij} > \frac{\pi}{2} + \alpha_1$	(4.28)-(4.30)	θ_{ij}	$\pi - \theta_{ij}$	—	—
Triangular	$\theta_{ij} \leq \frac{\pi}{2} + \alpha_1$	(4.13)	—	—	θ_{ij}	—
Square	$\theta_{ij} > \frac{3\pi}{4}$	(4.45)	—	θ_{ij}	—	—
Square	$\theta_{ij} \leq \frac{3\pi}{4}$	(4.13)	—	—	θ_{ij}	—

Eq. (4.16) with r_d replaced by the imbibition radius r_m gives the radius corresponding to the threshold capillary pressure of imbibition. The effective area and perimeter are given by:

$$A_{eff} = \frac{1}{2}\frac{R^2}{\tan\alpha} - \frac{1}{2}r_m b \sin(\alpha+\beta) + \frac{r_m^2\beta}{2} \tag{4.32}$$

$$P_{eff} = \left[\frac{R}{\tan\alpha} - b\right]\cos\theta_2 + r_m\beta \tag{4.33}$$

where θ_2 is the contact angle of the displacement. The meniscus-apex distance b, see Fig. (4.8), can be calculated by (see Appendix (A)):

$$b = r_{extreme}\frac{\cos(\alpha+\theta_1)}{\sin\alpha} \tag{4.34}$$

if the AM has not moved yet. The θ_1 is the contact angle that the interface moved with previous time. The $r_{extreme}$ is:

$$r_{extreme} = \frac{\sigma}{P_{c,extreme}} \tag{4.35}$$

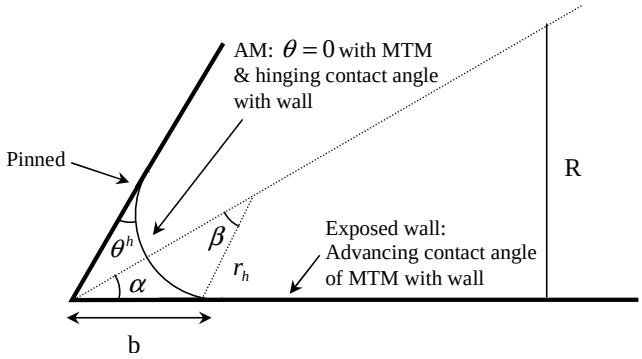

Figure 4.8: Imbibition by invasion of an MTM - conditions of the AM's at the corners [289].

where $P_{c,\,extreme}$ belongs to the last move of the interface.

If the AM has moved:

$$b = r_m \frac{\cos(\theta_2 + \alpha)}{\sin \alpha} \tag{4.36}$$

The angle β, see Fig. (4.8), is given by:

$$\beta = \sin^{-1}\left[\frac{b \sin \alpha}{r_m}\right] \tag{4.37}$$

if the AM has not moved yet. If the AM has moved:

$$\beta = \frac{\pi}{2} - \theta_2 - \alpha \tag{4.38}$$

The hinging contact angle is:

$$\theta^h = \cos^{-1}\left[\frac{r_{extreme}}{r_m}\cos(\theta_1 + \alpha_i)\right] - \alpha_i \tag{4.39}$$

if the AM has not moved yet. If the AM has moved:

$$\theta^h = \theta_2 \tag{4.40}$$

In contrast to the drainage case, there is not an analytical solution to find r_m. The r_m is found by an iterative procedure which solves Eq. (4.16) (with r_d replaced by the imbibition radius r_m) together with Eqs. (4.34)-(4.40)

simultaneously, and then the threshold capillary pressure of imbibition will be:

$$P_c = \frac{\sigma}{r_m} \tag{4.41}$$

For advancing contact angles less than $\frac{\pi}{2}$, the capillary pressure is always positive but it may also be positive for angles much larger $\frac{\pi}{2}$ depending on the effective perimeter, P_{eff}. The maximum advancing contact angle, θ_3, at which imbibition (defined as $P_c > 0$) may take place is when $P_{eff} = 0$. This happens when the AM's are flat and have a hinging contact angle of $\frac{\pi}{2} - \alpha$. It is given by:

$$\theta_3 = \cos^{-1}\left[\frac{-\cos(\alpha + \theta_1)\sin\alpha}{C_{n,r}\cos\alpha - \cos(\alpha + \theta_1)}\right] \tag{4.42}$$

where the $C_{n,r}$ is the curvature at which the saturation of the wetting phase started to increase and $C_{n,r} \geq C_{n,d}$.

For elements with square cross section, the r_m and θ_3 may be written as follows:

$$r_m = \frac{A_{eff}}{P_{eff}} = \frac{R^2 - r_m b\cos\theta^h + r_m^2(\frac{\pi}{2} - \theta^h - \alpha)}{2r_m\beta + 2[R-b]\cos\theta_2} \tag{4.43}$$

$$\theta_3 = \cos^{-1}\left[\frac{-r_{extreme}\beta}{R-b}\right] \tag{4.44}$$

If the advancing contact angle is larger than θ_3 then the capillary pressure is negative and the displacement is defined as *drainage*. For the threshold capillary pressures: *(I)* if $\theta_2 < \frac{\pi}{2} + \alpha$ then Eq. (4.13) is used with θ replaced by the advancing contact angle *(II)* but if $\theta_2 > \frac{\pi}{2} + \alpha$ then it is given by:

$$P_c = \frac{\sigma}{R}\left[\cos\theta_2 - \sqrt{\frac{tan\alpha}{2}(-\sin 2\theta_2 + 2\theta_2 - 2\alpha - \pi)}\right] \tag{4.45}$$

3. ***Irregular Triangular Elements***

The procedure is similar to that of the n-sided elements described above with expressions for r_m and θ_3 replaced by the following:

$$r_m = \frac{\frac{R^2}{4G} - r_m\sum_{i=1}^{n} b_i\cos\theta_i^h + r_m^2\sum_{i=1}^{n}(\frac{\pi}{2} - \theta_i^h - \alpha_i) - A}{2r_m\sum_{i=1}^{n}\beta_i + [\frac{R}{2G} - 2\sum_{i=1}^{3} b_i]\cos\theta_2} \tag{4.46}$$

where n is the number of contributing corners and A is the summation of corner areas (only those corners that do not have a contributing AM).

$$\theta_3 = \cos^{-1}[\frac{-2r_{extreme}\sum_{i=1}^{n}\beta_i}{\frac{R}{2G} - 2\sum_{i=1}^{3} b_i}] \tag{4.47}$$

or

$$\theta_3 = \cos^{-1}\left[\frac{-4G\sum_{i=1}^{3}\cos(\theta_1+\beta_i)}{(RP_{c,extreme}/\sigma) - \cos\theta_1 + 12G\sin\theta_1}\right] \tag{4.48}$$

For drainage: *(I)* if $\theta_2 < \frac{\pi}{2} + \alpha$ then the threshold capillary pressure is given by Eq. (4.13) with θ being the advancing contact angle *(II)* but if $\theta_2 > \frac{\pi}{2} + \alpha$ then Eqs. (4.28)-(4.30) are used.

(II) Snap-off Mechanism (Displacement by AM's)

Snap-off corresponds to an imbibition event where the non-wetting phase in the centre of a pore or throat is displaced by the AM's of the wetting phase residing in the corners or layers. This occurs only if there is no MTM present at the entrance of the element. The AM's will be present at the corners only if the contact angle by which the element is drained be less than $\frac{\pi}{2} - \alpha$ otherwise imbibition is possible only by invasion of an MTM.

If there is no contact angle hysteresis, when the pertinent capillary pressure is reduced, the AM's grow and move smoothly towards the centre of the element and meet to refill the element with the wetting phase.

But if there is contact angle hysteresis, when the relevant capillary pressure decreases, the invading phase starts swelling and consequently contributing AM's - starting from the sharpest corner - may hinge and eventually move - when the hinging contact angle reaches the advancing value - towards the centre to meet the other moving or pinned AM's. When AM's meet, the centre of the element is filled spontaneously by the wetting phase. Depending on the magnitude of the advancing contact angle, snap-off can be *spontaneous* or *forced*. When it occurs at a positive threshold capillary pressure ($\theta^a \leq \frac{\pi}{2} - \alpha_1$), it is an imbibition event, while it is forced (drainage) when the threshold capillary pressure is negative ($\theta^a > \frac{\pi}{2} - \alpha_1$). Snap-off is not favoured over a piston-like or pore-body filling event when there is a neighbouring element with the invading phase in the centre that is able to carry out the displacement. The threshold capillary pressures of snap-off events in angular

elements with different cross-sectional shape are given next.

1. ***Regular n-Sided Elements***

   For spontaneous snap-off the AM's meet each other when they reach halfway along the sides of the element. By equating the half length of one side of the element to the meniscus-apex distance of the moving AM's, the threshold capillary pressure is found:

$$P_c = \frac{\sigma}{R}\left[\cot\alpha\cos\theta_2 - \sin\theta_2\right] \qquad \theta_2 \leq \frac{\pi}{2} - \alpha \tag{4.49}$$

   But when the snap-off is forced, the threshold capillary pressure is a function of the curvature of the AM when it starts to move. This is because when the AM starts to move it can be unstable and may fill the element by the wetting phase immediately. The threshold capillary pressures are:

$$P_c = \frac{\sigma}{r_{extreme}}\frac{\cos(\theta_2+\alpha)}{\cos(\theta_1+\alpha)} \qquad \theta_2 \leq \pi - \alpha \tag{4.50}$$

$$P_c = \frac{\sigma}{r_{extreme}}\frac{-1}{\cos(\theta_1+\alpha)} \qquad \theta_2 \geq \pi - \alpha \tag{4.51}$$

2. ***Irregular Triangular Elements***

   If the snap-off is spontaneous then depending on how large is the advancing contact angle and whether AM's are present at all corners, different scenarios, on which moving AM meets which moving or pinned AM, are imaginable. These scenarios have different threshold capillary pressures. The event with the highest capillary pressure is most favourable. They are as follows:

$$P_c = \frac{\sigma}{R}\left[\cos\theta_2 - \frac{2\sin\theta_2}{\cot\alpha_1 + \cot\alpha_2}\right] \tag{4.52}$$

   if the moving AM's at corners 1 and 2 meet. If the moving AM at the corner 1 meets pinned AM at the corner 2:

$$P_c = \frac{\sigma(\cot\alpha_1\cos\theta_2 - \sin\theta_2)}{R(\cot\alpha_1 + \cot\alpha_2) - b_2} \tag{4.53}$$

$$P_c = \frac{\sigma}{R}\left[\cos\theta_2 - \frac{2\sin\theta_2}{\cot\alpha_1 + \cot\alpha_3}\right] \tag{4.54}$$

if the moving AM's at corners 1 and 3 meet. If the moving AM at the corner 1 meets pinned AM at the corner 3:

$$P_c = \frac{\sigma(\cot\alpha_1 \cos\theta_2 - \sin\theta_2)}{R(\cot\alpha_1 + \cot\alpha_3) - b_3} \tag{4.55}$$

$$P_c = \frac{\sigma}{R}\left[\cos\theta_2 - \frac{2\sin\theta_2}{\cot\alpha_2 + \cot\alpha_3}\right] \tag{4.56}$$

if the moving AM's at corners 2 and 3 meet. If the moving AM at the corner 2 meets pinned AM at the corner 3:

$$P_c = \frac{\sigma(\cot\alpha_2 \cos\theta_2 - \sin\theta_2)}{R(\cot\alpha_2 + \cot\alpha_3) - b_3} \tag{4.57}$$

If only one corner has a contributing AM, we *assume* that the element is filled when the AM moves and meets a *noncontributing* AM at one of the other corners.

$$P_c = \frac{\sigma(\cot\alpha_1 \cos\theta_2 - \sin\theta_2)}{R(\cot\alpha_1 + \cot\alpha_3)} \tag{4.58}$$

$$P_c = \frac{\sigma(\cot\alpha_1 \cos\theta_2 - \sin\theta_2)}{R(\cot\alpha_1 + \cot\alpha_2)} \tag{4.59}$$

if only corner 1 has a contributing AM and it meets a noncontributing AM at corners 3 or 2 respectively.

$$P_c = \frac{\sigma(\cot\alpha_2 \cos\theta_2 - \sin\theta_2)}{R(\cot\alpha_2 + \cot\alpha_3)} \tag{4.60}$$

$$P_c = \frac{\sigma(\cot\alpha_2 \cos\theta_2 - \sin\theta_2)}{R(\cot\alpha_2 + \cot\alpha_1)} \tag{4.61}$$

if only corner 2 has a contributing AM and it meets a noncontributing AM at corners 3 or 1 respectively.

$$P_c = \frac{\sigma(\cot\alpha_3 \cos\theta_2 - \sin\theta_2)}{R(\cot\alpha_2 + \cot\alpha_3)} \tag{4.62}$$

$$P_c = \frac{\sigma(\cot\alpha_3 \cos\theta_2 - \sin\theta_2)}{R(\cot\alpha_1 + \cot\alpha_3)} \tag{4.63}$$

if only corner 3 has a contributing AM and it meets a noncontributing AM at corners 2 or 1 respectively.

If the contact angle is the same at all corners then Eqs. (4.58) and (4.59) give the highest capillary pressure when only corner 1 has a contributing AM.

When the snap-off is forced, as soon as the hinging contact angle of the AM at the sharpest corner becomes as large as the advancing value, it starts moving towards the centre of the element while the other AM's are pinned. This means that the absolute value of the curvature decreases. The AM is not stable and spontaneously fills the element. The threshold capillary pressure for this case are given by Eqs. (4.50) and (4.51) where α is corner half angle of the sharpest corner if AM's are present at more than one corner.

The equations to compute the threshold capillary pressures for snap-off in two- and three-phase systems with different wettability conditions are tabulated in Tables (4.7), and (4.8).

Table 4.7: Threshold capillary pressures for snap-off displacements - oil to water, gas to water and gas to oil.

Cross-section	Contact Angle Range	Equation(s)	θ_1(1)	θ_2	Comment
Triangular	$\theta_{ij} \geq \frac{\pi}{2} + \alpha_1$	(4.52)-(4.63)	—	$\pi - \theta_{ij}$	Min $P_{c,ij}$
Triangular	$\theta_{ij} \geq \alpha_1$ & $\theta_{ij} \leq \frac{\pi}{2} + \alpha_1$	(4.50)	(2)	$\pi - \theta_{ij}$	—
Triangular	$\theta_{ij} < \alpha_1$	(4.51)	(2)	$\pi - \theta_{ij}$	—
Square	$\theta_{ij} > \frac{3\pi}{4}$	(4.49)	—	$\pi - \theta_{ij}$	—
Square	$\theta_{ij} \geq \frac{\pi}{4}$ & $\theta_{ij} \leq \frac{3\pi}{4}$	(4.50)	(2)	$\pi - \theta_{ij}$	—
Square	$\theta_{ij} < \frac{\pi}{4}$	(4.51)	(2)	$\pi - \theta_{ij}$	—

1. θ_1 is the contact angle that interface moved with last time.
2. It can be either $\pi - \theta_1$ or θ_1 based on the type of the AM that θ_1 belongs to. It is the angle that the AM makes with the surface towards the apex of the corner.

(III) Pore-body Filling Mechanism

This refers to the displacement of one phase in the centre of a pore by movement from the centre of adjoining throats(s). For drainage - the displacement of a wetting phase by non-wetting phase - the threshold capillary pressure is given by similar

Table 4.8: Threshold capillary pressures for snap-off displacements - water to oil, water to gas, and oil to gas.

Cross-section	Contact Angle Range	Equation(s)	θ_1(1)	θ_2	Comment
Triangular	$\theta_{ij} \leq \frac{\pi}{2} - \alpha_1$	(4.52)-(4.63)	—	θ_{ij}	Max $P_{c,ij}$
Triangular	$\theta_{ij} \leq \pi - \alpha_1$ & $\theta_{ij} > \frac{\pi}{2} - \alpha_1$	(4.50)	(2)	θ_{ij}	—
Triangular	$\theta_{ij} > \pi - \alpha_1$	(4.51)	(2)	θ_{ij}	—
Square	$\theta_{ij} \leq \frac{\pi}{4}$	(4.49)	—	θ_{ij}	—
Square	$\theta_{ij} > \frac{\pi}{4}$ & $\theta_{ij} \leq \frac{3\pi}{4}$	(4.50)	(2)	θ_{ij}	—
Square	$\theta_{ij} > \frac{3\pi}{4}$	(4.51)	(2)	θ_{ij}	—

1. θ_1 is the contact angle that interface moved with last time.
2. It can be either $\pi - \theta_1$ or θ_1 based on the type of the AM that θ_1 belongs to. It is the angle that the AM makes with the surface towards the apex of the corner.

expressions for piston-like advance. For imbibition - the displacement of a non-wetting phase by a wetting phase - the displacement is controlled by the largest radius of curvature. The threshold capillary pressure depends on inscribed radius of the pore-body and the number of neighbouring throats that either do *not* hold the invading phase in the centre or can not *contribute* to the displacement as they might be trapped. For a pore with coordination number m - number of throats connected to each pore - $m-1$ pore-body filling events are possible, called I_n, where n is the number of neighbouring throats that are not involved in the displacement $1 \leq n \leq m-1$ (see Fig. (4.9))[57, 58]. For instance, imagine an oil filled water-wet circular cross-section pore with 8 throats connected to it. If two of the throats contain oil in the centre, two gas, one trapped water, and only three continuous water, then for the water invasion of the pore: $n = 2 + 2 + 1 = 5$. One should note that when $n = 1$, the displacement is a piston-like event with the corresponding threshold capillary pressures (see sections (4.4.1) and (4.4.2)) [57, 58, 77]. Blunt [290] and Øren *et al.* [77] have proposed different empirical models to compute threshold capillary pressure of the pore-body filling as follows:

$$P_c = \frac{2\sigma\cos\theta}{R_p} - \sigma\sum_{i=1}^{n} e_i x_i \tag{4.64}$$

$$P_c = \frac{2\sigma\cos\theta}{R_p + \sum_{i=1}^{n} e_i R_{t,i} x_i} \tag{4.65}$$

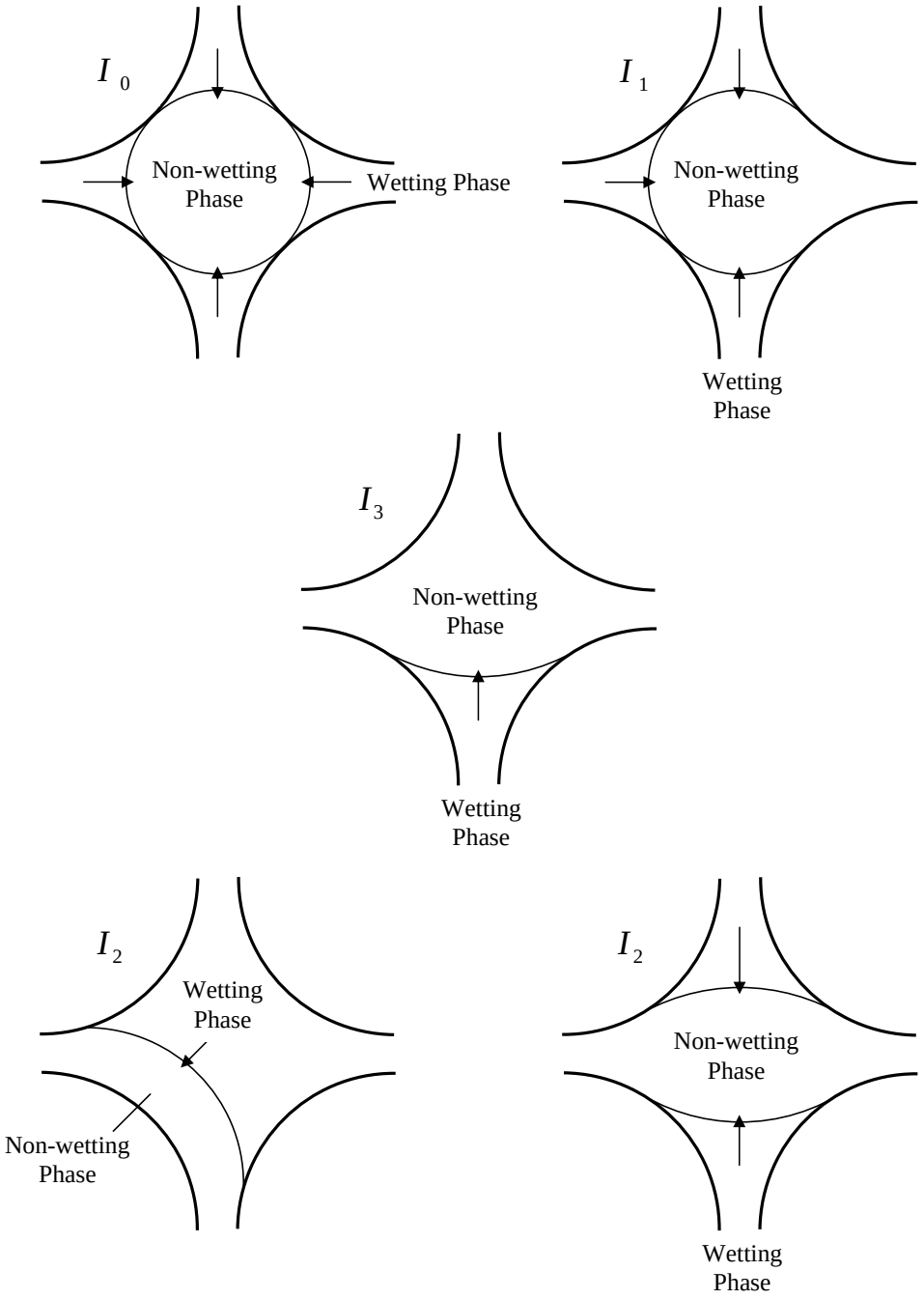

Figure 4.9: Diffrent pore-body filling events for imbibition in a pore with coordination number 4. For I_n, n means number of neighbouring throats that either do *not* hold the invading phase in the centre or can not *contribute* to the displacement as they might be trapped.

$$P_c = \frac{\sigma(1 + 2\sqrt{\pi G})\cos\theta}{R_p + \sum_{i=1}^{n} e_i R_{t,i} x_i} \tag{4.66}$$

where n indicates the order of the filling and is the number of throats that do not take part in the invasion of the bore body, $R_{t,i}$ are the inscribed radii of the such throats, x_i are random numbers, R_p is the inscribed radius of the pore, and e_i are predefined arbitrary parameters. Eqs. (4.64)- (4.66) show that pore-body filing is favoured when n is small. In this work, we use Eq. (4.64) with $e_1 = 0$ and $e_2 - e_n = 0.03\ \mu m^{-1}$ [135, 290].

The equations to compute threshold capillary pressures for piston-like and pore-body filling displacements in two- and three-phase systems with different wettability conditions are listed in Tables (4.3), (4.4), (4.5), and (4.6).

4.5 Layer Collapse and Formation

Piston-like and snap-off displacements – if the pertinent contact angles, capillary pressures, and corner half angles permit – allow the displaced phase to remain as layer(s) sandwiched between fluids in the corner(s) and centre of the element. The formation of layers in an element is also possible by displacement from fluids residing in the *layers* or *centre* of the neighbouring elements. The layers may spontaneously collapse by an increase in pressure of the fluids on either side of the layer. When a layer collapse event takes place, one of the two AM's bounding the layer will hinge and/or move towards the other one. However, there are cases where both AM's contribute into the layer collapse event, e.g. oil layer collapse event by water at a corner in a strongly oil-wet element (see chapter (5) for example configurations).

Based on whether the fluids residing on two sides of the layer are the same, layers may be categorized into two main groups; *(I): Identical* fluids, *(II): Different* fluids. The displacement history to form such layers in systems with different wettability and spreading coefficient will be discussed later. Here, the stability of the layers, i.e. the threshold capillary pressure for layer collapse and formation events, in each category is discussed [264, 265]:

4.5.1 Identical Fluids on Two Sides of a Layer

Fig. (4.10) illustrates this case. Since fluids residing on both sides of the layer are identical, when the capillary pressure of the fluid pair changes both bounding AM's contribute to the stability of the layer. The layer stays stable until two AM's touch each other at point C when the layer collapses immediately and the corner is filled completely by phase-2. This is the concept that is used to find the threshold

capillary pressure of collapse (or formation) of such a layer and is given by (see Appendix (A) for derivation):

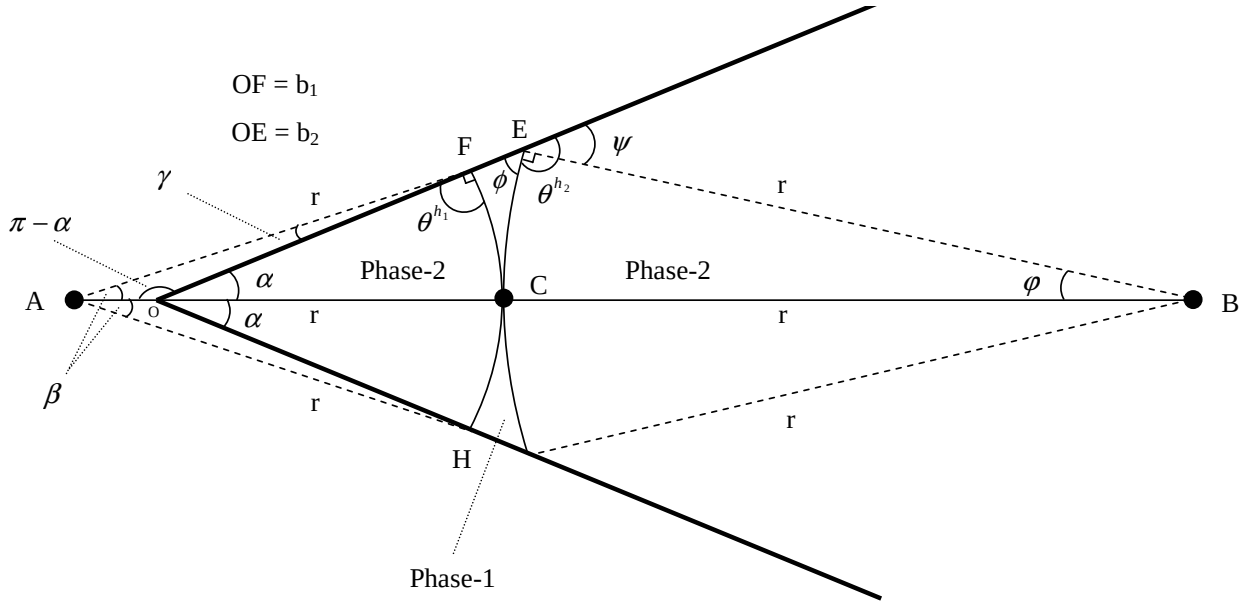

Figure 4.10: A layer sandwiched between identical fluids residing in the corner and centre.

$$P_c = \frac{\sigma(3\sin^2\alpha + 4\sin\alpha\cos\theta^{h_2} + \cos^2\theta^{h_2})}{b_1[\cos\alpha\sin\alpha(2\sin\alpha + \cos\theta^{h_2}) + \sin^2\alpha\sqrt{4\cos^2\alpha - 3 - cos^2\theta^{h_2} - 4\sin\alpha\cos\theta^{h_2}}]} \tag{4.67}$$

where

$$b_1 = r\frac{\cos(\alpha + \theta^{h_1})}{\sin\alpha} \tag{4.68}$$

4.5.2 Different Fluids on Two Sides of a Layer

Since the layer is surrounded by two different fluids, a change in the pressure of either fluids can result in layer collapse. In other words, the AM's bounding the layer act independently. Depending on the magnitude of the angle that each AM makes with the wall, two main groups of collapse scenario are imaginable:

1. $\theta_1 \leq \theta_2$

   Fig.(4.11) illustrates the case. The stability of the layer depends on the ratio of the curvature of the two AM's bounding the layer:

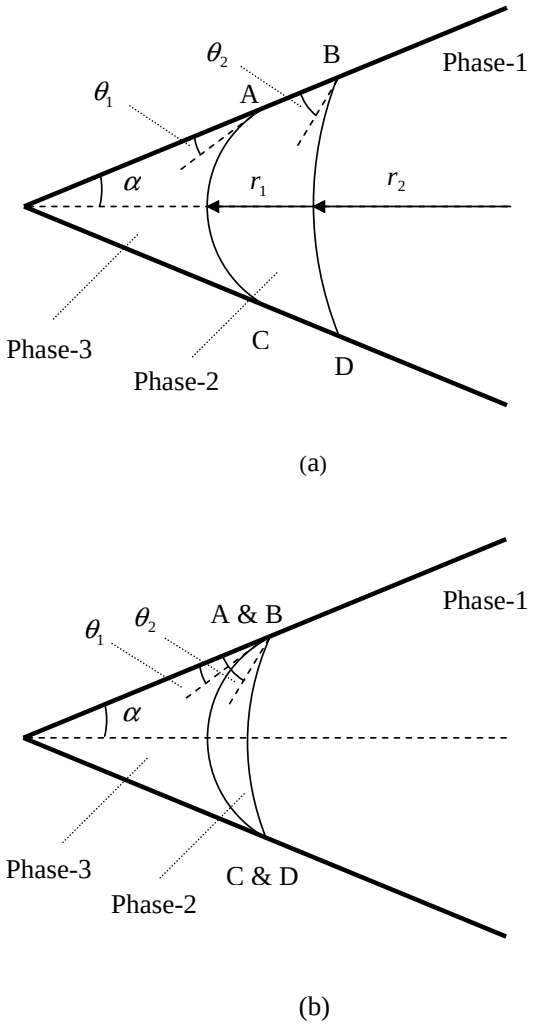

Figure 4.11: A layer sandwiched between different fluids residing in the corner and centre ($\theta_I^h < \theta_{II}^h$)(a) the layer before collapse (b) position of the AM's at the collapse moment.

$$\frac{r_1}{r_2} = \frac{\sigma_1 P_{c2}}{\sigma_2 P_{c1}} \tag{4.69}$$

where σ_1 and σ_2 are the interfacial tensions of the bounding interfaces of the layer and $P_{c,1}$ and $P_{c,2}$ are pertinent capillary pressures. The layer is stable until three-phase contact points meet each other (see Fig.(4.11)-(b)). This means that the layer collapses when the meniscus-apex distance, b, for two AM's become equal. Using Eq. (4.34) for meniscus-apex distance of each AM gives:

$$r_1 \frac{\cos(\theta_1 + \alpha)}{\sin \alpha} = r_2 \frac{\cos(\theta_2 + \alpha)}{\sin \alpha} \tag{4.70}$$

$$R_c = \frac{r_1}{r_2} = \frac{\cos(\theta_2 + \alpha)}{\cos(\theta_1 + \alpha)} \tag{4.71}$$

Then the two threshold capillary pressures of the layer collapse corresponding to the invasions by two surrounding fluids can be found by:

$$P_c = \frac{\sigma_1 P_{c2}}{\sigma_2 R_c} \tag{4.72}$$

$$P_c = \frac{\sigma_2 P_{c1} R_c}{\sigma_1} \tag{4.73}$$

2. $\theta_1 > \theta_2$

   Fig.(4.12) illustrates the case. The layer is stable until two AM's meet at their centres. The ratio of curvature of two AM's at the collapsing point is found by equating the centre-apex distance of one of the AM's to that of the other one (see Appendix (A) for derivation of centre-apex distance for an AM):

$$-r_1 \left[1 - \frac{\cos \theta_1}{\sin \alpha}\right] = -r_2 \left[1 - \frac{\cos \theta_2}{\sin \alpha}\right] \tag{4.74}$$

   Reordering Eq. (4.74) gives:

$$R_c = \frac{r_1}{r_2} = \frac{(\sin \alpha - \cos \theta_2)}{(\sin \alpha - \cos \theta_1)} \tag{4.75}$$

   The two threshold capillary pressures are then found from Eqs. (4.72) and (4.73).

One should not that if the curvature of any of the AM's is negative (see Fig. (4.13)-(a)), the threshold capillary pressures are found using the same procedure as above.

As we will show the relevant fluid configurations later, it is also possible to have a second layer sandwiched between the fluids residing in the centre of the element and the first layer (see Fig. (4.13)-(b)). The stability analysis for the second layer is also the same as that of the first layer.

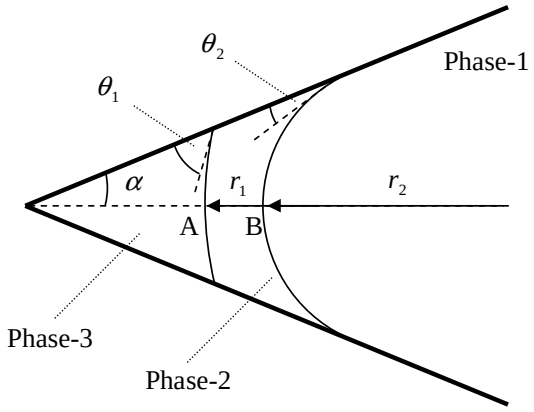

(a)

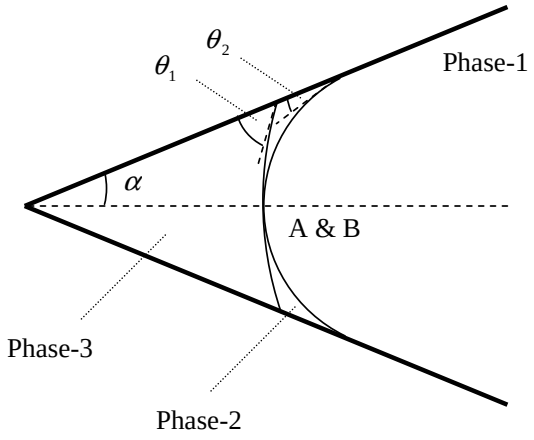

(b)

Figure 4.12: A layer sandwiched between different fluids residing in the corner and centre ($\theta_1 > \theta_2$) (a) the layer before collapse (b) position of the AM's at the moment of collapse.

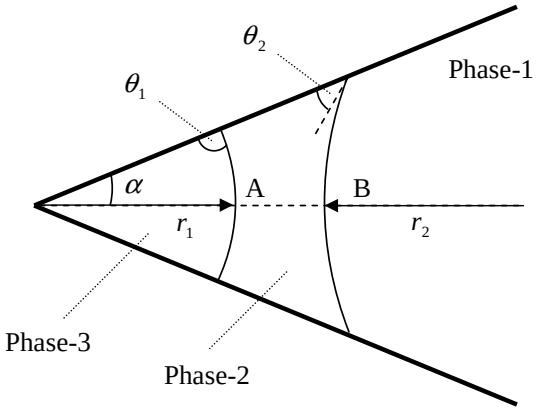

(a)

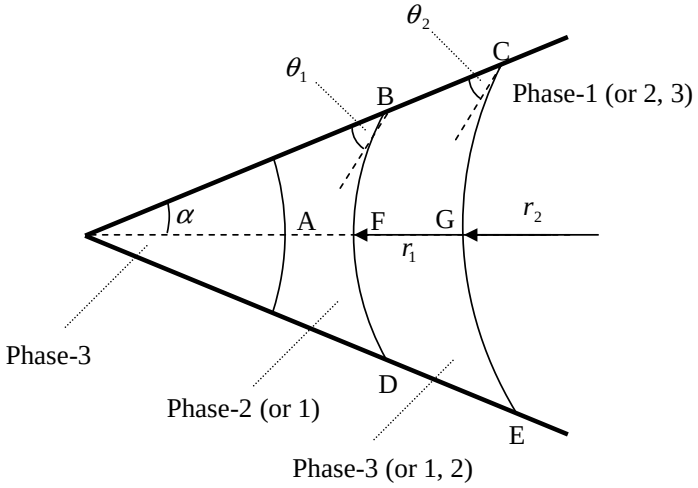

(b)

Figure 4.13: A layer sandwiched between different fluids (a) one of the AM's has negative curvature (b) a second layer sandwiched between fluids in the centre and the first layer.

Chapter 5

Two- and Three-Phase Fluid Generic Configurations

Different oil/water, gas/water and gas/oil contact angles and interfacial tensions make it theoretically possible to accommodate fluids in the corners of the pore space with different configurations. Figs. (5.1) and (5.2) illustrate all the possible generic configurations of one, two or three fluids in a single corner of an angular pore or throat with any values of two- and three-phase contact angles – the whole pore or throat is composed of no (circle), three (triangular) or four (square) corners. In all three-phase configurations the constraint among the three-phase contact angles given by Eq. 2.6 is satisfied. The configurations are equally applicable for any other angular pore or throat with any number of corners. Altered wettability surfaces are shown by thicker lines. Fluid located in the corner, layer or centre of a configuration is called a *phase location*. For example, configuration group F has three phase locations, water in a corner, an oil layer and gas in the centre. For single phase configurations – group A – only one phase location, i.e. water in the centre, is considered. Every phase location has a flag associated with it indicating whether the fluid that it accommodates is *continuous* or *trapped*. If it is trapped then the trapped cluster number that the phase location belongs to is also attached to it. A cluster of phase locations is trapped when it does not connect to the inlet and outlet; if is does then it is considered continuous. We shall discuss the details of how the phase locations are assigned to the clusters and how their continuity is determined later in this work. For elements with a circular cross-section, only one phase may occupy the pore or throat. For square and triangular cross-sections, the phase in the middle of the element must be the same for each corner, but different corners may have different configurations, depending on the corner angle. However, in a single

Table 5.1: The range of contact angles for which each configuration in Figs. (5.1) and (5.2) can exist.

Configuration	θ_{ow}	θ_{gw}	θ_{go}
A-1 , A-2	—	—	—
B-1 , B-2	$< \frac{\pi}{2} - \alpha^1$	—	—
B-3 , B-4	$\geq \frac{\pi}{2} - \alpha$	—	—
C-1 , C-2	—	$< \frac{\pi}{2} - \alpha$	—
C-3 , C-4	—	$\geq \frac{\pi}{2} - \alpha$	—
D-1 , D-2	$\geq \frac{\pi}{2} + \alpha$	—	—
E-1 , E-2	—	$\geq \frac{\pi}{2} + \alpha$	—
F-1 , F-2	$< \frac{\pi}{2} - \alpha$	—	$< \frac{\pi}{2} - \alpha$
F-3 , F-4	$\geq \frac{\pi}{2} - \alpha$	—	$< \frac{\pi}{2} - \alpha$
G-1 , G-2	—	$< \frac{\pi}{2} - \alpha$	$\geq \frac{\pi}{2} + \alpha$
G-3 , G-4	—	$\geq \frac{\pi}{2} - \alpha$	$\geq \frac{\pi}{2} + \alpha$
H-1 , H-2	$\geq \frac{\pi}{2} + \alpha$	$< \frac{\pi}{2} - \alpha$	—
I-1 , I-2	$< \frac{\pi}{2} - \alpha$	$\geq \frac{\pi}{2} + \alpha$	—
J-1 , J-2	$\geq \frac{\pi}{2} - \alpha$	$\geq \frac{\pi}{2} + \alpha$	$< \frac{\pi}{2} - \alpha$
K-1 , K-2	$\geq \frac{\pi}{2} + \alpha$	$\geq \frac{\pi}{2} - \alpha$	$\geq \frac{\pi}{2} + \alpha$

pore or throat, the contact angles in each corner are the same. Table (5.1) lists the range of contact angles for which each configuration in Figs. (5.1) and (5.2) may exist. A capillary pressure between any two phases, i.e. P_{cij}, is defined as $P_i - P_j$. The radius of curvature r of the interface between two phases i and j in Figs. (5.1) and (5.2) is related to the capillary pressure by Eq. (4.9).

One should note that when Eq. (4.9) is applied to calculate the radius of curvature for an interface, P_i and P_j may be different from the inlet or outlet pressures, i.e. the *global* absolute pressures of the two phases, if that phase is trapped. In such cases, the absolute pressures of the trapped clusters are used.

Capillary pressure is used in this work in two senses. The first is a threshold or entry capillary pressure at which a displacement in an element occurs. This has a precise definition dependent on the contact angles and pore geometry. The second is when there is some imposed pressure differences between phases in an element that is used to determine the radius of curvature of layers. This pressure difference always corresponds to a threshold capillary pressure for a recent displacement in one element.

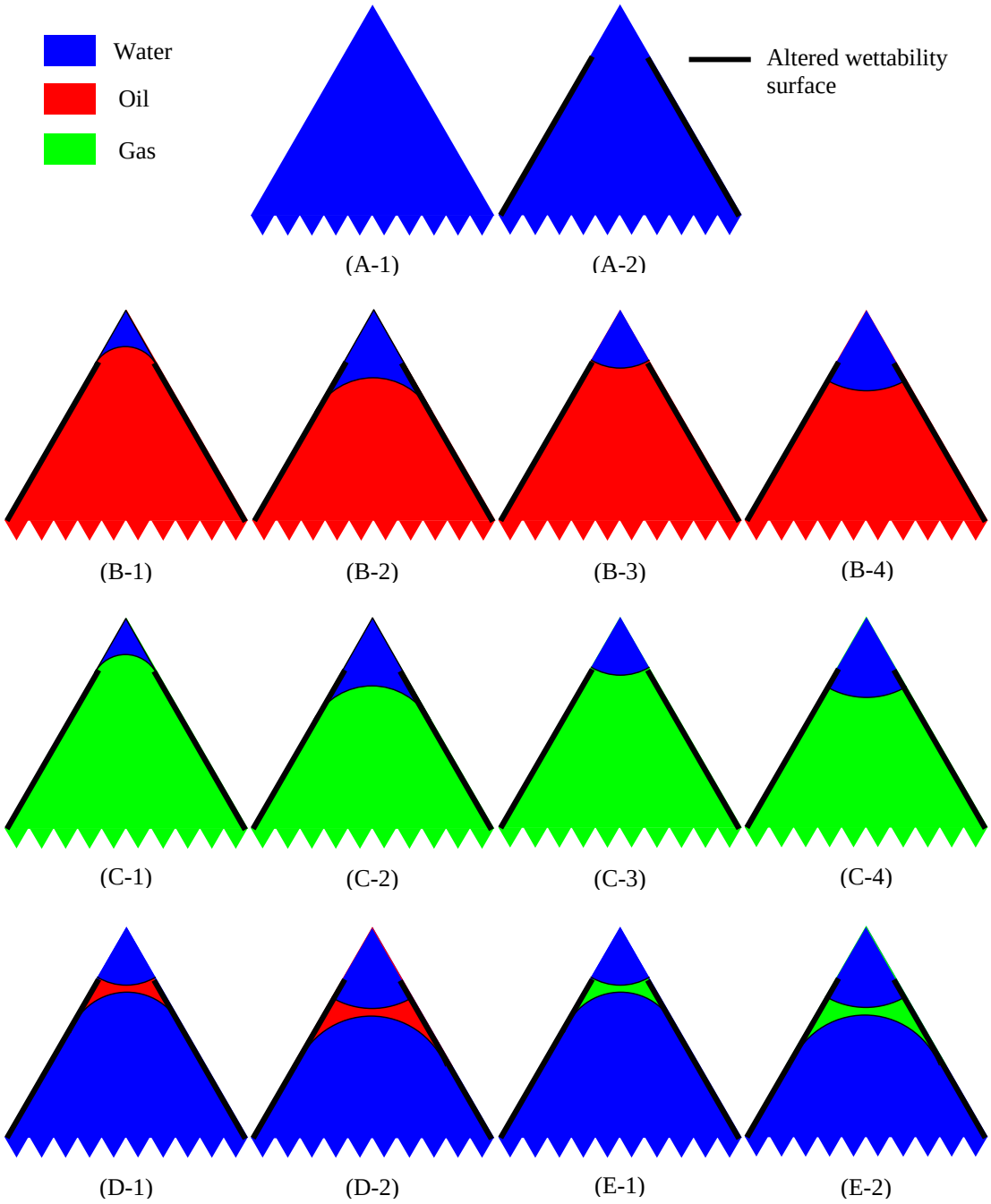

Figure 5.1: One- and two-phase configurations for a single corner. The bold solid line indicates regions of the surface with altered wettability. All the multiphase contact points may be pinned which means that as the capillary pressure changes, the curvature of the interface changes but that the location of the interface/solid contact is fixed. A phase may be present in the centre of the pore space or as a spreading or wetting layer, sandwiched between other phases. Water is always present in the corner. The network model simulates a sequence of displacement events that represent the change from one configuration to another. Chapter (4) presents the capillary pressures for each displacement.

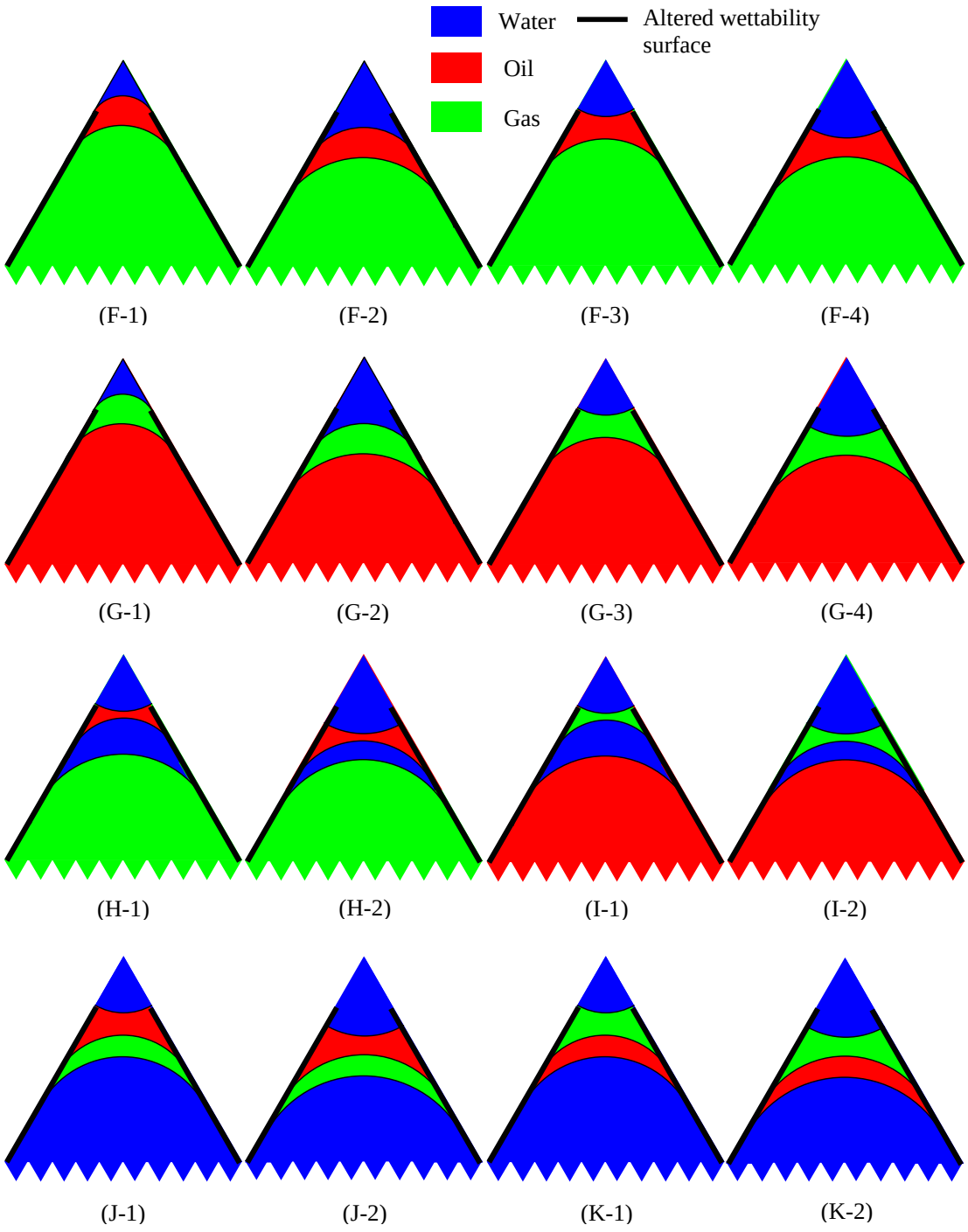

Figure 5.2: Three-phase configurations for a single corner, continued from Fig. (5.1).

5.1 Definitions

A *displacement* is defined as a change (see later for details) in generic configuration groups (indicated by letters in Figs. (5.1) and (5.2)) in an element by an *eligible* displacing phase which is the phase residing in a phase location that is topologically capable of doing the change(s). Based on the type of displacement this can be a configuration change in one or all corners of the element. For every configuration change, there might be *different* ways to carry out the displacement. In such a case each one is treated as a *separate* displacement. For instance, imagine configuration group change F to C due to oil layer collapse (see later for details). The change could be carried out either by invasion of water in the corner or gas in the centre which corresponds to a decrease in P_{cow} or an increase in P_{cgo} respectively. These two ways are treated as two separate displacements. A displacement occurs at a threshold capillary pressure. The network model simulates a sequence of displacements induced by imposed changes in phase pressures.

For every displacement, there are two phase locations associated with it. One accommodates the displacing fluid of the displacement, the *displacing phase location*, and the other one accommodates the displaced fluid, the *displaced phase location*. For example, consider configuration group change B to C by an invasion of gas residing in the centre of a neighbouring pore into oil in the centre of a throat. The displacing and displaced phase locations for this displacement are the gas centre in the pore and the oil centre in the throat, respectively.

A *process* is defined as a consecutive sequence of displacements that involve a change in the same capillary pressure in the same direction. The change in capillary pressure, P_{cij}, is due to injection of either phase i or j. For instance, primary drainage is a process involving an increase in oil/water capillary pressure. Water flooding is a different process involving a decrease in oil/water capillary pressure.

Because of contact angle hysteresis, the contact angle can hinge between its receding and advancing values without the contact line moving and is called the *hinging* contact angle. Every interface has two contact angles associated with it: *(I)*: a *target* contact angle, which is the contact angle that the *new* AM's will have just after a displacement in that element. The *existing* (old) AM's *might* reach this value just before displacement. This contact angle may be different from one process to another. For example, imagine a configuration group change A to B by oil primary drainage. The new AM's in configuration group B will have the target contact angle of θ_{ow}^{PD}. The target contact angle during water flooding for an existing oil/water interface in configuration group B is θ_{ow}^{a}. *(II)*: the *furthest* contact

angle, which is the maximum, or minimum, hinging contact angle that an interface reached during the last process when the pertinent capillary pressure was changing. This may not necessarily be the same as the target contact angle. For instance, imagine water flooding is being carried out after primary drainage in a strongly oil-wet system with $\theta^a_{ow} = \pi$. When the oil/water capillary pressure decreases the oil/water AM's start hinging from θ^{PD}_{ow} towards the target contact angle (θ^a_{ow}). If water flooding is stopped at some stage then there might be AM's, particularly in wide corners, that have not reached the advancing value yet. For such AM's the last hinging contact angle is considered as its furthest contact angle. For the AM's that reached the target contact angle, the furthest contact angle will be the same as the target contact angle. For the next process, for instance gas injection, the interface may start hinging from this furthest value towards the new target contact angle.

Every AM has a meniscus-apex distance, i.e. b (see Fig. (6.5)), associated with it and is calculated using Eq. (4.34) to be used in area and threshold capillary pressure calculations. b changes whenever the AM moves.

5.2 Configuration Changes

Configuration changes make it possible to simulate any sequence of fluid injection in two- and three-phase systems. All possible changes are discussed in this section. First we present points that one should consider to record configuration changes:

1. After every configuration group change, there will be some new displacements to be considered. These displacements are added into the *appropriate* lists (see details later). For every new displacement, the appropriate list is determined knowing what phase is displacing and whether the phases occupying the displacing and displaced phase locations are continuous or trapped.

2. Once a configuration group is changed, the type and the number of AM's in the corner may also change. There are two possibilities: *(I)* the number of AM's is the same but the type has been changed – fluid on one side of the AM has been replaced by a new fluid. For example, consider configuration group change B to C. In this case the furthest contact angle of the AM before the configuration change is given to the AM after the configuration change and then the interface may hinge from its furthest value towards the target contact angle (due to changes in the pertinent capillary pressure) and ultimately move. This will prevent any volume error of the fluid residing on the other side of

the AM – i.e. water in the corner in the example above. We may call this case an *old* AM case. *(II)* the number of AM's in the corner has either increased or decreased. If it has increased by piston-like or snap-off displacement then the *new* AM will have the furthest contact angle the same as the target value and moves according to the changes in the relevant capillary pressure. For example, imagine configuration group change B to F by piston-like invasion of gas. The furthest contact angle of the new gas/oil AM will be θ^r_{go}. If the number of AM's has increased by layer formation, see point (4). Finally if the number of AM's has decreased (by layer collapse) then it is treated as an old AM case. An example is the gas layer collapse event by water or oil in configuration group G to form an oil/water AM in configuration group B.

3. An AM moves once the hinging contact angle becomes as large as the advancing contact angle of the AM (when the related capillary pressure is decreasing) or as small as the receding contact angle of the AM (when the related capillary pressure is increasing). Once the AM moves, the new b is calculated. The value of b is updated as long as the AM keeps moving by changes in the pertinent capillary pressure in the same direction as when it started to move.

4. When a new layer formation event is considered, one should note that there are two displacements that may represent such an event and both must be added to the lists. Imagine an AM where a layer is going to be formed around it. The first displacement may displace some of the fluid above the AM to accommodate the layer while the other one displaces some of the fluid below the AM to make space for the layer. For example, consider gas layer formation resulting in configuration group change B to G. The two displacements may take place only if $\theta^r_{go} > \frac{\pi}{2} + \alpha$. By the first one, gas may displace some of the water in the corner to open enough space for the layer while forming a new gas/water interface for which the meniscus-apex distance b is calculated. Both target and furthest contact angles of the gas/water interface will be θ^r_{gw}. One should note that the gas/oil interface, in the new configuration, is treated as an old AM. π minus the furthest contact angle of the oil/water interface before the configuration group change is given as the furthest contact angle of the gas/oil interface. Then the gas/oil interface may start hinging from its furthest value towards θ^r_{go} if the gas/oil capillary pressure is increased during the process. Also the meniscus-apex distance of the oil/water interface b is given to the gas/oil interface. The threshold capillary pressure of the layer

formation is calculated using θ^r_{gw} and the furthest value of the gas/oil interface. But by the second displacement, gas may displace some of the oil in the centre to accommodate itself as a layer. A new gas/oil interface is created and so its meniscus-apex distance b is calculated. Both target and furthest contact angles of the gas/oil interface will be θ^r_{go}. The gas/water interface is considered as an old AM and the furthest contact angle of the oil/water interface before the configuration change is used as the furthest contact angle of the gas/water interface. Then the gas/water interface may hinge from its furthest value towards θ^r_{gw} if the gas/water capillary pressure is increased during the process. Also the meniscus-apex distance of the oil/water interface b is given to the gas/water interface. The threshold capillary pressure of the layer formation is calculated using θ^r_{go} and the furthest contact angle of the gas/water interface.

5. Once a displacement changes a configuration group, there might be other displacements that had been considered for the same configuration group change but through other routes. These displacements are not valid anymore and are omitted from the lists.

6. New piston-like displacements are considered only if the configuration group change has replaced the fluid at the centre of the element and there is at least one different phase residing in the centre of the neighbouring elements.

7. New layer formation displacements are added to the lists only when the phase that is expected to form the layer is located in neighbouring element(s) in the centre or layer.

8. New snap-off displacements are added to the list as soon as a new AM is formed or the type of an old AM has changed. One should note that this is considered only if the fluid in the centre of the element is residing on one side of the AM. A new layer collapse event is considered only if a new layer forms.

9. Once a new configuration group is formed, it might allow new displacements in the *neighbouring* elements. For instance, imagine a piston-like displacement by gas changes configuration group B to C in an element. Formation of a gas layer in the corners, as well as displacement of oil and water in the centre, of the neighbouring elements are considered if topological and contact angle circumstances permit.

10. There are some configurations (see Figs. (5.1) and (5.2)) that have more than one AM. The AM's and also layers are numbered from the apex inwards.

New configuration(s) to form by a displacement can be determined knowing the θ_{ow}, θ_{gw}, and θ_{go} of the displacement and the invading fluid. All changes that can happen to each configuration group, i.e. displacements, during different two- and three-phase processes are presented in detail next.

5.2.1 Configuration Group A

An oil layer formation event may change configuration group A to D. Both target and furthest contact angles of both new oil/water interfaces will be θ^r_{ow}. This may happen only when $\theta^r_{ow} \geq \frac{\pi}{2} + \alpha$. Since the interfaces are being freshly created, the meniscus-apex distance (b), which is the same for both interfaces, is calculated. The new displacements to add are: oil layer collapse by water in the corner, oil layer collapse by water in the centre, and snap-off of water in the centre by the oil in the layer. A very similar event by gas, i.e. gas layer formation, may change configuration group A to E. For both gas/water interfaces, target and furthest contact angles would be θ^r_{gw}. For the new interfaces, b is calculated. This may happen only when $\theta^r_{gw} \geq \frac{\pi}{2} + \alpha$. The new displacements to add are: gas layer collapse by water in the corner, gas layer collapse by water in the centre, and the snap-off of water in the centre by the gas.

Piston like displacement of water by oil may change configuration group A to B. Both target and furthest contact angles of the oil/water interface would be θ^r_{ow}. One should note that if oil has not touched the element before, i.e. wettability has not been altered, then $(\theta_{ow})^{PD}$ is used instead. The new displacements to add are: snap-off of oil in the centre by the water in the corner, piston-like displacement of oil in the centre by the other phases, i.e. gas and/or water, possibly located in the centre of the neighbouring elements. For the new oil/water interface, b is calculated. A similar displacement by gas may change configuration group A to C. Both target and furthest contact angles of the gas/water interface will be θ^r_{gw}. It should be noted that if the wettability of the element has not been altered before, then $(\theta_{gw})^{PD}$ is used instead. The new displacements to add are: snap-off of gas in the centre by water in the corner, piston-like displacement of gas in the centre by the other phases, i.e. oil and/or water. For the new gas/water interface, b is calculated. Fig. (5.3)-(a) indicates all the possible configuration changes that might happen to configuration A.

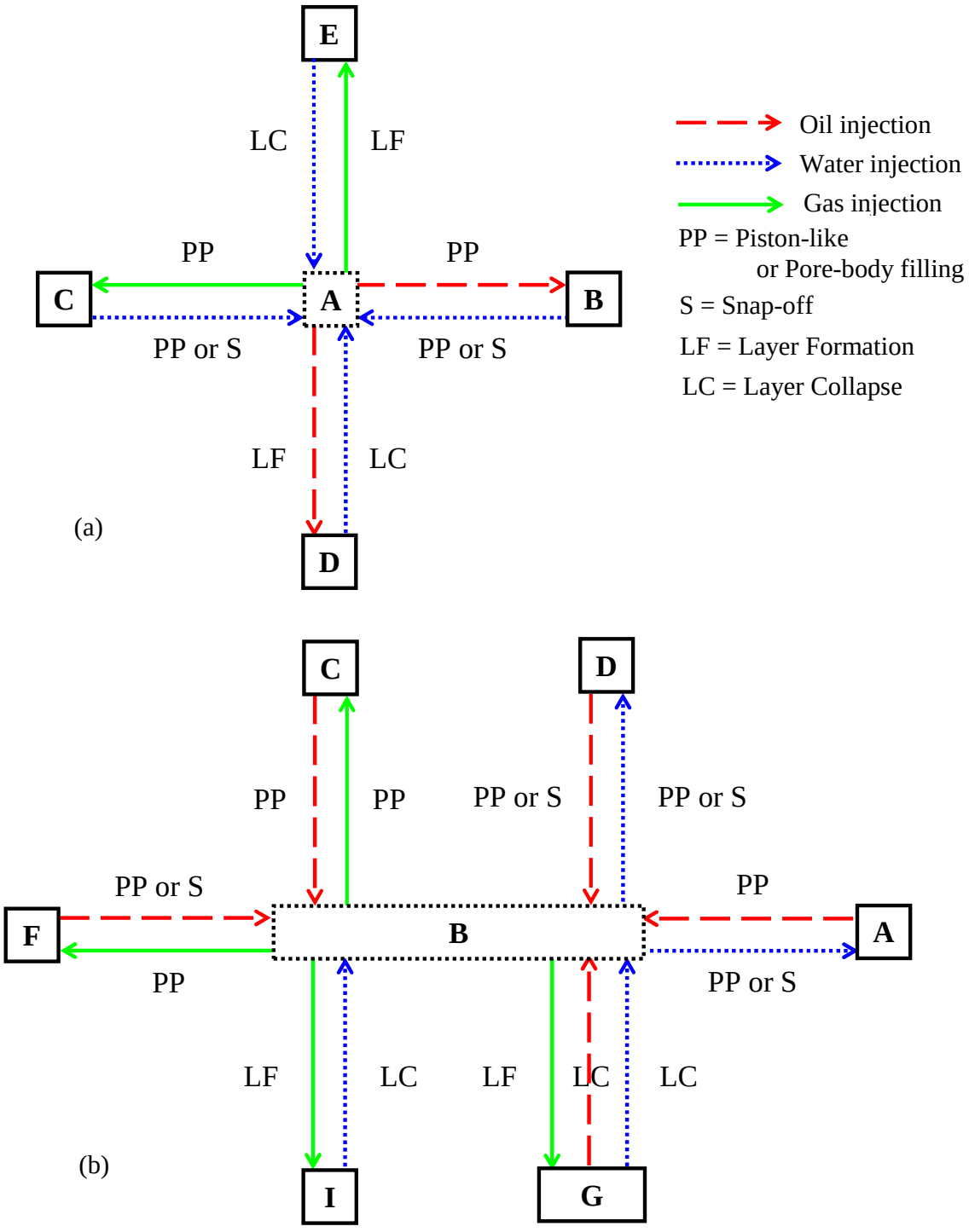

Figure 5.3: Possible configuration changes to configurations (a) A and (b) B.

5.2.2 Configuration Group B

A piston-like or snap-off displacement by water may change configuration group B to A. The contact angle at which the displacement is carried out is θ^a_{ow}. This happens only if $\theta^a_{ow} < \frac{\pi}{2} + \alpha$. No new interfaces are created. The new displacements to add are: oil layer formation, gas layer formation, and piston-like displacement of water in the centre by oil and/or gas. If $\theta^a_{ow} > \frac{\pi}{2} + \alpha$ then a piston-like or snap-off displacement by water may change configuration group B to D. A new oil/water interface is formed and so b is calculated. The new displacements to add are: oil layer collapse by water in the corner, oil layer collapse by water in the centre, snap-off of water in the centre by the oil in the layer, and piston-like displacement of water in the centre by oil and/or gas.

A piston-like displacement by gas may change configuration group B to C. The contact angle to carry out the displacement is θ^r_{go}. This may happen only if $\theta^r_{go} > \frac{\pi}{2} - \alpha$. The gas/water interface in the new configuration is not considered as a new interface. It is assigned the b and the furthest contact angle of the oil/water interface before the configuration change. The interface may hinge from its furthest contact angles towards θ^r_{gw} by an increase in gas/water capillary pressure. The new displacements to add are: snap-off of gas in the centre by the water in the corner, and piston-like displacement of gas in the centre by water and/or oil. The piston-like displacement by gas may change the configuration group B to F when $\theta^r_{go} \leq \frac{\pi}{2} - \alpha$. A new gas/oil interface is formed for which both target and furthest contact angles will be θ^r_{go}. b is calculated for the gas/oil interface. The new displacements to add are: oil layer collapse by water in the corner, oil layer collapse by gas in the centre, snap-off of gas in the centre by the oil in the layer, and piston-like displacement of gas in the centre by water and/or oil.

A gas layer formation event may change configuration group B to G. The new displacements to add are: gas layer collapse by water in the corner, gas layer collapse by oil in the centre, and snap-off oil in the centre by gas in the layer. Gas layer formation may also change configuration group B to I. The contact angle by which the displacement is carried out is θ^r_{gw}. Two new gas/water interfaces are formed and thus the b that is calculated will be the same for both. Target and furthest contact angles are θ^r_{gw} for the new interfaces. This may happen only when $\theta^r_{gw} \geq \frac{\pi}{2} + \alpha$. The new displacements to add are: the gas layer collapse by water in the corner, the gas layer collapse by water in the second layer, water layer collapse by gas in the first layer, water layer collapse by oil in the centre, and snap-off of oil in the centre by water in the second layer. Fig. (5.3)-(b) shows the possible configuration changes

to configuration B.

5.2.3 Configuration Group C

A piston-like or snap-off displacement by water may change configuration group C to A. The contact angle that is used to carry out the displacement is θ^a_{gw}. This occurs only if $\theta^a_{gw} < \frac{\pi}{2} + \alpha$. No new interface is formed. The new displacements to add are: oil layer formation, gas layer formation, and piston-like displacement of water in the centre by oil and/or gas. If $\theta^a_{gw} > \frac{\pi}{2} + \alpha$ then a piston-like or snap-off displacement by water may change configuration group C to E. A new gas/water interface is created and thus b is calculated. The new displacements to add are: gas layer collapse by water in the corner, gas layer collapse by water in the centre and water and snap-off of water in the centre by gas in the layer.

A piston-like displacement by oil could change configuration group C to B. The contact angle at which the displacement takes place is θ^a_{go}. This may happen only if $\theta^a_{go} < \frac{\pi}{2} + \alpha$. The oil/water interface is not treated as a new interface. b and the furthest contact angle of the gas/water interface before the configuration change are assigned to the oil/water interface. The oil/water interface may hinge from its furthest value towards θ^r_{ow} due to an increase in oil/water capillary pressure. The new displacements to add are: snap-off of oil in the centre by the water in the corner, and piston-like displacement of oil in the centre by water and/or oil. The piston-like displacement by oil could change the configuration group C to G when $\theta^a_{go} \geq \frac{\pi}{2} + \alpha$. A new gas/oil interface is created and so b is calculated. Both target and furthest contact angles will be θ^a_{go}. The new displacements to add are: gas layer collapse by water in the corner, gas layer collapse by oil in the centre, snap-off of oil in the centre by the gas in the layer, and piston-like displacement of oil in the centre by water and/or gas.

Oil layer formation could change configuration group C to F. As we described before, two displacement can cause this change. The two contact angles to be used are θ^r_{ow} and θ^a_{go}. The new displacements to add are: oil layer collapse by water in the corner, oil layer collapse by gas in the centre, and snap-off of gas in the centre by oil in the layer. Oil layer formation may also change configuration group C to H. The contact angle used to carry out the displacement is θ^r_{ow}. The displacement creates two fresh oil/water interfaces and so the same b is calculated for both. Both target and the furthest contact angles are θ^r_{ow} for the new interfaces. This may occur only if $\theta^r_{ow} \geq \frac{\pi}{2} + \alpha$. The new displacements to add are: oil layer collapse by water in the corner, oil layer collapse by water in the second layer, water layer collapse by

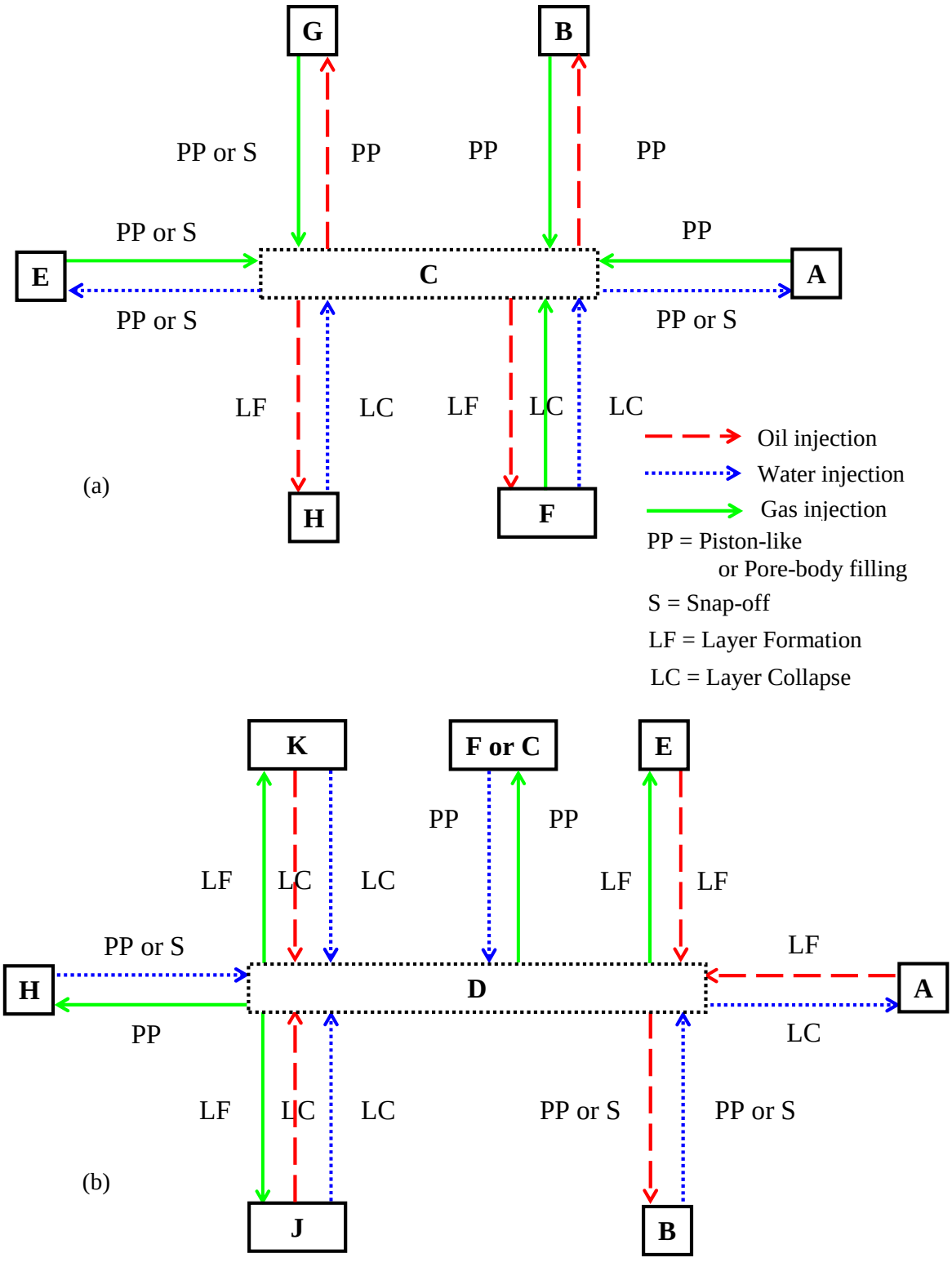

Figure 5.4: Possible configuration changes to configurations (a) C and (b) D.

oil in the first layer, water layer collapse by gas in the centre, and snap-off of gas in the centre by water in the second layer. Fig. (5.4)-(a) summarizes the possible configuration changes to configuration group C.

5.2.4 Configuration Group D

An oil layer collapse event by water may change configuration group D to A. The new displacements to add are: oil layer formation, and gas layer formation.

A piston-like or snap-off displacement by oil may change configuration group D to B. The contact angle at which the displacement is carried out is θ^r_{ow}. An oil/water interface is omitted. The contact angle of the oil/water interface in the corner may hinge from its furthest value to θ^r_{ow}. The new displacements to add are: snap-off of oil in the centre by water in the corner, two possible gas layer formations and piston-like displacement of oil in the centre by gas and/or water.

A piston-like displacement by gas may change configuration group D to F. The contact angle used for the displacement is θ^r_{gw}. This may happen only if $\theta^r_{go} < \frac{\pi}{2} - \alpha$. The gas/oil interface is not considered as a new interface. The furthest contact angle and b of the second oil/water interface before the configuration change are assigned to the gas/oil interface. Then the gas/oil interface may hinge from its furthest value towards θ^r_{go} due to an increase in the gas/oil capillary pressure. The new displacements to add are: snap-off of gas in the centre by oil in the layer, oil layer collapse by gas in the centre, water layer formation as a second layer, and piston-like displacement of the gas in the centre by water and/or oil. If $\theta^r_{go} < \frac{\pi}{2} - \alpha$ then the piston-like displacement may change the configuration D to C. The gas/water interface is not treated as a new interface and gets the furthest contact angle and b of the first oil/water interface before the configuration change. The gas/water interface may then hinge from its furthest value towards θ^r_{gw} due to an increase in gas/water capillary pressure. The new displacements to add are: snap-off of gas in the centre by water in the corner, and piston-like displacement of gas in the centre by water and/or oil.

A piston-like displacement by gas may convert configuration group D to H. The contact angle at which the displacement takes place is θ^r_{gw} which is considered to be both the furthest and target contact angles for the fresh gas/water interface. b is calculated. This event happens only if $\theta^r_{gw} < \frac{\pi}{2} - \alpha$. The new displacements to add are: water layer collapse by oil in the first layer, water layer collapse by gas in the centre, snap-off of gas in the centre by water in the second layer, and piston-like displacement of gas in the centre by oil and/or water.

A gas layer formation event may change configuration group D to K. As mentioned before, two displacements may carry out such a change. The two contact angles to use in the two displacements are θ^r_{gw} and θ^r_{go}. This may occur only if $\theta^r_{go} \geq \frac{\pi}{2} + \alpha$. The new displacements to add are: gas layer collapse by water in the corner, gas layer collapse by oil in the second layer, and oil layer collapse by gas in the first layer. Gas layer formation may also change configuration group D to J. The two contact angles applied in two displacements are θ^r_{gw} and θ^r_{go}. The event may take place only if $\theta^r_{go} \geq \frac{\pi}{2} - \alpha$ and $\theta^r_{gw} \geq \frac{\pi}{2} + \alpha$. The new displacements to add are: gas layer collapse by water in the centre, gas layer collapse by oil in the first layer, oil layer collapse by gas in the second layer, and snap-off of water in the centre by gas in the second layer. Fig. (5.4)-(b) summarizes the possible configuration changes to configuration group D.

5.2.5 Configuration Group E

Gas layer collapse by water could change configuration group E to A. The new displacements to add are: oil layer formation, and gas layer formation.

A piston-like or snap-off displacement by gas could change configuration group E to C. The contact angle for the displacement is: θ^r_{gw}. A gas/water interface is omitted. The gas/water interface in the corner may hinge from its furthest value towards θ^r_{gw}. The new displacements to add are: snap-off of gas in the centre by water in the corner, two possible oil layer formations, and piston-like displacement of gas in the centre by oil and/or water.

A piston-like displacement by oil may change configuration group E to I. The contact angle to use when the displacement is carried out is θ^r_{ow} which is considered as both the furthest and target contact angles for the new oil/water interface. b is calculated. The displacement happens only if $\theta^r_{ow} < \frac{\pi}{2} - \alpha$. The new displacements to add are: water layer collapse by oil in the centre, water layer collapse by gas in the first layer, snap-off of oil in the centre by water in the second layer, and piston-like displacement of oil in the centre by gas and/or water. If $\theta^r_{ow} \geq \frac{\pi}{2} - \alpha$ and $\theta^a_{go} \geq \frac{\pi}{2} + \alpha$ then the piston-like displacement by oil may change configuration group E to G. The contact angles used for the displacement are θ^r_{ow} and θ^a_{go}. The gas/oil interface is not treated as a new interface. The furthest contact angle and b of the second gas/water interface before the configuration change are given to the gas/oil interface. Then the gas/oil interface can hinge from its furthest value towards θ^a_{go} due to a decrease in gas/oil capillary pressure. The new displacements to add are: snap-off of oil in the centre by gas in the layer, gas layer collapse by oil in the centre,

water layer formation as a second layer, and piston-like displacement of the oil in the centre by water and/or gas. If $\theta^a_{go} < \frac{\pi}{2} + \alpha$ then piston-like displacement may change the configuration E to B. The furthest contact angle and b of the first gas/water interface before the configuration change are assigned to the oil/water interface as is not considered as a new interface. The oil/water interface may then hinge from its furthest value towards θ^r_{ow} due to an increase in oil/water capillary pressure. The new displacements to add are: snap-off of oil in the centre by water in the corner, and piston-like displacement of the oil in the centre by water and/or gas.

An oil layer formation event can change configuration group E to K. Two displacements may cause such an event. The two contact angles at which the displacements may occur are θ^r_{ow} and θ^a_{go}. This may occur only if $\theta^a_{go} \geq \frac{\pi}{2} + \alpha$ and $\theta^r_{ow} \geq \frac{\pi}{2} + \alpha$. The new displacements to add are: oil layer collapse by water in the centre, oil layer collapse by gas in the first layer, gas layer collapse by oil in the second layer, and snap-off of water in the centre by oil in the second layer. Oil layer formation can also convert configuration group E to J. The two contact angles used in these two displacements are θ^r_{ow} and θ^a_{go}. The displacement may occur only if $\theta^a_{go} < \frac{\pi}{2} - \alpha$. The new displacements to add are: oil layer collapse by water in the corner, oil layer collapse by gas in the second layer, and gas layer collapse by oil in the first layer. Fig. (5.5)-(a) indicates the possible configuration changes to configuration group E.

5.2.6 Configuration Group F

An oil layer collapse event may change configuration group F to C. The new displacements to add are: oil layer formation, and snap-off of gas in the centre by water in the corner.

A piston-like or snap-off displacement by oil may change configuration group F to B. The contact angle for the displacement is θ^a_{go}. No fresh interface is formed. The new displacements to add are: snap-off of oil in the centre by water in the corner, two gas layer formations, and piston-like displacement of oil in the centre by water and/or gas.

A piston-like displacement by water may change configuration group F to J. The contact angle used for the displacement is θ^a_{gw}. This may happen only if $\theta^a_{gw} \geq \frac{\pi}{2} + \alpha$. A new gas/water interface is created and thus b is calculated. Both target and furthest contact angles will be θ^a_{gw}. The new displacements to add are: gas layer collapse by oil in the first layer, gas layer collapse by water in the centre, snap-off of water in the centre by the gas in the layer, and piston-like displacement of water

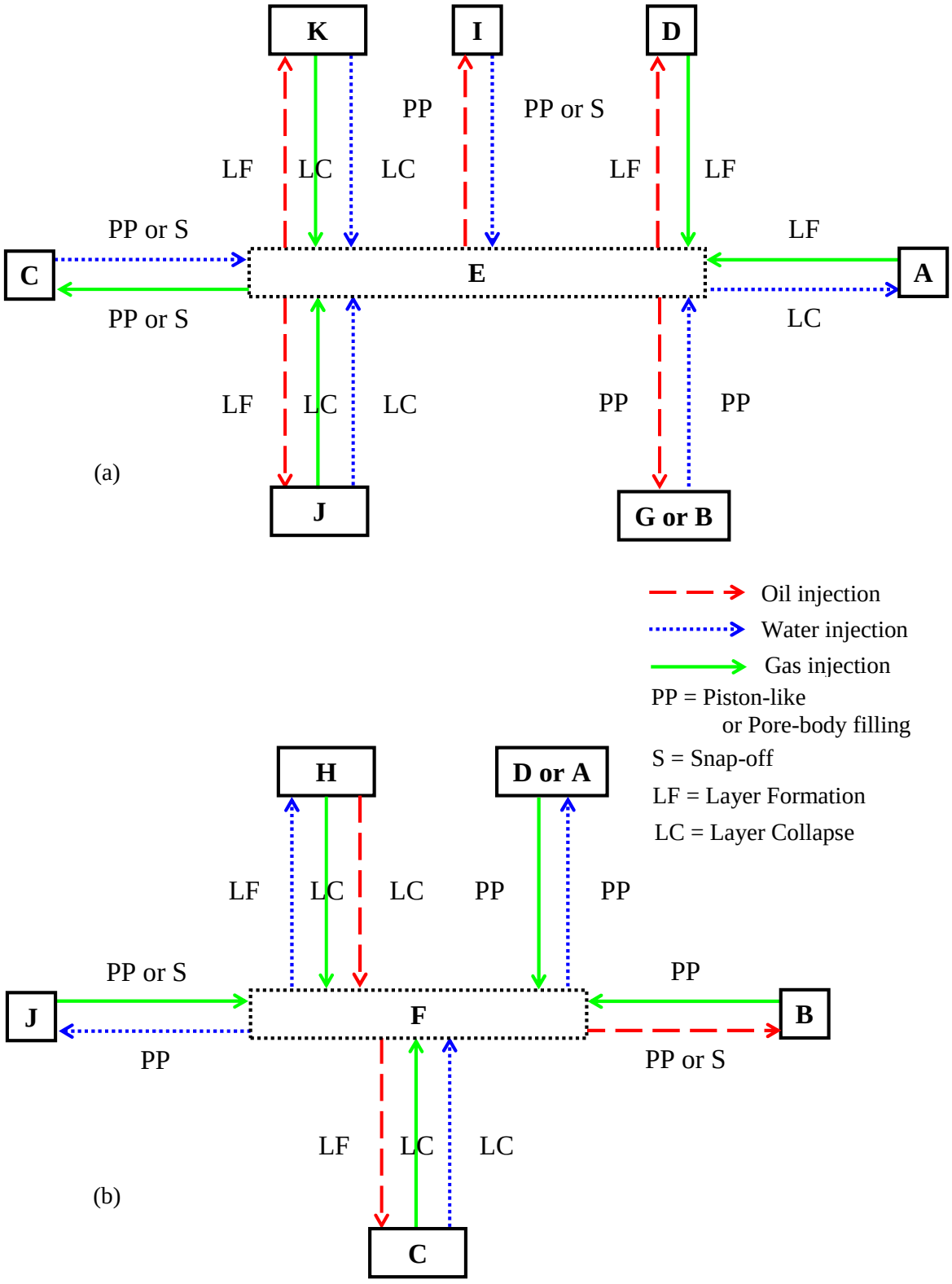

Figure 5.5: Possible configuration changes to configurations (a) E and (b) F.

in the centre by oil and/or gas. If $\theta^a_{gw} < \frac{\pi}{2} + \alpha$ then piston-like displacement by water may change configuration group F to D. The contact angles used for the displacement are θ^a_{gw} and θ^a_{ow}. This may occur only if $\theta^a_{ow} \geq \frac{\pi}{2} + \alpha$. The second oil/water interface is not considered as a new interface. The furthest contact angle and b of the the gas/oil interface before the configuration change are assigned to the second oil/water interface. The oil/water interface may hinge from its furthest value towards θ^a_{ow} due to a decrease in oil/water capillary pressure. The new displacements to add are: snap-off of water in the centre by oil in the layer, oil layer collapse by water in the centre, two gas layer formation events, and piston-like displacement of the water in the centre by gas and/or oil. If $\theta^a_{ow} < \frac{\pi}{2} + \alpha$ then the piston-like displacement may change the configuration F to A. No new interface is formed. The new displacements to add are: oil layer formation, gas layer formation, and piston-like displacement of water in the centre by oil and/or gas.

A water layer formation event may change configuration group F to H. Two displacements may carry out such a change. The two contact angles to use are θ^a_{gw} and θ^a_{ow}. This may occur only if $\theta^a_{ow} \geq \frac{\pi}{2} + \alpha$ and $\theta^a_{gw} < \frac{\pi}{2} - \alpha$. The new displacements to add are: oil layer collapse by water in the second layer, water layer collapse by oil in the first layer, water layer collapse by gas in the centre, and snap-off of gas in the centre by water in the second layer. Fig. (5.5)-(b) shows all possible configuration changes to configuration group F.

5.2.7 Configuration Group G

Gas layer collapse by water or oil may change configuration group G to B. The new displacements to add are: gas layer formation, and snap-off of oil in the centre by water in the corner.

A piston-like or snap-off displacement by gas could change configuration group G to C. The contact angle is θ^r_{go}. No new interface is created. The new displacements to add are: snap-off of gas in the centre by water in the corner, two oil layer formations, and piston-like displacement of gas in the centre by water and/or oil.

A piston-like displacement by water could convert configuration group G to K. The contact angle applied is θ^a_{ow}. b is calculated. This may happen only if $\theta^a_{ow} \geq \frac{\pi}{2} + \alpha$. The new displacements to add are: oil layer collapse by gas in the first layer, oil layer collapse by water in the centre, snap-off of water in the centre by the oil in the layer, and piston-like displacement of water in the centre by oil and/or gas. If $\theta^a_{ow} < \frac{\pi}{2} + \alpha$ then the piston-like displacement by water may change configuration group G to E. The contact angles used for the displacement are θ^a_{ow} and θ^a_{gw}. This

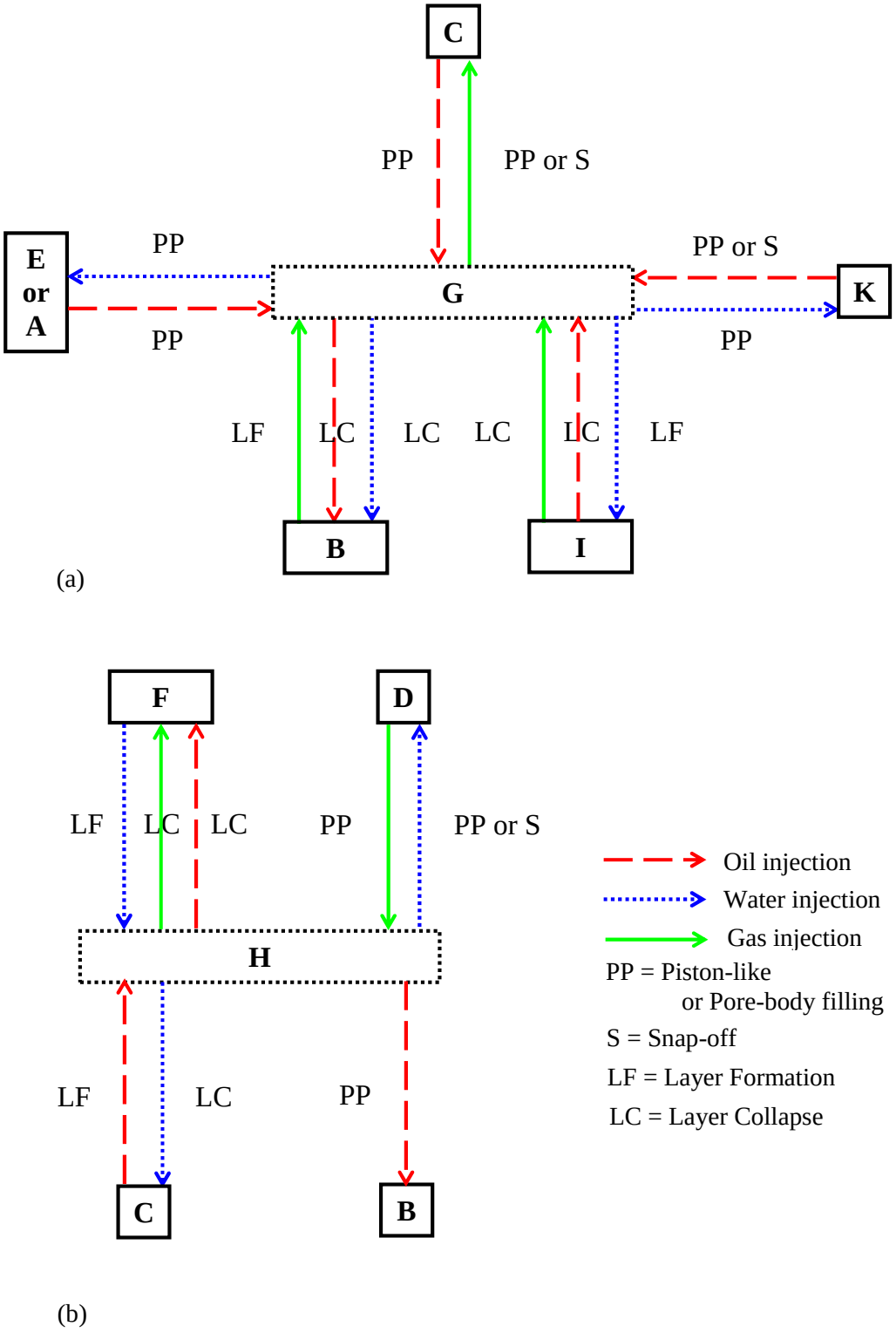

Figure 5.6: Possible configuration changes to configurations (a) G and (b) H.

may take place only if $\theta^a_{gw} \geq \frac{\pi}{2}+\alpha$. The second gas/water interface is not treated as a new interface. The furthest contact angle and b of the the gas/oil interface before the configuration change, are assigned to the second gas/water interface. The oil/water interface may then hinge from its furthest value towards θ^a_{gw} due to a decrease in gas/water capillary pressure. The new displacements to add are: snap-off of water in the centre by gas in the layer, gas layer collapse by water in the centre, two oil layer formation events, and piston-like displacement of the water in the centre by gas and/or oil. If $\theta^a_{gw} < \frac{\pi}{2} + \alpha$ then the piston-like displacement may convert the configuration G to A. The new displacements to add are: oil layer formation, gas layer formation, and piston-like displacement of water in the centre by oil and/or gas.

A water layer formation event may convert configuration group G to I. Two displacements may carry out such a change. Two displacement may carry out such a change which will use θ^a_{gw} and θ^a_{ow}. This may happen only if $\theta^a_{gw} \geq \frac{\pi}{2} + \alpha$ and $\theta^a_{ow} < \frac{\pi}{2} - \alpha$. The new displacements to add are: gas layer collapse by water in the second layer, water layer collapse by gas in the first layer, water layer collapse by oil in the centre, and snap-off of oil in the centre by water in the second layer. Fig. (5.6)-(a) indicates all possible configuration changes to configuration group G.

5.2.8 Configuration Group H

A water layer collapse event by gas or oil may change configuration group H to F. The new displacements to add are: water layer formation, oil layer collapse by gas in the centre, and snap-off of gas in the centre by oil in the layer.

A piston-like or snap-off displacement by water may change configuration group H to D. The contact angle is θ^a_{gw}. No new interface is formed. The new displacements to add are: snap-off of water in the centre by oil in the layer, two possible gas layer formation events, and piston-like displacement of water in the centre by gas and/or oil.

An oil layer collapse event by water may change configuration group H to C. The new displacements to add are: two oil layer formation events, and snap-off of gas in the centre by water in the corner.

A piston-like displacement by oil is assumed to change configuration group H to B, as we don't consider a third layer. The contact angle under which the displacement is carried out is θ^a_{og}. No new interface is formed. The new displacements to add are: snap-off oil in the centre by water in the corner, two possible gas layer formation events, and piston-like displacement of oil in the centre by gas and/or

water. Fig. (5.6)-(b) indicates all possible configuration changes to configuration group H.

5.2.9 Configuration Group I

A water layer collapse event by oil or gas can change configuration group I to G. The new displacements to add are: water layer formation, gas layer collapse by oil in the centre, and snap-off of oil in the centre by gas in the layer.

A piston-like or snap-off displacement by water may change configuration group I to E. The contact angle at which the displacement is carried out would is θ^a_{ow}. No new interface is created. The new displacements to add are: snap-off of water in the centre by gas in the layer, two possible oil layer formation events, and piston-like displacement of water in the centre by gas and/or oil.

A gas layer collapse event by water may change configuration group I to B. The new displacements to add are: two gas layer formation events, and snap-off of oil in the centre by water in the corner.

A piston-like displacement by gas is assumed to change configuration group I to C as we don't consider a third layer. The contact angle which is used to carry out the displacement is θ^r_{go}. No new interface is formed. The new displacements to add are: snap-off of gas in the centre by water in the corner, two possible oil layer formation events, and piston-like displacement of gas in the centre by oil and/or water. Fig. (5.7)-(a) indicates all possible configuration changes to configuration group I.

5.2.10 Configuration Group J

An oil layer collapse event may change configuration group J to E. The new displacements to add are: gas layer collapse by water in the corner and two oil layer formation events.

A gas layer collapse event by oil or water could change configuration group J to D. This may happen only if $\theta^a_{ow} \geq \frac{\pi}{2} + \alpha$ (water displacing) or $\theta^r_{ow} \geq \frac{\pi}{2} + \alpha$ (oil displacing). The new displacements to add are: oil layer collapse by water in the centre and two gas layer formation events. If the above oil/water contact angle condition is not satisfied then configuration group J may be converted to configuration group A. The new displacements to add are: oil and gas layer formation events.

A piston-like or snap-off displacement by gas may change configuration group J to F. The contact is θ^r_{gw}. No new interface is created. The new displacements to

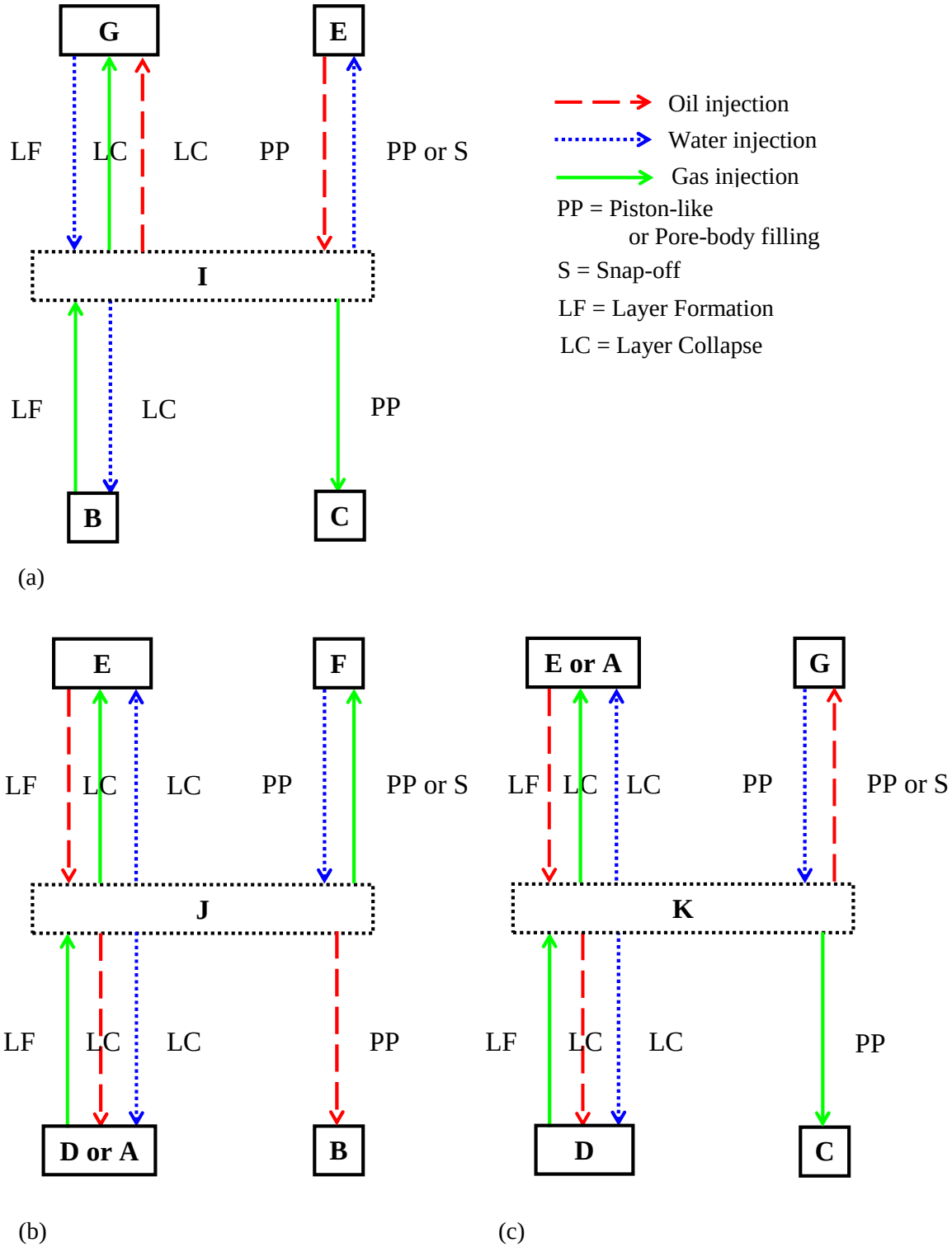

Figure 5.7: Possible configuration changes to configurations (a) I, (b) J, and (c) K.

add are: oil layer collapse by gas in the centre, snap-off of gas in the centre by oil in the layer, water layer formation event, and piston-like displacement of gas in the centre by water and/or oil.

A piston-like displacement by oil is assumed to change configuration group J to B as we don't consider a third layer. The contact angle is θ^r_{ow}. No new interface is formed. The new displacements to add are: snap-off of oil in the centre by water in the corner, two possible gas layer formation events, and piston-like displacement of oil in the centre by gas and/or water. Fig. (5.7)-(b) indicates all possible configuration changes to configuration group J.

5.2.11 Configuration Group K

Gas layer collapse by water or oil may change configuration group K to D. The new displacements to add are: oil layer collapse by water in the corner and two gas layer formation events.

An oil layer collapse event by water or gas could change configuration group K to E. This may happen only if $\theta^a_{gw} \geq \frac{\pi}{2} + \alpha$ (water displacing) or $\theta^r_{gw} \geq \frac{\pi}{2} + \alpha$ (gas displacing). The new displacements to add are: gas layer collapse by water in the centre and two oil layer formation events. If the above gas/water contact angle condition is not satisfied then configuration group K may be converted to configuration group A. The new displacements to add are: oil and gas layer formation events.

A piston-like or snap-off displacement by oil may change configuration group K to G. The contact angle is θ^r_{ow}. No new interface is created. The new displacements to add are: gas layer collapse by oil in the centre, snap-off of oil in the centre by gas in the layer, water layer formation, and piston-like displacement of oil in the centre by water and/or gas.

Piston-like displacement by oil is assumed to change configuration group K to C as we don't consider a third layer. The contact angle is θ^r_{gw}. No new interface is formed. The new displacements to add are: snap-off of gas in the centre by water in the corner, two possible oil layer formation events, and piston-like displacement of gas in the centre by oil and/or water. Fig. (5.7)-(c) indicates all possible configuration changes to configuration group K.

Chapter 6

Pore-Scale Network Modelling

6.1 Continuity and Clustering

In pore network modelling of multiphase flow, one of the most important and difficult tasks to be accomplished is the determination of whether or not a phase location is trapped as well as keeping this information updated during different processes in a robust way.

This is vitally important because for every displacement continuity of both displacing and displaced phase locations have to be known *a priori* (see section (6.4) for details). Also when it comes to compute the relative permeabilities, continuity of phase locations must be known as conductances are calculated only for continuous phase locations. (see section (6.6)).

The algorithm used to determine cluster distributions, critical percolation concentration, and percolation probabilities in network modelling was developed by Hoshen & Kopelman [260] which was later extended to irregular networks by Al-Futaisi & Patzek [291].

6.1.1 Hoshen & Kopelman Algorithm

The algorithm presented by Hoshen & Kopelman [260] was a method for determining of cluster distributions, critical percolation concentration and percolation probabilities in a finite lattice. The method was based on a multiple labelling scheme of members of a cluster in the lattice and was concerned with the determination and counting of the clusters of a particular type of occupant which were randomly distributed in a regular lattice of sites. Every site of the lattice was able to hold only one type of occupant and was connected to its neighbours by bonds. Every site

holding the particular type of occupant, was assigned a cluster label, m_t^α, where α was the name of the cluster. Such a cluster could have several labels as a directory of natural numbers.

A directory of positive and negative integer numbers was considered where the positive ones indicated the number of members in each cluster and the negative ones provided the links between different labels. The directory was updated when new members were assigned to the existing clusters, new clusters were found or coalescence occurred. Every new site was assigned a label in one of the following ways: *(I)* if there was not any already labelled neighbour with the same occupant, a new label was used, *(II)* if there was only one neighbour with the same occupant, the label of the neighbour was used *(III)* if there were more than one neighbour with the same occupant, the smallest label was used. The distinct feature of the multiple labelling scheme was that a new site could link two or more already labelled cluster fragments occupied by the same occupant into a bigger cluster without relabelling them. The algorithm was able to label the sites, find the clusters, and count them by a single scan of the lattice.

6.1.2 Displacement Based Algorithm

We use a *new* algorithm whose principles are described below. It is applicable to any two- or three-dimensional regular and random network with any number of phases, i.e. phase locations, residing in a pore or throat. In contrast, the original Hoshen-Kopelman algorithm [260] assumed that only a single phase occupied each element. Our algorithm, as we will discuss in detail shortly, is also different from the extension of Hoshen-Kopelman algorithm by Al-Futaisi & Patzek [291] since we *do not* – except for the first time – scan the entire network to update our information regarding the continuity status of different phases residing in every element.

First, the network at its initial condition is scanned to determine continuity of all its present phase locations. Flags are assigned to every single phase location indicating if it is continuous or trapped. If a phase location is trapped then the cluster number which it belongs to is also attached to it. To scan the network the algorithm shown in Fig. (6.1) is used. The algorithm uses Table (6.1) that lists the circumstances under which phase locations holding the same phase in adjacent pores and throats are considered connected. One should note that we assume that within a single pore or throat all the corners are connected and so are all the layers holding the same phase. This definition of connectivity is used to define clusters of each phase. During the scanning process, if a trapped cluster is found then all phase

locations belonging to the cluster are stored under the same cluster number.

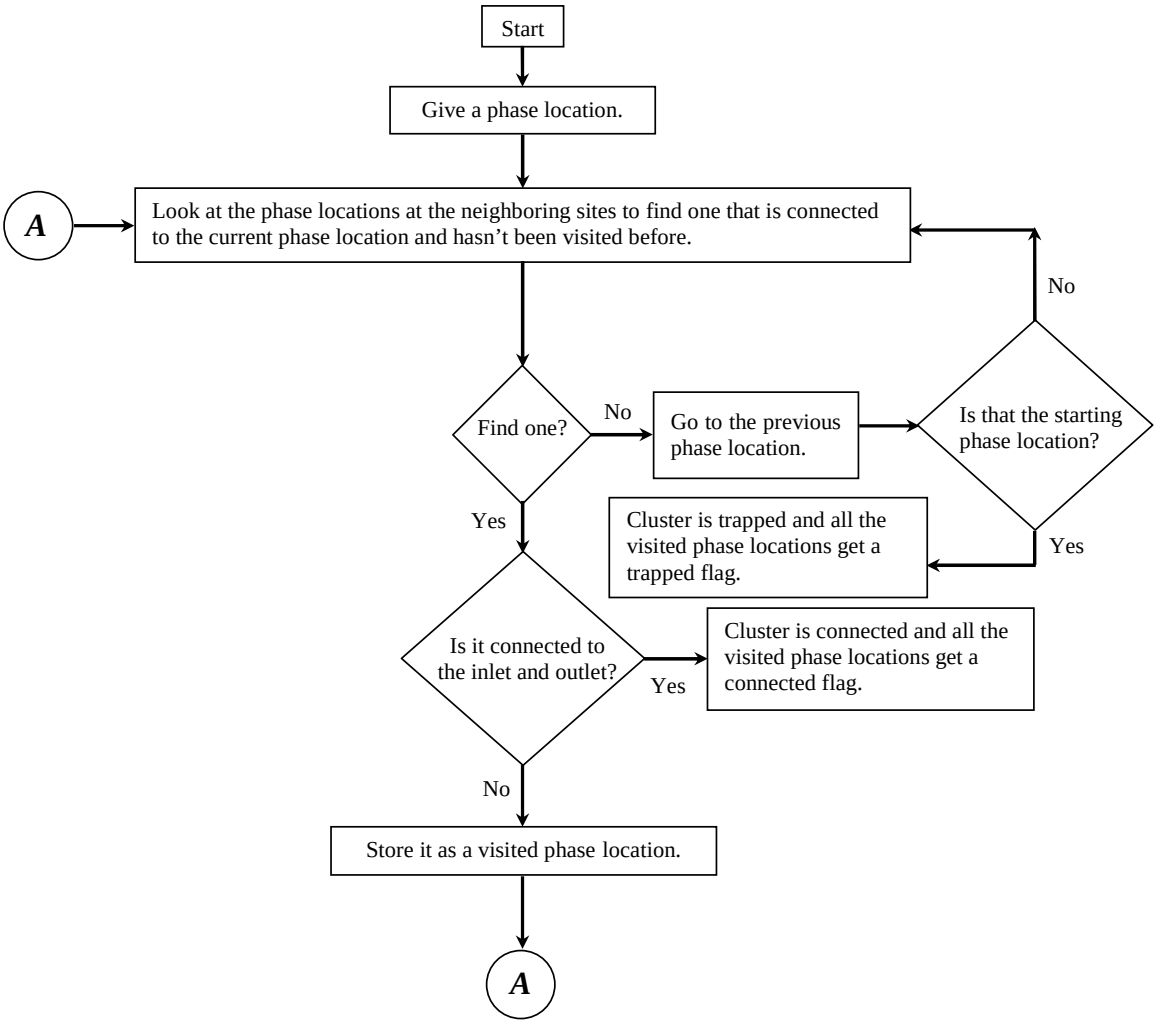

Figure 6.1: Flow chart used to determine clusters of each phase.

Once the scanning of the network at its initial status is finished, the injection of different phases and thus different displacements may start. Displacements may create new phase locations, form new trapped clusters and make old trapped clusters break, coalesce, or become continuous. This means that the old flags of phase locations may not be valid anymore and must be updated.

We present a series of *displacement-based* rules to update the flags where there will be *no need* to scan the *entire* network to update our information regarding the new continuity status of the phase locations after each displacement event. This means that flags will be *always* valid during all processes.

To present the rules, imagine a displacement occurring in a pore or throat. We

Table 6.1: Criteria for connectivity of phase locations holding the same phase in adjacent pores and throats.

Phase location(1)	Phase location(2)	Connected?
Corner	Corner	Yes
Corner	Layer	No
Corner	Centre	No
Layer	Layer	Yes
Layer	Centre	Yes
Centre	Centre	Yes

may call that pore or throat the *target* element which may have several *neighbours*. For a pore, the neighbours are the throats connected to it and for the throats, the pores. Neighbours do not necessarily contain the same fluid as the target element. Every phase location in the target element and its neighbours is considered as a member of a *chain* of phase locations with the same phase and will act as a *head*. If a chain stretches to the inlet and outlet, it is *continuous*, otherwise it is a *trapped* cluster.

The rules are itemized as follows:

1. Before the displacement takes place, all the chain heads in the target element and its neighbours are determined (i.e. *separately* in each pore and throat). For instance in a corner of an element with configuration group F, see Fig. (5.2), three chain heads, i.e. water corner, oil layer, and gas centre, are determined. One should note that at this stage, there is no need to know how far the chains stretch. Similar phase locations in an element will be members of the same chain and either of them could be used as the chain head. For example, in an element with triangular cross-section with all the corners having configuration group G, all the gas layers are considered as members of a gas chain and obviously should all have the same flags and only one of them is used as a chain head. This is also the case for the water corners. However, phase locations with the same phase but in a different *type* of location might not necessarily be considered as members of the same chain. For instance, in configuration group D, water in the centre is not considered as a member of the chain that the water corner is a member of, unless they touch each other in a corner where there is no oil layer. The water centre is considered as a head of another water chain.

2. Before the displacement, the connectivity of chain heads in the target element

with the chain heads in its neighbours are determined and stored using the criteria listed in Table (6.1).

3. The displacement is carried out which may omit some *old* phase locations while forming *new* ones in the target element. Only for the newly formed phase locations must flags be assigned. The new phase locations created by piston like, snap-off, and layer formation displacement events that hold *the same* phase as the displacing phase location will get flags exactly the same as those of the displacing phase location. For instance, for oil from the centre of a neighbour that creates an oil layer in the target element, the newly formed oil layer will get the same flags as the oil in the centre. But if the newly born phase location contains a phase similar to that of the displaced phase location, i.e. old, then it will get the same flags as the displaced phase location. For example, consider configuration group change B to F. The oil layers will get flags the same as those of oil in the centre before the displacement.

4. If the displacing phase location is trapped and forms new phase locations with the same flags then the new phase locations are added to the trapped cluster as new members.

5. If the displaced phase location was trapped and after the displacement it does not exist anymore, it is omitted from the list of the trapped cluster members.

6. If the target element is connected directly to the inlet or outlet and the new phase location is formed by the phase invading from the outside of the network, a continuous flag is assigned to the new phase location.

7. After the displacement, new possible chain heads are determined in the target element.

8. Connectivity of the new chain heads in the target elements with the chain heads in the neighbours are determined and stored.

9. Connectivity of every single chain head in the neighbours to the chain heads with the same phase in the target element before and after displacement are compared. If a chain head was disconnected (or connected) to the target element before the displacement and stays disconnected (or connected) after the displacement, there is no need to change the flags of the chain.

10. If a chain head in a neighbour was connected to the target element before the displacement and got disconnected after the displacement then: *(I)* If the chain head was continuous then its continuity is checked using the algorithm presented in Fig. (6.1) as the chain might have got trapped due to the disconnection from the target element. *(II)* If the chain head was trapped, disconnection from the target element *might* mean that a trapped cluster has *broken* into two or more smaller trapped clusters. This is called a *local break* and the next point describes how the algorithm realizes if a local break has actually broken the displaced trapped cluster into smaller ones.

11. In order to find if a local break is a *break*, one of the phase locations residing in a neighbour that belongs to the displaced (mother) trapped cluster is chosen. Then all the phase locations connected to it are found using the algorithm presented in Fig. (6.1). If *all* the other phase locations residing in the neighbour(s) that belong to the mother trapped cluster are among the found phase locations, then the disconnection has been only a local one and not a break. If not, it is a break and the found phase locations form a *new* trapped cluster with a new identity. Now all the other phase locations in the neighbour(s) that were members of the mother trapped cluster are also picked up one by one and all the connected phase locations are found and the process continues exactly the same as for the first phase location until there is no any phase location left that has not been assigned to a new smaller trapped cluster.

12. If a chain head in a neighbour was disconnected from the target element before the displacement and has become connected after the displacement then: *(I)* If the chain in the neighbour was trapped while the chain head in the target element is continuous then the trapped cluster has become continuous and flags of all its members are changed to continuous. The opposite case is also possible when the chain head in the target element is trapped while the one in the neighbour was continuous. *(II)* If the chain head in the neighbour was trapped and so was the chain head in the target element that it got connected to, then a *coalescence* has happened and both trapped clusters now will form a bigger trapped cluster (see section (6.3.1) for details). For all other cases there is no need to change the flags of the chains.

6.2 How to Choose the Right Displacement

Based on what phase displaces what phase, there are six possible two-phase processes: oil displacing water which is controlled by an increase in P_{cow}. This could be done either by an increase in oil pressure or a decrease in water pressure. Likewise, water displacing oil (decrease in $P_{cow} \equiv$ increase in water pressure or decrease in oil pressure), gas displacing water (increase in $P_{cgw} \equiv$ increase in gas pressure or decrease in water pressure), water displacing gas (decrease in $P_{cgw} \equiv$ increase in water pressure or decrease in gas pressure), gas displacing oil (increase in $P_{cgo} \equiv$ increase in gas pressure or decrease in oil pressure), and oil displacing gas (decrease in $P_{cgo} \equiv$ increase in oil pressure or decrease in gas pressure). Every displacement belongs to one or two of these six processes. For instance, collapse of the gas layer which leads to configuration group change G to B could occur by either water or oil invasion which corresponds to a decrease in P_{cow} or P_{cgo}, respectively. This means that this displacement belongs to both water displacing gas and oil displacing gas processes. But, for example, configuration group change B to A only belongs to a water displacing oil process.

A process can be carried out either by increasing the pressure of the displacing fluid or decreasing the pressure(s) of the displaced fluid(s). In two-phase processes, both methods may produce the same results but that may *not* necessarily be the case for three-phase systems. In this work, we shall model all the processes by increasing the pressure of the *injection* fluid. For example, gas injection into water and oil is carried out by increasing the gas pressure not by decreasing the pressures of oil and water.

For every single displacement, a threshold capillary pressure is calculated – see chapter (4) – which might depend on the relevant contact angles, corner angles and inscribed radius of the element of interest, other capillary pressures and the configuration of nearest neighbour pores and throats. Then depending on what fluid is displacing and what is displaced, the threshold absolute pressure of the *displacing* fluid for a *single* displacement is found from:

$$P_i^{threshold} = P_{cij}^{threshold} + P_j \tag{6.1}$$

or

$$P_j^{threshold} = P_i - P_{cij}^{threshold} \tag{6.2}$$

where P_i and P_j are pressures of phases i and j, respectively. The pressure of a

fluid is referred to the pressure of a continuous cluster of that fluid and is assumed to be the same as the inlet or outlet pressure of the fluid. There might be several such clusters of one fluid but they all will have the same pressure. The foregoing procedure is used for single displacements where one continuous phase location displaces another continuous one. When one or both of them is trapped, $P_i^{threshold}$ and $P_j^{threshold}$ are found in a slightly different way that shall be discussed in the Multiple Displacements section (6.4). Threshold pressures of all the displacements that have the same *displacing* fluid are ranked into the same *main sorted list*. Consequently, in three-phase systems there will be three main sorted lists for gas, oil and water as displacing phases. This means that every list may include entries from two different processes with the same displacing fluid. For instance, the water list may include threshold pressures from water displacing oil and water displacing gas processes.

Initially when the network is water-filled, only oil or gas can be injected and the only processes are those that displace water by oil or gas from the elements connected to the inlet. From this stage onwards, new displacements must be added, if there were any, to the appropriate list(s) regardless of whether they could occur during the current process or not (see chapter 5 for details). The exact configuration change associated with these new displacements may not be clear at this stage; and it is not necessary, as they may occur during other processes when the conditions, i.e. pressures and target contact angles, will be different. Before a new displacement is added to an appropriate list, its threshold capillary pressure is calculated. Before a new displacement is added to a main sorted list, it must be checked to see if both displacing and displaced phase locations are continuous. If one or both of them is trapped, then, based on what fluid is displacing and what fluid is displaced, the displacement is added into an appropriate *sorted sublist* in one of the 18 multiple displacement search categories tabulated in Tables (6.2), (6.3) and (6.4) (see details in Multiple Displacements section (6.4)). If both phase locations are continuous then it is added to an appropriate main sorted list.

By knowing the injection fluid, the relevant main sorted list is selected, for example the water list for water injection. The list is sorted in ascending order. Imagine the invading fluid is i. This means that we consider a displacement event where the volume of i in an element increases. Phase i can invade either phase j or k. The threshold pressure at the top of the list belongs to the *most favorable*, i.e. easiest, displacement. This could be displacement of j or k by i. If the displacement is *valid* then it takes place. A displacement is valid when the displacing and displaced phase locations are *present* and their continuity status flags are *consistent* with the

list that the threshold pressure is in. If a displacement is not valid, the event is taken off the sorted list and either discarded or moved to an appropriate list depending on the reason of invalidity. The next most favorable displacement is considered from the list. The advantage of having one list for both i to j and i to k displacements is that it assures that always the most favorable displacement is carried out *first*.

Displacements in the lists might no longer be valid because of other displacements that have already taken place. For instance, consider configuration group G. Collapse of the gas layer by water in the corner and oil in the centre are two possible displacements that should be in the water and oil lists, respectively. If the gas layer collapsed during water invasion by an increase in water pressure, the other displacement, i.e. collapse of the gas layer by oil, is no longer valid as there is no gas layer to be collapsed.

Multiple displacement search categories listed in Tables (6.2), (6.3), and (6.4) allow us to find the most favorable multiple displacement (see later for details), which then is compared with the most favorable single displacement that is determined from the main lists. This comparison would allow us to find the *globally* most favorable event.

Table 6.2: Multiple displacements search categories (continuous-trapped; c-t).

No.	Displacing	CS(1)	Displaced	CS	Name	CC(4)
1	oil	c(2)	water	t(3)	ocwt	wtot, wtoc, wtgt, wtgc
2	oil	c	gas	t	ocgt	gtwt, gtwc, gtot, gtoc
3	gas	c	water	t	gcwt	wtot, wtoc, wtgt, wtgc
4	gas	c	oil	t	gcot	otwt, otwc, otgt, otgc
5	water	c	oil	t	wcot	otwt, otwc, otgt, otgc
6	water	c	gas	t	wcgt	gtwt, gtwc, gtot, gtoc

1. Continuity Status
2. Continuous
3. Trapped
4. Chain-Categories

After a displacement, the pressure of the phase i (injection phase) is set to the *maximum* of the threshold pressure and the current pressure of phase i. All the displacements that have threshold pressures less than the pressure of the injection phase i are carried out until it is not possible to find a displacement with a threshold pressure less than or equal to the current value of the phase i pressure. This is done

Table 6.3: Multiple displacements search categories (trapped-continuous; t-c).

No.	Displacing	CS(1)	Displaced	CS	Name	CC(4)
1	oil	t(3)	water	c(2)	otwc	—
2	oil	t	gas	c	otgc	—
3	gas	t	water	c	gtwc	—
4	gas	t	oil	c	gtoc	—
5	water	t	oil	c	wtoc	—
6	water	t	gas	c	wtgc	—

1. Continuity Status
2. Continuous
3. Trapped
4. Chain-Categories

Table 6.4: Multiple displacements search categories (trapped-trapped; t-t).

No.	Displacing	CS(1)	Displaced	CS	Name	CC(3)
1	oil	t(2)	water	t	otwt	wtot, wtoc, wtgt, wtgc
2	oil	t	gas	t	otgt	gtwt, gtwc, gtot, gtoc
3	gas	t	water	t	gtwt	wtot, wtoc, wtgt, wtgc
4	gas	t	oil	t	gtot	otwt, otwc, otgt, otgc
5	water	t	oil	t	wtot	otwt, otwc, otgt, otgc
6	water	t	gas	t	wtgt	gtwt, gtwc, gtot, gtoc

1. Continuity Status
2. Trapped
3. Chain-Categories

in a way that the displacement with the *lowest* threshold pressure is ***always*** carried out *first*. At this time, all the configurations are stable and at *equilibrium* and the system is said to be *relaxed*.

The *maximum* of the threshold pressure and the current pressure of phase i is used because it is often the case that doing a displacement allows a subsequent displacement at a threshold pressure much lower than the current injection phase pressure. This event is more favorable than the next displacement in the list. An example of this is oil displacement into water in a water-wet medium. P_{oil} may be high to allow oil to fill a throat, but oil can then fill an adjoining pore at a

lower oil pressure. If we used this new lower value of P_{oil} to compute radii of curvature, then we would find that in some elements the radius is inconsistent with the fluid configuration – for instance, water AM in a corner would have a radius of curvature too large to fit in an element. In *strict capillary equilibrium*, the fluid would rearrange throughout the network to give configurations consistent with the prevailing capillary pressure. This is, however, a very difficult task for a general three-phase model. Instead, phase pressures are defined as the maximum value ever reached during the whole simulation. In other words, the pressure of the invading phase *never* acquires a lower value than its current one. Whenever a phase pressure reaches a new maximum, the fluid configurations are truly in a position of capillary equilibrium. In a simulation involving a complex displacement path, the phase pressures will continue to increase. However, since it is only pressure differences that control the displacement sequence, this is not a problem.

As mentioned earlier, threshold capillary pressures may be affected by the change in capillary pressure. In such circumstances, threshold capillary pressures for those displacements are recomputed taking into account the new arrangements of fluid and capillary pressures and re-ordered in the sorted lists. The new phase saturations and relative permeabilities are computed (see sections (6.5) and (6.6)) when the system is relaxed. If a new phase is injected then the sorted lists for displacements are re-ordered to account for latest changes in capillary pressures.

6.3 How to Treat the Trapped Clusters, Associated Radii of Curvatures and Displacements

Trapped phases will be in the form of clusters of phase locations. When a cluster of phase locations becomes trapped, *(1)*: A number is assigned to it. *(2)*: The phase of the cluster is stored. *(3)*: Addresses of all the phase locations belonging to it are stored. *(4)*: Two flags are assigned to every single phase location indicating that they are trapped and the the cluster number that they belong to. *(5)*: All the current capillary pressures, i.e. phase pressures, are stored. *(6)*: The volume of the trapped cluster, which is the summation of volume of its phase locations, when it is trapped is stored as the *original* volume of the cluster. The original volume is used in saturation calculations to account for volume errors caused by multiple displacements (see section (6.5)). *(7)*: If any of the phase locations of the cluster is involved in a displacement then it is moved to an appropriate sublist in one of the multiple displacement search categories. This could be a move from the main sorted

lists to the categories listed in Tables (6.2) and (6.3). If any of the phase locations is involved in displacements that are already in the search categories listed in Tables (6.2) and (6.3), then they need to be moved into corresponding categories in Table (6.4).

Every multiple displacement search category may contain several sorted sublists. Every sorted sublist within the categories named in Tables (6.2) and (6.3) has a cluster number associated with it and contains the threshold pressure of the valid displacements where a trapped cluster can displace continuous fluid or vice versa. Categories listed in Table (6.2) contain displacements where the displaced phase location is trapped while the categories named in Table (6.3) have the opposite situation. All the sublists are always sorted in ascending order. One should note that the sublists within each category are completely *independent* from each other.

During different three-phase processes, there may be cases where a trapped cluster touches one, two or several other trapped clusters with different phases. WAG flooding with several injection cycles is an example of such a case. The touching points represent displacements whose threshold pressures are stored in sublists within categories tabulated in Table (6.4). For every displacement both displacing and displaced phase locations are trapped. One trapped cluster might be involved in several sublists as every sublist represents the touching points between only *two* trapped clusters with different fluids. For every sublist displacing and displaced cluster, numbers are also stored.

When a trapped cluster forms, the curvature of all interfaces associated with it need to be kept fixed as long as the cluster is trapped and it has not become involved in multiple displacements. The conventional method in previously developed network models was that the interfaces were considered *frozen*. This was done regardless of the pressure of the phase inside the trapped cluster and pressures of the surrounding fluids. In this work, the pressure of the fluid inside the cluster is *not* a dummy value. It has a physical meaning during the modelling of different processes. The initial pressure of the cluster is the pressure of the phase when it was first trapped. However, the pressure of the cluster changes according to the change in the pressure of the surrounding phases in order to maintain the curvature of the interfaces at the same value as when the trapped cluster first formed. As an example, imagine water flooding into oil in a water-wet system. Trapped clusters of oil form at different stages of water injection, i.e. at different oil/water capillary pressures. Once each trapped cluster forms, it gets the current pressure of oil, i.e. P_{oil}. But since P_{oil} is fixed during water flooding, all the trapped clusters will have

the same oil pressure regardless of when they have trapped while the water pressure is increasing. To deal with this problem, we update the pressure of the trapped oil clusters according to the increase in pressure of water using:

$$P_{i,\,new}^{cluster\,k} = P_{cij}^{cluster\,k} + P_{j,\,new} \tag{6.3}$$

or

$$P_{j,\,new}^{cluster\,k} = P_{i,\,new} - P_{cij}^{cluster\,k} \tag{6.4}$$

where $P_{cij}^{cluster\,k} = (P_{i,\,old}^{cluster\,k} - P_{j,\,old})$ or $P_{cij}^{cluster\,k} = (P_{i,\,old} - P_{j,\,old}^{cluster\,k})$ is the capillary pressure exactly at the moment that the trapped cluster k formed. For the above water flooding example, it becomes:

$$P_{oil,\,new}^{cluster\,k} = (P_{oil,\,old}^{cluster\,k} - P_{water,\,old}) + P_{water,\,new} \tag{6.5}$$

The change in pressure of the trapped clusters affects on the selection of the most favorable multiple displacement as we shall describe later.

6.3.1 Coalescence

During different three-phase processes, trapped clusters may have to move under multiple displacement mechanisms in order to predict a physically correct occupancy. It is quite often the case that the moving trapped clusters meet other trapped clusters of the same phase. This will lead to a *coalescence* event. A coalescence event might also happen when a trapped cluster starts forming layers, if it is possible, between phase locations of the two other phases in the neighbouring pores and throats. Layer reformation allows the trapped clusters to extend their margins and meet other trapped clusters. This phenomenon is very well known when gas injection is carried out into water flood residual oil in a water-wet system [60, 62, 64, 65, 292]. But there are some subtleties associated with coalescence. It may well be the case that the merging trapped clusters have different pressures and volumes, as they might have been trapped at different times during different processes. In such circumstances, we assume that after coalescence the resultant trapped cluster has a *volume weighted* average pressure of the the merging trapped clusters. The *original* volume of the merging trapped clusters may be used in an average pressure calculation as follows:

$$P^{cluster} = \frac{\sum_{k=1}^{n} V_{original}^{cluster\,k} \times P^{cluster\,k}}{\sum_{k=1}^{n} V_{original}^{cluster\,k}} \tag{6.6}$$

where n is the number of merging trapped clusters.

The calculated average pressure of the newly formed trapped cluster is used in saturation calculations and also for multiple displacements. The volume of the trapped cluster formed by coalescence is given by:

$$V^{cluster} = \sum_{k=1}^{n} V_{original}^{cluster\,k} \tag{6.7}$$

When coalescence happens, all the phase locations of the merging trapped clusters are stored together and are assigned the same cluster number. If there are groups of displacements in categories listed in Tables (6.2) and (6.4) that any of the merging clusters were involved in, their threshold pressures are changed according to the new average pressure of the resultant trapped cluster. This is done by:

$$P_{i,\,new}^{threshold} = P_{j,\,new}^{cluster} + P_{i,\,old}^{threshold} - P_{j,\,old}^{cluster\,k} \tag{6.8}$$

or

$$P_{j,\,new}^{threshold} = P_{i,\,new}^{cluster} - P_{i,\,old}^{cluster\,k} + P_{j,\,old}^{threshold} \tag{6.9}$$

For the displacements in the categories listed in Table (6.3), threshold pressures are updated if the pressure of the displaced phase which is continuous changes.

In every multiple displacement search category listed in Tables (6.2), (6.3), and (6.4) all sublists associated with the merging clusters are re-ordered to represent one bigger cluster.

It is often the case that a trapped cluster meets a continuous cluster of the same phase. In such circumstances, the pressure of the continuous fluid is changed to that of the trapped cluster if it is bigger. All the volume error associated with that trapped cluster is ignored as the system is in contact with the inlet and outlet and the volume error would be compensated automatically. Note that this allows the phase pressures to change due to contact with previously trapped clusters. This method to update pressure is similar to the work of Van Dijke *et al.* [154, 155] but different from Fenwick & Blunt [142, 143] who kept the continuous cluster pressure constant. All the displacements associated with the trapped cluster are now transferred to the other lists, i.e. main sorted lists or sublists within search categories, as appropriate.

6.3.2 When a Trapped Cluster Breaks into Smaller Ones

In three-phase systems when multiple displacements take place, a trapped cluster might break into two or more smaller ones. For instance, consider an angular element with trapped oil in the centre that is invaded by gas. It is possible that the displaced trapped cluster cannot leave oil layers in the corners of the element and this might disconnect the other phase locations of the displaced trapped cluster that are residing in the neighbouring elements. This might also happen, for instance, when an existing layer phase location which is a member of a trapped cluster collapses.

After every multiple displacement, it must be checked if it has caused any *local* disconnection among the phase locations of the displaced trapped cluster(s) residing in neighbouring elements. If this has happened, it does not necessarily mean that the displaced clusters have broken into smaller ones as the phase locations might be connected to each other through other routes in the network, or the displaced phase location that has caused the local disconnection might simply be the dead end of a branch of the trapped cluster. If a break has happened then the number of the resultant smaller clusters and their members are determined and stored using the clustering algorithm described in section (6.1.2).

When a trapped cluster breaks into two or more smaller trapped clusters, the pressure of the smaller clusters are assumed to be *exactly the same* as that of the mother cluster at the time when the break took place. Now since the smaller trapped clusters have their own new independent identity, all the displacements associated with the mother trapped cluster in the different multiple displacement search categories must be distributed among the smaller clusters based on which cluster the trapped phase location involved in every displacement is associated with. The original volume of the mother cluster is assigned to the largest of the smaller clusters. The volume of the other clusters is set to zero. This does not create any problem as we shall show in section (6.5).

6.4 Multiple Displacements

One unique feature of three-phase flow at the pore level is multiple displacement. An invasion of phase j by phase i may be composed of a series of displacements starting with a displacement where i is the displacing fluid and ending with a displacement where j is the displaced fluid. If all the phases are continuous, this is simply equivalent to separate single displacements. However, the intermediate phases in the chain may be trapped. This means that a cascade of trapped clusters

nudge each other before a final displacement of a continuous phase. Trapped clusters of the intermediate phases can rearrange themselves in the pore space and/or reform layers, and may coalesce with other trapped clusters of the same phase to make bigger trapped clusters or become continuous by meeting continuous clusters. This happens simply due to capillary forces. Multiple displacements that involve more than one intermediate stage are only possible if there are trapped clusters of at least two phases [154]. If only one phase has any trapped clusters, a simpler version of multiple displacement, *double displacement*, may take place and this has been observed in micromodel experiments [64, 69, 72, 266] and coded into network models [140, 142, 143, 154], where one phase invades part of a trapped cluster that in turn displaces the third continuous phase.

Six possible double displacements are possible [142]. Table (6.5) lists all the possible cases for strongly water-wet system and Figs. (6.2)-(6.4) schematically illustrate three of them. Likewise, six double displacements can be considered in weakly and strongly oil-wet systems. They are tabulated in Tables (6.7) and (6.6), respectively.

Table 6.5: Possible double displacements in strongly water-wet systems.

No.	Mechanism	Type
1	Gas Displaces Oil Displaces Water	Double Drainage
2	Gas Displaces Water Displaces Oil	Drainage-Imbibition
3	Oil Displaces Gas Displaces Water	Imbibition-Drainage
4	Water Displaces Oil Displaces Gas	Double Imbibition
5	Water Displaces Gas Displaces Oil	Imbibition-Drainage
6	Oil Displaces Water Displaces Gas	Drainage-Imbibition

Table 6.6: Possible double displacements in strongly oil-wet systems.

No.	Mechanism	Type
1	Water Displaces Gas Displaces Oil	Double Drainage
2	Water Displaces Oil Displaces Gas	Drainage-Imbibition
3	Gas Displaces Water Displaces Oil	Imbibition-Drainage
4	Oil Displaces Gas Displaces Water	Double Imbibition
5	Oil Displaces Water Displaces Gas	Imbibition-Drainage
6	Gas Displaces Oil Displaces Water	Drainage-Imbibition

Here we present a search algorithm that is capable of finding the most favorable multiple displacement. In this work, we use it to find the most favorable double

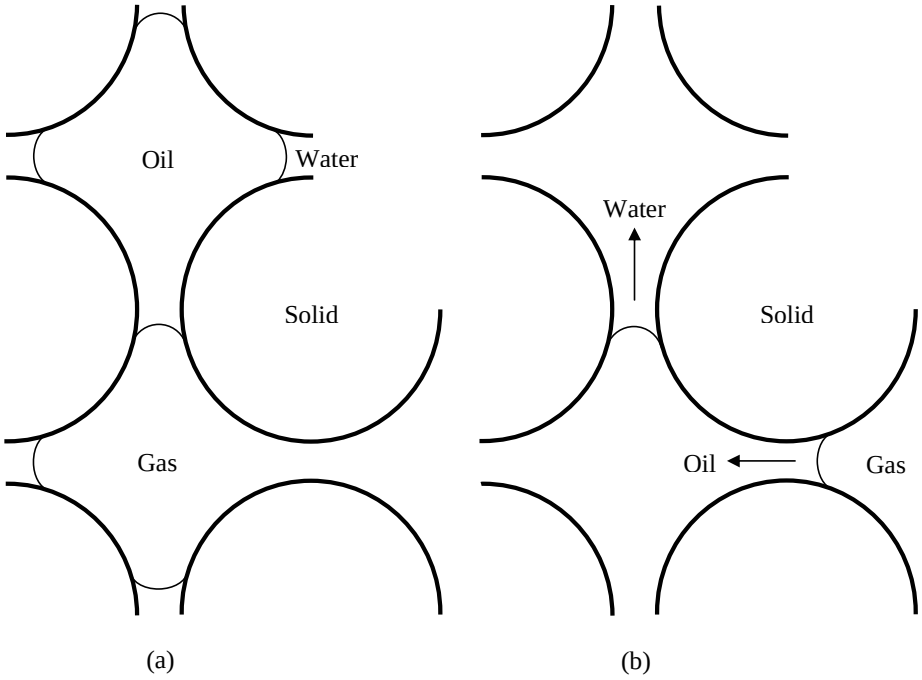

Figure 6.2: Double drainage in water-wet systems, (a) Trapped oil is in contact with water and gas in neighbouring elements, (b) Gas displaces oil which in turn displaces water [142].

Table 6.7: Possible double displacements in weakly oil-wet systems.

No.	Mechanism	Type
1	Gas Displaces Water Displaces Oil	Double Drainage
2	Gas Displaces Oil Displaces Water	Drainage-Imbibition
3	Oil Displaces Gas Displaces Water	Imbibition-Drainage
4	Oil Displaces Water Displaces Gas	Double Imbibition
5	Water Displaces Gas Displaces Oil	Imbibition-Drainage
6	Water Displaces Oil Displaces Gas	Drainage-Imbibition

displacement only. During each process, the most favorable double displacement is compared with the most favorable single displacement. The one that requires the lower pressure of the injection phase is the one that takes place. In order to find the most favorable double displacement, all the possible double events for all the trapped clusters in the system need to be considered.

The algorithm for considering such events is somewhat involved, since multiple events for all clusters need to be considered [154]. Here we present how the most favorable multiple displacement is found every time:

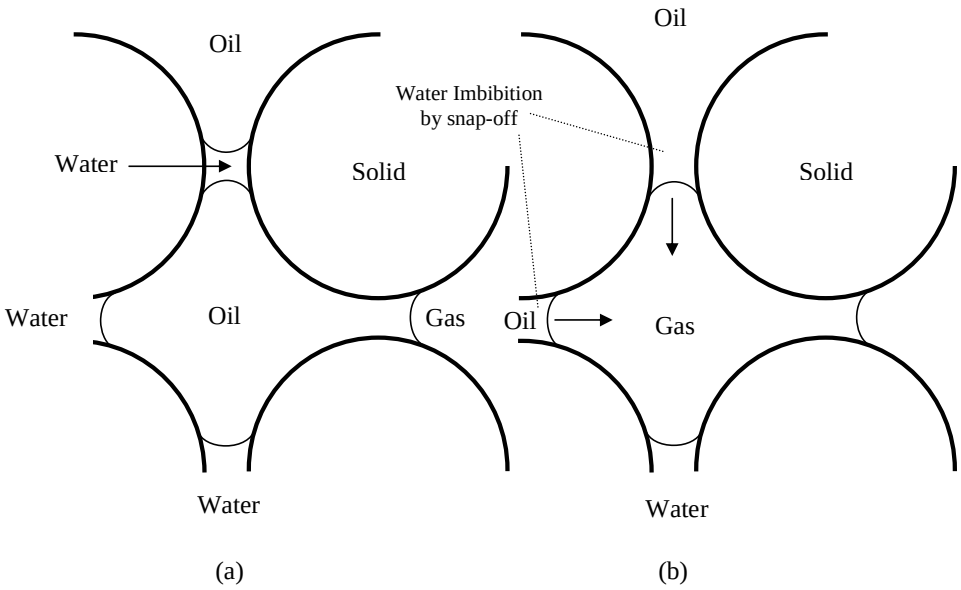

Figure 6.3: Double imbibition in water-wet systems, (a) Water imbibes into trapped oil which contacts gas, (b) Oil in turn displaces gas [142].

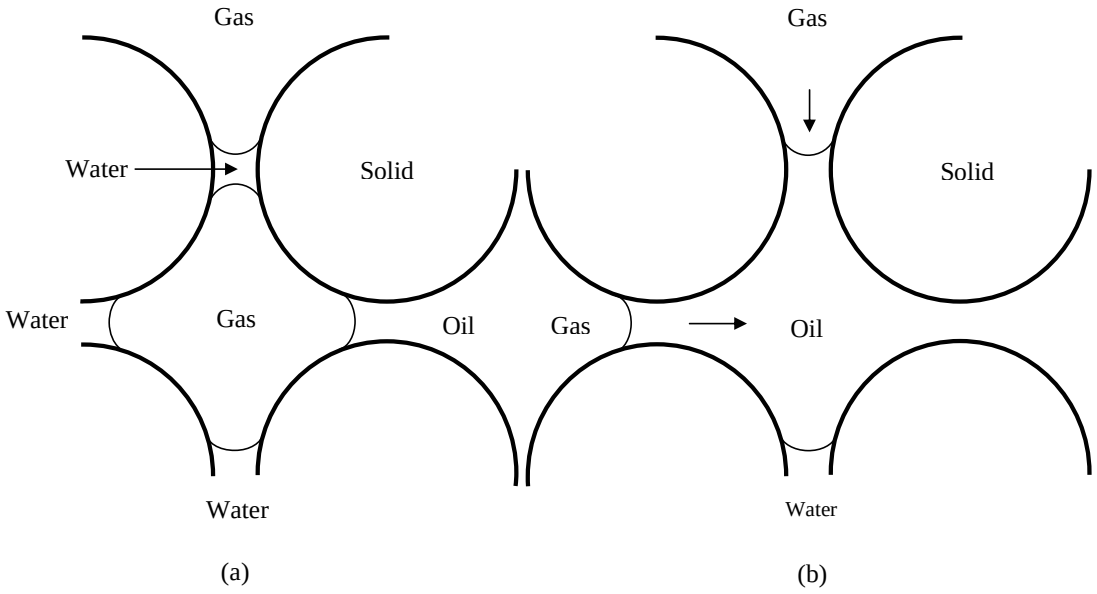

Figure 6.4: Imbibition-drainage in water-wet systems, (a) Water imbibes into trapped gas which contacts oil, (b) Gas in turn displaces oil.

First, based on what fluid is being injected into the system, the two categories from Table (6.2) that have the same displacing fluid as the injection fluid are considered and called *starting* categories. For instance, categories *gcwt* and *gcot* are considered (c indicates continuous and t trapped) when gas is being injected. Now all

the categories that could chain up with the starting categories are determined from Tables (6.2), and (6.4) and are called *chain-categories*. Chain-categories for *gcwt* and *gcot* would be *wtot*, *wtoc*, *wtgt*, *wtgc*, *otwt*, *otwc*, *otgt*, and *otgc*. As mentioned earlier, every category might include several sublists with one or two trapped cluster numbers associated with each one. The displacements at the top of each sublist within the starting categories can now chain up with the displacements at the top of the sublists within the chain-categories, if there are any, provided that the displacing trapped cluster number of the sublist within the chain-category is the *same* as the displaced trapped cluster number of the sublist within the starting category. This means that every trapped cluster involved in a multiple displacement contributes to two displacements. One should note that the displaced phase of a category must be always the same as the displacing phase of the category that it is going to chain up with. The displacement at the top of each sublist is the easiest, i.e. lowest invasion pressure, displacement of the sublist. So every multiple displacement is a chain of easiest displacements from sublists within categories that are allowed to chain up with each other. Chaining up with categories continues until the next category is one of those tabulated in Table (6.3). For example, the chain of *gcot*, *otwt*, *wtgt* and *gtwc* could give multiple displacements provided that sublists satisfying the foregoing conditions exist within the above categories. This in turn means that oil, water, and gas trapped clusters existed in the system. Continuous gas is touching trapped oil clusters which in turn touch trapped water clusters which in turn touch trapped gas clusters which in turn touch continuous water. For a multiple displacement with n trapped clusters involved, a series of $n+1$ chainlike displacements are carried out. Using the foregoing algorithm, all the possible multiple displacements are determined and their threshold absolute pressure are calculated using:

$$P_{i,\,MD}^{threshold} = P_i^{threshold} + \sum_{k=1}^{n} [(P_j^{threshold})^{cluster\,k} - P_{j,\,old}^{cluster\,k}] \tag{6.10}$$

where n is the number of trapped clusters involved, MD stands for multiple displacement, $P_i^{threshold}$ is the threshold pressure of the first displacement of the multiple displacement where the injection fluid is the displacing fluid, j is the fluid that cluster k accommodates, $(P_j^{threshold})^{cluster\,k}$ is the threshold absolute pressure of the displacement for which trapped cluster k is the *displacing* fluid, and $P_{j,\,old}^{cluster\,k}$ is the *old* pressure of the trapped cluster k, i.e. before the multiple displacement. Eq. (6.10) has been derived by summing up the threshold capillary pressures of all the displacements. One should note that the threshold capillary pressure of each

displacement in a multiple displacement is calculated using a contact angle that is defined according to what fluid is displacing what, *regardless* of what fluid is being injected into the system. When a multiple displacement is carried out pressures of the involved trapped clusters are increased to the value given by:

$$P_{j,\,new}^{cluster\ k} = (P_j^{threshold})^{cluster\ k} \tag{6.11}$$

We give an example of applying this algorithm by considering a double displacement which is used in this work. Imagine gas is being injected into oil and water where some of the oil is in trapped clusters. Since there are only trapped oil clusters the only possible multiple displacement is double displacement where continuous gas displaces trapped oil which in turn displaces continuous water. The double displacements are determined by chaining up categories *gcot* and *otwc* provided that the required sublists are present within each category. The threshold capillary pressure of the double displacement is:

$$P_{gas,\,DD}^{threshold} = P_{gas}^{threshold} + [(P_{oil}^{threshold})^{cluster} - P_{oil,\,old}^{cluster}] \tag{6.12}$$

where DD stands for double displacement. The new pressure of the trapped oil cluster is:

$$P_{oil,\,new}^{cluster} = (P_{oil}^{threshold})^{cluster} \tag{6.13}$$

Once a multiple displacement is recognized as a *global* most favorable event, it is carried out. But there is one subtlety involved. It is quite often the case that $P_{i,\,MD}^{threshold}$ is smaller than P_i. In other words, the multiple displacement could be carried out without any increase in pressure of phase i. The difference between these two pressures needs to be accounted for in the pressures of trapped clusters involved in multiple displacement by increasing them by $(P_i - P_{i,\,MD}^{threshold})$.

When it comes to calculate the threshold pressure of a multiple displacement, one may use threshold pressures of the displacements involved regardless of their type. This means that displacements may well be layer formation or collapse events. Theoretically this is fine but not *technically*. *(I)* This approach might increase the volume error associated with multiple displacement as piston-like, pore-body filling and snap-off events might chain up with the layer formation or collapse events which would obviously be detrimental for volume-mass conservation. *(II)* The simulator might be trapped in an infinite loop of forming and collapsing layers. To prevent these problems, we shall use a slightly different approach where only threshold pres-

sures of piston-like, pore-body filling and snap-off events are used in calculating the threshold pressure of a multiple displacement. In this approach, when a multiple displacement is to be carried out, all the layer formation or collapse events in the involved sublists that are *more favorable* to the displacements used in $P_{i,MD}^{threshold}$ calculations, are carried out *first*.

As we mentioned earlier, when a multiple displacement is taking place, pressures of the involved trapped clusters increase. Once this happens, we then *update all* the AM's associated with the trapped clusters according to their new pressures. This means that the volumes of the trapped clusters are always kept updated. Also the *new* AM's formed during the multiple displacements will have radii of curvatures according to the new pressures of the trapped clusters that they belong to.

After every multiple displacement event, new displacements that are now available have to be added to the sublists within the correct categories. This means that we might have new chains of displacements, i.e. multiple displacements, for the next round. Also there might be phase locations that must be added to or omitted from the involved trapped cluster(s). For example, imagine a trapped gas cluster is to displace trapped oil in the centre of a triangular throat. Before the displacement, configurations in all the corners are from group B and the centre phase location is a member of a trapped oil cluster. Also imagine corner half angles, contact angles and capillary pressures allow oil to reside as a layer in at least one corner after the oil in the centre is displaced by gas. After the displacement, the configurations in two corners are changed to C and in one corner to F. Once the configurations are changed, the centre phase location must be omitted from the trapped oil cluster and added to the trapped gas cluster as it now accommodates gas. Also one oil layer phase location residing in one of the corners must be added to the displaced trapped oil cluster. The new displacements that must be added to the appropriate lists are: oil layer collapse by water in the corner to be added into the *right* sublist, i.e. the sublist with the same cluster number, within the *wcot* category provided that water in the corner is continuous, oil layer collapse by gas in the centre to be added into the right sublist within the *gtot* category, snap-off of the gas in the centre by oil layer to be added into the right sublist within the *otgt* category, snap-off of gas in the centre by water in the corners to be added into the right sublist within the *wcgt* category and other displacements in connection with continuous and trapped fluids residing in the neighbouring elements.

6.5 Saturation Computation

Saturation is computed when the phase pressure reaches a new maximum - this means that the system is at equilibrium and it is not possible to carry out any displacements with the current phase pressures. If V_p^i is the volume of phase p in element i (including the water volume in clay) then the saturation of phase p is given by:

$$S_p = \frac{\sum_{i=1}^{n_e} V_p^i + V_p^{error}}{\sum_{j=1}^{n_p} \sum_{i=1}^{n_e} V_j^i + \sum_{j=1}^{n_p} V_j^{error}} \tag{6.14}$$

where n_p is the number of phases, n_e is the total number of pores and throats, and V_p^{error} is the volume error of phase p caused by multiple displacements and is given by:

$$V_p^{error} = \sum_{i=1}^{n_p^c} (V_p^{original} - V_p^{present})_i \tag{6.15}$$

where n_p^c is the number of trapped clusters of phase p. The total volume, inscribed radius, and shape of each element are read in as input data. The volume of a phase in an element is the total volume multiplied by the fraction of the cross-sectional area occupied by that phase. One should note that saturation is computed within the selected region, i.e. between inlet and outlet surfaces of the network rather than over the whole network (see section (6.6) for details). Expressions used to compute areas are given next.

6.5.1 Area Open to Flow

The equations used to compute the total area of a pore or throat with different cross-sections are:

$$A_t = \pi R^2 \qquad Circular\ cross-section \tag{6.16}$$

$$A_t = 4R^2 \qquad Square\ cross-section \tag{6.17}$$

$$A_t = \frac{R^2}{4G} \qquad Triangular\ cross-section \tag{6.18}$$

where R and G are the inscribed radius and shape factor of the pore or throat, respectively.

The corner area open to flow is calculated using:

$$A_c = r^2[\cos\theta(\cot\alpha\cos\theta - \sin\theta) + \theta + \alpha - \frac{\pi}{2}] \tag{6.19}$$

$$A_c = \left[r\frac{\cos(\theta+\alpha)}{\sin\alpha}\right]^2 \sin\alpha\cos\alpha \qquad if \quad \alpha+\theta = \frac{\pi}{2} \tag{6.20}$$

where r is the radius of curvature which corresponds to the ratio of interfacial tension to the capillary pressure of the interface, α is the corner half angle and θ is the angle that the interface makes with the solid surface towards the corner not necessarily the contact angle of the interface, e.g. θ_I and θ_{II} in Fig. (6.5).

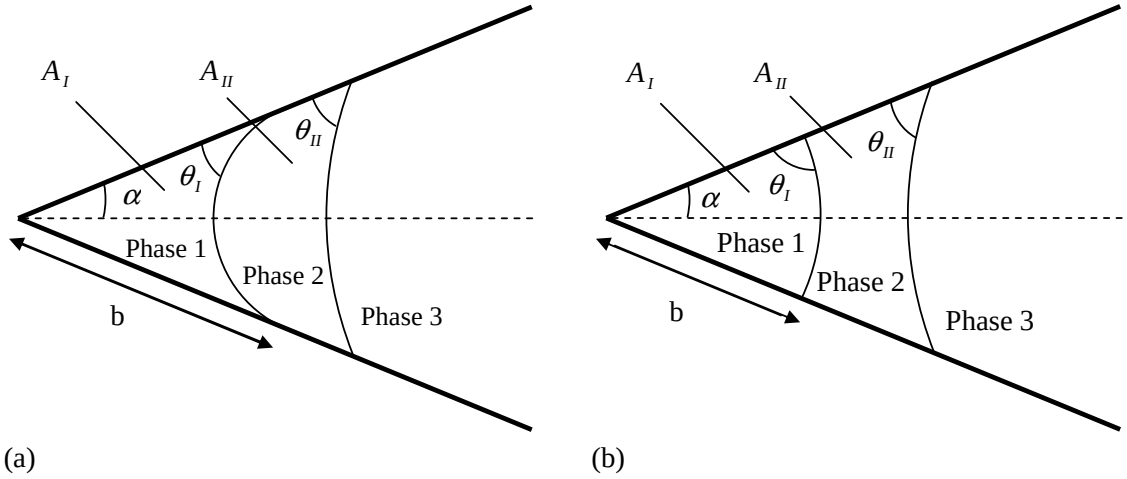

Figure 6.5: Corners with a sandwiched layer, (a) positive first interface (b) negative first interface.

If a layer is present in the corner, the layer area is the total area of the corner including the layer minus the corner area excluding the layer and both are calculated using Eqs. (6.19) and (6.20) but with pertinent r and θ. For instance, in configuration group F, first the total corner area, $A_c = A_{w\,corner} + A_{o\,layer}$, is calculated with r and θ of the gas/oil interface and then $A_{w\,corner}$ is found using r and θ of the oil/water interface. Then $A_{o\,layer} = A_c - A_{w\,corner}$. The same procedure is used to calculate the area of the the second layer, if present.

The area open to flow to a phase in the centre of an angular element is the total area of the element minus the summation of the corner areas, including the layers (if present).

6.6 Conductances - Absolute and Relative Permeabilities

When saturation is computed, relative permeability and capillary pressure can also be found. This is not done after every saturation computation to save computer time. Typically, relative permeability is calculated around 20 - 40 times during a simulation. To compute absolute and relative permeability, conductances of each continuous phase location in each element are first computed. Normally exact analytic results are not possible, and empirical expressions derived from solutions of the Stoke's equation for flow in pores of different geometries and for different fluid configurations are used [76–78, 127, 264, 293, 294]. See later for expressions for the conductances of each phase for the configurations shown in Figs. (5.1) and (5.2). Then the average conductance for each phase in the whole network is computed by explicitly calculating the flow through the network assuming conservation of volume. From this absolute and relative permeability can be found [77, 127, 142, 290].

Solving the system of linear equations for each phase gives the pressure of that phase in all the pores that contain that continuous phase. If there is an interface between any of the phases in a pore or between the pore and connected throats then the difference between the pressures of those two phases in that pore corresponds to capillary pressure between those two phases [146].

In order to minimize *end* effects on calculated macroscopic properties, we calculate the properties within two surfaces perpendicular to the main flow direction bounding the central 90% of the network. However, the pressure is solved over whole network to find the pressure in each pore. The pressure of the fluid whose permeability is being calculated is found at the two surfaces by:

$$P_a = \frac{\sum_{i=1}^{n} P_a^i \, A_a^i}{\sum_{i=1}^{n} A_a^i} \tag{6.21}$$

where P_a is the pressure of phase a at the surface, P_a^i is the pressure of phase a in a pore or throat at the point that touches the surface, A_a^i is the area open to flow for phase a through that pore or throat, and n is the number of pores and throats touching the surface. When the element that touches the surface is a pore then the pressure of the phase a at the touching point will be the pore pressure of fluid a and is known after the pressure is solved over the whole network. But if it is a throat, then the pressure at the touching point is found by a *linear interpolation* between the pressures of phase a in two connecting pores located in two sides of the surface.

This is similar to the procedure used by Øren *et al.* [77].

The absolute permeability of the network is calculated using Darcy's law:

$$K = \frac{\mu_a \, Q_a^{total} L}{A \Delta P} \tag{6.22}$$

where K is the absolute permeability, μ_a the viscosity of fluid a, L is the distance and ΔP is the corresponding pressure drop between the vertical surfaces. A is the cross-sectional area perpendicular to the main direction of flow, Q_a^{total} is the total flow rate of fluid a.

First it is assumed that the network is completely filled with only one phase, e.g. a. Conductance is calculated using the following equations [77, 281]:

$$g = \frac{0.5GA^2}{\mu} \qquad Circular\ cross-section \tag{6.23}$$

$$g = \frac{0.5623GA^2}{\mu} \qquad Square\ cross-section \tag{6.24}$$

And for triangular cross-sections:

$$g = \frac{3R^2A}{20\mu} \tag{6.25}$$

A pore might be connected to several other pores by throats (see Fig. (6.6)). The conductance of a phase a, through an assembly of two pores connected to each other by a throat, is considered to be the *harmonic* mean of the conductance to the phase through the pores and the connecting throat [142]:

$$\frac{L_{ij}}{g_{ij}^a} = \frac{L_{t_{ij}}}{g_{t_{ij}}^a} + \frac{L_{p_{ij}}}{g_{p_i}^a} + \frac{L_{p_{ji}}}{g_{p_j}^a} \tag{6.26}$$

where L_{ij} is the distance between the centres of two connected pores, g_{ij}^a is the conductance of the assembly to phase a, $L_{t_{ij}}$ is the throat length, $g_{t_{ij}}^a$ the throat conductance to phase a, $L_{p_{ij}}$ and $L_{p_{ji}}$ are the half length of the pores, and $g_{p_i}^a$ and $g_{p_j}^a$ are conductance of the pores i and j to phase a, respectively, see Fig. (6.6).

The flow rate of the phase between two connected pores, i.e. q_{ij}^a is then given by [142]:

$$q_{ij}^a = \frac{g_{ij}^a}{L_{ij}} (P_{p_i}^a - P_{p_j}^a) \tag{6.27}$$

where $P_{p_i}^a$ and $P_{p_j}^a$ are the pressures of fluid a in pores i and j respectively.

Conserving volume for fluid a in each pore gives:

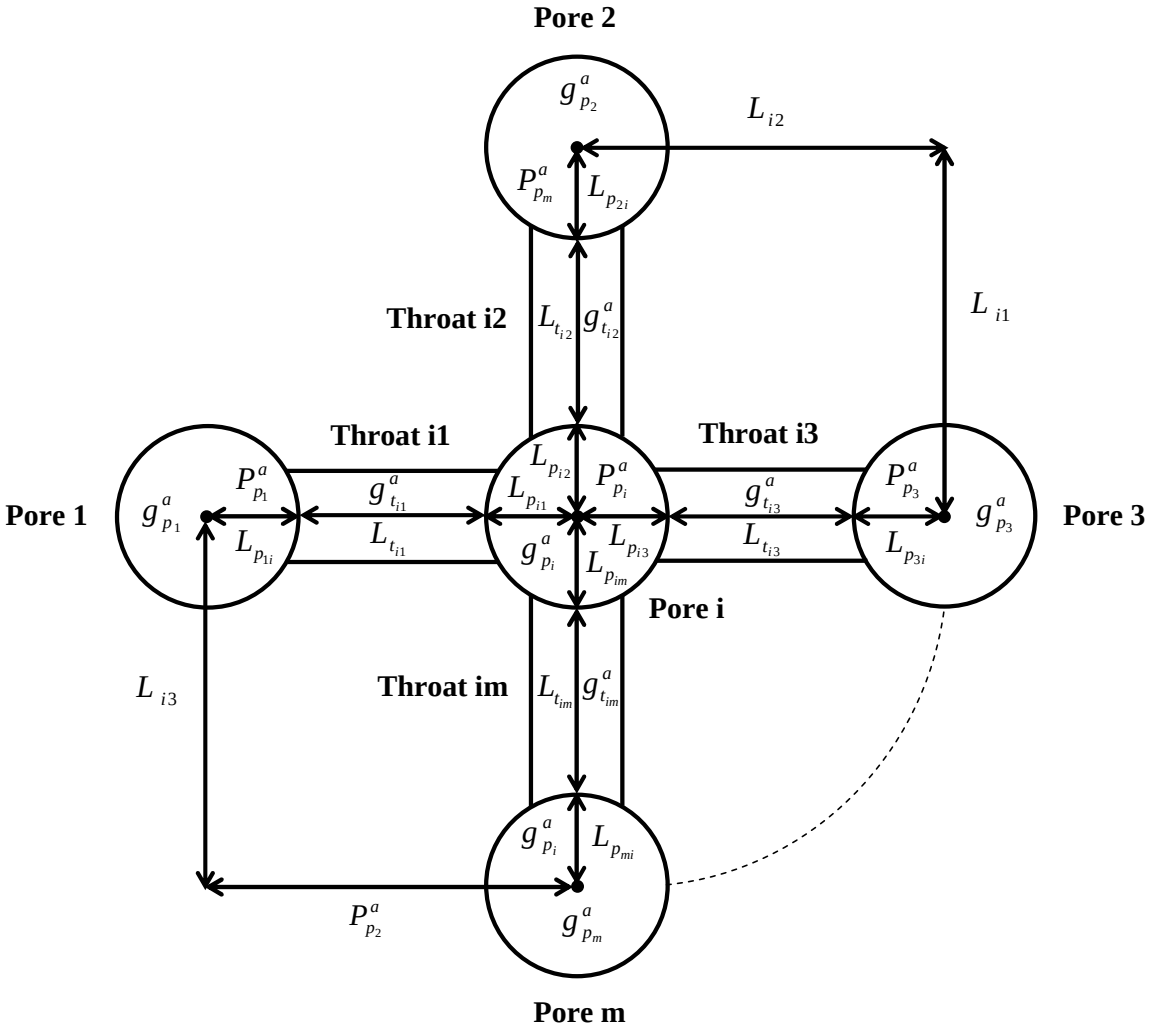

Figure 6.6: Schematic assemblies of pores connected to each other by throats.

$$\sum_{i=1}^{m_i} q_{ij}^a = 0 \tag{6.28}$$

where m_i is the number of connected throat-pores containing continuous phase a. If Eq. (6.26) is written for all such throat-pores and then inserted into Eq. (6.28), a system of linear equations is formed:

$$
\begin{aligned}
P^a_{p_1} \sum_{j=1}^{m_1} \frac{g^a_{1j}}{L_{1j}} - \sum_{j=1}^{m_1} \frac{g^a_{1j}}{L_{1j}} P^a_{p_j} &= 0 \\
P^a_{p_2} \sum_{j=1}^{m_2} \frac{g^a_{2j}}{L_{2j}} - \sum_{j=1}^{m_2} \frac{g^a_{2j}}{L_{2j}} P^a_{p_j} &= 0 \\
&\dots \\
P^a_{p_n} \sum_{j=1}^{m_n} \frac{g^a_{nj}}{L_{nj}} - \sum_{j=1}^{m_n} \frac{g^a_{nj}}{L_{nj}} P^a_{p_j} &= 0
\end{aligned} \tag{6.29}
$$

The resultant system of linear equations for the pore pressures is solved using the *Conjugate Gradient* method [77]. Having the pore pressures allows us to calculate the total flow rate of the phase, i.e. Q^a_{total}, which in turn is used in Eq. (6.22) to calculate the absolute permeability of the network, K.

Relative permeabilities are computed only when the network contains more than one phase. They are calculated only for phases that have at least one network-spanning cluster (a cluster that is continuous from inlet to outlet).

First the conductance in all the pore and throats containing continuous phase a is computed. Then using the same procedure used for the calculation of absolute permeability, the pressures of the phase in the pores that are a member of spanning cluster(s) are found which in turn allows us to calculate relative permeability of the phase by:

$$
k^a_r = \frac{Q^a_{total}}{Q^{single\,phase}_{total}} \tag{6.30}
$$

Relative permeabilities are calculated only when the system is relaxed otherwise there will be configurations that are not stable at the pressure at which the relative permeabilities are calculated. The number of linear equations to be solved will be lower than that for single-phase flow simply because the network is filled by multiple phases meaning that not all the elements might contain continuous phase a.

When a network has elements with non-circular cross-section, a single element might accommodate up to three fluids in it. A fluid, as it was shown in Figs. (5.1) and (5.2), might be residing in corners, layers or the centre of a non-circular element. For the fluid flowing through the centre of an element, Eqs. (6.23), (6.24), and (6.25) are still used with A being only the area open to flow to the fluid at the centre.

Fluid flow through the corners and layers is yet more complex considering the

involved physics. Parameters such as wettability, fluid-fluid and fluid-solid boundary conditions, corner half angle, surface shear viscosity and physical properties of fluids affect the conductances. This have been investigated by several authors. One group has tried to solve the fluid flow numerically using Navier-Stokes equations and then empirically correlate the numerical results and propose expressions for laminar corner flow [77, 112, 293, 295–297]. Another approach is to apply the hydraulic diameter approximation which was used by Lenormand and Zarcone [58] for flow in square cross-section tubes. Blunt *et al.* [68] used a thin film flow approximation to study the oil layer flow regime in a gravity drainage process. Later, Zhou *et al.* [294] combined the hydraulic diameter and the thin film flow approximations to derive expressions for corner and layer flow which were later modified by Hui & Blunt [264, 265]. The proposed expressions were successful in predicting experimental measurements [294, 298]. The authors found free and no-flow boundary conditions suitable for gas/oil and oil/water interfaces, respectively.

In this work, we use the expressions proposed by Hui & Blunt [264, 265] to compute the conductance of wetting and spreading layers.

When $\theta_I \leq \frac{\pi}{2} - \alpha$, see Fig. (6.5)-(a), the conductance of the element to the phase flowing at the corner can be estimated by:

$$g = \frac{A_c^2(1-\sin\alpha)^2(\varphi_2\cos\theta - \varphi_1)\varphi_3^2}{12\mu\sin^2\alpha(1-\varphi_3)^2(\varphi_2 + f\varphi_1)^2} \tag{6.31}$$

$$\varphi_1 = (\frac{\pi}{2} - \alpha - \theta) \tag{6.32}$$

$$\varphi_2 = \cot\alpha\cos\theta - \sin\theta \tag{6.33}$$

$$\varphi_3 = (\frac{\pi}{2} - \alpha)\tan\alpha \tag{6.34}$$

where $\theta = \theta_I$, $A_c = A_I$, $f = 1$ for a no-flow boundary condition suitable for oil/water interfaces, and $f = 0$ when a free boundary condition is applied for gas/oil or gas/water interfaces.

If $\theta_I > \frac{\pi}{2} - \alpha$, see Fig. (6.5)-(b), the corner conductance is calculated using:

$$g = \frac{A_c^2\tan\alpha(1-\sin\alpha)^2\varphi_3^2}{12\mu\sin^2\alpha(1-\varphi_3)(1+f\varphi_3)^2} \tag{6.35}$$

When there is a fluid layer sandwiched between the phases residing in the corner and centre, corner and layer or layer and centre (see Figs. (5.1) and (5.2)), the

conductance of the element to the sandwiched phase can be estimated by:

$$g = \frac{A_1^3(1-\sin\alpha)^2\tan\alpha\varphi_3^2}{12\mu A_c \sin^2\alpha(1-\varphi_3)\left[1+f_1\varphi_3-(1-f_2\varphi_3)\sqrt{\frac{A_2}{A_c}}\right]^2} \tag{6.36}$$

where A_1 is the area of the layer that the conductance is being calculated for, A_c is a summation of areas of corner and layer (if present) above the layer of interest, and $A_2 = A_c - A_1$. For instance, to calculate the conductance of the gas layer in configuration group J, see Fig.(5.2), $A_1 = A_{g\,layer}$, $A_c = A_{w\,corner} + A_{o\,layer} + A_{g\,layer}$, and $A_2 = A_{w\,corner} + A_{o\,layer}$. The corner and layer areas are calculated using Eqs. (6.19) and (6.20).

6.7 Saturation Path Tracking

As several authors have shown (see section (3.1)), macroscopic properties in three-phase systems are strongly dependent on the saturation history of the system. This means that prediction of experimental measurements is possible only if the experimental saturation history is reproduced by the model. It is only then that the computed properties are comparable with their experimental counterparts. In this work, we present an algorithm to track the experimental saturation paths on a point by point basis.

Every given saturation path is composed of a series of points in saturation space. The first saturation target (of oil, water, and gas) is specified. The difference between the present saturations and the target saturations are found. The phase with the most *negative* difference is the next to be injected. Imagine this is phase i. This means that we consider a displacement where the volume of i in an element increases. Injection of phase i continues until the difference between the present and the target saturation of phase i is not the most negative difference. Another phase with the most negative difference is then injected. This continues until the saturation differences fall within a predefined tolerance. Then a new saturation target is considered. This process continues until the desired saturation path is produced, see Fig. (6.7).

Tracking an experimental path using a network model is practically very complex and difficult. This is because of finite size effects, the percolation nature of the processes and hysteresis. For instance, in some cases during a saturation tracking procedure, the system does not *relax* before several thousand displacements have been performed which will take the saturations far away from the desired path.

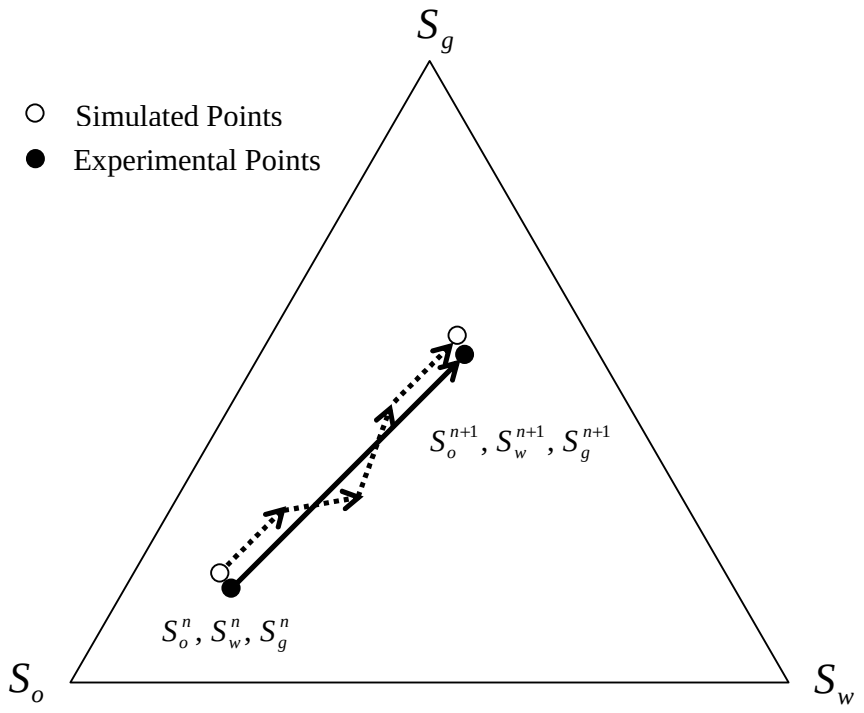

Figure 6.7: Schematic presentation of saturation tracking method.

However, in the cases we present in this work, this does not significantly affect the results.

Chapter 7

Two- and Three-Phase Relative Permeabilities

7.1 Comparison with Experiment

In this section, we use our model to simulate different two- and three-phase processes at the pore-level and compare the results with their experimental counterparts.

The experiments we compare against will be two- and three-phase steady-state measurements of relative permeability performed by Oak on water-wet Berea sandstone [1]. The fluids used by Oak were dodecane with 10% iodooctane, brine, and air (nitrogen). Oak did not measure interfacial tensions. Pure dodecane/water/air systems have a negative spreading coefficient; however it is known that the presence of even small amounts of other alkanes in the oil can affect the spreading behaviour significantly [245]. The low oil saturations reached in Oak's experiments indicate a spreading system as assumed by other authors who have studied this data [53, 149]. Consequently in this section we will use interfacial tensions for a spreading hexane/water/air system – Table (7.1). These values are likely to be similar to those in the experiments – small changes in the interfacial tensions, as long as the system remains spreading, have a negligible impact on the results.

Oak studied three cores with permeabilities of 1000 mD, 800 mD, and 200 mD. Our network has a permeability of 3055 mD (Table (4.2)). Oak found that the measured two-phase relative permeabilities for the least permeable core were different from the other two. In our study we will only compare against data from the two more permeable cores since their permeability and hence pore structure is likely to be more representative of our network.

Table 7.1: Interfacial tensions and spreading coefficient (mN/m) used in this work [264, 298].

Fluids	σ_{ow}	σ_{go}	σ_{gw}	C_s
Hexane-water-air	48	19	67	0

7.1.1 Two-Phase Simulations/Primary Drainage

During primary drainage, the receding contact angle is assumed to be 0°; in predicting Berea data there are no other parameters to adjust. Fig. (7.1) shows the prediction against experimental data for oil/water, gas/oil, and gas/water drainage. The predictions are excellent and similar to those obtained using a two-phase net-

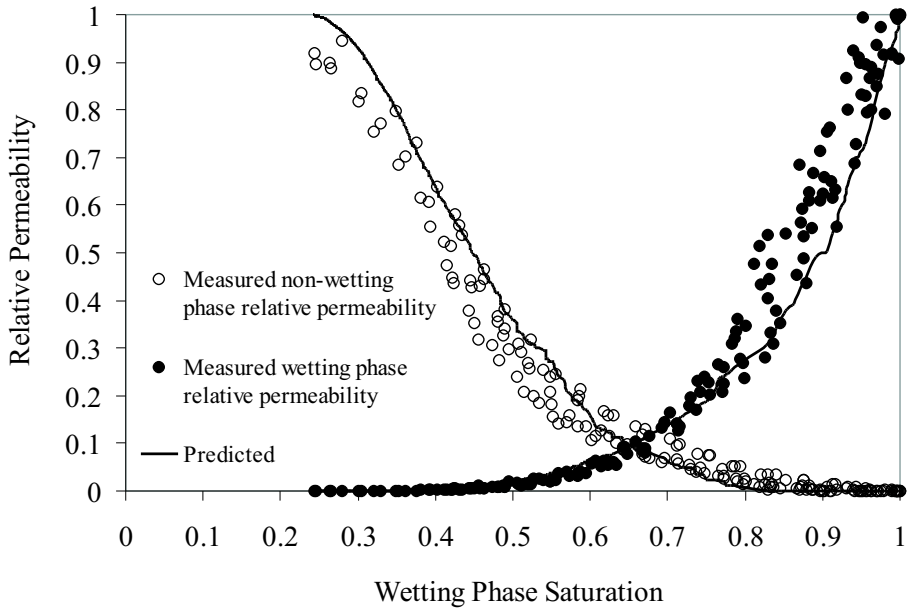

Figure 7.1: Comparison of experimental [1] and predicted relative permeabilities during primary drainage in Berea sandstone.

work model by Valvatne & Blunt [134, 135]. If we have a good representation of the pore structure and the displacement physics is straightforward, we can readily make reliable predictions.

7.1.2 Two-Phase Simulations/Imbibition

To predict imbibition data, we assumed a uniform distribution of advancing contact angles. In all cases the initial condition was an irreducible saturation of the wetting

phase, with all possible pores and throats occupied by non-wetting phase at the end of primary drainage.

In imbibition there is a competition between pore-body filling and snap-off. A large aspect ratio (pores much larger than throats) and a low contact angle favors snap-off leading to a large trapped non-wetting phase saturation. As the contact angle increases, there is less trapping as the displacement is more connected [55, 104]. We adjusted the range of contact angle to match the trapped non-wetting phase saturation at the end of imbibition. The advancing oil/water and gas/oil contact angles were in the range $63^\circ - 80^\circ$ and $30^\circ - 70^\circ$ respectively. These values are representative of effective contact angles on microscopically rough surfaces [32, 254]. Furthermore, we expect oil to be more wetting in the presence of gas than water in the presence of oil, since there are virtually no molecular interactions between gas and oil. The results are shown in Figs. (7.2) and (7.3). Small changes in the

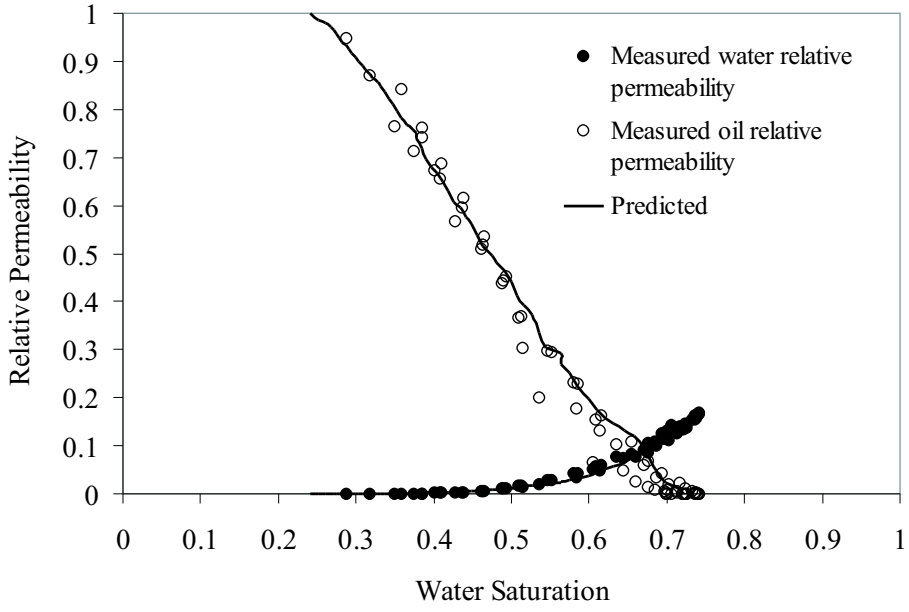

Figure 7.2: Comparison of measured [1] and predicted oil/water two-phase relative permeabilities for imbibition in Berea sandstone.

contact angle distribution did not adversely affect the match with experiment. With a representative range of contact angle we are able to predict relative permeabilities in imbibition.

As discussed in chapter (2) in three-phase flow once two contact angles are known, the third can be predicted using Eq. (2.6). Eq. (2.6) was used to find the advancing gas/water contact angles from the advancing oil/water and gas/oil values and

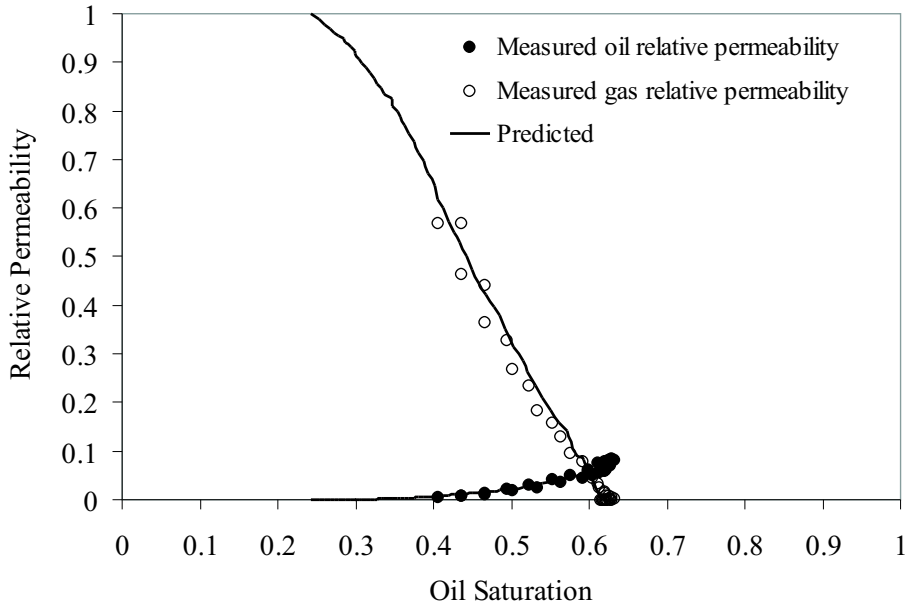

Figure 7.3: Comparison of measured [1] and predicted two-phase gas/oil relative permeabilities for imbibition in Berea sandstone.

these were used in a simulation of water displacing gas. The advancing gas/water contact angle was distributed between 55.2°-77.2°. Water in the presence of gas is less wetting than oil in gas, but more wetting than water in oil. The comparison of predicted and measured relative permeabilities is shown in Fig. (7.4). The predictions are excellent. However, the two-phase experimental imbibition data were not necessarily measured in the presence of the third phase, which means that using Eq. (2.6) to find the gas/water contact angles may not be appropriate.

Table 7.2: Contact angles (degrees) used to predict the experiments.

$\theta_{ow}^{PrimaryDrainage(PD)}$	θ_{gw}^{PD}	θ_{ow}^{r}	θ_{ow}^{a}	θ_{go}^{r}	θ_{go}^{a}	θ_{gw}^{r}	θ_{gw}^{a}
0	0	43-60	63-80	10-50	30-70	36.6-57.3	55.2-77.2

7.1.3 Three-Phase Simulations

We will now predict three-phase relative permeability. We use the same advancing contact angles as for two-phase flow. We assume that the receding contact angles are 20° lower than the advancing values, which is a typical amount of hysteresis for water-wet media [32]. The contact angles used are given in Table (7.2).

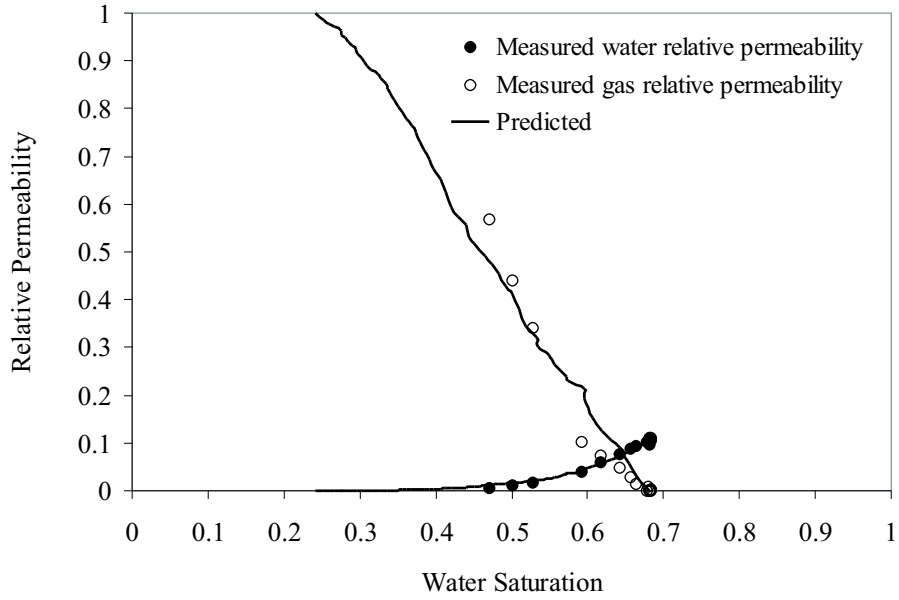

Figure 7.4: Comparison of measured [1] and predicted two-phase gas/water relative permeabilities for imbibition in Berea sandstone.

1. General Behaviour

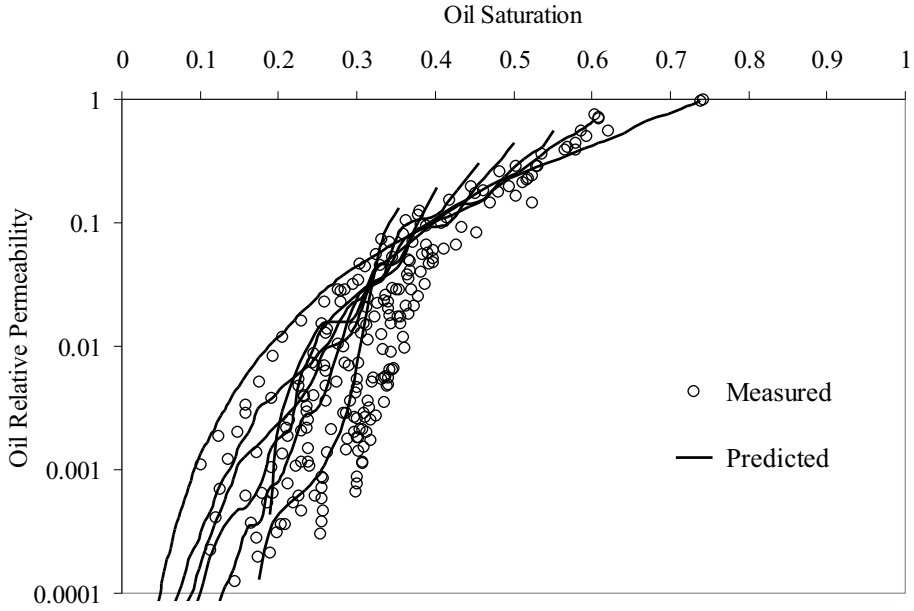

Figure 7.5: Comparison of measured [1] and predicted three-phase oil relative permeability during gas injection.

Fig. (7.5) shows a comparison of predicted three-phase oil relative permeability during gas injection with the measured steady-state values published by Oak [1]. The predicted results are produced by simulating tertiary gas injection into different initial oil saturations after water flooding maintaining a constant oil/water capillary pressure. The experimental data and predictions are scattered in a similar manner. The scatter arises because in a water-wet system oil is the intermediate-wet phase and its relative permeability is a strong function of saturation history and initial oil saturation [151–153, 264, 265]. These predictions are similar to those obtained using a water-wet three-phase network model by Lerdahl *et al.* [149].

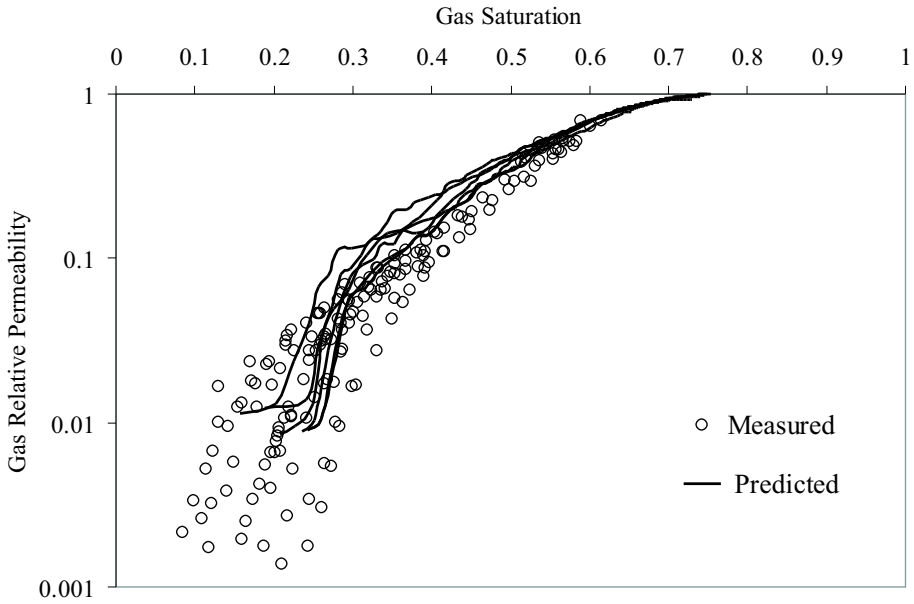

Figure 7.6: Comparison of measured and predicted three-phase gas relative permeability during gas injection.

Fig. (7.6) illustrates the comparison between predicted and measured three-phase gas relative permeability. Again the predictions are in good agreement with the measured values. At high gas saturation, predictions and experimental data are not very scattered because gas is the most non-wetting phase in a water-wet system, and its relative permeability is a function of only its own saturation. However, the measured values at low gas saturations are quite scattered and this is because of difficulties in the experiments [1, 149]. Predicted values at low gas saturation are zero due to finite size effects. This is again similar to the results of Lerdahl *et al.* [149].

Fig. (7.7) presents the comparison between predicted three-phase water relative

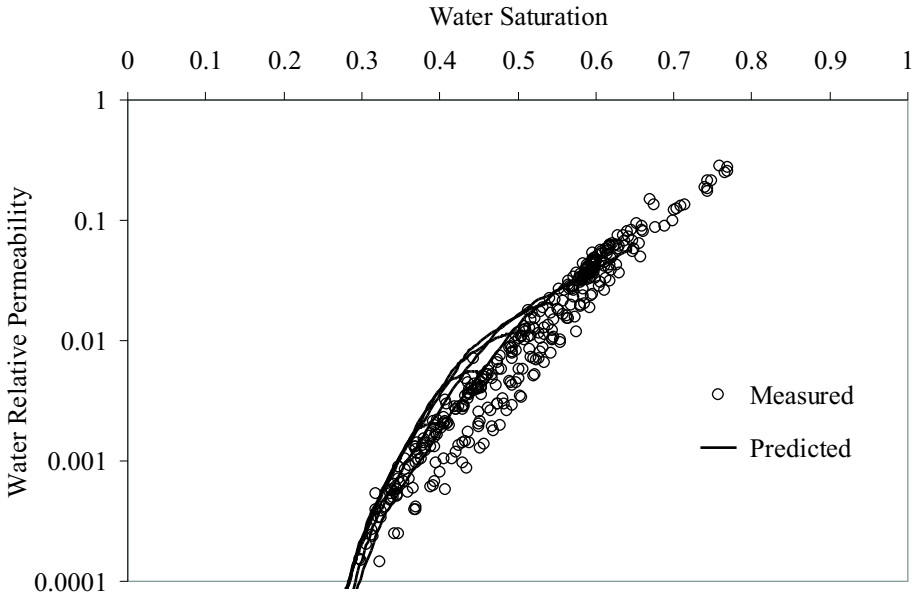

Figure 7.7: Comparison of measured and predicted three-phase water relative permeability during gas injection.

permeability and measured values. The water relative permeability is slightly overestimated. The reason for this is not known, but it may be due to measurement difficulties. In water-wet systems the water relative permeability is expected to be a function of only its own saturation and similar to two-phase values. Recall that we predict the two-phase water relative permeabilities accurately.

While these results are very encouraging, we are comparing two clouds of points with considerable scatter. In the next section we go one step further and attempt a more rigorous analysis by comparing experiments on a point-by-point basis.

2. Comparison with Experiment Using Saturation Tracking

We apply our saturation tracking algorithm presented in section (6.7) to produce identical saturation paths as the measured ones and then compare the predicted and measured relative permeabilities. This is of interest in three-phase flow due to the fact that three-phase macroscopic properties are a strong function of saturation history (path). We analyze two experiments.

Experiment (I): Fig. (7.8) shows the tracked and measured saturation path for a high initial oil saturation experiment, Experiment 9 - Sample 13. The initial point was produced by primary drainage and the saturation tracking algorithm was used to reproduce the experimental path. We were able to reproduce the same path

as the experiment.

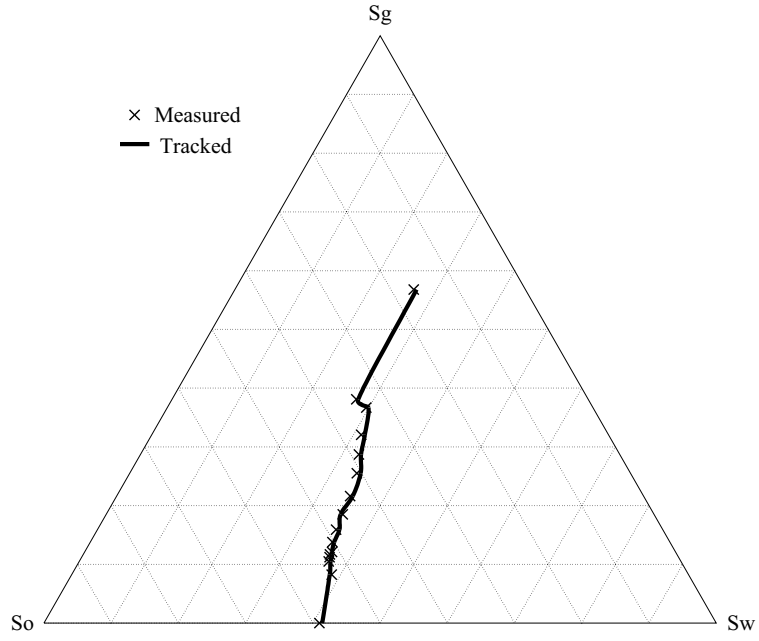

Figure 7.8: Comparison of measured and tracked saturation paths for Experiment 9 - Sample 13 of Oak experiments [1].

Fig. (7.9) compares the predicted and measured three-phase oil relative permeability for Experiment (I). The prediction compares well with the measured values at high oil saturations but tends to over-predict at low oil saturations. The reason for this is not very clear at this stage but it may be due to scatter in the data, the uncertainty associated with the layer conductance estimations and also the representation of the void space of the rock by different idealized angular geometries.

Fig. (7.10) illustrates the comparison between the predicted and measured three-phase gas relative permeability. Due to finite size effects the predicted values at low gas saturations are zero.

Fig. (7.11) compares the predicted three-phase water relative permeability with the measured values. The agreement is fairly good. We slightly over-estimate the relative permeability, as discussed in the previous section.

Experiment (II): Fig. (7.12) shows the measured and tracked saturation paths for another high initial oil saturation experiment, Experiment 10 - Sample 14. Again the initial oil saturation is established by primary drainage.

Fig. (7.13) compares the predicted and measured three-phase oil relative permeability. Similar to the previous experiment predicted values at low oil saturations

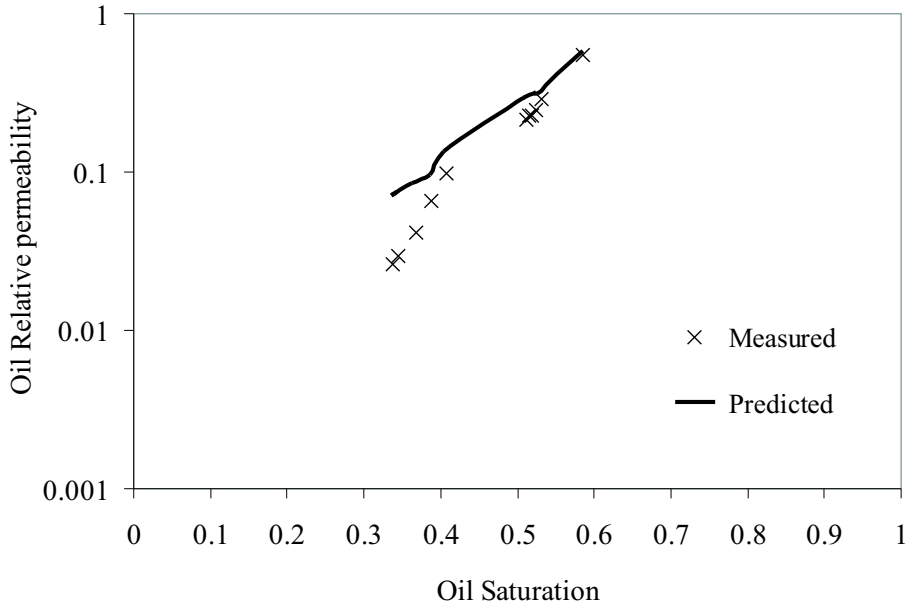

Figure 7.9: Comparison of measured and predicted three-phase oil relative permeabilities for Experiment 9 - Sample 13 of Oak experiments [1].

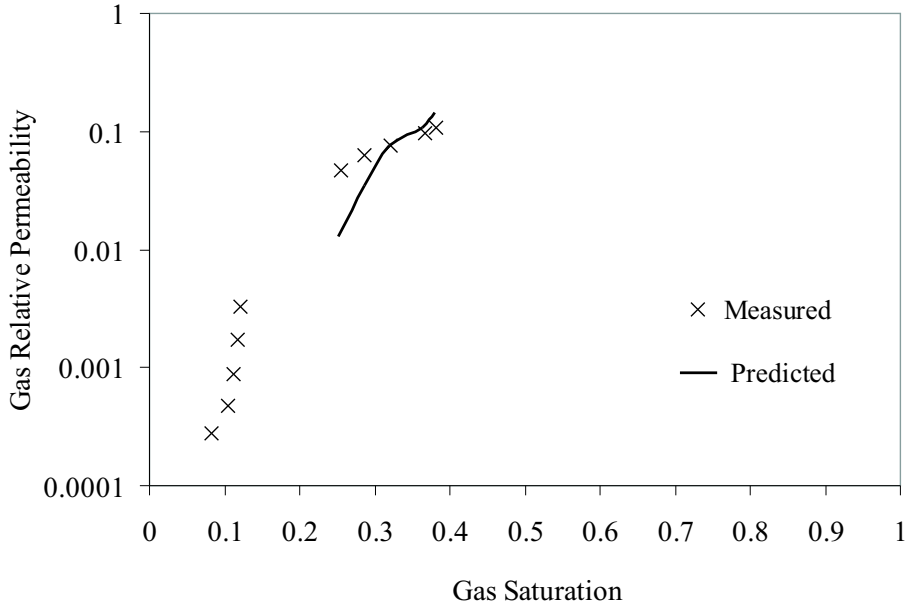

Figure 7.10: Comparison of measured and predicted three-phase gas relative permeabilities for Experiment 9 - Sample 13 of Oak experiments [1].

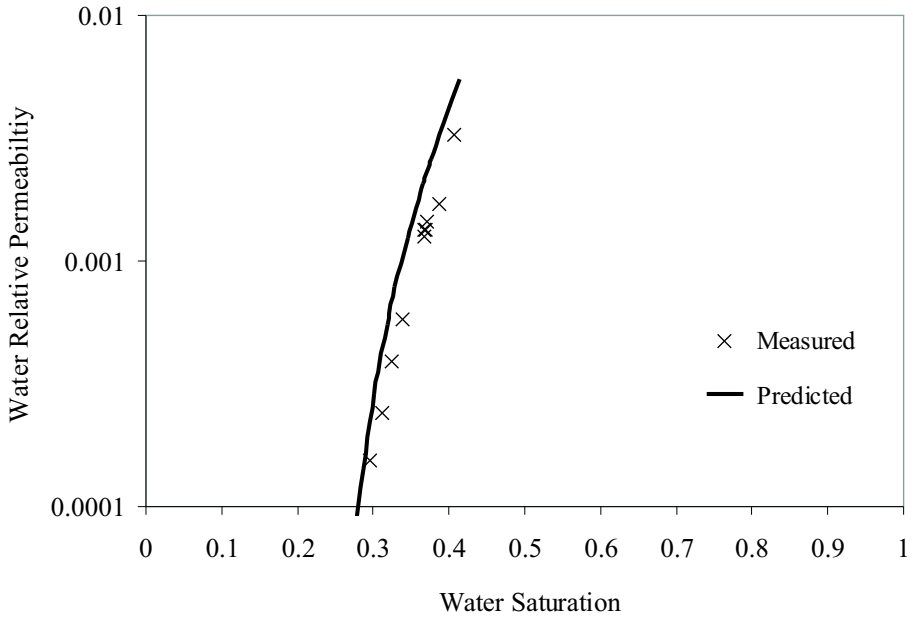

Figure 7.11: Comparison of measured and predicted three-phase water relative permeabilities for Experiment 9 - Sample 13 of Oak experiments [1].

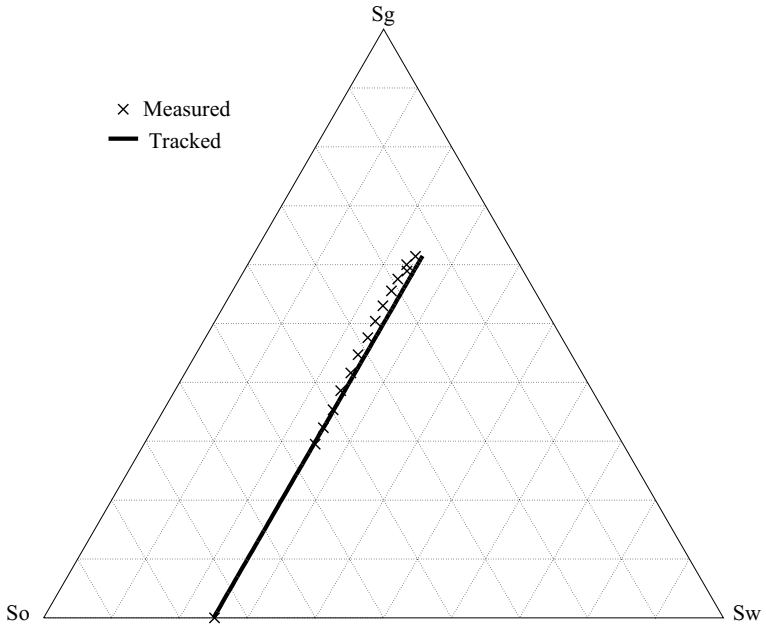

Figure 7.12: Comparison of measured and tracked saturation paths for Experiment 10 - Sample 14 of Oak experiments [1].

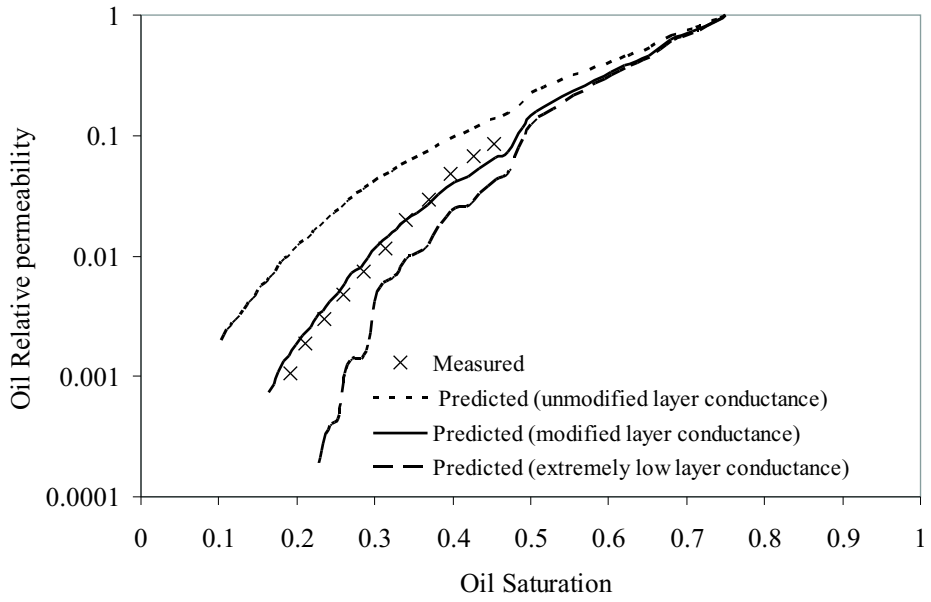

Figure 7.13: Comparison of measured and predicted three-phase oil relative permeabilities for Experiment 10 - Sample 14 of Oak experiments [1].

are over-estimated. This is the region where oil relative permeability is controlled by flow of oil through the layers. The sensitivity of the oil relative permeability to oil layer conductance was tested by multiplying the layer conductance by constant factors of 0.08 and 0.001. The effect is significant, Fig. (7.13), and indicates that the predicted oil relative permeability is very sensitive to how layer flow is modelled.

Fig. (7.14) indicates the very good agreement between predicted and measured three-phase gas relative permeability. Variations in the oil layer conductance does not have any impact on the gas relative permeability. Gas flows in the centre of the larger pores and throats as it is the most non-wetting phase and is unaffected by oil layers.

We analyzed other experiments for both secondary (after primary drainage) and tertiary (after water flooding) gas injection. In all cases the results were similar to those shown here. The predictions of gas and water relative permeabilities were good, and we predicted the oil relative permeability at high saturation accurately. However, at low saturation we systematically over-estimated the oil relative permeability. Where we make good predictions flow is controlled by the sub-networks of pores and throats whose centres are filled with each phase. As we have shown in the two-phase analysis, with a geologically representative network and a range of contact angles that captures the correct balance between pore body filling and

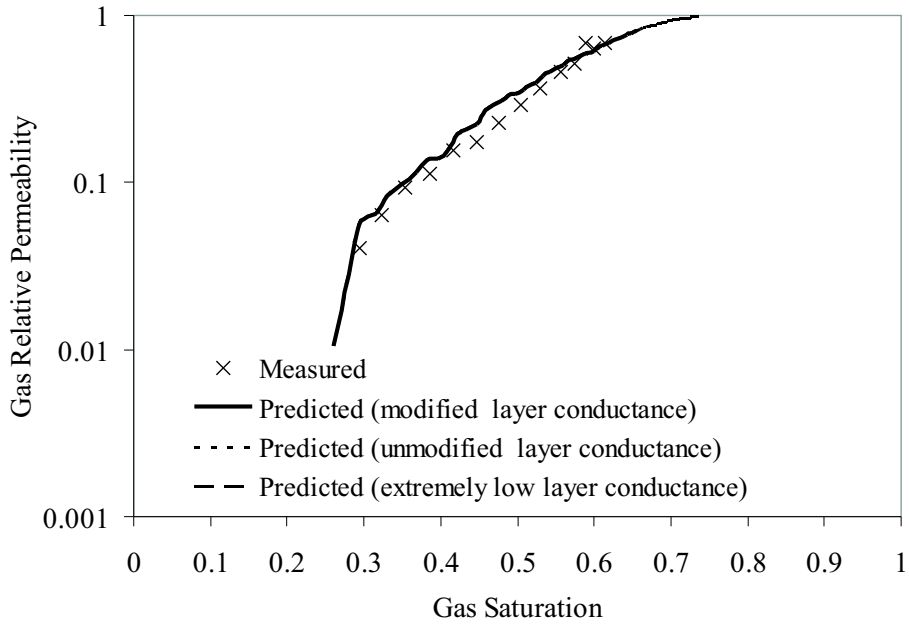

Figure 7.14: Comparison of measured and predicted three-phase gas relative permeabilities for Experiment 10 - Sample 14 of Oak experiments [1].

snap-off in imbibition, we can predict relative permeability accurately.

However, the oil relative permeability in gas injection for oil saturations below approximately 0.5 is controlled by oil layers – these layers provide connectivity of the oil phase and without them the oil would be completely trapped at a saturation of around 0.2. This is a situation unique to three-phase flow. It would appear that we significantly over-estimate the layer conductance. This is probably because our simplistic representation of connected layers in a corner fails to capture parts of the pore space where the layers are much less stable or conductive.

7.2 Simulation of Different Processes

We now use our model to study different cases that have not necessarily been studied experimentally. We consider two systems with different wettability whose contact angles are tabulated in Table (7.3). We use the same interfacial tensions as before – Table (7.1).

Table 7.3: Contact angles (degrees) used to simulate different processes.

System	$\theta_{ow}^{PD(1)}$	θ_{gw}^{PD}	θ_{ow}^{r}	θ_{ow}^{a}	θ_{go}^{r}	θ_{go}^{a}	θ_{gw}^{r}	θ_{gw}^{a}
A	0	0	10-50	30-70	0	0	8.46-41.9	25.3-58.1
B	0	0	90-160	110-180	0	0	73.5-112.9	87.8-115.6

1. Primary Drainage

7.2.1 Secondary Gas Injection

Here we simulate gas injection into different initial oil saturations S_{oi} after primary drainage (secondary gas injection) assuming a fixed oil/water capillary pressure. In this section we consider the water-wet system A in Table (7.3). Fig. (7.15) presents the saturation paths taken by each simulation. Since the gas/oil interfacial tension is lower than that of the gas/water, gas displaces oil first and then at the residual or trapped oil saturation (close to zero), it starts displacing water.

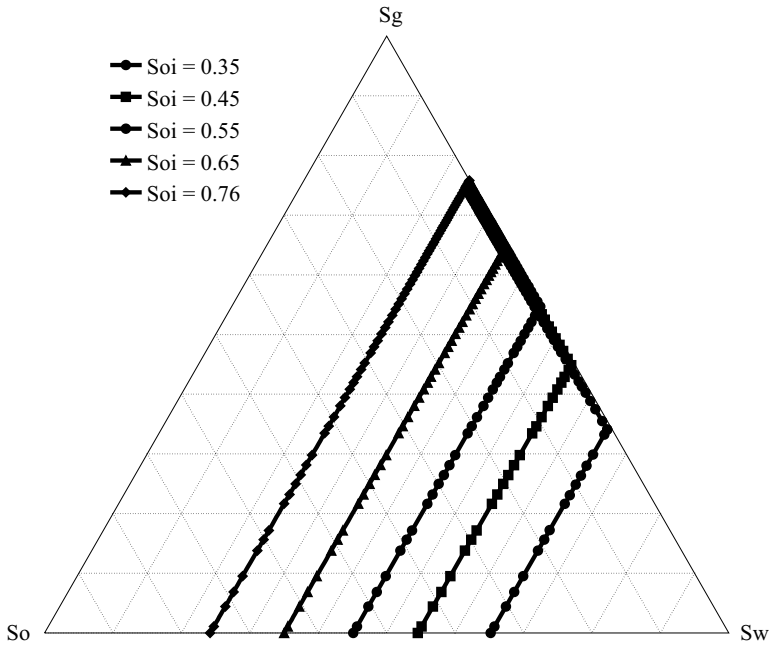

Figure 7.15: Saturation paths for secondary gas injection with different initial oil saturations in a spreading system.

Fig. (7.16) compares the three-phase oil relative permeability for secondary gas injection with different initial oil saturations. At high oil saturations, the higher the initial oil saturation, the lower the oil relative permeability. Initially oil occupies

the largest elements. Gas then invades the oil-filled pores and throats in decreasing order of size. For a low initial oil saturation, oil only occupies large elements giving a larger relative permeability than for a high initial oil saturation where oil remains in small elements [151–153, 264, 265]. However, at low oil saturations, the higher the initial oil saturation, the higher the oil relative permeability. This is due to the effect of initial oil saturation on oil layer stability. At high initial oil saturations the oil/water capillary pressure, or oil pressure, is high. Oil pushes water far into the corners in configuration group F (Fig. (5.2)). For low S_{oi}, the oil/water capillary pressure is lower, water occupies more of the corners and oil layers are thinner. Thicker layers have a larger conductance and will collapse later in the displacement, leading to higher oil relative permeabilities.

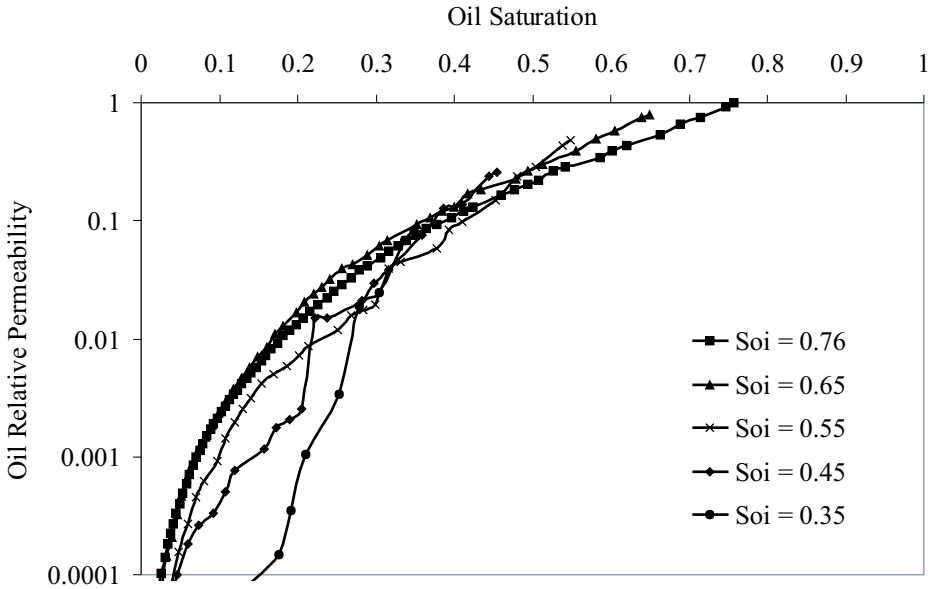

Figure 7.16: Three-phase oil relative permeabilities for secondary gas injection with different initial oil saturations.

Figs. (7.17) and (7.18) illustrate three-phase gas and water relative permeabilities for secondary gas injection with different initial oil saturations respectively. Since the system is water-wet, gas and water relative permeabilities are a function of only their own saturations – water occupies the smallest elements while gas occupies the largest elements – regardless of the initial oil saturation.

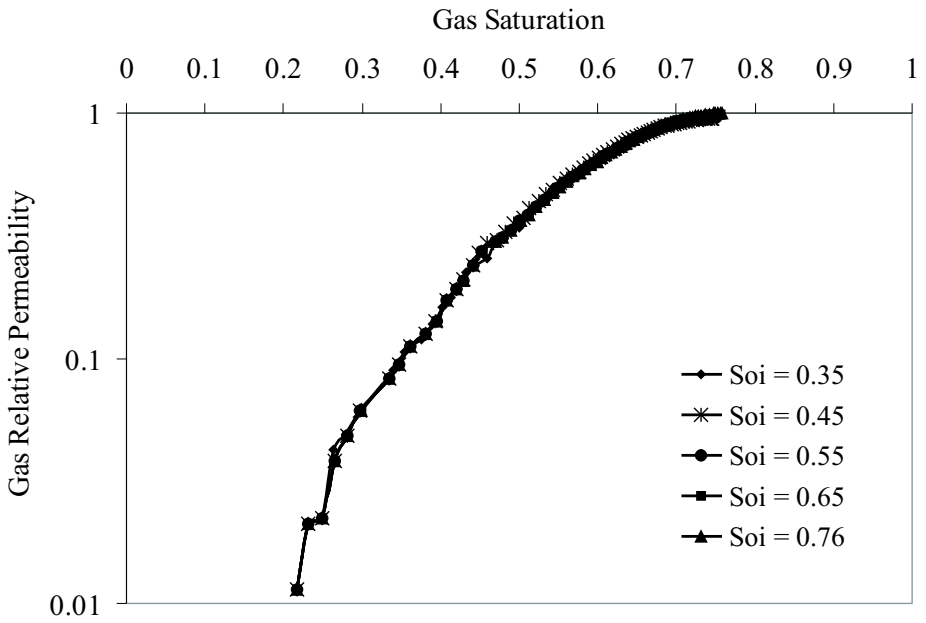

Figure 7.17: Three-phase gas relative permeabilities for secondary gas injection with different initial oil saturations.

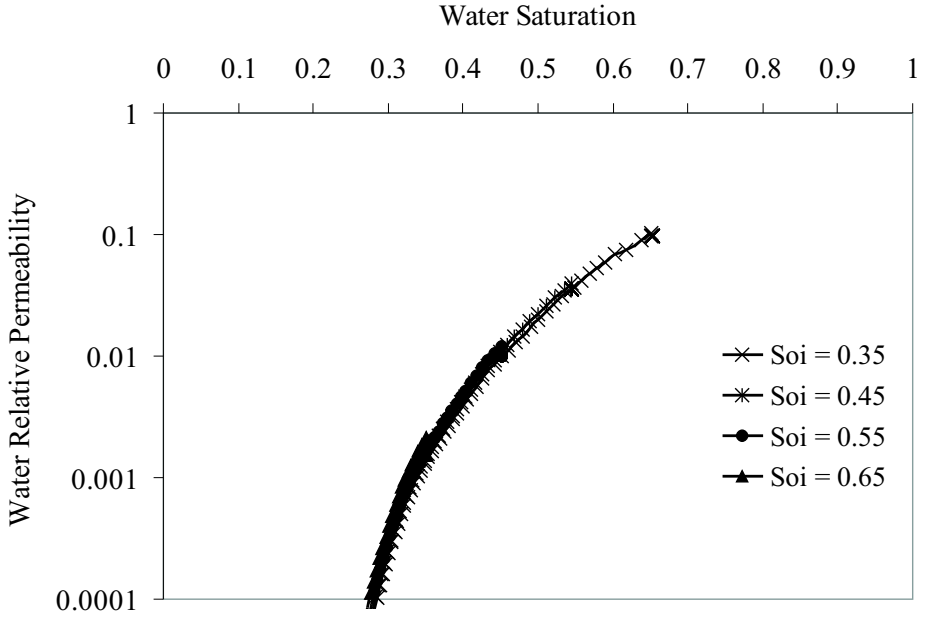

Figure 7.18: Three-phase water relative permeabilities for secondary gas injection with different initial oil saturations.

7.2.2 Comparison of Secondary and Tertiary Gas Injection

Here we compare secondary with tertiary gas injection again for the water-wet system A, Table (7.3). Fig. (7.19) shows the three-phase oil relative permeability for secondary and tertiary gas injection into an initial oil saturation of 0.55. The oil relative permeability for secondary gas injection is not very different from tertiary gas injection at high oil saturations where layer flow is not dominant. At low oil saturations, oil flows mainly through layers. Theses layers are thicker and more stable during secondary gas injection due to the higher oil/water capillary pressure in comparison with tertiary gas injection where the oil layers are thinner and less stable because the oil/water capillary pressure is lower after water flooding. This gives higher oil relative permeabilities for secondary gas injection than for tertiary gas injection with the same initial oil saturation.

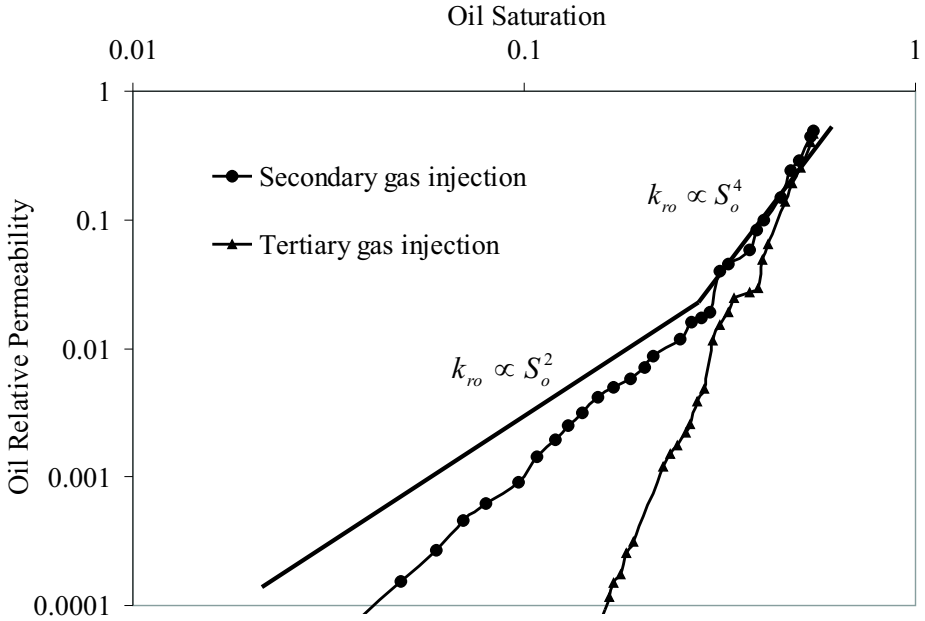

Figure 7.19: Comparison of three-phase oil relative permeability for secondary and tertiary gas injection with an initial oil saturation of 0.55.

In Fig. (7.19) at high oil saturation we see, approximately, $k_{ro} \propto S_o^4$. The oil relative permeability is controlled by the network of pores and throats filled with oil in the centres and it drops rapidly with oil saturation as this network becomes less well connected. For secondary gas injection, at an oil saturation approximately equal to the water flood residual, we see a cross-over to a layer drainage regime where approximately $k_{ro} \propto S_o^2$. This is easily explained theoretically [53, 143, 299–

301]. The hydraulic conductance of the layers is proportional to the square of the cross-sectional area of oil (see Appendix (6.6)). When most oil is flowing in layers, the oil saturation is proportional to the oil area, leading to the quadratic relative permeability. This behaviour has been observed in gas injection and gravity drainage experiments [143, 263, 299–301]. Notice that the apparent log-log slope at low saturation is slightly larger than 2, as seen for sandstones [143, 263]. This is because some small throats are still oil-filled in the layer drainage regime and when they are occupied by gas, their contribution to the oil relative permeability drops significantly. For tertiary gas injection, this oil layer drainage regime is not observed – this is because oil layers collapse during the displacement leading to very low oil relative permeabilities.

The three-phase gas (Fig. (7.20)) and water (Fig. (7.21)) relative permeabilities are the same in secondary and tertiary gas injection. Again this is because they depend on only their own saturations and are relatively insensitive to saturation path, as long as it is a drainage-dominated displacement.

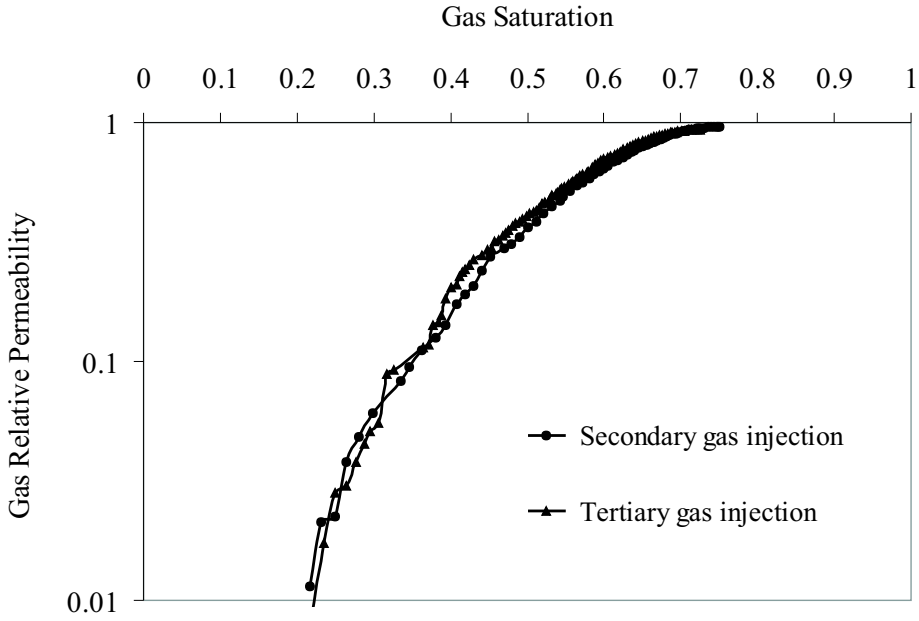

Figure 7.20: Comparison of three-phase gas relative permeability for secondary and tertiary gas injection with an initial oil saturation of 0.55.

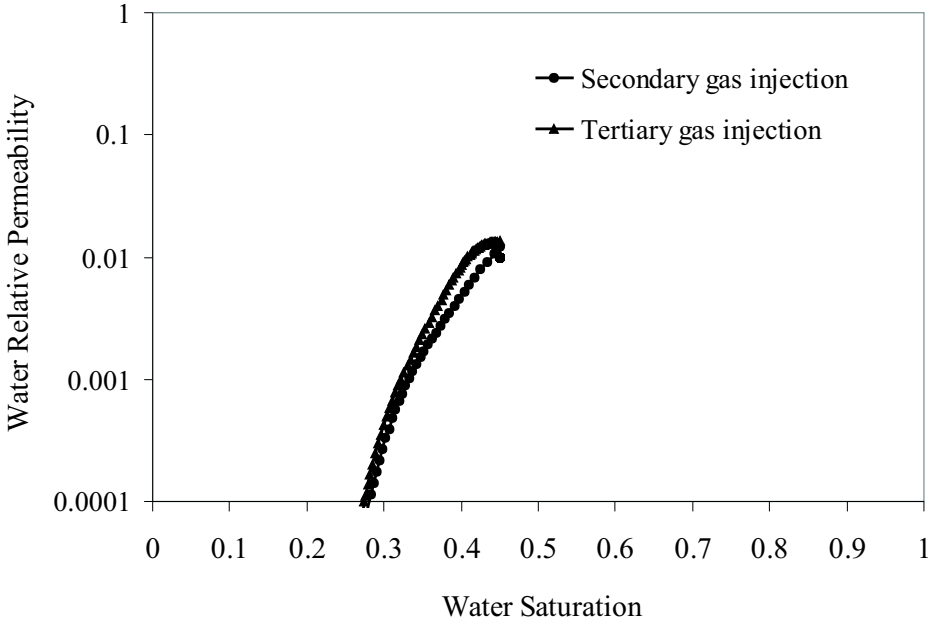

Figure 7.21: Comparison of three-phase water relative permeability for secondary and tertiary gas injection with an initial oil saturation of 0.55.

7.2.3 Tertiary Gas Injection into Water Flood Residual Oil

The physics involved with gas injection into water flood residual oil is very complex. Several micromodel experiments [60–69, 71, 72] have shown that when gas is injected into such a spreading system the two phenomena of *double displacement* and oil *layer formation* make the initially trapped oil continuous which allows it to drain to very low saturation. This in turn involves coalescence, formation and break-up of trapped clusters of oil. We have implemented these mechanisms in our model and Figs. (7.22), (7.29), and (7.30) show the three-phase oil, water, and gas relative permeabilities for this process again in our water-wet system, A. The oil relative permeability is zero at the end of water flooding (beginning of gas injection) as all the oil is trapped, but it jumps to a non-zero value as it gets reconnected during the early stages of gas injection. This happens at low gas saturation, see Fig. (7.31), where the trapped oil saturation is plotted against gas saturation.

Figs. (7.22) also compares the oil relative permeability of the tertiary gas injection with that of a secondary gas injection with a similar initial oil saturation ($S_{oi} = 0.38$). At high oil saturations, oil relative permeability of the tertiary case is lower than that of the secondary gas injection. This is because at the beginning of secondary gas injection all the oil resides in the large pores and throats, see Fig.

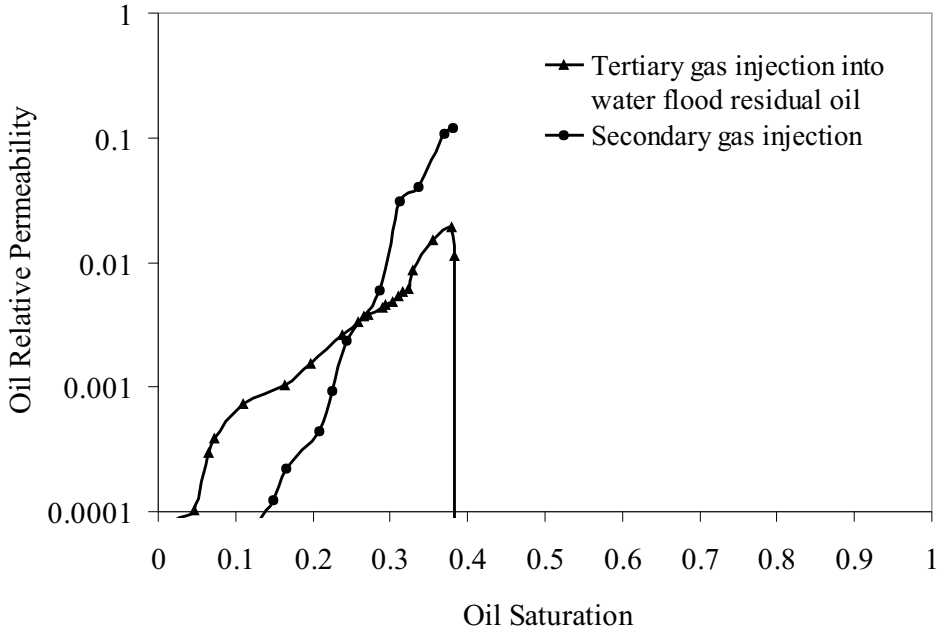

Figure 7.22: Three-phase oil relative permeability for tertiary gas injection into water flood residual oil ($S_{oi} = 0.384$) and for secondary gas injection with a similar initial oil saturation ($S_{oi} = 0.38$).

(7.23), while at the beginning of the tertiary gas injection some of the oil stays in the small elements due to trapping during water flooding, see Fig. (7.24). In other words, the fraction of large oil filled elements at the starting point of secondary gas injection is larger than that of tertiary case leading to lower oil relative permeabilities for tertiary gas injection. However, at low oil saturations when the layer flow is dominant, the oil relative permeability of the tertiary gas injection is higher since during the displacement, double drainage causes an increase in oil/water capillary pressure making oil layers thicker and more conductive.

Fig. (7.24) shows the pore and throat occupancy at the end of water flooding. The trapped oil resides in the larger elements. During gas injection, double displacement causes the oil to be pushed into smaller pores and throats while the gas occupies the larger elements, see Figs. (7.25)-(7.28). The oil is now connected, since it also resides in layers in gas-filled elements. This allows oil to be displaced and results in a non-zero oil relative permeability, Fig. (7.22).

Fig. (7.29) shows the gas relative permeability compared to an equivalent secondary gas injection with ($S_{oi} = 0.38$). The gas relative permeability for the tertiary case is lower, in contrast to Fig. (7.20). The reason is that here the oil is trapped

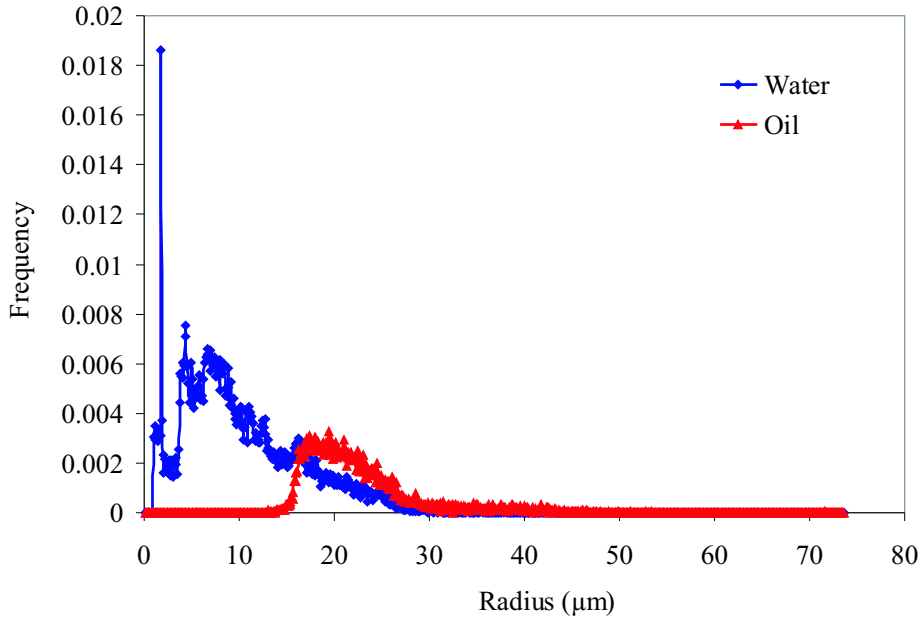

Figure 7.23: Pore and throat occupancy as a function of size after primary drainage ($S_o = 0.38$).

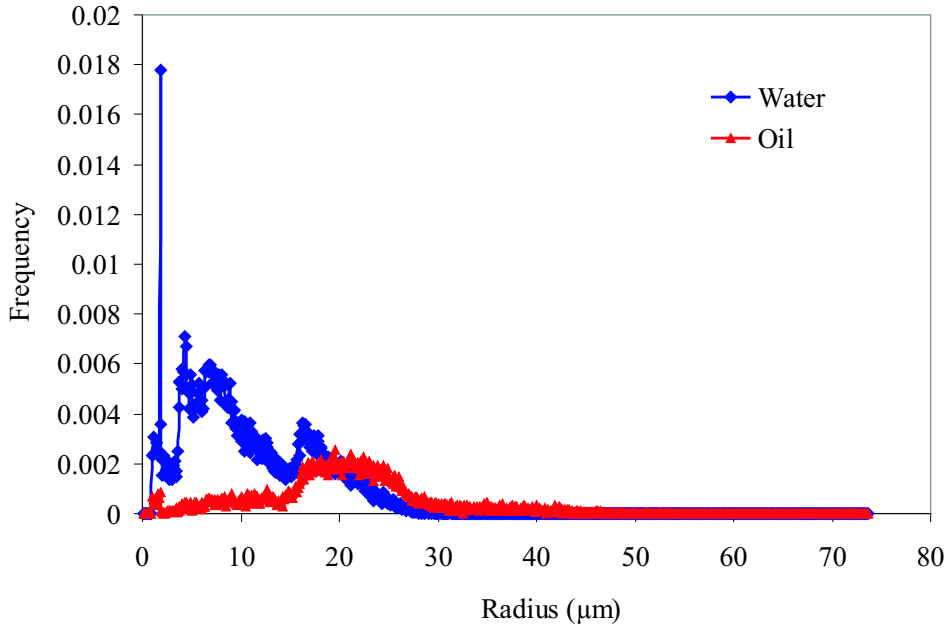

Figure 7.24: Pore and throat occupancy as a function of size after water flooding. The trapped oil resides in the larger elements.

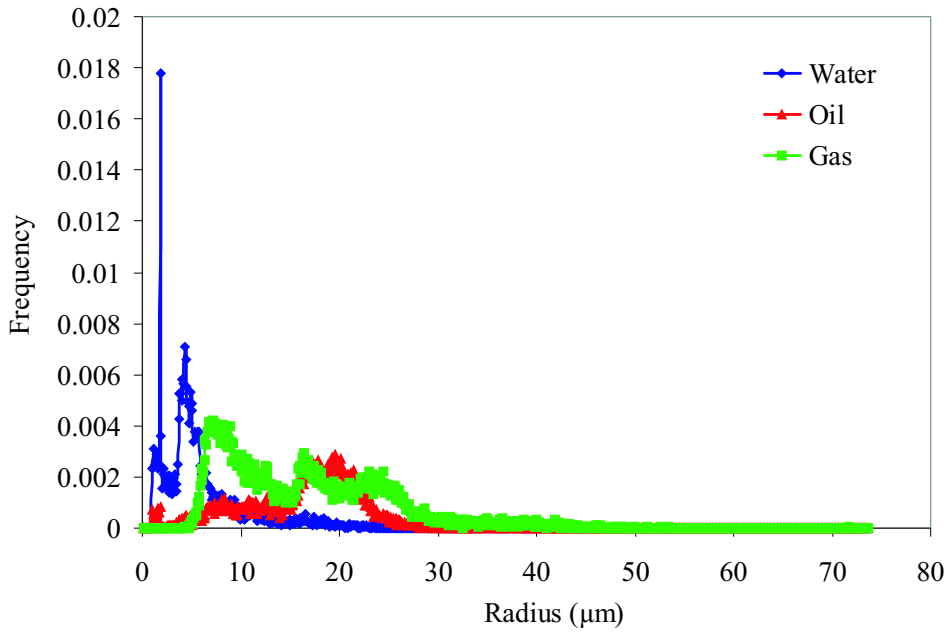

Figure 7.25: Pore and throat occupancy as a function of size during tertiary gas injection into water flood residual oil when $S_o \approx 0.23$. Double displacement shifts the oil into intermediate-sized elements.

and gas is displacing oil by double displacement and hence is less well connected – the trapped oil is blocking the larger pores and throats. Similarly the tertiary water relative permeability is lower, Fig. (7.30). During the displacement, double drainage causes an increase in oil/water capillary pressure giving a drainage-type displacement for water, pushing it into smaller elements. This is not seen if oil is initially well connected, see Fig. (7.21).

Table (7.4) shows the displacement statistics for tertiary gas injection into water flood residual oil ($S_{oi} = 0.384$) compared to secondary gas injection with a similar initial oil saturation ($S_{oi} = 0.38$). In tertiary gas injection there is significant amount of double displacement and oil layer formation that reconnects the oil and rearranges its occupancy (Fig. (7.26)). In contrast, secondary gas injection is controlled by direct gas-oil displacement alone since the oil is initially already connected. The number of gas-oil displacements involved in double displacement is much lower than number of oil-water ones since once a trapped cluster becomes continuous by oil-water piston-like displacement and/or layer formation the gas-oil displacement of the double displacement is automatically carried out under direct gas-oil displacement scheme and that is why number of direct gas-oil displacements in tertiary gas

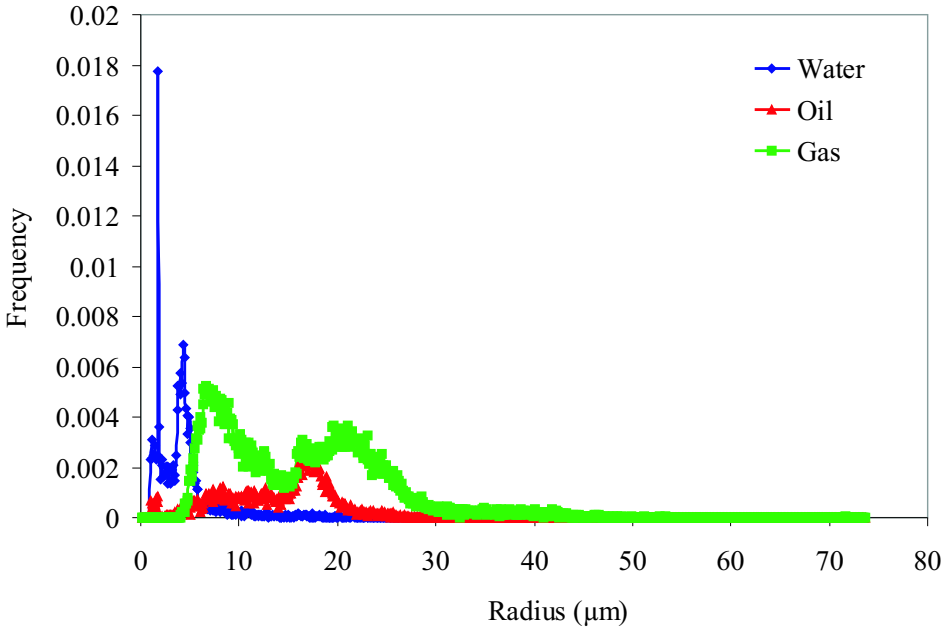

Figure 7.26: Pore and throat occupancy as a function of size during tertiary gas injection into water flood residual oil when $S_o \approx 0.16$. Double displacement shifts the oil into intermediate-sized elements.

Table 7.4: The number of different types of displacement for tertiary gas injection into water flood residual oil ($S_{oi} = 0.384$) and for secondary gas injection with a similar initial oil saturation ($S_{oi} = 0.38$).

	Number of Displacements	
Displacement Type	TGI(1)	SGI(2)
Double displacement gas-oil (piston-like)	1345	0
Double displacement oil-water (piston-like)	3856	0
Direct gas-oil (piston-like)	13699	10091
Direct gas-water (piston-like)	22688	27804
Oil layer collapse	6178	8640
Oil layer formation	1356	0

1. Tertiary Gas Injection
2. Secondary Gas Injection

injection is higher than that of the secondary gas injection. At the end of water flooding there were 1864 trapped clusters of oil and during the tertiary gas injection into water flood residual oil 507 coalescence, 90 break, and 1040 reconnection events took place.

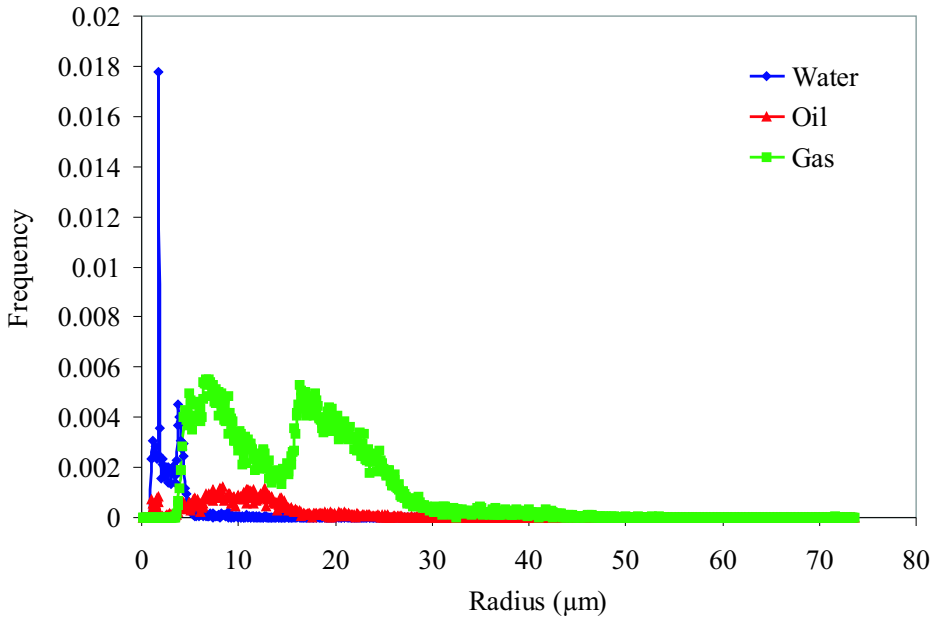

Figure 7.27: Pore and throat occupancy as a function of size during tertiary gas injection into water flood residual oil when $S_o \approx 0.07$. Double displacement shifts the oil into intermediate-sized elements.

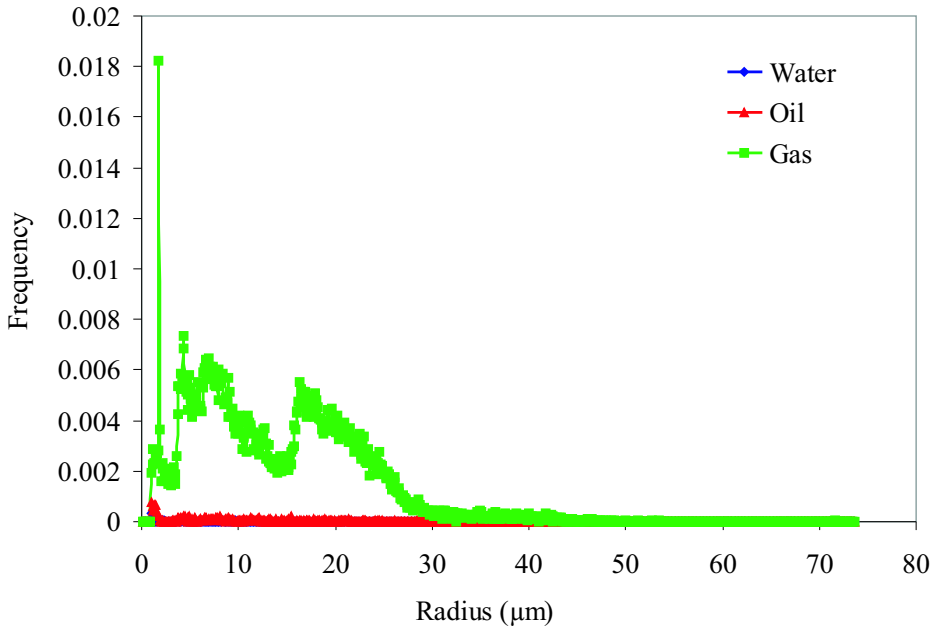

Figure 7.28: Pore and throat occupancy as a function of size during tertiary gas injection into water flood residual oil when $S_o \approx 0.01$.

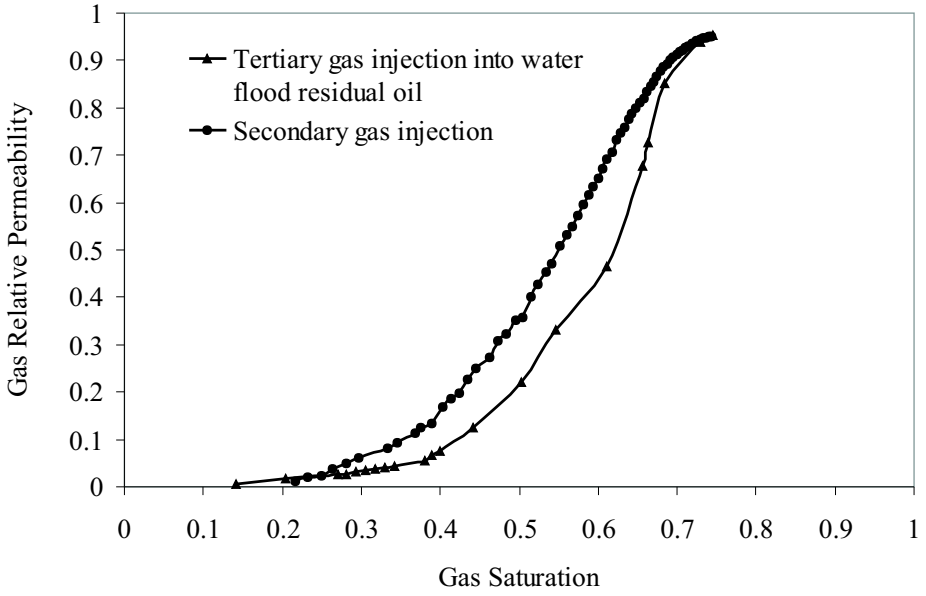

Figure 7.29: Three-phase gas relative permeability for tertiary gas injection into water flood residual oil ($S_{oi} = 0.384$) and for secondary gas injection with a similar initial oil saturation ($S_{oi} = 0.38$).

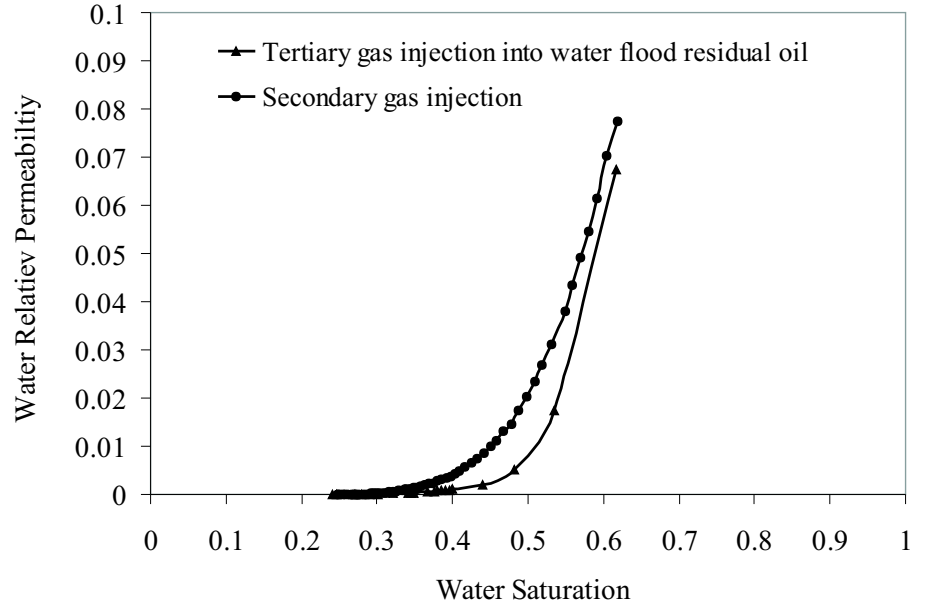

Figure 7.30: Three-phase water relative permeability for tertiary gas injection into water flood residual oil ($S_{oi} = 0.384$) and for secondary gas injection with a similar initial oil saturation ($S_{oi} = 0.38$).

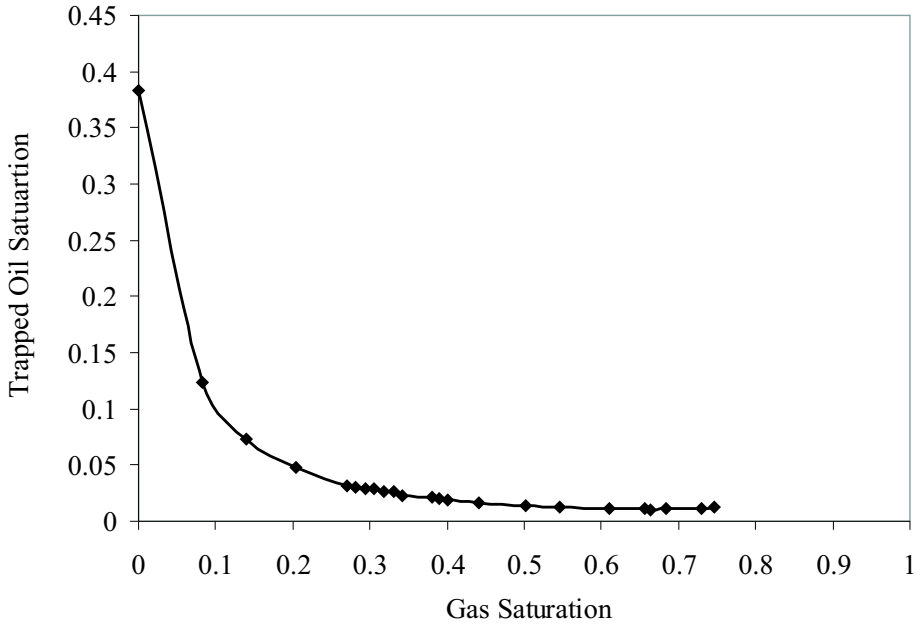

Figure 7.31: Trapped oil saturation as a function of gas saturation during tertiary gas injection into water flood residual oil.

7.2.4 Effects of Wettability

We will now use our model to predict the effect of wettability on two- and three-phase relative permeabilities. In this case, we do not have experimental data to compare against, but the success of network modelling predictions for mixed-wet two-phase systems [135, 302] and water-wet two- and three-phase systems gives us some confidence that our results are valid. We compare two cases: water-wet A and oil-wet B where the distribution of advancing oil/water contact angle is uniform between $30^\circ - 70^\circ$ and $110^\circ - 180^\circ$ respectively (Table (7.3)). Again the interfacial tensions are given in Table (7.1).

1. Two-Phase

Fig. (7.32) shows oil and water relative permeabilities for water flooding for these two cases. The water relative permeability for the oil-wet system at low water saturation is lower than that of the water-wet case. At low water saturation there are not many network-spanning water-filled oil-wet elements since water flooding is a drainage process and the biggest pores and throats are filled first. At higher

water saturation once water-filled elements span the system, the water relative permeability in the oil-wet system is larger since water occupies the larger pore spaces. When the wettability changes from water-wet to oil-wet, the oil relative permeability decreases since oil becomes the wetting phase and occupies the smaller pores and throats.

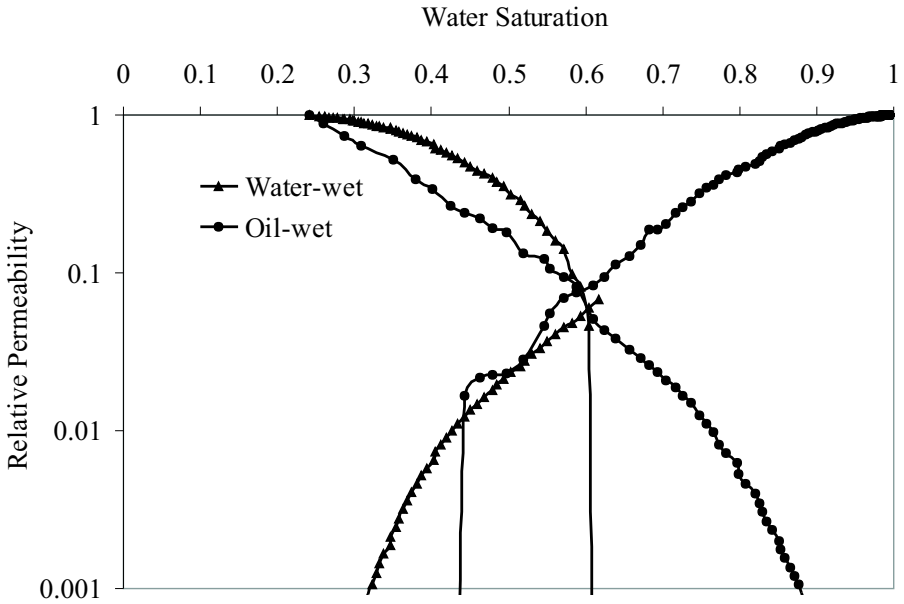

Figure 7.32: Oil and water relative permeability of water flooding in: (I) water-wet, $\theta^a_{ow} = 30^\circ - 70^\circ$ (system A), and (II) oil-wet, $\theta^a_{ow} = 110^\circ - 180^\circ$ (system B) Berea sandstone.

The water-wet system has the higher residual oil saturation, 0.384, because snap-off traps oil. A lower residual oil saturation, 0.0055, is found in the oil-wet system since oil layers prevent trapping. This behaviour is consistent with that found by other authors [113, 119, 120, 122, 303, 304]. Fig. (7.33) shows the pore and throat occupancy as a function of size after water flooding in the oil-wet system, B.

2. Three-Phase

We consider primary drainage to irreducible water saturation followed by water flooding to $S_w = 0.4$ ($S_{oi} = 0.6$). Then gas is injected at a constant oil/water capillary pressure.

Fig. (7.34) shows the oil relative permeability. In the oil-wet case, oil remains in smaller pores and throats after water flooding than for a water-wet medium,

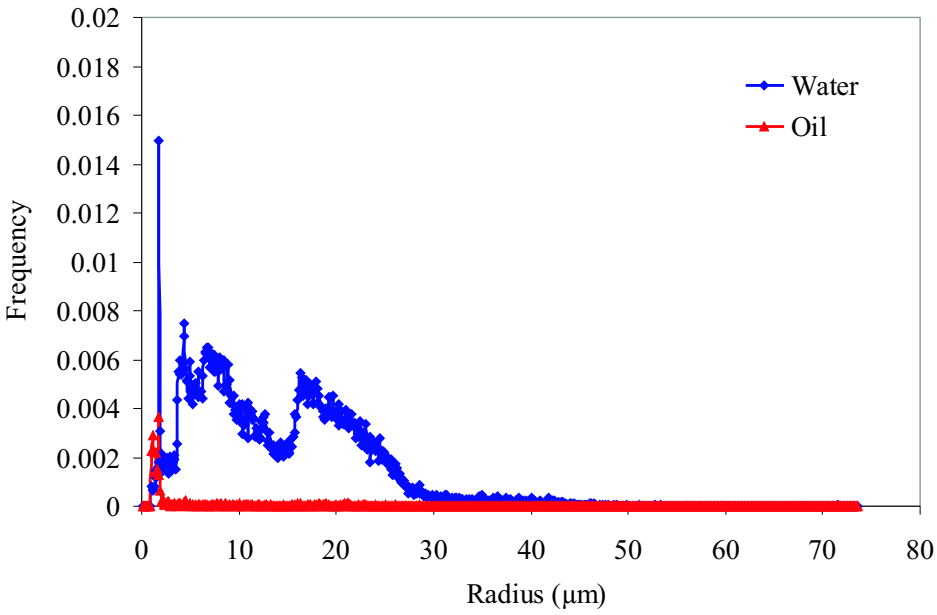

Figure 7.33: Pore and throat occupancy as a function of size after water flooding in the oil-wet system, B.

giving a lower relative permeability. This is seen in Fig. (7.34) for oil saturations larger than approximately 0.4. At lower oil saturations, gas has invaded most of the oil-filled elements. The relative permeability is limited by the connectivity of the oil phase. In the water-wet medium, oil layers collapse during gas injection, whereas oil layers remain stable throughout the displacement for the oil-wet case. A higher gas pressure is required to collapse oil layers, since water is pinned in the corners – configurations $F-3$ and $F-4$ in Fig. (5.2). Thus, the oil-wet oil relative permeability is larger at low oil saturation.

The water-wet gas relative permeability in Fig. (7.35) is larger than the oil-wet case at high gas saturation. In a water-wet medium, the gas always occupies the largest pores and throats. For an oil-wet system, gas is not the most non-wetting phase in the presence of water (in Table (7.3) some values of θ_{gw} are greater than 90°) and will displace water from some of the smaller pores, resulting in poorer connectivity and conductance. This effect of wettability has been discussed previously [264] and is well established experimentally [148, 300, 301]. This result is a direct consequence of the constraint on contact angles, Eq. (2.6) [248].

The water relative permeability in Fig. (7.36) is at first sight surprising. One might expect that the water relative permeability for the oil-wet case to be higher than for the water-wet medium, since water can be non-wetting to both oil and gas

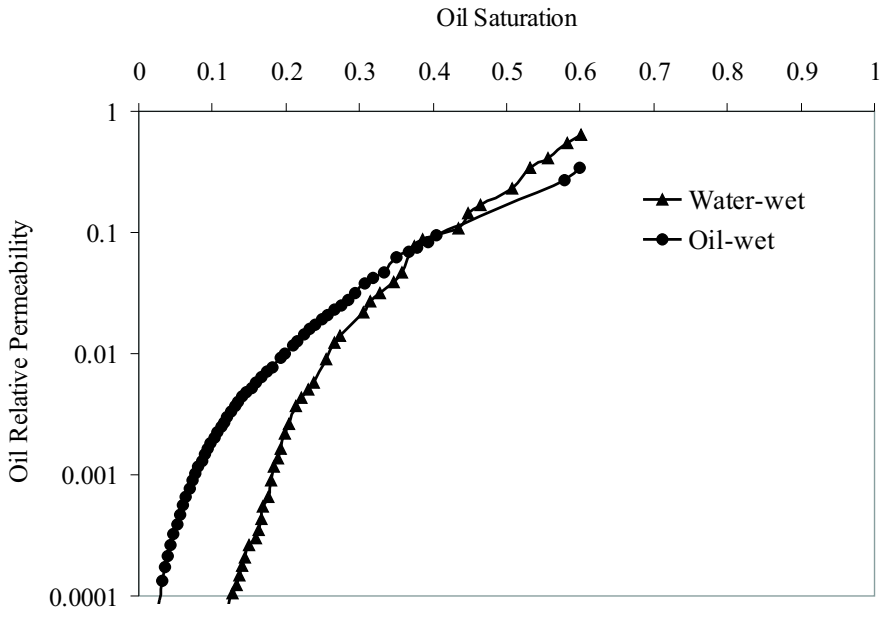

Figure 7.34: Effects of wettability on three-phase oil relative permeability. Curves for tertiary gas injection into a water-wet and oil-wet system with initial oil saturation of 0.6 are shown.

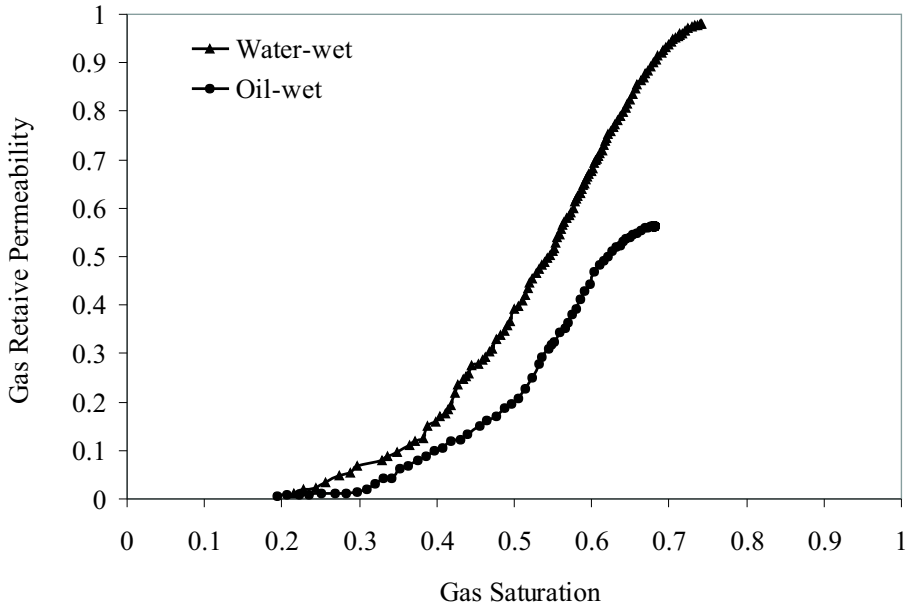

Figure 7.35: Effects of wettability on three-phase gas relative permeability. Curves for tertiary gas injection into a water-wet and oil-wet system with initial oil saturation of 0.6 are shown.

in oil-wet systems, occupying the larger pore spaces. The explanation is that during water flooding water invades the larger pores and throats in the oil-wet medium. This results in an increase in water saturation, but the oil-wet water-filled elements fail to span the network, meaning that the water relative permeability remains very low (see Fig. (7.32) - $S_w = 0.4$ is just before water is well connected). During gas injection, since gas displaces water, the water relative permeability can only decrease from its already negligible value.

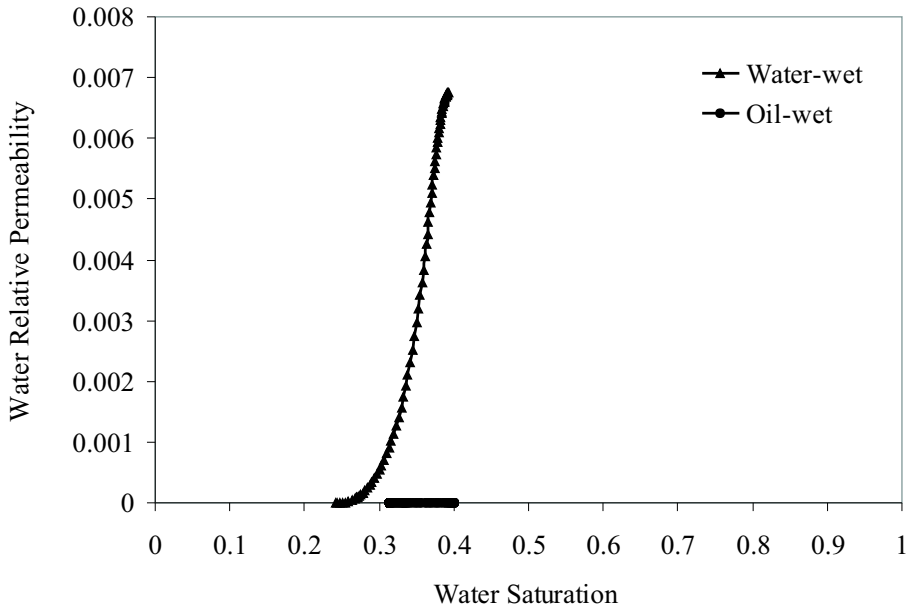

Figure 7.36: Effects of wettability on three-phase water relative permeability. Curves for tertiary gas injection into a water-wet and oil-wet system with initial oil saturation of 0.6 are shown.

Chapter 8

Final Remarks

8.1 Conclusions

Based on today's knowledge on physics of two- and three-phase flow in porous media at the pore-level, a definitive capillary dominated three-phase network model was developed that combines three essential components:

1. A description of the pore space and its connectivity that mimics *real* systems
2. A physically-based model of *wettability alteration*
3. A *full description of fluid configurations* for two- and three-phase flow

We described in detail how the model was developed and works. We also presented a novel and robust clustering algorithm to account for trapping and double displacement. The model includes the following features:

- Mixed wettability
- Wetting layers
- Spreading layers
- Hysteresis and wettability alteration are fully accounted for. Any values of receding and advancing oil/water, gas/water, and gas/oil contact angles can be considered.
- Any random/regular two- and three-dimensional networks can be used.
- Direct two-phase displacements

- Layer reformation
- Double displacement
- Multiple injections
- Saturation tracking

The model successfully predicted two-phase water-wet relative permeabilities measured on Berea sandstone by Oak [1]. For primary drainage there were no parameters to adjust. For oil/water and gas/oil imbibition the advancing contact angles were chosen to match the residual non-wetting phase saturation. Using these contact angles excellent agreement between experiment and predictions was made. For gas/water data we used a constraint, Eq. (2.6), to predict the gas/water contact angles from the oil/water and gas/oil results. Again the match to experiment was excellent.

We then predicted three-phase gas injection relative permeabilities from Oak [1]. We used a saturation tracking algorithm to follow exactly the same displacement path as in the experiments. The predictions of gas and water relative permeabilities and the oil relative permeability at high oil saturation were good. However, at low oil saturations, where flow is dominated by spreading layers, we systematically over-predicted the oil relative permeability. This was likely to be due to us over-estimating the oil layer conductance.

We computed relative permeabilities for cases that had not been studied experimentally. We showed that the oil relative permeability in tertiary gas injection – after water flooding – is lower than in secondary gas injection – after primary drainage, since oil layers are less stable and thinner due to a low initial oil/water capillary pressure. For secondary gas injection we observed an approximately quadratic variation of oil relative permeability with oil saturation when flow was controlled by layers, as seen experimentally. We then compared relative permeabilities of a tertiary gas injection into water flood residual oil with those of a secondary gas injection with a similar initial oil saturation. Oil relative permeability of the tertiary case was non-zero and higher than that of the secondary gas injection at low oil saturations since double-displacement caused an increase in oil/water capillary pressure – in tertiary gas injection – leading to thicker and more conductive oil layers. The increase in the oil/water capillary pressure also lowered gas and water relative permeabilities of the tertiary case comparing to their secondary counterparts. These results were different from the tertiary gas injection into oil that was initially already connected. We also

showed the effects of wettability on relative permeability by comparing tertiary gas injection relative permeabilities for water-wet and oil-wet systems. The behaviour of all three relative permeabilities was different from that observed in two-phase flow and was explained in terms of the pore-scale physics.

The model could now be used to study a wide range of other phenomena in three-phase flow, including water alternate gas (WAG) flooding and gas gravity drainage.

8.2 Recommendations for Future Work

Still there is a great amount of work that can be done to improve, even further, the abilities of the two- and three-phase pore-scale network models:

- More accurate layer conductance models for different boundary conditions which are critically important for prediction of relative permeabilities at low saturation
- Improved pore-body filling models
- Better estimations of three-phase equilibrium interfacial tensions
- More representative networks for different types of rocks, in particular carbonates

Also there are many interesting subjects to be studied using three-phase network modeling:

- Solution gas drive
- Effects of asphalt precipitation on three-phase relative permeabilities due to composition variation, e.g. CO_2 sequestration, or pressure drop below the bubble point
- Gas condensates
- Coupling pore-scale network model to a 3D simulator to capture displacement paths
- Dispersion in three-phase systems
- Water alternate gas (WAG) injection

Bibliography

[1] M. J. Oak. Three-phase relative permeability of water-wet Berea. *Paper SPE 20183, Proceedings of the SPE/DOE Seventh Symposium on Enhanced Oil Recovery, Tulsa, Oklahoma, 22-25 April*, 1990.

[2] M. C. Leverett and W. B. Lewis. Steady flow of gas-oil-water mixtures through unconsolidated sands. *Transactions of the American Institute of Mining, Metallurgical, and Petroleum Engineers*, **142**(107):107–116, 1940.

[3] B. H. Caudle, R. L. Slobod, and E. R. Brownscombe. Further developments in the laboratory determination of relative permeability. *Transactions of the American Institute of Mining, Metallurgical, and Petroleum Engineers*, **192**: 145–150, 1951.

[4] A. T. Corey, C. H. Rathjens, J. H. Henderson, and M. R. J. Wyllie. Three-phase relative permeability. *Transactions of the American Institute of Mining, Metallurgical, and Petroleum Engineers*, **207**:349–351, 1956.

[5] J. Naar and R. J. Wygal. Three-phase imbibition relative permeability. *SPE Journal*, **December**:254–258, 1961.

[6] R. W. Snell. Three phase relative permeability in an unconsolidated sand. *Journal of the Institute of Petroleum*, **48**:80–88, 1962.

[7] A. M. Sarem. Three-phase relative permeability measurement by unsteady-state method. *SPE Journal*, **September**:199–205, 1966.

[8] E. C. Donaldson and G. W. Dean. Two- and three-phase relative permeability studies. *United States Department of the Interior Bureau of Mines*, **6826**:1–23, 1966.

[9] D. N. Saraf and I. Fatt. Three-phase relative permeability measurement using nuclear magnetic resonance technique for estimating fluid saturation. *SPE Journal*, **September**:235–242, 1967.

[10] D. N. Saraf, J. P. Batycky, C. H. Jackson, and D. B. Fisher. An experimental investgation of three-phase flow of water-oil-gas mixtures through water-wet sandstones. *Paper SPE 10761, Proceedings of the SPE Regional Meeting, San Francisco, CA, 24-26 March*, 1982.

[11] E. V. Spronsen. Three-phase relative pemeability measurements using the centrifuge method. *Paper SPE 10688, Proceedings of the 3rd SPE/DOE joint Symposium on Enhanced Oil Recovery, Tulsa, Oklahoma, 4-7 April*, 1982.

[12] R. J. Lenhard and J. C. Parker. Measurement and prediction of saturation-pressure relationships in three-phase porous media systems. *Journal of Contaminant Hydrology*, **1**(4):407–424, 1987.

[13] A. S. Grader and D. J. O'Meara. Dynamic displacement measurements of three-phase relative permeabilities using three immiscible liquids. *Paper SPE 18293, Proceedings of the 63rd SPE Annual Technical Conference and Exhibition, Houston, TX, 2-5 October*, 1988.

[14] R. J. Lenhard and J. C. Parker. Experimental validation of the theory of extending two-phase saturation-pressure relations to three-fluid phase systems for monotonic drainage paths. *Water Resources Research*, **24**:373–380, 1988.

[15] B. B. Maini, S. Kokal, and K. Jha. Measurements and correlations of three-phase relative permeability at elevated temperatures and pressures. *Paper SPE 19677, Proceedings of the 64th SPE Annual Technical Conference and Exhibition, San Antonio, Texas, 8-11 October*, 1989.

[16] M. J. Oak, L. E. Baker, and D. C. Thomas. Three-phase relative permeability of Berea sandstone. *Journal of Petroleum Technology*, **42**(8):1054–1061, 1990.

[17] B. B. Maini, F. Nicola, J. Goldman, and H. K. Sarma. Measurements and estimation of three-phase relative permeability. *Petroleum Recovery Institute, Calgary, Canada, October*, 1990.

[18] L. A. Ferrand, P. C. D. Milly, G. F. Pinder, and R. P. Turrin. A comparison of capillary pressure-saturation relations for drainage in two- and three-fluid porous media. *Advances in Water Resources*, **13**(2):54–63, 1990.

[19] J. L. Wilson, S. H. Conrad, W. R. Mason, W. Peplinski, and E. Hagen. Laboratory investigation of residual liquid organics from spills, leaks and the disposal

of hazardous wastes in groundwater. *EPA Report no. EPA/600/6-90/004, EPA, Ada, OK, April*, 1990.

[20] B. F. Marek, K. J. Hartman, and A. E. MacDonald. Three-phase relative permeability of limestones having bimodal pore-size distribution. *Paper SPE 21374, Proceedings of the SPE Middle East Oil Show held in Bahrain, 16-19 November*, 1991.

[21] M. J. Oak. Three-phase relative permeability of intermediate-wet Berea sandstone. *Paper SPE 22599, Proceedings of the 66th SPE Annual Technical Conference and Exhibition, Dallas, TX, 6-9 October*, 1991.

[22] R. J. Lenhard. Measurement and modeling of three-phase saturation-pressure hysteresis. *Journal of Contaminant Hydrology*, **9**(3):243–269, 1992.

[23] D. E. Dria, G. A. Pope, and K. Sepehrooni. Three-phase gas/oil/brine relative permeabilities measured under CO_2 flooding conditions. *SPE Reservoir Engineering*, **8**(2):143–150, 1993.

[24] F. J. M. Kalaydjian, J. C. Moulu, O. Vizika, and P. K. Munkerud. Three-phase flow in water-wet porous media:determination of gas/oil relative permeability under various spreading conditions. *Paper SPE 26671, Proceedings of the 68th SPE Annual Technical Conference and Exhibition, Houston, TX, 3-6 October*, 1993.

[25] J. E. Nordtvedt, E. Ebeltoft, J. E. Iversen, A. Sylte, H. Urkedal, K. O. Vatne, and A. T. Watson. Determination of three-phase relative permeabilities from displacement experiments. *Paper SPE 36683, Proceedings of the SPE Annual Technical Conference and Exhibition, Denver, Colorado, 6-9 October*, 1996.

[26] S. Siddiqui, P. J. Hicks, and A. S. Grader. Verfication of buckley-leverett three-phase theory using computerised tomography. *Journal of Petroleum Science and Engineering*, **15**(1):1–21, 1996.

[27] F. J. M. Kalaydjian, J. C. Moulu, O. Vizika, and P. K. Munkerud. Three-phase flow in water-wet porous media: gas/oil relative permeabilities for various spreading conditions. *Journal of Petroleum Science and Engineering*, **17**(3-4): 275–290, 1997.

[28] E. J. Mackay, G. D. Henderson, D. H. Tehrani, and A. Danesh. The importance of interfacial tension on fluid distribution during depressurisation. *Paper SPE*

38919, Proceedings of the SPE Annual Technical Conference and Exhibition, San Antonio, Texas, 5-8 October, 1997.

[29] S. Siddiqui, J. Yang, and M. Ahmed. Dynamic displacement measurement of three-phase relatrive permeabilities in berea sandstone cores. *Paper SPE 49306, Proceedings of the SPE Annual Technical Conference and Exhibition, New Orleans, Louisiana, 27-30 September*, 1998.

[30] C. A. Grattoni, R. I. Hawes, and R. A. Dawe. Production of gas from waterflood residual oil: gas saturation build-up and relative permeabilities. *Petroleum Geoscience*, **7**:131–136, 2001.

[31] M. Honarpour, L. Koederitz, and A. H. Harvey. *Relative Permeability of Petroleum Reservoirs*. CRC Press, Florida, 1st edition, 1986.

[32] F. A. L. Dullien. *Porous Media: Fluid Transport and Pore Structure*. Academic Press, San Diego, 2nd edition, 1992.

[33] M. C. Leverett. Capillary behaviour in porous solids. *Transactions of the American Institute of Mining, Metallurgical, and Petroleum Engineers*, **142**: 152–169, 1941.

[34] C. S. Land. Calculation of imbibition relative permeability for two- and three-phase flow from rock properties. *SPE Journal*, **June**:149–156, 1968.

[35] H. L. Stone. Probability model for estimating three-phase relative permeability. *Journal of Petroleum Technology*, **22**(2):214–218, 1970.

[36] H. L. Stone. Estimation of three-phase relative permeability and residual oil data. *Journal of Canadian Petroleum Technology*, **12**(4):53–61, 1973.

[37] J. K. Dietrich and P. L. Bondor. Three-phase oil relative permeability models. *Paper SPE 6044, Proceedings of the 51st SPE Annual Technical Conference and Exhibition, New Orleans, LA, 3-6 October*, 1976.

[38] K. Aziz and A. Settari. *Petroleum Reservoir Simulation*. Elsevier Applied Science, London, 1st edition, 1979.

[39] F. J. Fayers and J. D. Matthews. Evaluatin of normalized Stone's method for estimating three-phase relative permeabilities. *SPE Journal*, **April**:224–232, 1984.

[40] J. C. Parker, R. J. Lenhard, and T. Kuppusamy. A parametric model for constitutive properties governing multiphase flow in porous media. *Water Resources Research*, **23**(4):618–624, 1987.

[41] J. C. Parker and R. J. Lenhard. A model for hysteretic constitutive relations governing multiphase flow. 1.Saturation-pressure relations. *Water Resources Research*, **23**(12):2187–2196, 1987.

[42] R. J. Lenhard and J. C. Parker. A model for hysteretic constitutive relations governing multiphase flow. 2.Permeability-saturation relations. *Water Resources Research*, **23**(12):2197–2206, 1987.

[43] L. E. Baker. Three-phase relative permeability correlations. *Paper SPE 17369, Proceedings of the SPE/DOE Enhanced Oil Recovery Symposium, Tulsa, Oklahoma, 17-20 April*, 1988.

[44] M. A. Aleman and J. C. Slattery. Estimation of three-phase relative permeabilities. *Transport in Porous Media*, **3**(2):111–131, 1988.

[45] F. J. Fayers. Extension of stone's method i and conditions for real characteristics in three-phase flow. *SPE Reservoir Engineering*, **4**:437–445, 1989.

[46] M. Delshad and G. A. Pope. Comparison of the three-phase oil relative permeability models. *Transport in Porous Media*, **4**(1):59–83, 1989.

[47] J. C. Parker and R. J. Lenhard. Determining three-phase permeability-saturation-pressure relations from two-phase measurements. *Journal of Petroleum Science and Engineering*, **4**:57–65, 1990.

[48] O. S. Hustad and A. G. Hansen. A consistent correlation for three-phase relative permeabilities and phase pressures based on three sets of two-phase data. *Proceedings of the Eightth European Symposium on Improved Oil Recovery, Vienna, 15-17 May*, 1995.

[49] G. R. Jerauld. General three-phase relative permeability model for Purdhoe Bay. *Paper SPE 36178, Proceedings of the 7th ADIPEC, Abu Dhabi, 13-16 October*, 1996.

[50] G. R. Jerauld. Prudhoe Bay gas/oil relative permeability. *SPE Reservoir Engineering*, **12**(1):66–73, 1997.

[51] E. F. Balbinski, T. P. Fishlock, S. G. Goodyear, and P. I. R. Jones. Key characteristics of three-phase oil relative permeability formulations for improved oil recovery predictions. *Petroleum Geoscience*, **5**(4):339, 1999.

[52] F. J. Fayers. An improved three-phase flow model incorporating compositional variance. *Paper SPE 59313, Proceedings of the SPE/DOE Improved Oil Recovery Symposium, Tulsa, Oklahoma, 3-5 April*, 2000.

[53] M. J. Blunt. An empirical model for three-phase relative permeability. *SPE Journal*, **5**(4):435–445, 2000.

[54] O. S. Hustad. A coupled model for three-phase capillary pressure and relative permeability. *SPE Journal*, **7**(1):59–69, 2002.

[55] M. J. Blunt. Pore level modeling of the effects of wettability. *SPE Journal*, **2**(4):494–510, 1997.

[56] G. G. Pereira, W. V. Pinczewski, D. Y. C. Chan, L. Paterson, and P. E. Øren. Pore-scale network model for drainage-dominated three-phase flow in porous media. *Transport in Porous Media*, **24**(2):167–201, 1996.

[57] R. Lenormand, C. Zarcone, and A. Sarr. Mechanisms of the displacement of one fluid by another in a network of capillary ducts. *Journal of Fluid Mechanics*, **135**(October):337–353, 1983.

[58] R. Lenormand and C. Zarcone. Role of roughness and edges during imbibition in square capillaries. *Paper SPE 13264, Proceedings of the 59th SPE Annual Technical Conference and Exhibition, Houston, TX, 16-19 September*, 1984.

[59] J. D. Chen and J. Koplik. Immiscible fluid displacement in small networks. *Journal of Colloid and Interface Science*, **108**(2):304–330, 1985.

[60] I. Chatzis, A. Kantzas, and F. A. L. Dullien. On the investigation of gravity-assisted inert gas injection using micromodels, long Berea sandstone cores, and computer-assisted tomography. *Paper SPE 18284, Proceedings of the 63rd SPE Annual Technical Conference and Exhibition, Houston, TX, 2-5 October*, 1988.

[61] A. Kantzas, I. Chatzis, and F. A. L. Dullien. Mechanisms of capillary displacement of residual oil by gravity-assisted inert gas injection. *Paper SPE 17506, Proceedings of the SPE Rocky Mountain Regional Meeting, Casper, WY, 11-13 May*, 1988.

[62] A. Kantzas, I. Chatzis, and F. A. L. Dullien. Enhanced oil recovery by inert gas injection. *Paper SPE 17379, Proceedings of the SPE/DOE Enhanced Oil Recovery Symposium, Tulsa, Oklahoma, 17-20 April*, 1988.

[63] P. E. Øren and W. V. Pinczewski. The effect of film-flow on the mobilization of waterflood residual oil by gas flooding. *Proceedings of the 6th European IOR Symposium, Stavanger, May*, 1991.

[64] P. E. Øren and W. V. Pinczewski. Mobilization of waterflood residual oil by gas injecton for water wet conditions. *SPE Formation Evaluation*, **7**:70–78, 1992.

[65] P. E. Øren and W. V. Pinczewski. The effect of wettability and spreading coefficients on the recovery of waterflood residual oil by immiscible gasflooding. *Paper SPE 24881, Proceedings of the 67th SPE Annual Technical Conference and Exhibition, Washington, DC, 4-7 October*, 1992.

[66] W. E. Soll, M. A. Celia, and J. L. Wilson. Micromodel studies of three-fluid porous media systems: pore-scale processes relating to capillary pressure-saturation relationships. *Water Resources Research*, **29**(9):2963–2974, 1993.

[67] P. E. Øren and W. V. Pinczewski. Effect of wettability and spreading coefficients on recovery of waterflood residual oil by immiscible gasflooding. *SPE Formation Evaluation*, **9**(2):149–156, 1994.

[68] M. J. Blunt, D. Zhou, and D. H. Fenwick. Three-phase flow and gravity drainage in porous media. *Transport in Porous Media*, **20**(1-2):77–103, 1995.

[69] P. E. Øren and W. V. Pinczewski. Fluid ditribution and pore-scale displacement mechanisms in drainage dominaed three-phase flow. *Transport in Porous Media*, **20**(1-2):105–133, 1995.

[70] M. Dong, F. A. L. Dullien, and I. Chatzis. Imbibition of oil in film form over water present in edges of capillaries with an angular cross section. *Journal of Colloid and Interface Science*, **172**(1):21–36, 1995.

[71] O. Vizika and J. M. Lombard. Wettability and spreading: Two key parameters in oil recovery with three-phase gravity drainage. *SPE Reservoir Engineering*, **11**(1):54–60, 1996.

[72] A. A. Keller, M. J. Blunt, and P. V. Roberts. Micromodel observation of the role of oil layers in three-phase flow. *Transport in Porous Media*, **26**(3): 277–297, 1997.

[73] P. M. Adler, C. G. Jacquin, and J. A. Quiblier. Flow in simulated porous media. *International Journal of Multiphase Flow*, **16**(4):691–712, 1990.

[74] A. P. Roberts. Statistical reconstruction of three-dimesional porous media from two-dimensional images. *Physical Review E*, **56**(3):3203–3212, 1997.

[75] C. L. Y. Yeong and S. Torquato. Reconstructing random media II. three-dimensional media from two-dimensinal cuts. *Physical Review E*, **58**(1):224–233, 1998.

[76] S. Bakke and P. E. Øren. 3-D pore-scale modelling of sandstones and flow simulations in the pore networks. *SPE Journal*, **2**(2):136–149, 1997.

[77] P. E. Øren, S. Bakke, and O. J. Arntzen. Extending predictive capabilities to network models. *SPE Journal*, **3**(4):324–336, 1998.

[78] P. E. Øren and S. Bakke. Process based reconstruction of sandstones and prediction of transport properties. *Transport in Porous Media*, **46**(2-3):311–343, 2002.

[79] J. H. Dunsmuir, S. R. Ferguson, K. L. D'Amico, and J. P. Stokes. X-ray microtomography: a new tool for the characterization of porous media. *Paper SPE 22860, Proceedings of the 66th SPE Annual Technical Conference and Exhibition, Dallas, TX, 6-9 October*, 1991.

[80] P. Spanne, J. F. Thovert, C. J. Jacquin, W. B. Lindquist, K. W. Jones, and P. M. Adler. Synchrotron computed microtomography of porous media: topology and transports. *Physical Review Letters*, **73**(14):2001–2004, 1994.

[81] A. K. Gunstensen, D. H. Rothman, S. Zaleski, and G. Zanetti. Lattice boltzmann model of immiscible fluids. *Physical Review A*, **43**(8):4320–4327, 1991.

[82] D. Grunau, S. Chen, and K. Eggert. A lattice boltzmann model for multiphase fluid flows. *Physics of Fluids A - Fluid Dynamics*, **5**(10):2557–2562, 1993.

[83] B. Ferreol and D. H. Rothman. Lattice-Boltzmann simulations of flow through Fontainebleau porous media. *Transport in Porous Media*, **20**(1-2):3–20, 1995.

[84] F. M. Van Katz and P. J. P. Egberts. Simulation of three-phase displacement mechanisms using a 2D Lattice-Boltzmann model. *Transport in Porous Media*, **37**(1):55–68, 1999.

[85] J. F. Delerue and E. Perrier. Dxsoil, a library for 3d image analysis in soil science. *Computational Geosciences*, **28**(9):1041–1050, 2002.

[86] I. Fatt. The network model of porous media I. capillary pressure characteristics. *Transactions of the American Institute of Mining, Metallurgical, and Petroleum Engineers*, **207**:144–159, 1956.

[87] I. Fatt. The network model of porous media II. dynamic properties of a single size tube network. *Transactions of the American Institute of Mining, Metallurgical, and Petroleum Engineers*, **207**:160–163, 1956.

[88] I. Fatt. The network model of porous media III. dynamic properties of networks with tube radius distribution. *Transactions of the American Institute of Mining, Metallurgical, and Petroleum Engineers*, **207**:164–181, 1956.

[89] M. A. Celia, P. C. Reeves, and L. A. Ferrand. Recent advances in pore scale models for multiphase flow. *Reviews of Geophysics, Supplement*, **33**:1049–1057, 1995.

[90] M. J. Blunt. Flow in porous media- pore-network models and multiphase flow. *Current Opinion in Colloid and Interface Science*, **6**(3):197–207, 2001.

[91] M. J. Blunt, M. D. Jackson, M. Piri, and P. H. Valvatne. Detailed physics, predictive capabilities and macroscopic consequences for pore-network models of multiphase flow. *Advances in Water Resources*, **25**(8-12):1069–1089, 2002.

[92] K. K. Mohanty and S. J. Salter. Multiphase flow in porous media:II Pore-level modeling. *Paper SPE 11018, Proceedings of the 57th SPE Annual Fall Technical Conference and Exhibition, New Orleans, LA, 26-29 September*, 1982.

[93] C. Y. Lin and J. C. Slattery. 3-dimensional, randomized, network model for two phase flow through porous-media. *AIChE Journal*, **28**(2):311–324, 1982.

[94] R. Chandler, J. Koplik, K. Lerman, and J. F. Willemsen. Capillary displacement and percolation in porous media. *Journal of Fluid Mechanics*, **119**(June): 249–267, 1982.

[95] K. K. Mohanty and S. J. Salter. Multiphase flow in porous media:III Oil mobilization, Transverse dispersion, and Wettability. *Paper SPE 12127, Proceedings of the 58th SPE Annual Technical Conference and Exhibition, San Francisco, CA, 5-8 October*, 1983.

[96] A. A. Heiba, H. T. Davis, and L. E. Scriven. Effect of wettability on two-phase relative permeabilities and capillary pressures. *Paper SPE 12172, Proceedings of the 58th SPE Annual Technical Conference and Exhibition, San Francisco, CA, 5-8 October*, 1983.

[97] J. Koplik and T. J. Lasseter. Two-phase flow in random network models of porous media. *SPE Journal*, **February**:89–100, 1985.

[98] A. A. Heiba, G. R. Jerauld, H. T. Davis, and L. E. Scriven. Mechanism-based simulation of oil recovery processes. *Paper SPE 15593, Proceedings of the 61st SPE Annual Technical Conference and Exhibition, New Orleans, LA, 5-8 October*, 1986.

[99] M. M. Dias and A. C. Payatakes. Network models for two-phase flow in porous media. Part 1. immiscible micro-displacements of non-wetting fluids. *Journal of Fluid Mechanics*, **164**:305–336, 1986.

[100] C. E. Diaz, I. Chatzis, and F. A. L. Dullien. Simulation of capillary pressure curves using bond correlated site percolation on a simple cubic network. *Transport in Porous Media*, **2**(3):215–240, 1987.

[101] J. Bear, C. Braester, and P. C. Menier. Effective and relative permeabilities of anisotropic porous media. *Transport in Porous Media*, **2**:301–316, 1987.

[102] R. Lenormand, E. Touboul, and C. Zarcone. Numerical models and experiments on immiscible displacements in porous media. *Journal of Fluid Mechanics*, **189**(April):165–187, 1988.

[103] D. Y. C. Chan, B. D. Hughes, and L. Paterson. Simulating flow in porous media. *Physical Review A*, **38**(8):4106–4120, 1988.

[104] G. R. Jerauld and S. J. Salter. The effect of pore structure on hysteresis in relative permeability and capillary pressure: Pore-level modelling. *Transport in Porous Media*, **5**(2):102–151, 1990.

[105] M. J. Blunt and P. King. Relative permeabilities from two- and three-dimensional pore-scale network modelling. *Transport in Porous Media*, **6**: 407–433, 1991.

[106] M. J. Blunt, M. J. King, and H. Scher. Simulation and theory of two-phase flow in porous media. *Physical Review A*, **46**:7680–7699, 1992.

[107] S. Bryant and M. J. Blunt. Prediction of relative permeability in simple porous media. *Physical Review A*, **46**(4):2004–2011, 1992.

[108] A. A. Heiba, M. Sahimi, L. E. Scriven, and H. T. Davis. Percolation theory of two-phase relative permeability. *SPE Reservoir Engineering*, **7**:123–132, 1992.

[109] J. A. Billiotte, H. DeMoegen, and P. E. Øren. Experimental micromodeling and numerical simulation of gas/water injection/withdrawal cycles as applied to underground gas storage reservoirs. *SPE Aadvanced Technology Series*, **1**(1):133–139, 1993.

[110] M. A. Ioannidis and I. Chatzis. A mixed-percolation model of capillary hysteresis and entrapment in mercury porosimetry. *Journal of Colloid and Interface Science*, **161**:278–291, 1993.

[111] S. L. Bryant, D. W. Mellor, and C. A. Cade. Physically representative network models of transport in porous media. *AIChE Journal*, **39**(3):387–396, 1993.

[112] P. A. Goode and T. S. Ramakrishnan. Momentum transfer across fluid-fluid interfaces in porous media: a network model. *AIChE Journal*, **39**(7):1124–1134, 1993.

[113] S. R. McDougall and K. S. Sorbie. The impact of wettability on waterflooding: Pore-scale simulation. *SPE Reservoir Engineering*, **10**(3):208–213, 1995.

[114] M. I. Lowry and C. T. Miller. Pore-scale modeling of nonwetting-phase residual in porous media. *Water Resources Research*, **31**(3):455–473, 1995.

[115] S. H. Lee, L. Padmanabhan, and H. A. Al-Sunaidi. Simulation of linear displacement experiments on massively parallel computers. *Paper SPE 30721, Proceedings of the SPE Annual Technical Conference and Exhibition, Dallas, TX, 22-25 October*, 1995.

[116] P. C. Reeves and M. A. Celia. A functional relationship between capillary pressure, saturation, and interfacial area as revealed by a pore-scale network model. *Water Resources Research*, **32**(8):2345–2358, 1996.

[117] L. Paterson, S. Painter, X. Zhang, and W. V. Pinczewski. Simulation residual saturation and relative permeability in heterogeneous formations. *Paper SPE 36523, Proceedings of the SPE Annual Technical Conference and Exhibition, Denver, Colorado, 6-9 October*, 1996.

[118] L. S. Nilsen, P. E. Øren, S. Bakke, and A. Henriquez. 3-D pore-scale modelling of heterogeneous sandstone reservoir rocks and quantitative analysis of the architecture, geometry and spatial continuity of the pore network. *Paper SPE 35531, in Proceedings of the European 3-D Reservoir Modelling Conference, Stavanger, Norway, 16-17 April*, 1996.

[119] M. J. Blunt. Effects of heterogeneity and wetting on relative permeability using pore level modeling. *SPE Journal*, **2**:70, 1997.

[120] A. B. Dixit, S. R. McDougall, and K. S. Sorbie. A pore-level investigation of relative permeability hysteresis in water-wet systems. *Paper SPE 37233, Proceedings of the SPE International Symposium on Oilfield Chemistry, Houston, Texas, 18-21 February*, 1997.

[121] H. Rajaram, L. A. Ferrand, and M. A. Celia. Prediction of relative permeabilities for unconsolidated soils using pore-scale network models. *Water Resources Research*, **33**(1):43–52, 1997.

[122] A. S. Dixit, S. R. McDougall, K. S. Sorbie, and J. S. Buckley. Pore-scale modelling of wettability effects and their influence on oil recovery. *SPE Reservoir Evaluation and Engineering*, **2**(1):25–36, 1999.

[123] U. Fischer and M. A. Celia. Prediction of relative and absolute permeabilities for gas and water from soil water retention curves using a pore-scale network model. *Water Resources Research*, **35**(4):1089–1100, 1999.

[124] B. Xu, J. Kamath, Y. C. Yortsos, and S. H. Lee. Use of pore-network models to simulate laboratory coreflods in a heterogeneous carbonate sample. *SPE Journal*, **4**(3):179–186, 1999.

[125] C. Laroche, O. Vizika, and F. Kalaydjian. Network modeling to predict the effect of wettability heterogeneities on multiphase flow. *Paper SPE 56674,*

Proceedings of the SPE Annual Technical Conference and Exhibition, Houston, TX, 3-6 October, 1999.

[126] A. Maximenko and V. V. Kadet. Determination of relative permeabilities using the network models of porous media. *Journal of Petroleum Science and Engineering*, **28**(3):145–152, 2000.

[127] T. W. Patzek. Verification of a complete pore network simulator of drainage and imbibition. *SPE Journal*, **6**(2):144–156, 2001.

[128] M. A. Knackstedt, A. P. Sheppard, and M. Sahimi. Pore network modelling of two-phase flow in porous rock: the effect of correlated heterogeneity. *Advances in Water Resources*, **24**(3-4):257–277, 2001.

[129] R. J. Held and M. A. Celia. Modeling support of functional relationships between capillary pressure, saturation, interfacial area and common lines. *Advances in Water Resources*, **24**(3-4):325–343, 2001.

[130] M. Hilpert and C. T. Miller. Pore-morphology-based simulation of drainage in totally wetting porous media. *Advances in Water Resources*, **24**:243–255, 2001.

[131] R. J. Held and M. A. Celia. Pore-scale modeling extension of constitutive relationships in the range of residual saturations. *Water Resources Research*, **37**(1):165–170, 2001.

[132] M. Piri and M. J. Blunt. Pore-scale modeling of three-phase flow in mixed-wet systems. *Paper SPE 77726, Proceedings of the SPE Annual Technical Conference and Exhibition, San Antonio, Texas, 29 September-2 October*, 2002.

[133] M. Ferer, G. S. Bromhal, and D. H. Smith. Pore-level modeling of drainage: Crossover from inavsion percolasion fingering to compact flow. *Physical Review E*, **67**:051601.1–051601.12, 2003.

[134] P. H. Valvatne and M. J. Blunt. Predictive pore-scale modeling of two-phase flow in mixed-wet media. *Submitted to Water Resources Research*, , 2003.

[135] P. H. Valvatne and M. J. Blunt. Predictive pore-scale network modeling. *Paper SPE 84550, Proceedings of the SPE Annual Technical Conference and Exhibition, Denver, Colorado, 5-8 October*, 2003.

[136] P. E. Øren and S. Bakke. Reconstruction of Berea sandstone and pore-scale modelling of wettability. *Journal of Petroleum Science and Engineering*, **39**(3-4):177–199, 2003.

[137] A. Al-Futaisi and T. W. Patzek. Impact of wettability alteration on two-phase flow characteristics of sandstones: A quasi-static description. *Water Resources Research*, **39**(2)(SBH12):1–13, 2003.

[138] A. A. Heiba, H. T. Davis, and L. E. Scriven. Statistical network theory of three-phase relative permeabilities. *Paper SPE 12690, Proceedings of the SPE/DOE Symposium on Enhanced Oil Recovery, Tulsa, Oklahoma, 15-18 April*, 1984.

[139] W. E. Soll and M. A. Celia. A modified percolation approach to simulating three-fluid capillary pressure-saturation relationships. *Advances in Water Resources*, **16**:107–126, 1993.

[140] P. E. Øren, J. Billiotte, and W. V. Pinczewski. Pore-scale network modelling of waterflood residual oil recovery by immiscible gas flooding. *Paper SPE 27814, Proceedings of the SPE/DOE Symposium in Improved Oil Recovery, Tulsa, Oklahoma, 17-20 April*, 1994.

[141] L. Paterson, J. Y. Lee, and W. V. Pinczewski. Three-phase relative permeability in heterogeneous formations. *Paper SPE 38882, Proceedings of the SPE Annual Technical Conference and Exhibition, San Antonio, Texas, 5-8 October*, 1997.

[142] D. H. Fenwick and M. J. Blunt. Three-dimensional modeling of three phase imbibition and drainage. *Advances in Water Resources*, **21**(2):121–143, 1998.

[143] D. H. Fenwick and M. J. Blunt. Network modeling of three-phase flow in porous media. *SPE Journal*, **3**(1):86–97, 1998.

[144] V. Mani and K. K. Mohanty. Effect of the spreading coefficient on three-phase flow in porous media. *Journal of Colloid and Interface Science*, **187**(1):45–56, 1997.

[145] V. Mani and K. K. Mohanty. Pore-level network modeling of three-phase capillary pressure and relative permeability curves. *SPE Journal*, **3**:238–248, 1998.

[146] C. Laroche, O. Vizika, and F. Kalaydjian. Network modeling as a tool to predict three-phase gas injection in heterogeneous wettability porous media. *Journal of Petroleum Science and Engineering*, **24**(2-4):155–168, 1999.

[147] G. G. Pereira. Numerical pore-scale modeling of three-phase fluid flow:Comparison between simulation and experiment. *Physical Review E*, **59**(4):4229–4242, 1999.

[148] J. C. Moulu, O. Vizika, P. Egermann, and F. Kalaydjian. A new three-phase relative permeability model for various wettability conditions. *Paper SPE 56477, Proceedings of the SPE Annual Technical Conference and Exhibition, Houston, TX, 3-6 October*, 1999.

[149] T. R. Lerdahl, P. E. Øren, and S. Bakke. A predictive network model for three-phase flow in porous media. *Paper SPE 59311, Proceedings of the SPE/DOE Symposium in Improved Oil Recovery, Tulsa, Oklahoma, 3-5 April*, 2000.

[150] J. K. Larsen, N. Bech, and A. Winter. Three-phase immiscible WAG injection: micromodel experiments and network models. *Paper SPE 59324, Proceedings of the SPE/DOE Improved Oil Recovery Symposium, Tulsa, Oklahoma, 3-5 April*, 2000.

[151] M. I. J. van Dijke, K. S. Sorbie, and S. R. McDougall. A process-based approach for three-phase capillary pressure and relative permeability relationships in mixed-wet systems. *Paper SPE 59310, Proceedings of the SPE/DOE Symposium in Improved Oil Recovery, Tulsa, Oklahoma, 3-5 April*, 2000.

[152] M. I. J. van Dijke, K. S. Sorbie, and S. R. McDougall. Saturation-dependencies of three-phase relative permebilities in mixed-wet and fractionally wet systems. *Advances in Water Resources*, **24**:365–384, 2001.

[153] M. I. J. van Dijke, S. R. McDougall, and K. S. Sorbie. Three-phase capillary pressure and relative permeability relationships in mixed-wet systems. *Transport in Porous Media*, **44**:1–32, 2001.

[154] M. I. J. van Dijke, K. S. Sorbie, M. Sohrabi, D. Tehrani, and A. Danesh. Three-phase flow in WAG processes in mixed-wet porius media: pore-scale network simulations and comparison with micromodel experiments. *Paper SPE 75192, Proceedings of the SPE/DOE Tenth Symposium on Improved Oil Recovery, Tulsa, Oklahoma, 13-17 April*, 2002.

[155] M. I. J. van Dijke and K. S. Sorbie. Pore-scale network model for three-phase flow in mixed-wet porous media. *Physical Review E*, **66**:046302.1–046302.14, 2002.

[156] N. Silpngarmlers and T. Ertekin. Artificial neural network architectures for predicting two-phase and three-phase relative permeabilitiy characteristics. *Paper SPE 77704, Proceedings of the SPE Annual Technical Conference and Exhibition, San Antonio, Texas, 29 September-2 October*, 2002.

[157] B. Guler, T. Ertekin, and A. S. Grader. An artificial neural network based relative permeability predictor. *Paper 9991, Proceedings of the 8th Petroleum Conference of the South Saskatchewan Section, The Petroleum Society of CIM, Regina, 18-21 October*, 1999.

[158] N. Silpngarmlers, B. Guler, T. Ertekin, and A. S. Grader. Development and testing of two-phase relative permeability predictrs using artificial neural networks. *Paper SPE 69392, Proceedings of the SPE Latin American and Caribbean Petroleum Engineering Conference, Buenos Aires, Argentina, 25-28 March*, 2001.

[159] G. P. Androutsopoulos and R. Mann. Evaluation of mercury porosimetry using a network pore structure model. *Chemical Engineering Science*, **34**:1203–1212, 1979.

[160] I. Chatzis and F. A. L. Dullien. The modeling of mercury porosimetry and relative permeability of mercury in sandstones using percolation theory. *Int. Chem. Eng.*, **25**:47–65, 1985.

[161] C. D. Tsakiroglou and A. C. Payatakes. A new simulator of mercury porosimetry for the characterization of the porous materials. *Journal of Colloid and Interface Science*, **137**:315–339, 1990.

[162] P. G. Toledo, L. E. Scriven, and H. T. Davis. Pore-space statistics and capillary pressure curves from volume-controlled porosimetry. *SPE Formation Evaluation*, **9**(1):46–54, 1994.

[163] C. D. Tsakiroglou and A. C. Payatakes. Characterization of the pore structure of reservoir rocks with the aid of serial sectioning analysis, mercury porosimetry and network simulation. *Advances in Water Resources*, **23**(7):773–789, 2000.

[164] Y. Li, W. G. Laidlaw, and N. C. Wardlaw. Sensitivity of drainage and imbibition to pore structures as revealed by computer simulation of displacement process. *Advances in Colloid and Interface Science*, **26**:1–68, 1986.

[165] C. D. Tsakiroglou and M. Fleury. Resistivity index of frcational wettability porous media. *Journal of Petroleum Science and Engineering*, **22**:253–274, 1999.

[166] H. N. Man and X. D. Jing. Network modelling of wettability and pore geometry effects on electrical resistivity and capillary pressure. *Journal of Petroleum Science and Engineering*, **24**(2-4):255–267, 1999.

[167] C. D. Tsakiroglou and M. Fleury. Pore network analysis of resistivity index for water-wet porous media. *Transport in Porous Media*, **35**(1):89–128, 1999.

[168] H. N. Man and X. D. Jing. Pore network modelling of electrical resistivity and capillary pressure characteristics. *Transport in Porous Media*, **41**(3):263–286, 2000.

[169] H. N. Man and X. D. Jing. Network modelling of strong and intermediate wettability on electrical resistivity and capillary pressure. *Advances in Water Resources*, **24**(3-4):345–363, 2001.

[170] H. N. Man and X. D. Jing. Network modelling of mixed-wettability on electrical resistivity, capillary pressure and wettability indices. *Journal of Petroleum Science and Engineering*, **33**(1-3):101–122, 2002.

[171] R. P. Ewing and B. Berkowitz. A generalized growth model for simulating initial migration of dense non-aqueous phase liquids. *Water Resources Research*, **34**(4):611–622, 1998.

[172] C. Jia, K. Shing, and Y. C. Yortsos. Visualization and simulation of non-aqueous phase liquids solubilization in pore networks. *Journal of Contaminant Hydrology*, **35**(4):363–387, 1999.

[173] C. Jia, K. Shing, and Y. C. Yortsos. Advective mass transfer from stationary sources in porous media. *Water Resources Research*, **35**(11):3239–3251, 1999.

[174] D. Zhou, L. A. Dillard, and M. J. Blunt. A physically based model of dissolution of nonaqueous phase liquids in the saturated zone. *Transport in Porous Media*, **39**(2):227–255, 2000.

[175] L. A. Dillard and M. J. Blunt. Development of a pore network simulation model to study nonaqueous phase liquid dissolution. *Water Resources Research*, **36**(2):439–454, 2000.

[176] A. Ahamdi, A. Aigueperse, and M. Quintard. Calculation of the effective properties decribing active dispersion in porous media: from simple to complex unit cells. *Advances in Water Resources*, **24**:423–438, 2001.

[177] L. A. Dillard, H. I. Essaid, and M. J. Blunt. A functional relation for field-scale nonaqueous phase liquid dissolution developed using a pore network model. *Journal of Contaminant Hydrology*, **48**(1-2):89–119, 2001.

[178] R. J. Held and M. A. Celia. Pore-scale modeling and upscaling of nonaqueous phase liquid mass transfer. *Water Resources Research*, **37**(3):539–549, 2001.

[179] C. E. Knutson, C. J. Werth, and A. J. Valocchi. Pore-scale modeling of dissolution from variably distributed nonaqueous phase liquid blobs. *Water Resources Research*, **37**(12):2951–2963, 2001.

[180] C. Satik and Y. C. Yortsos. A pore network study of bubble growth in porous media driven by heat transfer. *Journal of Heat Transfer*, **118**:455–462, 1995.

[181] X. Li and Y. C. Yortsos. Theory of multiple bubble growth in porous media by solute diffusion. *Chemical Engineering Science*, **50**(8):1247–1271, 1995.

[182] C. Du and Y. C. Yortsos. A numerical study of the critical gas saturation in a porous media. *Transport in Porous Media*, **35**(2):205–225, 1999.

[183] R. Bora, B. B. Maini, and A. Chakma. Flow visualization studies of solution gas drive process in heavy oil reservoirs with a glass micromodel. *SPE Reservoir Evaluation and Engineering*, **3**(3):224–229, 2000.

[184] M. E. Kainourgiakis, A. K. Stubos, N. D. Konstantinou, N. K. Kanellopoulos, and V. Milisic. A network model for the permeability of condensable vapours through mesoporous media. *Journal of Membrane Science*, **114**:215–225, 1996.

[185] X. Wang and K. K. Mohanty. Critical condensate saturation in porous media. *Journal of Colloid and Interface Science*, **214**:416–426, 1999.

[186] X. Wang and K. K. Mohanty. Pore-network model of flow in gas/condensate reservoirs. *SPE Journal*, **5**(4):426–434, 2000.

[187] M. Jamiolahmady, A. Danesh, D. H. Tehrani, and D. B. Duncan. A mechanistic model of gas-condensate flow in pores. *Transport in Porous Media*, **41**: 17–46, 2000.

[188] M. Jamiolahmady, A. Danesh, D. H. Tehrani, and D. B. Duncan. Positive effect of flow velocity on gas-condensate relative permeability: network modelling and comparison with experimental rsults. *Transport in Porous Media*, **52**:159–183, 2003.

[189] M. Prat. Isothermal drying of non-hygroscopic capillary-porous materials as an invasion percolation process. *International Journal of Multiphase Flow*, **21**(5):875–892, 1995.

[190] J. B. Laurindo and M. Prat. Numerical and experimental network study of evaporation in capillary porous media. Phase Distribution. *Chemical Engineering Science*, **51**(23):5171–5185, 1996.

[191] J. B. Laurindo and M. Prat. Numerical and experimental network study of evaporation in capillary porous media.Drying rates. *Chemical Engineering Science*, **53**(12):2257–2269, 1996.

[192] I. N. Tsimpanogiannis and Y. C. Yortsos. Scaling theory of drying in porous media. *Physical Review E*, **59**(4):4353–4365, 1999.

[193] A. G. Yiotis, A. K. Stubos, A. G. Boudouvis, and Y. C. Yortsos. A 2-D pore-network model of the drying of single-component liquids in porous media. *Advances in Water Resources*, **24**:439–460, 2001.

[194] M. Prat. Recent advances in pore-scale models for drying of porous media. *Chemical Engineering Journal*, **86**(1-2):153–164, 2002.

[195] F. Plourde and M. Prat. Pore network simulations of drying of capillay porous media. influence of thermal gradients. *International Journal of Heat and Mass Transfer*, **46**(7):1293–1307, 2003.

[196] D. S. Freitas and M. Prat. Pore network simulation of evaporation of a binary liquid from a capillary porous medium. *Transport in Porous Media*, **40**:1–25, 2000.

[197] J. Carmeliet, F. Descamps, and G. Houvenaghel. A multiscale network model for simulating moisture transfer properties of porous media. *Transport in Porous Media*, **35**(1):67–88, 1999.

[198] K. Mogensen and E. Stenby. A dynamic pore-scale model of imbibition. *Paper SPE 39658, Proceedings of the SPE/DOE Symposium in Improved Recovery, Tulsa, Oklahoma, 19-22 April*, 1998.

[199] E. Aker, K. J. Maløy, A. Hansen, and G. G. Batrouni. A two-dimensional networksimulator for two-phase flow in porous media. *Transport in Porous Media*, **32**(2):163–186, 1998.

[200] K. Mogensen and E. Stenby. A dynamic two-phase pore-scale model of imbibition. *Transport in Porous Media*, **32**(3):299–327, 1998.

[201] H. K. Dahle and M. A. Celia. A dynamic network model for two-phase immiscible flow. *Computational Geosciences*, **3**(1):1–22, 1999.

[202] K. Mogensen, E. Stenby, S. Banerjee, and V. A. Barker. Comparison of iterative methods for computing the pressure field in a dynamic network model. *Transport in Porous Media*, **37**:277–301, 1999.

[203] R. G. Hughes and M. J. Blunt. Pore scale modeling of rate effects in imbibition. *Transport in Porous Media*, **40**(3):295–322, 2000.

[204] G. N. Constantinides and A. C. Payatakes. Effects of precursor wetting films in immiscible displacement through porous media. *Transport in Porous Media*, **38**(3):291–317, 2000.

[205] M. S. Valavanides and A. C. Payatakes. True-to-mechanism model of steady-state two-phase flow in porous media, using decomposition into prototype flows. *Advances in Water Resources*, **24**:385–407, 2001.

[206] M. Singh and K. K. Mohanty. Dynamic modeling of drainage through three-dimensional porous material. *Chemical Engineering Science*, **58**:1–18, 2003.

[207] M. D. Santiago and R. A. Dawe. The network simulation of diplacement processes in fractured reservoir matrix. *The Mathematics of oil recovery: based on the proceedings of a conference on the mathematics of oil recovery organized by the Institute of Mathematics and its Applications in association with the Society of Petroleum Engineers and held at Robinson College Cambridge in July 1989 ; edited by P. R. King.*, pages 551–572, 1992.

[208] R. J. Glass, M. J. Nicholl, and L. Yarrington. A modified invasion percolation model for low-capillary number immiscible displacements in horizontal

rough-walled fractures: Influence of local in-plane curvature. *Water Resources Research*, **34**(12):3215–3234, 1998.

[209] H. Amundsen, G. Wagner, U. Oxaal, P. Meakin, J. Feder, and T. Jøssang. Slow two-phase flow in artificial fractures: Experiments and simulations. *Water Resources Research*, **35**(9):2619–2626, 1999.

[210] A. A. Keller, M. J. Blunt, and P. V. Roberts. Behavior of nonaqueous phase liquids in fractured porous media under two-phase flow conditions. *Transport in Porous Media*, **38**(1-2):189–203, 2000.

[211] R. G. Hughes and M. J. Blunt. Pore-scale modeling of multiphase flow in fractures and matrix/fracture transfer. *SPE Journal*, **6**(2):126–136, 2001.

[212] R. G. Hughes and M. J. Blunt. Network modeling of multiphase flow in fractures. *Advances in Water Resources*, **24**:409–421, 2001.

[213] R. S. Maier, D. M. Kroll, R. S. Bernard, S. E. Howington, J. F. Peters, and H. T. Davis. Pore-scale simulation of dispersion. *Physics of Fluids*, **12**(8): 2065–2079, 2000.

[214] D. Cohen, T. W. Patzek, and C. J. Radke. Two-dimensional network simulation of diffusion-driven coarsening of foam inside a porous medium. *Journal of Colloid and Interface Science*, **179**(2):357–373, 1996.

[215] H. Kharabaf and Y. C. Yortsos. Pore network model for foam formation and propagation in porous media. *SPE Journal*, **3**:42–53, 1998.

[216] H. H. Al-Sharji, C. A. Grattoni, R. A. Dawe, and R. W. Zimmerman. Pore-scale study of the flow of oil and water through polymer gels. *Paper SPE 56738, Proceedings of the SPE Annual Technical Conference and Exhibition, Houston, Texas, 3-6 October*, 1999.

[217] B. J. Suchomel, B. M. Chen, and M. B. Allen. Macroscale properties of porous media from a network model of biofilm processes. *Transport in Porous Media*, **31**:39–66, 1998.

[218] H. J. Dupin, P. K. Kitanidis, and P. L. McCarty. Pore-scale modeling of biological clogging due to aggregate expansion: A material mechanics approach. *Water Resources Research*, **37**(12):2965–2979, 2001.

[219] F. Thauvin and K. K. Mohanty. Network modeling on non-darcy flow through porous media. *Transport in Porous Media*, **31**:19–37, 1998.

[220] Y. Zhang, M. Shariati, and Y. C. Yortsos. The spreading of immiscible fluids in porous media under the influence of gravity. *Transport in Porous Media*, **38**:117–140, 2000.

[221] R. P. Ewing and B. Berkowitz. Stochastic pore-scale growth models of DNAPL migration in porous media. *Advances in Water Resources*, **24**(3-4):309–323, 2001.

[222] A. Leventis, D. A. Verganelakis, M. R. Halse, and J. B. Webber. Capillary imbibition and pore characterisation in cement pastes. *Transport in Porous Media*, **39**:143–157, 2000.

[223] J. Stark and M. Manga. The motion of long bubbles in a network of tubes. *Transport in Porous Media*, **40**:201–218, 2000.

[224] S. P. Friedman and N. A. Seaton. Critical path analysis of the relationship between permeability and electrical conductivity of three-dimensional pore networks. *Water Resources Research*, **34**(7):1703–1710, 1998.

[225] A. G. Hunt. Applications of percolation theory to porous media with distributed local conductances. *Advances in Water Resources*, **24**:279–307, 2001.

[226] X. Lopez, P. H. Valvatne, and M. J. Blunt. Predictive network modeling of single-phase non-newtonian flow in porous media. *Journal of Colloid and Interface Science*, **264**:256–265, 2003.

[227] M. Sahimi, A. R. Mehrabi, N. Mirzaee, and H. Rassamdana. The effect of asphalt percipitation on flow behavior and production of a fractured carbonate oil reservoir during gas injection. *Transport in Porous Media*, **41**:325–347, 2000.

[228] J. E. P. Monteagudo, K. Rajagopal, and P. L. C. Lage. Simulating oil flow in porous media under asphaltene deposition. *Chemical Engineering Science*, **57**:323–337, 2002.

[229] J. E. P. Monteagudo, L. F. L. R. Silva, and P. L. C. Lage. Scaling laws for network model permeability: application to wellbore oil flow simulation with solid deposition. *Chemical Engineering Science*, **58**:1815–1829, 2003.

[230] J. Ghassemzadeh, M. Hashemi, L. Sartor, and M. Sahimi. Pore network simulation of fluid imbibition into paper during coating processes: I. Model development. *AIChE Journal*, **47**:519–535, 2001.

[231] M. Dadvar, M. Sohrabi, and M. Sahimi. Pore network model of deactivation of immobilized glucose isomerase in packed-bed reactors. I: Two-dimensional simulations at the particle level. *Chemical Engineering Science*, **56**(8):2803–2819, 2001.

[232] M. Dadvar and M. Sahimi. Pore network model of deactivation of immobilized glucose isomerase in packed-bed reactors. II: Three-dimensional simulations at the particle level. *Chemical Engineering Science*, **57**(6):939–952, 2002.

[233] J. Wood and L. F. Gladden. Modelling diffusion and reaction accompanied by capillary condensation using three-dimensional pore networks. Part 1. Fickian diffusion and pseudo-first-order reaction kinetics. *Chemical Engineering Science*, **57**(15):3033–3045, 2002.

[234] J. Wood, L. F. Gladden, and F. J. Keil. Modelling diffusion and reaction accompanied by capillary condensation using three-dimensional pore networks. part 2. Dusty gas model and general reaction kinetics. *Chemical Engineering Science*, **57**(15):3047–3059, 2002.

[235] J. J. Meyers and A. I. Liapis. Network modeling of the intraparticle convection and diffusion of molecules in porous particles packed in a chromatographic column. *Journal of Chromatography A*, **827**(2):197–213, 1998.

[236] A. I. Liapis, J. J. Meyers, and O. K. Crosser. Modeling and simulation of the dynamic behavior of monoliths: Effects of pore structure from pore network model analysis and comparison with columns packed with porous spherical particles. *Journal of Chromatography A*, **865**(1-2):13–25, 1999.

[237] J. J. Meyers and A. I. Liapis. Network modeling of the convective flow and diffusion of molecules adsorbing in monoliths and in porous particles packed in a chromatographic column. *Journal of Chromatography A*, **852**(1):3–23, 1999.

[238] B. A. Grimes, J. J. Meyers, and A. I. Liapis. Determination of the intraparticle electroosmotic volumetric flow-rate, velocity and peclet number in capillary electrochromatography from pore network theory. *Journal of Chromatography A*, **890**(1):61–72, 2000.

[239] J. J. Meyers, O. K. Crosser, and A. I. Liapis. Pore network modelling: determination of the dynamic profiles of the pore diffusivity and its effect on column performance as the loading of the solute in the adsorbed phase varies with time. *Journal of Chromatography A*, **908**(1-2):35–47, 2001.

[240] J. J. Meyers, S. Nahar, D. K. Ludlow, and A. I. Liapis. Determination of the pore connectivity and pore size distribution and pore spatial distribution of porous chromatographic particles from nitrogen sorption measurements and pore network modelling theory. *Journal of Chromatography A*, **907**(1-2):57–71, 2001.

[241] L. M. Bryntesson. Pore network modelling of the behaviour of a solute in chromatography media: transient and steady-state diffusion properties. *Journal of Chromatography A*, **945**(1-2):103–115, 2002.

[242] B. C. E. Schwarz, J. S. Devinny, and T. T. Tsotsis. A biofilter network model importance of the pore structure and other large-scale heterogeneities. *Chemical Engineering Science*, **56**(2):475–483, 2001.

[243] H. F. Nordhaug, M. Celia, and H. K. Dahle. A pore network model for calculation of interfacial velocities. *Advances in Water Resources*, **26**(10):1061–1074, 2003.

[244] S. Bryant, P. R. King, and D. W. Mellor. Network model evaluation of permeability and spatial correlation in a real random sphere packing. *Transport in Porous Media*, **11**(1):53–70, 1993.

[245] A. W. Adamson and A. P. Gast. *Physical Chemistry of Surfaces*. John Wiley and Sons, Inc., New York, 6th edition, 1997.

[246] D. Zhou and M. J. Blunt. Effect of spreading coefficient on the distribution of light non-aqueous phase liquid in the subsurface. *Journal of Contaminant Hydrology*, **25**(1):1–19, 1997.

[247] F. E. Bartell and H. J. Osterhoff. Determination of the wettability of a solid by a liquid. *Industrial and Engineering Chemistry*, **19**:1277–1287, 1927.

[248] M. J. Blunt. Constraints on contact angles for multiple phases in thermodynamic equilibrium. *Journal of Colloid and Interface Science*, **239**:281–282, 2001.

[249] N. R. Morrow, H. T. Lim, and J. S. Ward. Effect of crude-oil-induced wettability changes on oil recovery. *SPE Formation Evaluation*, **2**:89–103, 1986.

[250] O. Fassi-Fihri, M. Robin, and E. Rosenberg. Wettability studies at the pore level: Anew approach by the use of Cycro-Scanning Electron Microscopy. *Paper SPE 22596, Proceedings of the 66th SPE Annual Technical Conference and Exhibition, Dallas, TX, 6-9 October*, 1991.

[251] A. R. Kovscek, H. Wong, and C. J. Radke. A pore-level scenario for the development of mixed wettability in oil reservoirs. *AIChE Journal*, **39**(6): 1072–1085, 1993.

[252] J. S. Buckley, Y. Liu, and S. Monsterleet. Mechanisms of wetting alteration by crude oils. *SPE Journal*, **3**(1):54–61, 1998.

[253] L. W. Lake. *Improved Oil Recovery*. Prentice Hall, Englewood Cliffs, NJ, 1989.

[254] N. R. Morrow. Effects of surface roughness on contact angle with special reference to petroleum recovery. *Journal of Canadian Petroleum Technology*, **14**(4):42–53, 1975.

[255] N. R. Morrow. Capillary pressure correlations for uniformely wetted porous media. *Journal of Canadian Petroleum Technology*, **15**(4):49–69, 1976.

[256] N. J. Hayden and T. C. Voice. Microscopic observation of a napl in a three-fluid-phase soil system. *Journal of Contaminant Hydrology*, **12**(3):217–226, 1993.

[257] M. Dong and I. Chatzis. The imbibition and flow of a wetting liquid along the corners of a square capillary tube. *Journal of Colloid and Interface Science*, **172**(2):278–288, 1995.

[258] R. B. Stinchcombe. Conductivity and spinwave stiffness in disordered systems - an exactly soluble model. *Journal of Physics C. Solid State Physics*, **7**: 179–203, 1974.

[259] D. Wilkinson and J. F. Willemsen. Invasion percolation: a new form of percolation theory. *Journal of Physics A: Mathematical and General*, **16**(14): 3365–3376, 1983.

[260] J. Hoshen and R. Kopelman. Percolation and cluster distribution. I. cluster multiple labeling technique and critical concentration algorithm. *Physical Review B*, **14**(8):3438–3445, 1976.

[261] S. G. Goodyear and P. I. R. Jones. Relative permeabilities for gravity stabilised gas injection. *Proceedings of the 7th European IOR Symposium, Moscow, Russia, 27-29 October*, 1993.

[262] P. Naylor, N. C. Sargent, A. J. Crosbie, A. P. Tilsed, and S. G. Goodyear. Gravity drainage during gas injection. *Proceedings of the 8th European IOR Symposium, Vienna, Austria, 15-17 May*, 1995.

[263] A. Sahni, J. Burger, and M. J. Blunt. Measurement of three phase relative permebility during gravity drainage using CT scanning. *Paper SPE 39655, Proceedings of the SPE/DOE Improved Oil Recovery Symposium, Tulsa, Oklahoma, 19-22 April*, 1998.

[264] M. H. Hui and M. J. Blunt. Effects of wettability on three-phase flow in porous media. *Journal of Physical Chemistry B*, **104**(16):3833–3845, 2000.

[265] M. H. Hui and M. J. Blunt. Pore-scale modeling of of three-phase flow and the effects of wettability. *Paper SPE 59309, Proceedings of the SPE/DOE Improved Oil Recovery Symposium, Tulsa, Oklahoma, 3-5 April*, 2000.

[266] M. Sohrabi, G. D. Henderson, D. H. Tehrani, and A. Danesh. Visualisation of oil recovery by water alternating gas wag injection using high pressure micromodels water wet system. *Paper SPE 63000, Proceedings of the SPE Annual Technical Conference and Exhibition, Dallas, TX, 1-4 October*, 2000.

[267] M. Sohrabi, D. H. Tehrani, A. Danesh, and G. D. Henderson. Visualisation of oil recovery by water alternating gas (WAG) injection using high pressure micromodels - oil-wet & mixed-wet systems. *Paper SPE 71494, Proceedings of the SPE Annual Technical Conference and Exhibition, New Orleans, Louisiana, 30 September - 3 October*, 2001.

[268] M. A. Ioannidis and I. Chatzis. On the geometry and topology of 3D stochastic porous media. *Journal of Colloid and Interface Science*, **229**(2):323–334, 2000.

[269] M. Pillotti. Reconstruction of clastic porous media. *Transport in Porous Media*, **41**(3):359–364, 2000.

[270] Z. R. Liang, P. C. Philippi, C. P. Fernandes, and F. S. Magnani. Prediction of permeability from the skeleton of three-dimensional pore structure. *SPE Reservoir Evauation and Engineering*, **2**:161–168, 1999.

[271] R. D. Hazlett. Simulation of capillay dominated displacements in microtomographic images of reservoir rocks. *Transport in Porous Media*, **20**:21–35, 1995.

[272] D. A. Coker, S. Torquato, and J. H. Dunsmuir. Morphology and physical properties of Fontainebleau sandstone via tomographic analysis. *Journal of Geophysical Research*, **101**(B8: Solid earth and planets):17497–17506, 1996.

[273] Z. R. Liang, C. P. Fernandes, F. S. Magnani, and P. C. Philippi. A reconstruction technique for three-dimensional porous media using image analysis and Fourier transforms. *Journal of Petroleum Science and Engineering*, **21**: 273–283, 1998.

[274] Z. R. Liang, M. A. Ioannidis, and I. Chatzis. Permeability and electrical conductivity of porous media from 3D stochastic replicas of the microstructure. *Chemical Engineering Science*, **55**:5247–5257, 2000.

[275] S. Bekri, K. Xu, F. Yousefian, P. M. Adler, J.-F. Thovert, J. Muller, K. Iden, A. Psyllos, A. K. Stubos, and M. A. Ioannidis. Pore geometry and transport properties in North Sea chalk. *Journal of Petroleum Science and Engineering*, **25**:107–134, 2000.

[276] J. Quiblier. A new three dimensional modeling technique for studying porous media. *Journal of Colloid and Interface Science*, **98**:84–102, 1984.

[277] P. M. Adler, C. J. Jacquin, and J. F. Thovert. The formation factor of reconstructed porous media. *Water Resources Research*, **28**:1571–1576, 1992.

[278] H. J. Vogel and K. Roth. Quantitative morphology and network representation of soil pore structure. *Advances in Water Resources*, **24**:233–242, 2001.

[279] R. Ehrlich and D. K. Davies. Image analysis of pore geometry: relationship to reservoir engineering and modeling. *Paper SPE 19054, Proceedings of the SPE Gas Technology Symposium , Dallas, TX, 7-9 June*, 1989.

[280] G. Mason and N. R. Morrow. Capillary behavior of a perfectly wetting liquid in irregular triangular tubes. *Journal of Colloid and Interface Science*, **141**(1): 262–274, 1991.

[281] T. W. Patzek and D. B. Silin. Shape factor and hydraulic conductance in noncircular capillaries. I. One-phase creeping flow. *Journal of Colloid and Interface Science*, **236**(2):295–304, 2001.

[282] R. P. Mayer and R. A. Stowe. Mercury porosimetry-breakthrough pressure for penetration between packed spheres. *Journal of Colloid Science*, **20**:893–911, 1965.

[283] H. M. Princen. Capillary phenomena in assemblies of parallel cylinders I. Capillary rise between two cylinders. *Journal of Colloid and Interface Science*, **30**(1):69–75, 1969.

[284] H. M. Princen. Capillary phenomena in assemblies of parallel cylinders II. Capillary rise in systems with more than two cylinders. *Journal of Colloid and Interface Science*, **30**(3):359–371, 1969.

[285] H. M. Princen. Capillary phenomena in assemblies of parallel cylinders III. Liquid columns between horizontal parallel cylinders. *Journal of Colloid and Interface Science*, **34**(2):171–184, 1970.

[286] B. Legait. Laminar flow of two phases through a capillary tube with variable square cross section. *Journal of Colloid and Interface Science*, **96**:28–38, 1983.

[287] N. R. Morrow. Pore level displacement mechanisms. *Proceedings of the First Intl. Symposium on Evaluation of Reservoir wettability and Its Effect on Oil Recovery, Socorro, New Mexico, 18-21 September*, 1990.

[288] M. I. J. van Dijke and K. S. Sorbie. Three-phase capillary entry conditions in pores of noncircular cross-section. *Journal of Colloid and Interface Science*, **260**:385–397, 2003.

[289] S. Ma, G. Mason, and N. R. Morrow. Effect of contact angle on drainage and imbibition in regular polygonal tubes. *Colloids and Surfaces A: Physicochemical and Engineering Aspects*, **117**(3):273–291, 1996.

[290] M. J. Blunt. Physically-based network modeling of multiphase flow in intermediate-wet porous media. *Journal of Petroleum Science and Engineering*, **20**(3-4):117–125, 1998.

[291] A. Al-Futaisi and T. W. Patzek. Extension of Hoshen-Kopelman algorithm to non-lattice environments. *Physica A*, **321**(3-4):665–678, 2003.

[292] F. J. M. Kalaydjian. Performance and analysis of three-phase capillary pressure curves for drainage and imbibition in porous media. *Paper SPE 24878, Proceedings of the 67th SPE Annual Technical Conference and Exhibition, Washington, DC, 4-7 October*, 1992.

[293] T. C. Ransohoff and C. J. Radke. Laminar flow of a wetting liquid along the corners of a predominantly gas-occupied noncircular pore. *Journal of Colloid and Interface Science*, **121**(2):392–401, 1988.

[294] D. Zhou, M. J. Blunt, and F. M. Orr. Hydrocarbon drainage along corners of noncircular capillaries. *Journal of Colloid and Interface Science*, **187**(1): 11–21, 1997.

[295] T. C. Ransohoff, P. A. Gauglitz, and C. J. Radke. Snap-off of gas-bubbles in smoothly constricted noncircular capillaries. *AIChE Journal*, **33**(5):753–765, 1987.

[296] T. W. Patzek and J. G. Kristensen. Shape factor and hydraulic conductance in noncircular capillaries. II. Two-phase creeping flow. *Journal of Colloid and Interface Science*, **236**(2):305–317, 2001.

[297] A. Al-Futaisi and T. W. Patzek. Three-phase hydraulic conductances in angular capillaries. *SPE Journal*, **8**(3):252–261, 2003.

[298] T. Firincioglu, M. J. Blunt, and D. Zhou. Three-phase flow and wettability effects in triangular capillaries. *Colloids and Surfaces A: Physicochemical and Engineering Aspects*, **155**(2-3):259–276, 1999.

[299] D. A. DiCarlo, A. Sahni, and M. J. Blunt. The effect of wettability on three-phase relative permeability. *Paper SPE 49317, Proceedings of the SPE Annual Technical Conference and Exhibition, New Orleans, Louisiana, 27-30 September*, 1998.

[300] D. A. DiCarlo, A. Sahni, and M. J. Blunt. The effect of wettability on three-phase relative permeability. *Transport in Porous Media*, **39**:347–366, 2000.

[301] D. A. DiCarlo, A. Sahni, and M. J. Blunt. Three-phase relative permeability of water-wet, oil-wet and mixed-wet sandpacks. *SPE Journal*, **5**(1):82–91, 2000.

[302] M. D. Jackson, P. H. Valvatne, and M. J. Blunt. Prediction of wettability variation and its impact on waterflooding using pore-to reservoir-scale simulation. *Paper SPE 77543, Proceedings of the SPE Annual Technical Conference and Exhibition, San Antonio, Texas, 29 September-2 October*, 2002.

[303] A. B. Dixit, S. R. McDougall, and K. S. Sorbie. Analysis of relative permeability hysteresis trends in mixed-wet porous media using network models. *Paper SPE 39656, Proceedings of the SPE/DOE Improved Oil Recovery Symposium, Tulsa, Oklahoma, 19-22 April*, 1998.

[304] A. B. Dixit, J. S. Buckley, S. R. McDougall, and K. S. Sorbie. Empirical measures of wettability in porous media and the relationship between them derived from pore-scale modelling. *Transport in Porous Media*, **40**:27–54, 2000.

Appendix A

Threshold Layer Collapse Capillary Pressure

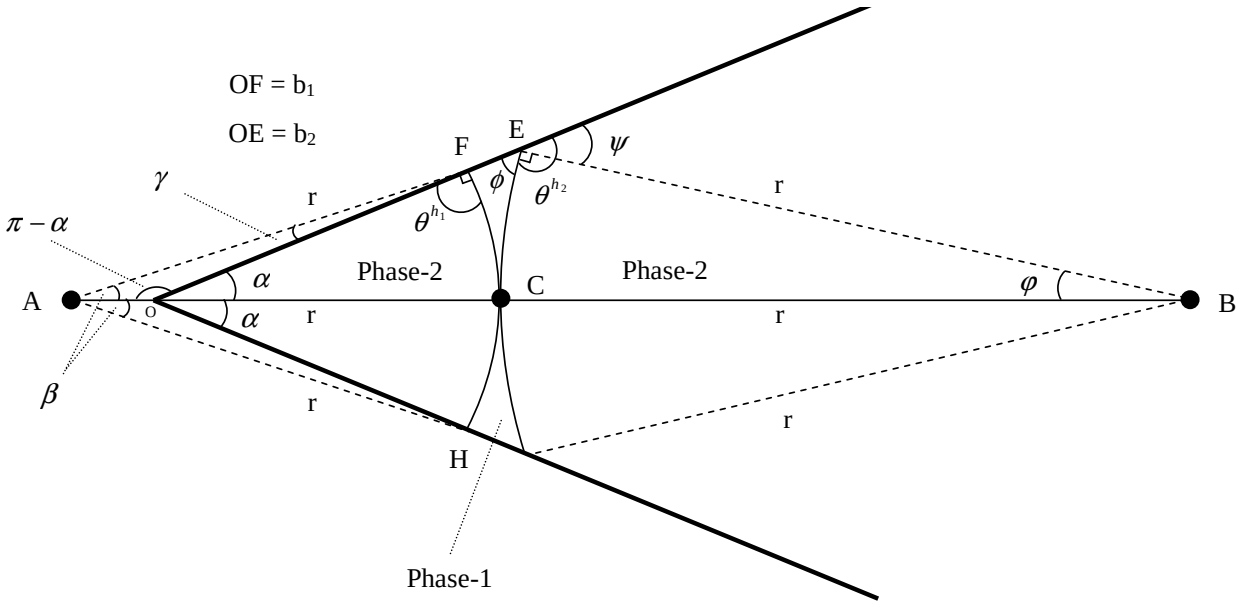

Figure A.1: A layer sandwiched between identical fluids residing in the corner and the centre.

Consider the triangle OEB:

$$\frac{r}{\sin\alpha} = \frac{OB}{\sin(\pi - \psi)} \tag{A.1}$$

$$\psi = \theta^{h_2} - \frac{\pi}{2}$$
$$\therefore \frac{r}{\sin\alpha} = \frac{OB}{\sin(\frac{3\pi}{2} - \theta^{h_2})} \tag{A.2}$$

$$OB = \frac{r}{\sin\alpha}\sin(\frac{3\pi}{2} - \theta^{h_2})$$
$$\sin(\frac{3\pi}{2} - \theta^{h_2}) = -\cos\theta^{h_2}$$
$$\therefore OB = -r\frac{\cos\theta^{h_2}}{\sin\alpha} \tag{A.3}$$

$$OC = OB - r = -r\left[1 + \frac{\cos\theta^{h_2}}{\sin\alpha}\right] \tag{A.4}$$

Consider triangle AOF:

$$\frac{r}{\sin(\pi - \alpha)} = \frac{b_1}{\sin\beta} \tag{A.5}$$

$$\sin(\pi - \alpha) = \sin\alpha$$
$$\therefore \sin\beta = \frac{b_1}{r}\sin\alpha \tag{A.6}$$

$$\gamma = \pi - (\pi - \alpha) - \beta = \alpha - \beta \tag{A.7}$$

In triangle AOF:

$$\frac{AO}{\sin\gamma} = \frac{b_1}{\sin\beta} \tag{A.8}$$

From Eqs. (A.6), (A.7), and (A.8):

$$\frac{AO}{\sin(\alpha - \beta)} = \frac{r}{\sin\alpha} \tag{A.9}$$

$$AO = \frac{r}{\sin\alpha}\sin(\alpha - \beta) = \frac{r}{\sin\alpha}(\sin\alpha\cos\beta - \cos\alpha\sin\beta) \tag{A.10}$$

From Eqs. (A.6) and (A.10):

$$AO = r\cos\beta - b_1\cos\alpha \tag{A.11}$$

$$OC = r - AO \tag{A.12}$$

$$OC = r - r\cos\beta + b_1\cos\alpha \tag{A.13}$$

From equating Eqs. (A.4) and (A.13):

$$r(2 + \frac{\cos\theta^{h_2}}{\sin\alpha}) + b_1\cos\alpha = r\cos\beta \tag{A.14}$$

$$r^2(4 + 4\frac{\cos\theta^{h_2}}{\sin\alpha} + \frac{\cos^2\theta^{h_2}}{\sin^2\alpha}) + b_1^2\cos^2\alpha + 2b_1 r\cos\alpha(2 + \frac{\cos\theta^{h_2}}{\sin\alpha}) = r^2\cos^2\beta \tag{A.15}$$

$$r^2\cos^2\beta = r^2(1 - \sin^2\beta) = r^2(1 - \frac{b_1^2}{r^2}\sin^2\alpha) = r^2 - b_1^2\sin^2\alpha \tag{A.16}$$

$$r^2(3 + 4\frac{\cos\theta^{h_2}}{\sin\alpha} + \frac{\cos^2\theta^{h_2}}{\sin^2\alpha}) + b_1^2 + 2b_1 r\cos\alpha(2 + \frac{\cos\theta^{h_2}}{\sin\alpha}) = 0 \tag{A.17}$$

$$r = \frac{-2b_1\cos\alpha[2 + (\cos\theta^{h_2}/\sin\alpha)] \pm [A]}{\left[6 + 8(\cos\theta^{h_2}/\sin\alpha) + 2(\cos^2\theta^{h_2}/\sin^2\alpha)\right]} \tag{A.18}$$

$$A = \left[4b_1^2\cos^2\alpha(4 + 4\frac{\cos\theta^{h_2}}{\sin\alpha} + \frac{\cos^2\theta^{h_2}}{\sin^2\alpha}) - 12b_1^2 - 16b_1^2\frac{\cos\theta^{h_2}}{\sin\alpha} - 4b_1^2\frac{\cos^2\theta^{h_2}}{\sin^2\alpha}\right]^{\frac{1}{2}} \tag{A.19}$$

$$\frac{r}{b_1} = \frac{-2\sin^2\alpha\cos\alpha - \cos\alpha\sin\alpha\cos\theta^{h_2} \pm [A]}{3\sin^2\alpha + 4\sin\alpha\cos\theta^{h_2} + \cos^2\theta^{h_2}} \tag{A.20}$$

$$A = [4\cos^2\alpha\sin^4\alpha + 4\sin^3\alpha\cos\theta^{h_2}\cos^2\alpha + \cos^2\alpha\sin^2\alpha\cos^2\theta^{h_2} - 3\sin^4\alpha - 4\cos\theta\sin^3\alpha - \cos^2\theta^{h_2}\sin^2\alpha]^{\frac{1}{2}} \tag{A.21}$$

$$\frac{r}{b_1} = \frac{-\cos\alpha\sin\alpha(2\sin\alpha+\cos\theta^{h_2}) \pm \sin^2\alpha\left[-4\sin\alpha\cos\theta^{h_2} - 3 + 4\cos^2\alpha - \cos^2\theta^{h_2}\right]^{\frac{1}{2}}}{3\sin^2\alpha + 4\sin\alpha\cos\theta^{h_2} + \cos^2\theta^{h_2}} \tag{A.22}$$

$$P_{c12} = -\frac{\sigma_{12}}{r} \tag{A.23}$$

$$P_{c12} = \frac{\sigma_{12}(3\sin^2\alpha + 4\sin\alpha\cos\theta^{h_2} + \cos^2\theta^{h_2})}{b_1[\cos\alpha\sin\alpha(2sin\alpha + \cos\theta^{h_2}) + \sin^2\alpha\sqrt{4\cos^2\alpha - 3 - cos^2\theta^{h_2} - 4\sin\alpha\cos\theta^{h_2}}]} \tag{A.24}$$

For b_1:

$$\gamma + \theta^{h_1} = \frac{\pi}{2} \tag{A.25}$$

From Eqs. (A.6), (A.7), and (A.25):

$$\beta = (\alpha + \theta^{h_1}) - \frac{\pi}{2} \tag{A.26}$$

$$\begin{aligned} b_1 &= \frac{r}{\sin\alpha}\sin[(\alpha+\theta^{h_1}) - \frac{\pi}{2}] \\ \sin[(\alpha+\theta^{h_1}) - \frac{\pi}{2}] &= -\cos(\alpha+\theta^{h_1}) \\ \therefore b_1 &= \frac{r}{\sin\alpha}[-\cos(\alpha+\theta^{h_1})] \end{aligned} \tag{A.27}$$

Since the curvature is negative then:

$$b_1 = r\frac{\cos(\alpha+\theta^{h_1})}{\sin\alpha} \tag{A.28}$$

For b_2, consider triangle OEB:

$$\frac{r}{\sin\alpha} = \frac{b_2}{\sin(\varphi)} \tag{A.29}$$

$$\begin{aligned}
\varphi &= \pi - (\frac{3\pi}{2} - \theta^{h_2}) - \alpha \\
\varphi &= -\frac{\pi}{2} + \theta^{h_2} - \alpha \\
\theta^{h_2} &= \pi - \phi \\
\therefore \varphi &= \frac{\pi}{2} - (\alpha + \phi)
\end{aligned} \tag{A.30}$$

From Eqs. (A.29) and (A.30):

$$\begin{aligned}
\sin\varphi = \sin[\frac{\pi}{2} - (\alpha + \phi)] &= \cos(\alpha + \phi) \\
\therefore b_2 &= r\frac{\cos(\alpha + \phi)}{\sin\alpha}
\end{aligned} \tag{A.31}$$

Appendix B

Parameters in the Model

Input parameters of the model are summarized here. For each item the value(s)/equations(s) that are used in this work are given within the parentheses.

- Fraction of the clay volume saturated with water to control irreducible water saturation (1).
- Interfacial tensions to be used in capillary pressure and area calculations (see Table (7.1)).
- A section of the network where saturations and relative permeabilities are computed (the central 90% of the network).
- A large positive integer number to be used in random number generation, seed (12357).
- Maximum number of iterations to be used in pressure solver (30000).
- Convergency criterion to be used in pressure solver ($5.0E-06$).
- Pore-body filling model to be used in calculation of threshold capillary pressures for imbibition in pores (Eq. (4.64), see section (4.4.2)).
- Parameters of pore-body filling model ($e_1 = 0$ and $e_2 - e_n = 0.03\ \mu m^{-1}$, see section (4.4.2)).
- Contact angles to be used in threshold capillary pressure and area calculations (see Tables (7.2) and (7.3)).